AD-784 950

FEASIBILITY STUDY AND DEMONSTRATION OF NITROGEN GENERATION FOR FUEL TANK INERTING

Scott A. Manatt

AiResearch Manufacturing Company

Prepared for:

Federal Aviation Administration

June 1974

NOTICE

The United States government does not endorse products or manufacturers. Trade or manufacturers' names appear herein solely because they are considered essential to the object of this report.

NOTICE

This document contains material reprinted from DC-10 Schematics, American Airlines Series 10 by permission of McDonnell Douglas Corporation. Year of first publication 6-30-1970. Doc. No. WZZ7111.

NOTICE

This document is disseminated under the sponsorship of the U.S. Department of Transportation in the interest of information exchange. The United States government assumes no liability for its contents or use thereof.

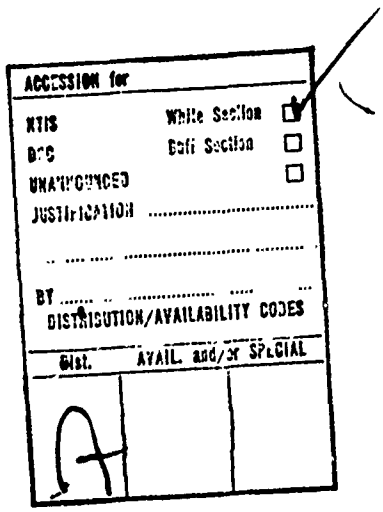

Technical Report Documentation Page

1. Report No.	2. Government Accession No.	3. Recipient's Catalog No.
FAA-RD-74-112		AD-784950

4. Title and Subtitle	5. Report Date
FEASIBILITY STUDY AND DEMONSTRATION OF NITROGEN GENERATION FOR FUEL TANK INERTING	June 1974
	6. Performing Organization Code
7. Author(s)	8. Performing Organization Report No.
Scott A. Manatt	74-10261
9. Performing Organization Name and Address	10. Work Unit No. (TRAIS)
AiResearch Manufacturing Company of California Division of The Garrett Corporation 2525 W. 190th Street, Torrance, Calif. 90509	36344
	11. Contract or Grant No.
	DOT FA72WA-3140
12. Sponsoring Agency Name and Address	13. Type of Report and Period Covered
U.S. Department of Transportation Federal Aviation Administration Systems Research and Development Service Washington, D. C. 20591	Final July 1972 - June 1974
	14. Sponsoring Agency Code

15. Supplementary Notes

16. Abstract

Nitrogen fuel tank inerting has been shown to be an effective means of providing aircraft explosion prevention by reducing the O_2 concentration below the lower limit for fuel vapor ignition. Inerting systems using LN_2 storage have been demonstrated on aircraft flown by both the USAF and the FAA. A reduction of O_2 concentration to a level of 9% or less is sufficient to produce an incombustible environment for jet fuels and potential ignition sources. Generation of an inert gas from air has been investigated to reduce the weight and logistics penalties associated with inert gas storage.

A program for the feasibility study and laboratory demonstration of fuel tank inerting by nitrogen generation has been conducted to determine the viability of the inert gas generation approach to fuel tank inerting. Typical system requirements have been defined using the McDonnell Douglas DC-10 as a transport aircraft representative of potential applications. The study concluded that both the catalytic combustion of air with turbine engine fuels and air separation by hollow fiber permeable membranes are viable candidates.

The program evaluated the potential application of hollow fiber membrane air separation to fuel tank inerting. A preliminary design for a DC-10 system based on hollow fiber permeable membranes has been established. Data from laboratory testing demonstrate system operation as an inert gas generator and good compliance with performance predictions.

17. Key Words	18. Distribution Statement
Air separation, explosion prevention, fire prevention, aviation safety, fuel systems, fuel tank inerting, inert gas generation, inerting, nonflammable atmosphere, permeable membranes.	Document is available to the public through the National Technical Information Service, Springfield, Virginia 22151

19. Security Classif. (of this report)	20. Security Classif. (of this page)	21. No. of Pages	22. Price
Unclassified	unclassified	207	5.75

Form DOT F 1700.7 (8-72)

FOREWORD

The Feasibility Study and Demonstration of Nitrogen Generation for Fuel Tank Inerting Program was conducted by AiResearch Manufacturing Company of California, a division of The Garrett Corporation under the U.S. Department of Transportation Contract No. DOT FA72WA-3140. The work was sponsored by the Federal Aviation Administration's Systems Research and Development Service, Crashworthiness Section under the direction of Mr. Thomas G. Horeff, Section Chief. During the performance period of the contract, Navy Commanders William McAdoo and Joseph Shea acted as contract technical monitors for the FAA.

The contractual period was from July 1972 through June 1974. The principal investigator for AiResearch was Mr. Scott A. Manatt of the Aerospace Systems Department under a section managed by Mr. Joseph M. Ruder. Significant contributions were also made by Mr. Christopher Gibson - materials, Mr. Kim Linnett - design analysis, and Dr. Harold Strumpf - data analysis, all of AiResearch. McDonnell-Douglas was extremely helpful in supplying the information and schematics defining the features of the DC-10 airplane.

The program was conducted in two phases. The first phase, started in July 1972, consisted of an analytical evaluation of various inert gas generation concepts to be used as a part of an airborne fuel tank inerting system. This phase concluded in an interim presentation given by AiResearch personnel in April 1973. The second phase of the program was chiefly concerned with experimental evaluation and further assessment of the hollow fiber permeable membrane air separation concept, identified during the first phase program. This report presents a summation and compilation of both phases of the program.

All work reported was performed at the AiResearch facility in Torrance, California, with the exception of the membrane fiber manufacture and test module fabrication. This activity was subcontracted to Dow Chemical, USA, and accomplished in Dow's Walnut Creek, California, facilities to AiResearch's specifications.

This final report has been assigned AiResearch report No. 74-10261.

TABLE OF CONTENTS

		Page
SECTION 1	INTRODUCTION	1-1
	PROGRAM BACKGROUND AND PURPOSE	1-1
	SUMMARY	1-3
	CONCLUSION	1-5
SECTION 2	INERT GAS GENERATION SUBSYSTEM TRADEOFFS	2-1
	DESIGN BASELINE	2-1
	Selection of the DC-10 Aircraft	2-1
	Fuel Tank Inert Gas Requirements	2-2
	Flight Profiles	2-5
	1. Normal Flight Profiles	2-6
	2. Basic Mission Profile	2-13
	3. Emergency Descent	2-13
	Installation Considerations	2-13
	CANDIDATE INERT GAS GENERATION SUBSYSTEMS	2-28
	Permeable Membrane Separation Concept and Operation	2-28
	Fuel/Air Combustion	2-30
	1. Concept and Operation	2-30
	2. DC-10 System Preliminary Design	2-32
	Physical Sorption Concept and Operation	2-35
	Chemical Sorption	2-39
	1. Concept and Operation	2-39
	2. DC-10 System Preliminary Design	2-43
	Air Rectification	2-47
	1. Concept and Operation	2-47
	2. DC-10 System Preliminary Design	2-49
	Evaluation Summary	2-51
SECTION 3	HOLLOW FIBER PERMEABLE MEMBRANE INERT GAS GENERATION SUBSYSTEM INVESTIGATION	3-1
	ANALYTICAL EVALUATION	3-1
	Separation Principle	3-2
	Hollow Fiber Configuration	3-3
	Mathematical Model	3-4

TABLE OF CONTENTS (Continued)

		Page
	SYSTEM PRELIMINARY DESIGN	3-9
	Operating Principle	3-9
	Design Point Selection	3-11
	System Operation	3-18
	1. Inert Gas Flow	3-18
	2. Temperature Control	3-21
	3. Ground Cooling Air Supply	3-22
	4. Emergency Descent Provisions	3-22
	5. Typical Operating Conditions	3-24
	Component Description	3-24
	1. Item 12, Inertial Dirt Separator	3-24
	2. Item 13, Filter	3-25
	3. Item 14, Air Separation Module	3-26
	Air Separation Module Design	3-27
	FEASIBILITY TEST PROGRAM	3-41
	Test Hardware	3-41
	1. Polymethyl Pentene Fibers	3-41
	2. Small Scale Spiral Wrapped Module	3-42
	3. Large Scale Parallel Fiber Module	3-47
	Test Program	3-47
	1. Chemical Degradation Life Test	3-50
	2. Apparent Permeability Coefficient Measurement	3-51
	3. Air Separation Test and Performance Prediction	3-72
SECTION 4	OWNERSHIP CONSIDERATIONS	4-1
	OPERATING SUPPORT	4-1
	COST CONSIDERATIONS	4-1
	Initial Costs	4-2
	Maintenance Cost	4-2
	Operating Costs	4-5
SECTION 5	PROGRAM CONCLUSIONS	5-1

TABLE OF CONTENTS (Continued)

		Page
APPENDIX		
A	MEMBRANE GAS TRANSFER	A-1
B	TEST MODULE CHARACTERISTICS	B-1
C	1000 HOUR DEGRADATION CHECK TEST DATA	C-1
D	SINGLE GAS PERMEATION TEST DATA	D-1
E	AIR SEPARATION TEST DATA	E-1
F	PRE-REPAIR TEST DATA	F-1
REFERENCES		R-1

LIST OF ILLUSTRATIONS

Figure		Page
2-1	Fuel Tank Capacity and Location	2-3
2-2	Oxygen Released from Fuel	2-5
2-3	DC-10 Flight Profile - Ground Operation	2-7
2-4	DC-10 Flight Profile - Enroute Climb	2-8
2-5	DC-10 Flight Profile - Cruise	2-9
2-6	DC-10 Flight Profile - Optional Low Altitude Cruise	2-10
2-7	DC-10 Flight Profile - Long Range Descent	2-11
2-8	DC-10 Flight Profile - High Speed Descent	2-12
2-9	DC-10 Basic Mission Profile Characteristics	2-14
2-10	DC-10 Flight Profile - Emergency Descent	2-15
2-11	Fuel Tank Inerting System	2-17
2-12	DC-10 Pneumatic System	2-18
2-13	Bleed Air Availability (Idle Descent Settings)	2-19
2-14	DC-10 Profile View	2-21
2-15	DC-10 Air Conditioning System	2-23
2-16	ECS Pack Ram Air	2-24
2-17	DC-10 Fuel Vent System	2-25
2-18	Schematic Diagram of a Basic Permeable Membrane IGG	2-29
2-19	Schematic Diagram of a Basic Catalytic Reactor IGG	2-31
2-20	Catalytic Reactor IGG	2-33
2-21	Conceptual Operation of Physical Sorption IGG	2-35
2-22	Molecular Sieve Co-Adsorption Equilibrium Curves	2-36
2-23	Oxygen Loading Within a Molecular Sieve	2-37
2-24	Outlet Oxygen Concentration versus Time	2-38

ILLUSTRATIONS (cont)

Figure		Page
2-25	Molecular Sieve 4A Required Weight	2-38
2-26	Conceptual Operation of Chemical Sorption IGG	2-40
2-27	Fluomine Equilibrium Curves	2-41
2-28	Equilibrium Oxygen Concentration	2-42
2-29	Typical Bed Structure Temperature as a Function of Time	2-44
2-30	Inert Gas Oxygen Concentration as a Function of Time	2-44
2-31	DC-10 Chemical Absorption IGG Preliminary System Design	2-45
2-32	Conceptual Operation of an Air Rectification IGG	2-47
2-33	Nitrogen-Oxygen Phase Diagram	2-48
2-34	DC-10 Rectification IGG System	2-50
3-1	Hollow Fiber Permeable Membrane Tube Element	3-7
3-2	Schematic Diagram, Permeable Membrane	3-10
3-3	Sample Computer Output Design Point Performance	3-15
3-4	Sample Computer Output Off-Design Performance	3-17
3-5	Typical Membrane IGG Performance	3-19
3-6	Pressure Drop in Membrane Tubing	3-29
3-7	Polymethyl Pentene Structural Consideration	3-30
3-8	Silicone Rubber Structural Consideration	3-30
3-9	Membrane Material Weight	3-32
3-10	Bleed Air Pressure Variation	3-34
3-11	Ram Air Pressure Variation	3-34
3-12	Reduction in Inert Gas Oxygen Concentration	3-35
3-13	The Effect of Reduced Ram Air Flow	3-35
3-14	The Effect of Tube Diameter	3-36

ILLUSTRATIONS (cont)

Figure		Page
3-15	The Effect of Increased Wall Thickness	3-36
3-16	The Effect of Permeability Coefficient Variation on Separator Bleed Air Inlet Flow	3-38
3-17	The Effect of Permeability Coefficient Variation on Separator Membrane Weight	3-39
3-18	The Effect of Permeability Coefficient Variation on System Weight	3-40
3-19	Small Spiral Wrapped Test Module Overall Assembled View	3-43
3-20	Small Spiral Wrap Air Separation Module	3-44
3-21	Small Spiral Wrapped Test Unit Fiber Wrap Detail	3-45
3-22	Small Spiral Wrapped Test Module End View	3-46
3-23	Large Scale Parallel Fiber Air Separation Module	3-48
3-24	Large Scale Parallel Fiber Test Module	3-49
3-25	IGG Membrane 1000 Hour Performance Test	3-52
3-26	Large Scale Parallel Fiber Test Module	3-54
3-27	Large Scale Test Module Hollow Fiber Permeable Membrane Module Insert	3-55
3-28	Large Scale Test Module During Tube Sheet Void Repair	3-56
3-29	Large Scale Module Following Tube Sheet Void Repair	3-57
3-30	Initial Leakage Indication	3-58
3-31	Time Dependent Leakage and Permeation Indication	3-58
3-32	Large Scale Polymethyl Pentene Test Module, Experimental Nitrogen Permeability at a Nominal 10 psig Bleed Air Pressure	3-60

ILLUSTRATIONS (cont)

Figure		Page
3-33	Large Scale Polymethyl Pentene Test Module, Experimental Nitrogen Permeability	3-64
3-34	Large Scale Polymethyl Pentene Test Module, Experimental Oxygen Permeability	3-65
3-35	Experimental Coefficient as a Function of Test Pressure	3-67
3-36	Large Scale Polymethyl Pentene Test Modules, Experimental Nitrogen Permeability at 30 psig Nominal Bleed Air Pressure	3-68
3-37	Large Scale Polymethyl Pentene Test Module, Experimental Oxygen Permeability at 30 psig Nominal Bleed Air Pressure	3-69
3-38	The Influence of Internal Leakage on Separation Factor	3-71
3-39	Large Scale Polymethyl Pentene Test Module, Experimental Permeability	3-73
3-40	Large Scale Polymethyl Pentene Test Module, Air Separation Test at 60°F	3-75
3-41	Large Scale Polymethyl Pentene Test Module, Air Separation Test at 40°F	3-76
3-42	Large Scale Polymethyl Pentene Test Module, Air Separation at 140°F	3-77
3-43	Large Scale Polymethyl Pentene Test Module, Air Separation Performance for Varying Ram Air Flow Rates	3-79
4-1	Schematic Diagram, Permeable Membrane Fuel Tank Inerting System	4-3

ILLUSTRATIONS IN APPENDIXES

Figure		Page
D-1	Single Gas Permeation Test Data Schematic Diagram	D-10
E-1	Air Separation Test Data Schematic Diagram	E-3
E-2	Sample Test Data Predictions Using Performance Computer Program	E-7

LIST OF TABLES

Table		Page
2-1	DC-10 Performance and Design Data	2-2
2-2	Performance Characteristics Summary	2-52
3-1	Membrane Properties	3-28
3-2	Large Scale Parallel Fiber Air Separation Module Test Sequence	3-61
4-1	Summary of Maintenance Cost of Ownership Elements	4-4
4-2	Maintenance Cost Assumptions	4-6
4-3	Estimated Energies Used During a Standard DC-10 Flight Profile	4-7
4-4	Penalties for Power Usage and Weight	4-8
4-5	Fuel Consumption Per Flight Segment	4-9

Tables in Appendixes

Table		
B-1	Small Spiral Wrapped Test Module Configuration	B-1
B-2	Large Scale Parallel Fiber Module Configuration	B-2
C-1	1000 Hour Performance Degradation Check Test Data Summary	C-3
D-1	Single Gas Permeation Test Data Summary (Post Leakage Repair)	D-2
D-2	Test Equipment List	D-12
E-1	Air Separation Test Data Summary (Post Leakage Repair)	E-2
F-1	Single Gas Permeation Test Data Summary (Pre-Leakage Repair)	F-2
F-2	Air Separation Test Data Summary (Pre-Leakage Repair)	F-8

LIST OF ABBREVIATIONS

APPROX	Approximately
APU	Auxiliary Power Unit
ASTM	American Society for Testing Materials
ATM	Atmosphere
BTU	British Thermal Units
COMP	Compartment
CONC	Concentration
COND	Condition
CU FT, cu ft	cubic foot
cfm	Cubic feet per minute
CM, cm	centimeter
CM Hg	Centimeter of mercury
DES	Design
DOT	U.S. Department of Transportation
ECS	Environmental Control System
FAA	Federal Aviation Administration
FAR	Federal Aviation Regulations
fpm	foot-per-minute
FT, ft	Foot
FWD	Forward
GAL	Gallon
HR, hr	Hour
ICC	Interstate Commerce Commission
ICI	Imperial Chemical Industries
IGG	Inert Gas Generation
ILS	Integrated Logistics Support
in.	inch
Lab	Laboratory
LB, lb	pound

LIST OF ABBREVIATIONS (Continued)

LN_2	Liquid Nitrogen
MIN, min	Minute
MMH/FH	Maintenance Man Hours per Flight Hour
MMH/OH	Maintenance Man Hours per Overhaul Hour
NO.	number
NOV	November
NTP	Normal Temperature and pressure (70° and 14.7 psia)
OCT	October
O_2	Oxygen
N_2	Nitrogen
ppm	parts-per-million
PSI, psi	Pounds per square inch
PSIA, psia	Pounds per square inch (absolute)
PSID, psid	Pounds per square inch (differential)
PSIG, psig	Pounds per square inch (gauge)
PTS	points
ROM	Rough order of magnitude
SAT	Saturation
STA	Station
Sec, sec	seconds

LIST OF SYMBOLS

A, A_s	Mass transfer surface area (log-mean area for tubes)
C	Gas concentration
c	Oxygen concentration in tube
c'	Oxygen concentration around tube
CO_2	Carbon dioxide
D	Diffusion coefficient
D_o	Diffusion frequency factor
E_D	Diffusion activation energy
E_P	Psuedo activation energy for permeability
e	Base of Naperian logaritham system (2.718 . . .)
^oF	Temperature in degrees Farenheit
H_2O	Water (used in pressure measurement in H_2O)
J	Mass flux
KW	Power in killowatts
L	Length
$\dot{M}_B$	Bleed air mass flow rate
$\dot{M}_P$	Permeant mass flow rate
$\dot{M}_R$	Ram air mass flow rate
O_2	Oxygen gas
OUT	Subscript denoting outlet condition
N_2	Nitrogen gas
P	Pressure in tube
P'	Pressure around tube
P_B	Bleed air pressure
$\bar{P}_B$	Average bleed air pressure
$\bar{P}_R$	Average ram air pressure
Pu	Ullage Gas Pressure
$\dot{Q}$	Mass flow rate

R	Gas constant
S	Solubility coefficient
S_o	Solubility frequency factor
T	Absolute temperature
T_u	Ullage gas temperature
T_R	Ram air temperature
t	Time
th	Tube wall thickness
Vu	Ullage gas volume
$\dot{W}s$	Sweep gas mass flow rate
α	Proportional to
ΔHs	Heat of Solution
ΔP	Pressure difference
ΔX	Displacement difference
δ	Very small increment of time
μ	Unit of length, micron
∂	Indicates partial differential
$\mathfrak{C}$	Centerline
%	Percent
$\frac{dw}{dt}$	Ullage demand airflow rate
TP	Permeability coefficient
TP_o	Permeability frequency factor

Subscripts

i	i^{th} gas
1	Node number 1
2	Node number 2
P	Permeant

LIST OF SYMBOLS (Continued)

Subscripts

IN	Inlet
OUT	Outlet
O	Oxygen
N	Nitrogen

SECTION 1

INTRODUCTION

This final report is a summary of the work conducted under Federal Aviation Administration contract DOT FA72WA-3140 by the AiResearch Manufacturing Company of California, a Division of The Garrett Corporation, during the period of contract performance from July 1972 through June 1974. The program was conducted under the technical direction of the Crashworthiness Section of the Research and Development Service of the Federal Aviation Administration.

PROGRAM BACKGROUND AND PURPOSE

A potential hazard exists due to the susceptibility of aircraft fuel tanks and vent systems to overpressure and subsequent explosion induced by the ignition of flammable fuel air mixtures in these zones. The combination of atmospheric environment and turbine engine fuel properties in current transport aircraft expose the aircraft to this danger. It is the evaluation of the feasibility of onboard inert gas generation as a method of eliminating this exposure to which the program addresses itself.

Data collected by FAA, and others, indicate that numerous aircraft explosions have occurred due to ignition of the flammable mixture within the fuel tanks and vent systems of commercial aircraft causing extensive damage, loss of equipment, and causing injury and death to the aircraft passengers and crew. Following data evaluation by the FAA-Industry Advisory Committee, it was concluded that fuel systems fires and explosions were primarily caused or aggravated by electrostatic discharge during refueling, penetration of the fuel tank resulting from engine failure where hot parts caused ignitio , lightning strokes on the aircraft skin, and impact-survivable crashes where resultant fires spread or caused wing explosions prohibiting aircraft evacuation prior to the occurrence of intense heat and the generation of toxic combustion products.

Evaluation of a number of means of eliminating or substantially reducing this hazard has been explored with various degrees of success. Of these, two types of systems have been identified which are felt to offer the most promise for eventual adoption by commercial transport operators. The first of these techniques is flame suppression exemplified by reticulated foam filled fuel tanks and by flame extinguishment systems using a stored material such as

bromotrifloromethane rapidly disbursed upon flame detection. The second technique, with perhaps the widest potential application to transport aircraft, is to provide a nonflammable ullage and vent mixture which will not allow ignition to occur. Since the system to control the mixture in the ullage and vent spaces has little or no latitude in adjusting the fuel vapor concentration, such systems have been principally directed toward reduction of the oxidizer concentration. With air, this is accomplished by replacing the air with an inert gas. While both carbon dioxide and nitrogen gas have been successfully utilized as the inert gas, logistics and economics have tended to favor nitrogen gas. Since this concept requires the delivery of a considerable quantity of nitrogen, its storage has been found to be at a considerable expense of weight and volume. Systems demonstrated for aircraft use have tended to store the nitrogen gas as a liquid to reduce these penalties.

While nitrogen fuel tank inerting offers perhaps the optimum performance solution for explosion prevention in the ullage and fuel vent spaces, the storage of inert gas entails considerable penalties. These penalties of weight, volume, logistics of resupply, additional vehicles required during aircraft turn-around, operating costs, cryogenic equipment related maintenance training, and operational flexibility constraints are undesirable from the operator's point of view.

The purpose of this study and demonstration has been the evaluation of alternatives to the storage of nitrogen by utilization of the vast reservoir of nitrogen gas, which constitutes almost eighty percent of the air through which the aircraft operates. This requires the elimination of oxygen from that air. Studies conducted under government sponsorship, both military and civilian, have concluded that complete elimination of oxygen is not required to maintain a nonflammable mixture for current turbine fuels and potential ignition sources. These studies vary somewhat in the evaluation of the minimum allowable oxygen concentration, but generally fell into a range of 10-12 percent oxygen by volume required for ignition at optimum fuel vapor concentrations.[1,2,3] Thus, a system to remove about 50 percent of the oxygen in air

[1] S. V. Zinn, Jr., Inerted Fuel Tank Oxygen Concentration Requirements, Federal Aviation Administration, Interim Report FAA-RD-71-42, August 1971

[2] P. B. Stewart and E. S. Starkman, Inerting Conditions for Aircraft Fuel Tanks, WADC Technical Report 55-418, University of California, September 1955

[3] M. G. Zabetakis, Flammability Characteristics of Combustible Gases and Vapors, Bureau of Mines Bulletin 627, U.S. Department of the Interior

could be utilized in place of the cumbersome liquid nitrogen storage vessels as a source of inert gas. The purpose of this program, then, is the detail evaluation of these inert gas generators (IGG). For the purpose of this study, a maximum oxygen concentration of 9 percent has been established as the limiting criteria. The successful development of a nitrogen fuel tank inerting system based on the IGG concept will greatly increase the overall acceptability by potential users due to significant reduction in the penalties delineated above.

SUMMARY

The program has been organized into two phases. The first phase consisted of evaluation of alternative IGG concepts capable of airborne generation of inert gas. In order to make a realistic comparison of various potential IGG subsystems which are basically dependent upon a wide variety of other available aircraft services and requirements, it was necessary to select a representative aircraft as a common denominator. The DC-10, series 10, of the American Airlines configuration was selected for the study. The DC-10 is representative of today's fleets of wide bodied jet transport aircraft and has enabled the study to continue with a meaningful common baseline.

The selection of this representative aircraft allows the report to consider significant parameters above and beyond the basic operating characteristics of the various IGG concepts; specifically, the integration of the system into the airframe and the consideration of the system's interface with other aircraft systems. The phase I study included aircraft integration studies and several trips to actual operational aircraft in the field to observe the functioning and fueling operation and the structure and system layout aboard the DC-10.

From the flight data published by McDonnell-Douglas[4], actual DC-10 ground and flight profiles were examined. Also from this data, a hypothetical mission profile was evaluated to represent the worst case demands on a fuel tank inerting system. This profile included three different descent profiles including the emergency descent mission, a contingency for aircraft depressurization at high altitude. Each of the candidate IGG systems was then evaluated against this design profile for the DC-10.

[4] DC-10 Flight Crew Operating Manual, Reference and Performance CAI-52, Vol. 2

Of the possible means of generating inert gas originally screened, five were considered for detailed Phase 1 analyses. These were; (1) the separation of air by hollow fiber permeable membranes; (2) the catalytic combustion of oxygen from air using aircraft fuel; (3) air rectification (that is, the liquification and separation of air); (4) physical sorption of oxygen from air using molecular sieve materials and (5) chemical sorption of oxygen from air using a chemical developed for the oxygen concentrator work being done for aviator breathing oxygen. Several of these concepts have shown a potential for operation at a fraction of the weight of liquid nitrogen systems; two were judged to warrant further consideration at this time. These were the catalytic combustion of oxygen from air, a concept under which considerable activity sponsored by the Air Force Aero Propulsion Lab, has already taken place, and, secondly, the separation of air by hollow fiber permeable membranes.

Although activity continues at a high level on the catalytic combustion process under Air Force sponsorship, the possibility of a permeable membrane system of competing size and weight was identified. The membrane system offers additional potential advantages since it does not represent an additional fire zone aboard the aircraft and since no potentially troublesome combustion products are generated which can be accummulated in the fuel tanks. For these reasons, it was recommended that the permeable membrane air separation process offered an extremely high potential return and should be investigated further in the Phase 2 program. The Phase 2 program consisted of a more detailed investigation of the requirements and system for a hollow fiber permeable membrane air separation IGG subsystem and included successful laboratory demonstration. All components of the inerting system were carefully examined and those components not normally a part of transport category aircraft systems were investigated. This included filtering devices required to establish bleed air sufficiently free of particulant matter to prevent clogging of the hollow fibers, detail investigation of the fibers, and the fiber air separation modules themselves. The program included the actual development of a fiber of the material and geometry selected in the Phase 1 study. A fiber of sufficient uniformity was developed which was then integrated into test modules. Two different modules were built for the program. The first test unit, the small scale spiral wrap module was built for normal laboratory research activity. This unit was evaluated in the laboratory

for preliminary values of apparent permeability coefficient, that property which describes the ability of the permeable membranes to transfer the oxygen and nitrogen constituant components of air. The small scale module was subjected to a one-thousand hour continuous testing period in which the unit was operated to produce an outlet process gas concentration of approximately 8 percent oxygen. At nominal 250 hour intervals, the output flow rate was varied throughout the test range and data recorded. Data taken during each of the five performance checks was then compared. No trend towards degradation was noted for any of the five sets of data points. In addition, this data was compared with predicted values using a computer analysis developed at AiResearch. Very close correlation was achieved.

The second module supplied, the large scale parallel fiber module, was constructed with approximately 2600 square feet of mean surface area. This unit, capable of withstanding representative test pressures, was tested in the laboratory for a period of several months. Data recorded using this test unit clearly indicated the ability of the permeable membrane IGG concept to separate air and to reduce oxygen concentration below the 9 percent limit. The module was tested throughout a broad range of operating temperatures from 0 to 160^{o}F. In addition to air separation performance, the unit was used to evaluate basic permeability data. Computer predictions based upon this basic data closely correlated with actual measured air separation performance throughout the temperature range using experimentally determined apparent permeability coefficients.

Phase 2 activity considered a representative membrane IGG fuel tank inerting system for DC-10 design. The preliminary design presented shows the application of the hollow fiber permeable membrane separation IGG to a fuel tank inerting system including controls. A cost of ownership study has been conducted upon this design and the data is presented herein as a projection of actual costs associated with initial acquisition, maintenance and operation.

CONCLUSIONS

Based on the work covered by this report, and from the previous work of other investigators on earlier fuel tank inerting related programs, the conclusions of Section 5 were established.

As a result of the successful feasibility study and demonstration reported herein, the following conclusions were drawn:

- The use of nitrogen gas to replace air in fuel tank ullage and vent systems is an attractive means of fuel related explosion suppression.
- The application requires a considerable quantity of inert gas to provide repressurization and reasonable safety margin.
- One means of somewhat reducing the weight and volume penalty associated with inert gas storage is the use of LN_2, although at certain expense to airline operations.
- The complete elimination of oxygen is not required to maintain a non-flammable ullage and vent system; a limit of 9% oxygen allows a sufficient safety margin even at optimum fuel vapor concentrations.
- The feasibility of systems capable of generating a product from air having less than 9% oxygen has been successfully demonstrated both analytically and in the laboratory.
- The development of such a system, using hollow fiber permeable membrane technology for air separation, appears very attractive to commercial transport operations due to low operating penalties and a low projected cost of ownership.
- Using hollow fiber permeable membrane air separation, a preliminary design for an inert gas generation (IGG) fuel tank inerting system for a DC-10 has been completed. The total estimated fuel tank inerting system weight is 320 lb.
- The feasibility study indicates further development may even reduce the membrane air separator module penalties below current estimates, which are a fraction of those for LN_2 systems.
- 1000 hours of simulated operation has been performed without any degradation of performance.
- Module repair feasibility has been demonstrated.

SECTION 2

INERT GAS GENERATION SUBSYSTEM TRADEOFFS

Fuel tank explosion prevention systems of several different types have been evaluated and experimentally demonstrated. While nitrogen fuel tank inerting systems which maintain a nonflamable gas in the fuel tank vapor and vent spaces offers attractive protection for transport aircraft, the approach of on-board storage of the large quantities of nitrogen required has led to the selection of cryogenic storage for reduction of weight and volume.[5] Still, the penalties of weight, volume and unfamiliar maintenance and servicing requirements as well as the complications of regular servicing requirements have reduced the attractiveness of nitrogen fuel tank inerting to potential users.

Phase I of the program to study and demonstrate the feasibility of on-board inert gas generation (IGG) systems as an alternate to liquid nitrogen storage, has considered several approaches and evaluated their feasibility for application to a typical aircraft installation. This section discusses the Phase I evaluation of candidate IGG subsystems for the DC-10 aircraft.

DESIGN BASELINE

For the purposes of limiting the number of subsystem trade studies, selection of a baseline aircraft is presented in order to provide a common comparison between candidate IGG concepts. Following selection of a baseline system, various flight profiles for the baseline design are analyzed to determine ullage gas requirements for all modes of operation.

Selection of the DC-10 Aircraft

The DC-10, Series 10, of the American Airlines configuration was chosen as a baseline for the IGG subsystem tradeoff study. The DC-10 has been selected for two basic reasons: (1) a common denominator is required in order to make meaningful comparison, and (2) the comparison should be realistic in terms of the current wide-body jet-type application. To this end, the DC-10 has been

---

[5] E.P. Klueg, W.C. McAdoo and W.E. Neese, Performance of a DC-9 Aircraft Liquid Nitrogen Fuel Tank Inerting System, Federal Aviation Administration, Final Report FAA-RD-72-53, August 1972

selected as a typical aircraft and is a potential candidate for application and is used for the design baseline for the IGG subsystem comparison presented in this report.

General data for the DC-10 baseline aircraft which have been used for this analysis are found in Table 2-1.

TABLE 2-1

DC-10 PERFORMANCE AND DESIGN DATA

Parameter	Assumed Value
Maximum Take-off Weight	430,000 lb
Maximum Operation Altitude	42,000 ft
Maximum Descent Rate	8100 fpm to 25,000 ft 6100 fpm to 15,000 ft
Propulsion	3 General Electric Turbofan CF6-6D
Primary Fuel	ASTM-D 1655-65T (Jet A and A1)

For the purposes of this study, the fuel tank capacity, although subject to some variation, can be summarized in Figure 2-1. The fuel compartments are divided into six elements, two associated with each of the propulsion engines. The fuel tanks combined volume used in this study was slightly less than 3,000 cubic feet.

Fuel Tank Inert Gas Requirements

Basic inert gas consumption can be categorized by several uses, that is, volume repressurization due to pressure change such as occurs in aircraft descent, fuel consumption volume replacement, and miscellaneous applications such as ullage sweeps, control requirements, and so forth. In addition, small consumption rates may be associated with the ullage gas temperature decrease and resultant increase in ullage gas density. The resultant inert gas fuel tank inflow rate can be summarized by the following equation.

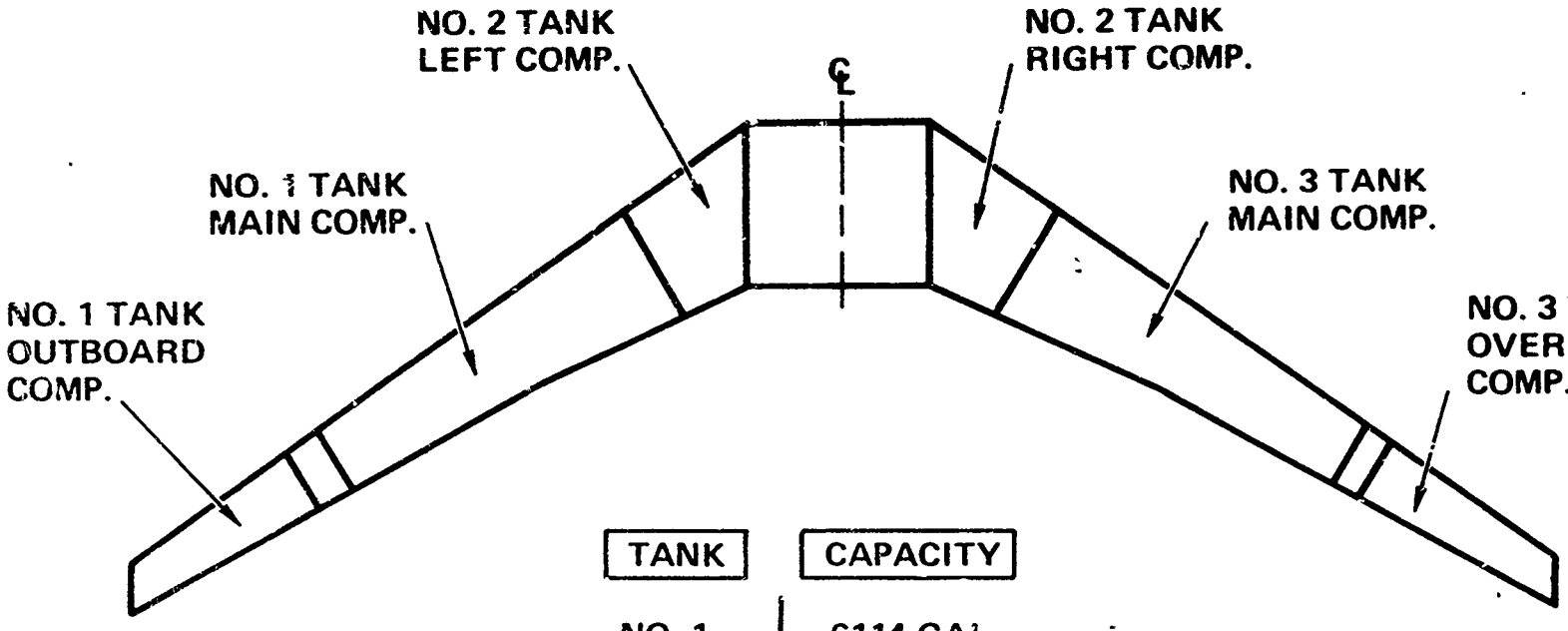

TANK	CAPACITY
NO. 1	6114 GAL
NO. 2	9914 GAL
NO. 3	6114 GAL
TOTAL	22,142 GAL ≈ 2970 CU FT

SPA 3241-15

Figure 2-1. Fuel Tank Capacity and Location

$$\frac{dw}{dt} = \frac{1}{RT_u}\left(P_u \frac{\partial V_u}{\partial t} + V_u \frac{\partial P_u}{\partial t}\right) + \dot{W}_s \qquad (2\text{-}1)$$

where: $\frac{dw}{dt}$ = inert gas demand rate

R = inert gas constant

T_u = ullage gas temperature

P_u = ullage gas pressure

V_u = ullage gas volume

$\dot{W}_s$ = ullage sweep rate

t = time

This general inflow equation shows that inert gas demand rate is directly proportional to the rate of volumetric replacement (fuel usage) and to the rate of pressure increase (descent repressurization), plus miscellaneous uses. An evaluation of aircraft operation reveals that repressurization upon descent is by far the largest source of inert gas consumption. At any given condition, this rate is proportional to the altitude (pressure), the volume of ullage being repressurized and the descent rate.

One additional consideration for inert gas requirements occurs when operational or ground considerations prevent the scrubbing or removal of oxygen from fuel at the time of fueling. An alternate means of operation is to provide sufficient gas to the ullage during climbout to keep oxygen concentrations below 9 percent by volume. Since the fuel will tend to release dissolved oxygen in proportion to the ullage pressure, the amount of oxygen potentially evolved from fuel must be carefully considered. Aircraft jet A type fuel will saturate with air by 14.7 psia and 70°F with 75 ppm oxygen. Figure 2-2 shows the cumulative amount of oxygen released per 100,000 lb of fuel as a function of altitude (total pressure) and initial fuel air saturation at sea level. Data is presented for fuel containing from 25 to 100 percent air saturation indicating total oxygen released as a function of altitude. Maximum initial fuel for the case considered is approximately 145,000 lb, however, during climb to altitude, some fuel is expended. This tends to increase the ullage (accumulator) volume as well as decreasing the potential oxygen to be released.

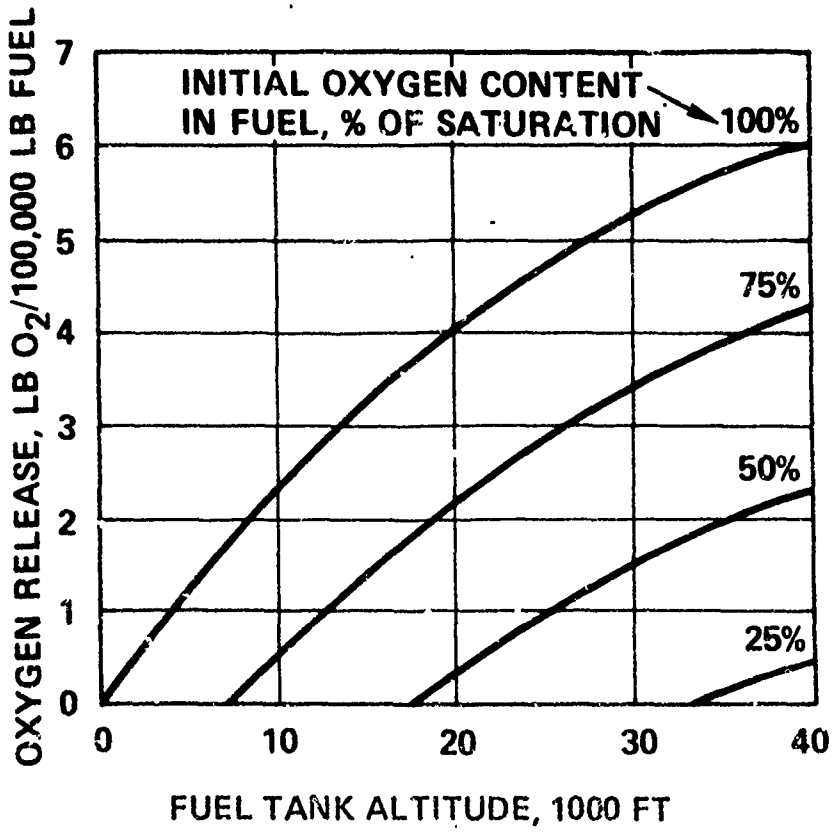

Figure 2-2. Oxygen Released from Fuel During Climb Operations

Flight Profiles

In order to consider the aircraft requirements in terms of inert gas generation systems, typical operation of DC-10 aircraft must be considered. A typical basic flight operation has assumed the following occurrence of events:

- Ground Operation (12 minutes)
- Take-off
- Enroute Climb (30 minutes)
- Cruise (several hours)
- Descent (30 minutes)

Evaluation of inert gas requirements for the above modes of operation during normal flight profiles (and emergency descent operations) are found below. These typical missions are for standard day conditions with inert gas inflow at 60°F. The data used in the evaluation of flight profile is from the DC-10 flight crew operating manual.[4]

The profile selected is unrealistic in terms of actual DC-10 flight time, but represents the most severe case for the operation of a nitrogen fuel tank inerting system.

Although the assumption of slightly different flight characteristics will necessarily result in altitude and inert gas demand flow rates which deviate from the data which follows, these values are representative of typical operation and most importantly, are of sufficient accuracy to establish a reasonable base for IGG subsystem feasibility comparison.

1. Normal Flight Profiles

   a. Ground Operation

      The first mode of operation to be considered during the normal flight profile is for the assumed period of ground operation. Figure 2-3 shows inert gas inflow for this period. The plot for ground operation considers sea level conditions at a weight of 420,000 lb gross at time of takeoff. The plot shows that inflow is steady during ground operations until the propulsion engines are throttled up to takeoff thrust at which time a flow spike of slightly in excess of 1 lb per minute of inert gas is required to replace fuel consumed. Demand inflow then begins to decrease as a result of a partially compensating pressure decrease (increase in altitude).

   b. Enroute Climb

      The hypothetical mission requirement then continues for the first 30 minutes of enroute climb. Aircraft operation is assumed to be Mach 0.85 above 10,000 feet up to a gross weight limited maximum operating altitude for the aircraft which occurs at about 33,000 feet. Figure 2-4 illustrates the inert gas requirements during this mode of operation. The inflow demand can be seen to decrease as the aircraft climbs with slight fluctuations represented by changes in throttle settings and ascent rates. During the period from 10,000 feet to 33,000 feet, the inflow demand due to fuel consumption is almost exactly counterbalanced by the negative effects of decreasing pressure. As a result of tabulated input data, slight flow requirements were computed for altitudes between 25,000 and 28,000 feet.

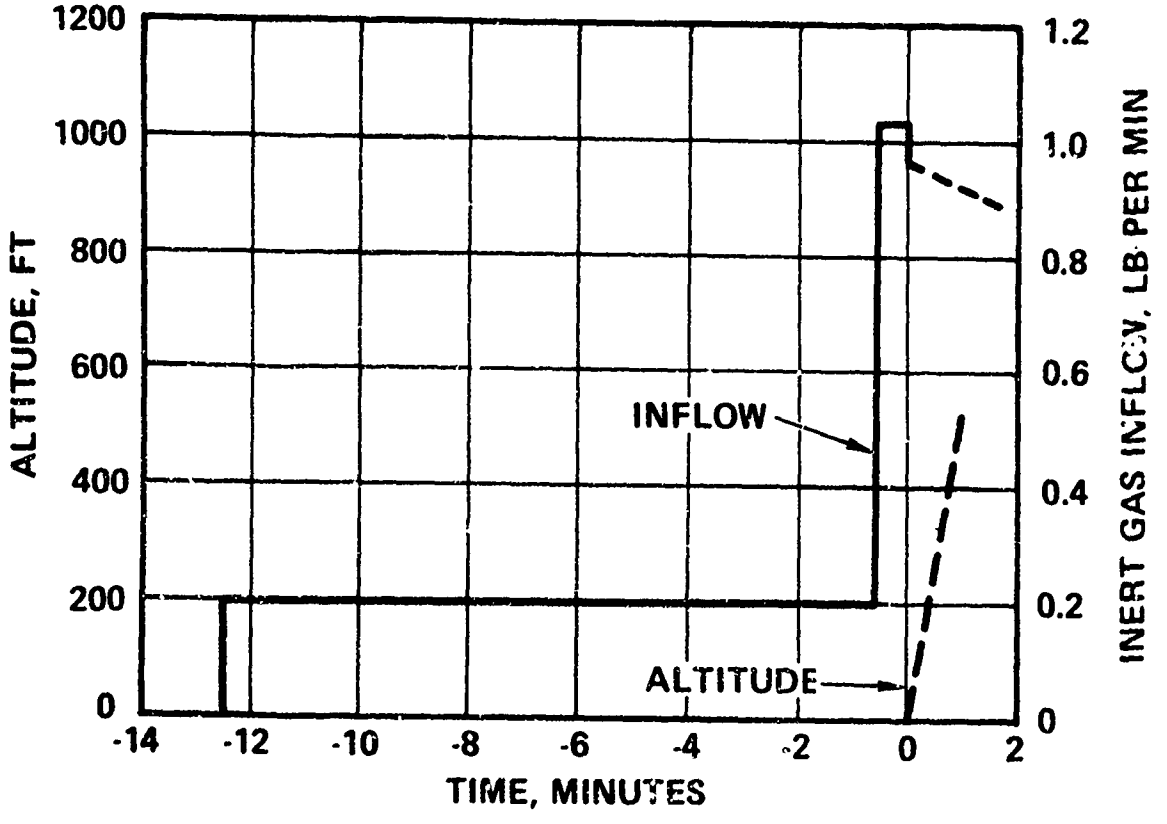

SPA 3241-16

Figure 2-3. DC-10 Flight Profile - Ground Operation

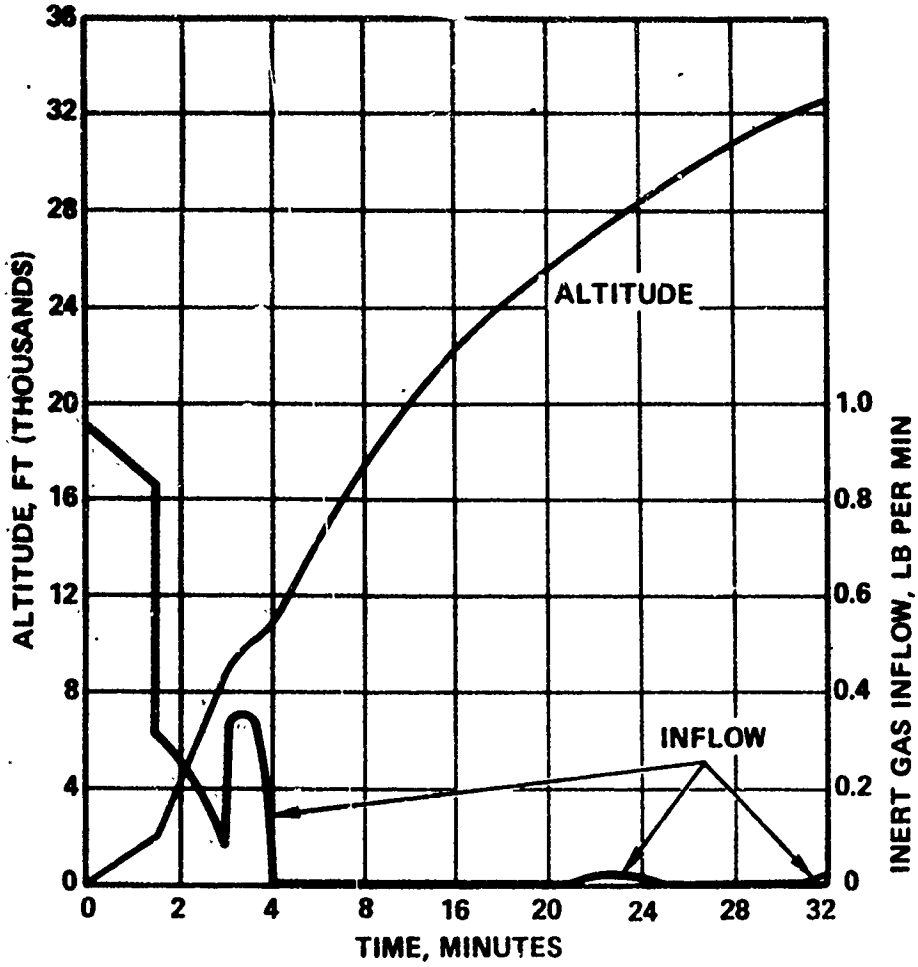

SPA 3241-17

Figure 2-4. DC-10 Flight Profile - Enroute Climb

c. Enroute Climb and Cruise

The flight condition is continued for a hypothetical possible mission lasting in excess of 8 hours (to near fuel exhaustion). The altitude profile shown in Figure 2-5 illustrates continual operation at weight limited aircraft ceiling to an assumed cruise at 41,000 feet.

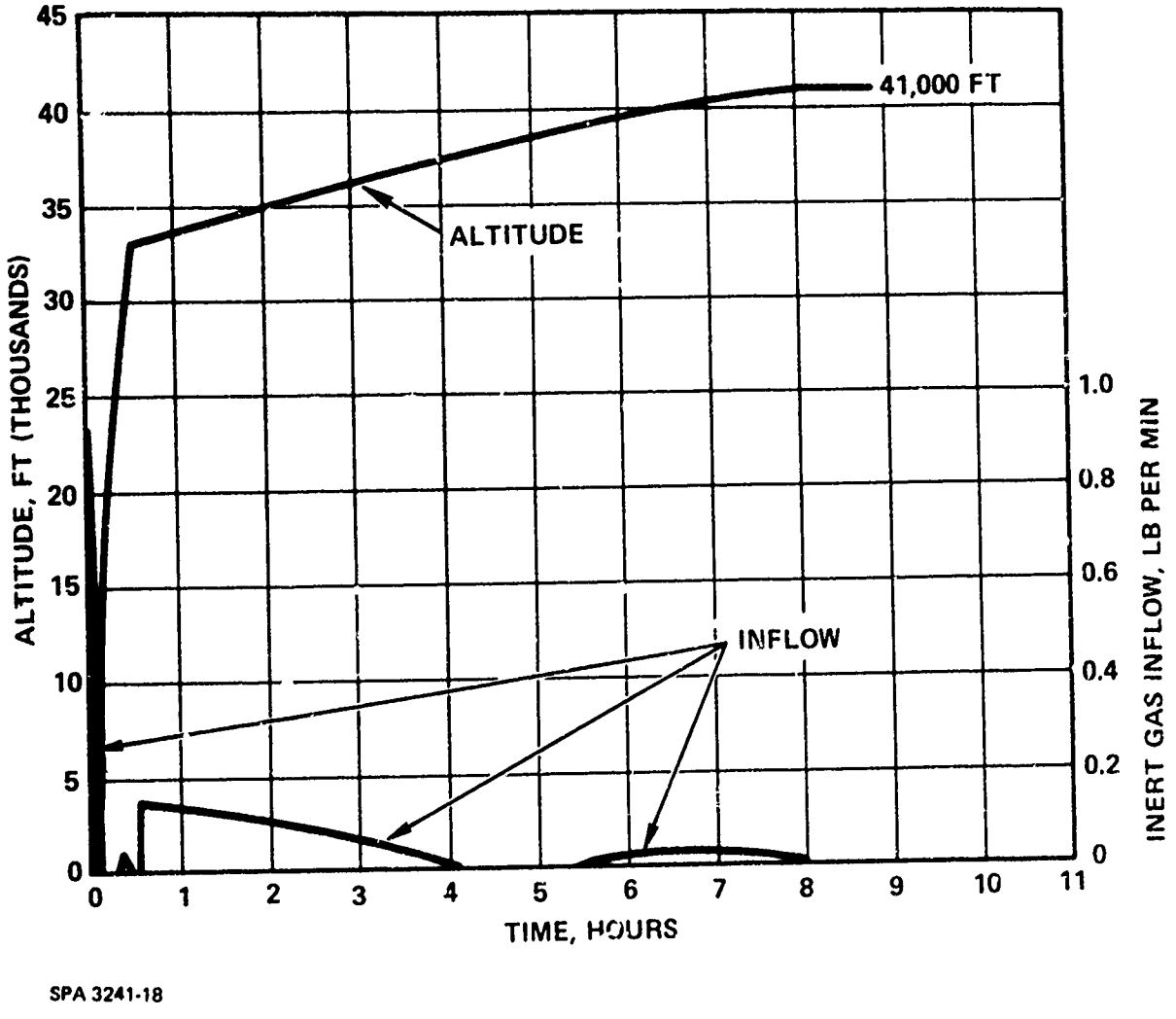

Figure 2-5. DC-10 Flight Profile - Cruise

d. Low Altitude Cruise

An optional mode of operation, shown in Figure 2-6, is for cruise at lower than ceiling altitudes. This results in increased inert gas flow demand over high altitude operations due to: (1) increased density of pressurizing gas, and (2) increased power requirements by propulsion engines. The case shown in Figure 2-6 is for an 11,000 foot maximum speed cruise which results in inert gas inflow requirements of approximately 0.4 lb per minute.

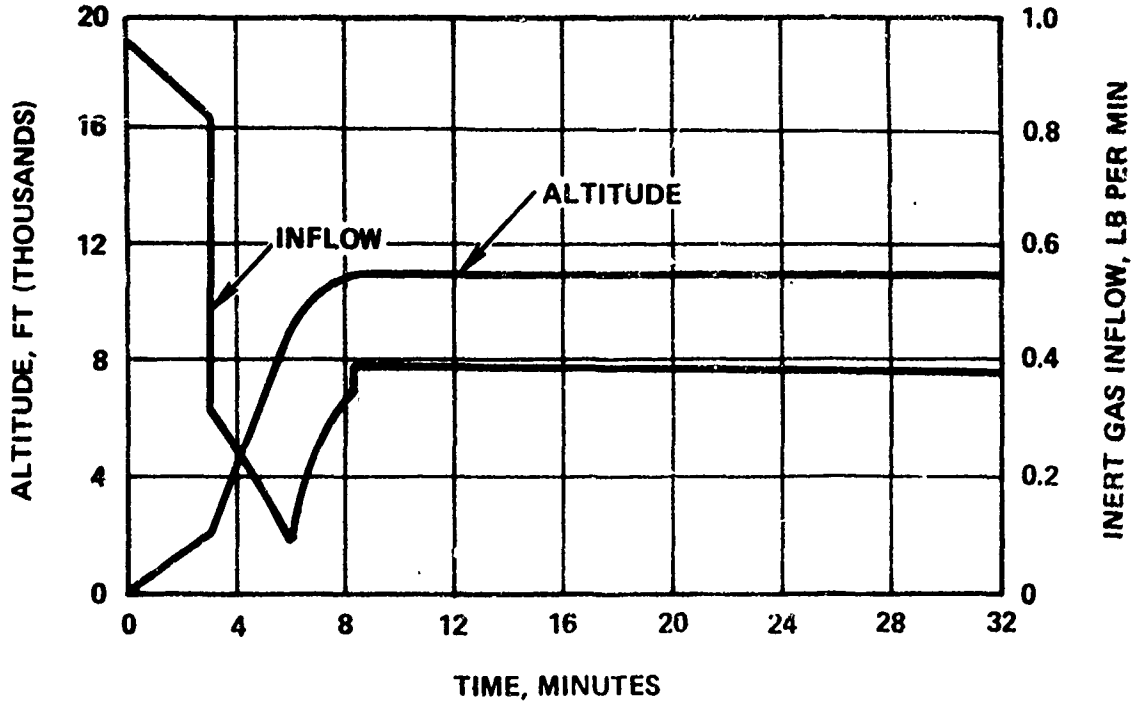

Figure 2-6. DC-10 Flight Profile - Optional Low Altitude Cruise

e. Descent

Two separate descent profiles are considered for normal flight operations. The first, and most probable operation, is a descent over a considerable distance taking approximately 30 minutes as shown in Figure 2-7. In order to arrive at worst case conditions, the analysis allowed the aircraft to land with only 300 lb of fuel remaining onboard, thereby ensuring maximum demand inflow requirements due to the largest possible ullage (see equation 2-1). The steady descent rate results in increased inflow requirements as a function of inflow gas pressure (density) which peaks at the descent profile break at approximately 2,500 feet altitude. This results in a peak inflow demand of 11.2 lb of inert gas per minute to the fuel ullage as seen in Figure 2-7.

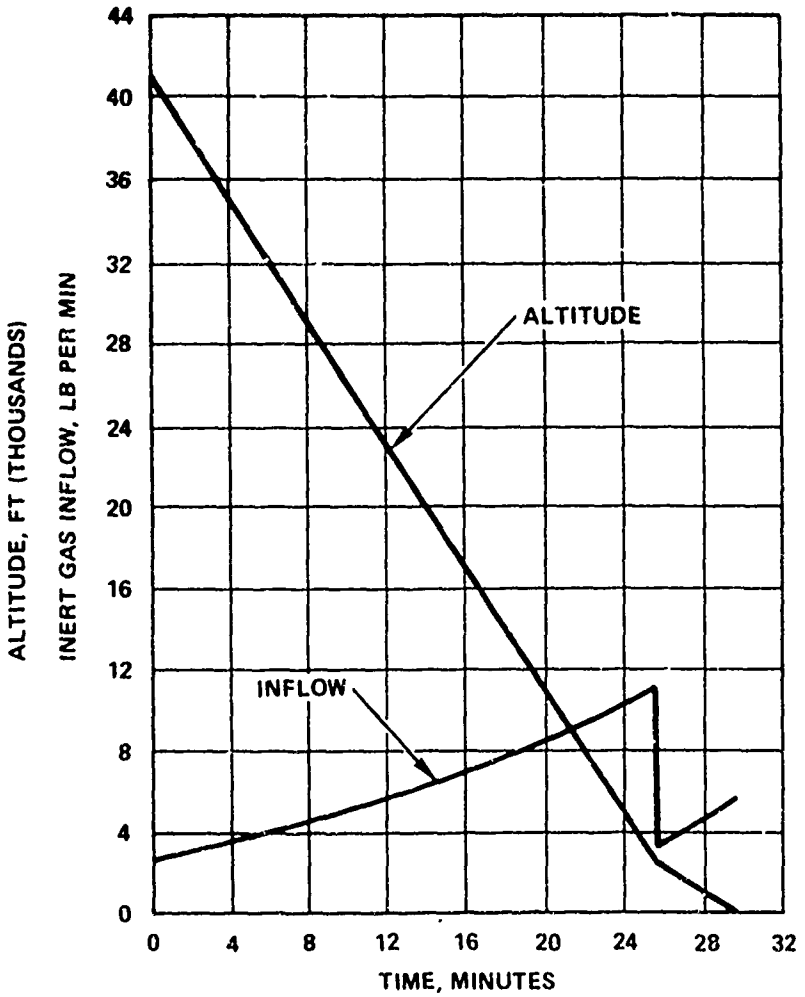

SPA 3241-20 Figure 2-7. DC-10 Flight Profile - Long Range Descent

The case of a high speed descent has also been considered. This descent profile results in an earlier landing due to increased descent rates. The unique curve shows two distinct peaks, one occurring at the break in the initial descent rate at about 12,000 feet, and the second occurring at 2,500 feet. Again minimum aircraft fuel at landing has been considered to maximize demand flow rates. Figure 2-8 illustrates this second descent. These two descents are representative of normal descent operations experienced by DC-10 aircraft.

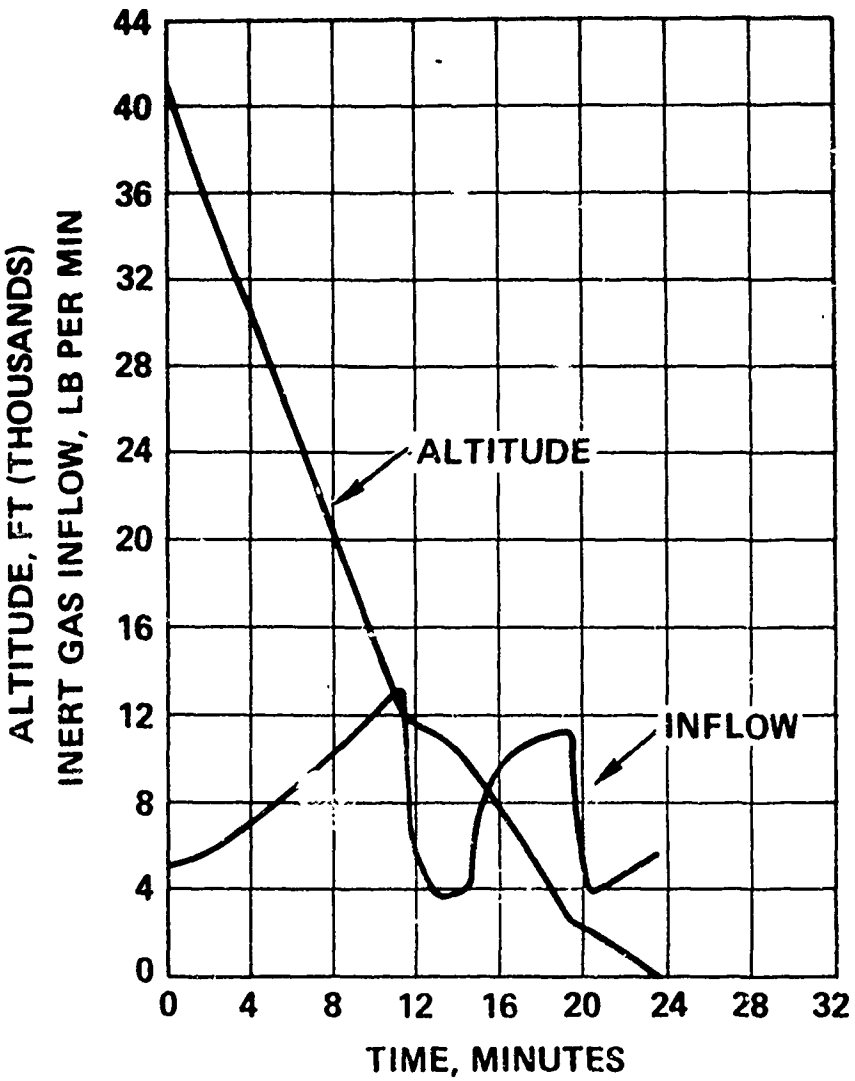

SPA 3241-21

Figure 2-8. DC-10 Flight Profile - High Speed Descent

2. Basic Mission Profile

The basic mission profile as shown in Figure 2-9 has been established from the data presented above. The inert gas inflow rate curves associated with this profile, as presented in the upper portion of the graph indicate that both the peak rates, and the total gas required (the time integral of the flow rate) are predominant during the descent portion of the profile. For this reason, nitrogen fuel tank inerting systems requiring either LN_2 storage (which are total gas sensitive), or IGG systems (which are peak flow rate sensitive), have designs strongly influenced by descent requirements.

3. Emergency Descent

One planned abnormal operating mode which can occur as a result of cabin depressurization or other serious aircraft damage is "emergency descent". In emergency situations such as these, the aircraft is descended at the maximum rates compatible with the structural design. A rate of 8,100 feet per minute to 25,000 feet altitude, followed by 6,100 feet per minute to 12,000 feet altitude, followed by descent in accordance with high speed descent profiles has been assumed. The resultant inflow demand rate is shown in Figure 2-10. Three distinct peaks in inflow demand result. The first two peaks are associated with the rapid descent rates, and a third associated with the lower altitude high speed descent profile. It should be noted that emergency descent profiles are not common occurrences. Design of IGG type systems, which, by their nature are inflow rate sensitive, should consider the possibility of alternate means to meet emergency descent profiles. Although alternate means to meet emergency descent rates may require the storage of special chemicals, rapid turnaround is not a normal requirement following the occurrance of an event resulting in an emergency descent. The inclusion of an alternate means of meeting the emergency descent rates has the added advantage of providing redundancy. This may be particularly advantageous since the occurrence requiring an emergency descent may involve damage to the primary IGG or to an onboard system which provides services for the primary IGG.

Installation Considerations

In order to complete a design baseline evaluation for an inert gas generation subsystem, integration of the system into the aircraft must be considered. For any IGG inerting system, the major required elements are bleed air and

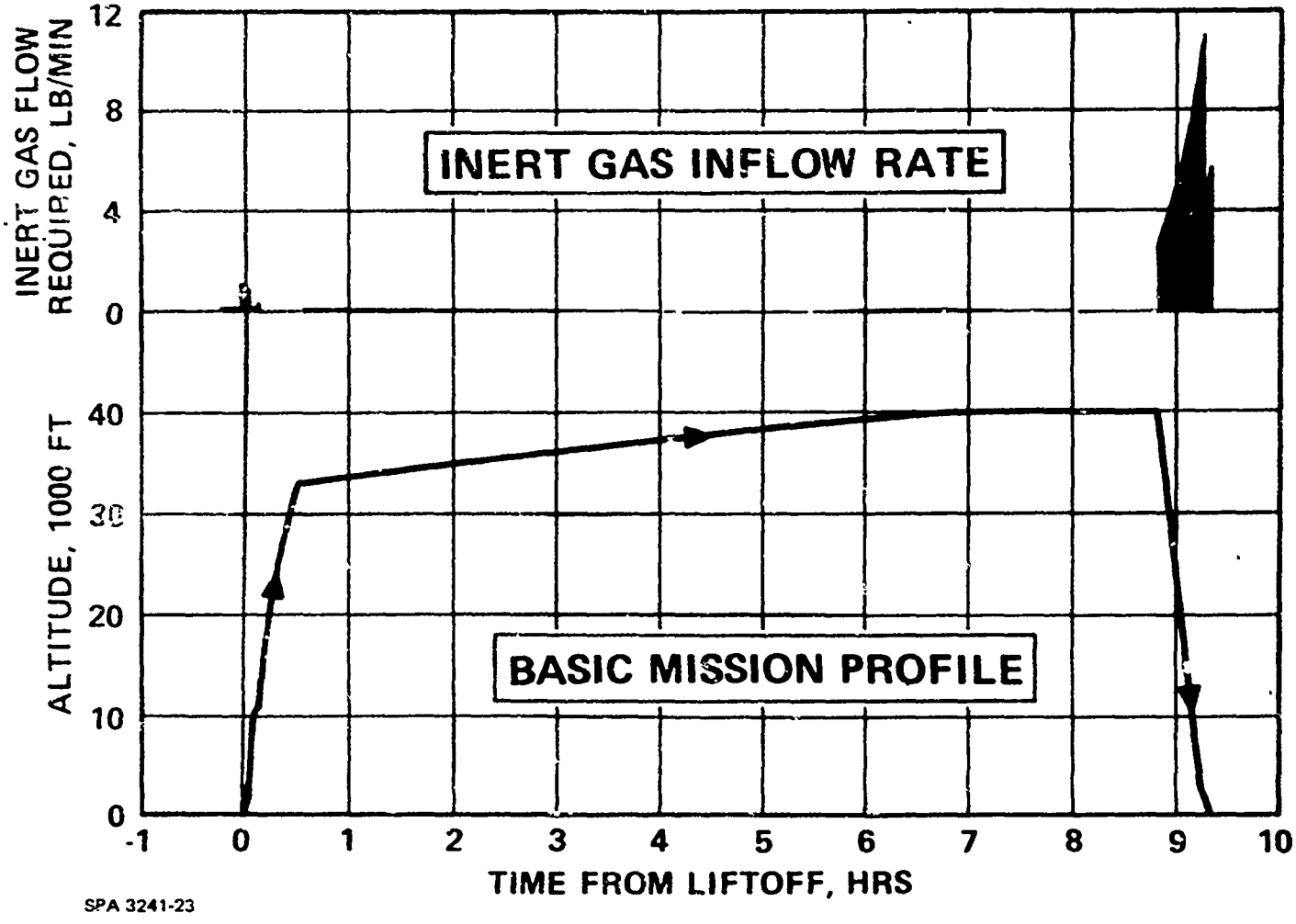

Figure 2-9. DC-10 Basic Mission Profile Characteristics

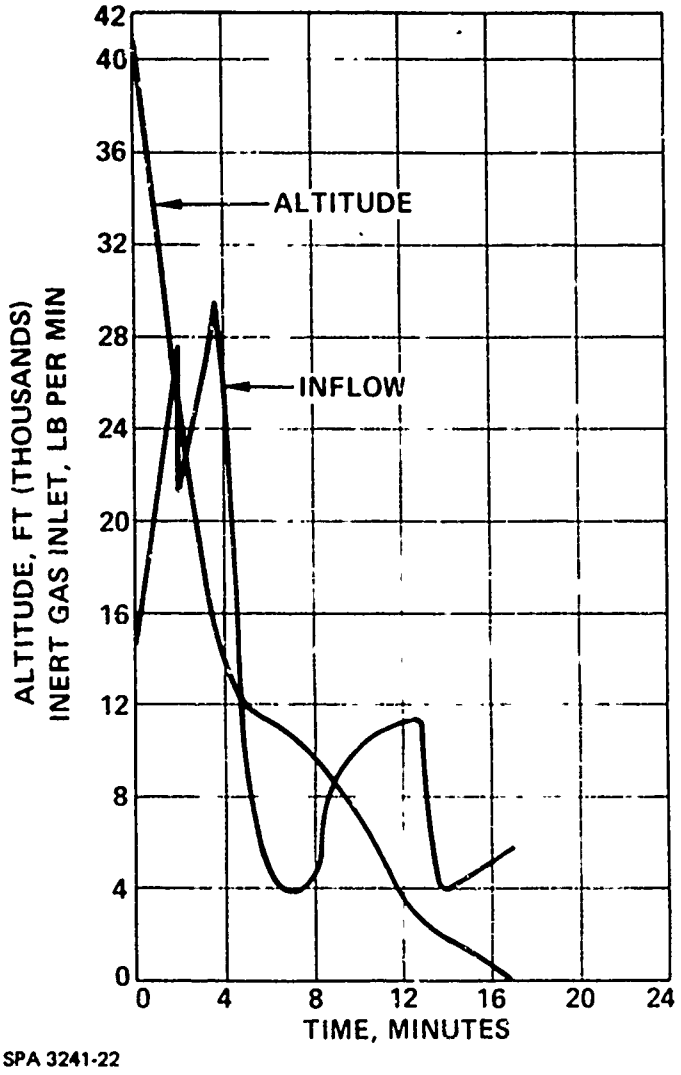

Figure 2-10. DC-10 Flight Profile - Emergency Descent

other services such as ram air, electrical power, fuel, and so forth. Besides the IGG system and its requirements, additional system requirements for the aircraft itself include consideration of a fuel tank ullage demand inflow valve, the fuel tank ullage itself, and a vent control valve placed between the existing vent stand-pipe and the fuel tanks. Ullage sweep control may also be desirable for operating modes in which ground scrubbing during fueling is not practical. In addition, emergency descent inert gas flow augmentation may prove to be optimum from system operation and weight standpoints. An integrated inerting system with the above elements is shown in Figure 2-11.

Availability of bleed air and other aircraft services is of prime concern in IGG selection and installation of the subsystem into the aircraft. The logical source of pressurized air is from the existing DC-10 pneumatic system. Potential sources of air, as shown in Figure 2-12, are from each of the three propulsion engines, from the APU, and from ground pneumatic connectors during certain ground operations. The primary source of process air is, of course, bleed air via the existing bleed air system as shown in Figure 2-12. Air from the compressor storage first passes through a bleed air precooler located in the engine nacelle to reduce temperature within the bleed air manifold to a maximum of 425°F. Pressure is regulated by a pressure regulating valve which limits pressure to a nominal 48 psig above local ambient conditions. Pressure regulating is controlled by the action of the high pressure bleed control valve upstream, which senses the pressure in the 16th stage of the compressor. If this pressure falls below 96 psig above local ambient conditions, high pressure bleed air is selected by this valve. When pressure at this stage is above 96 psig, mid stage bleed air from the eighth stage of the compressor is selected.

A key consideration in the selection of an IGG is its impact on other airborne systems and current operating modes. A principle concern is the use of bleed air. While normal aircraft operation provides a potential for the use of considerably more bleed air than is currently required by the existing systems, possible abnormal operation must also be considered.

Figure 2-13 shows data from the DC-10, Series 10, Air Conditioning and Pneumatic System Design Control Document. The resultant unused available bleed air for the most severe case (idle descent) at the current engine settings

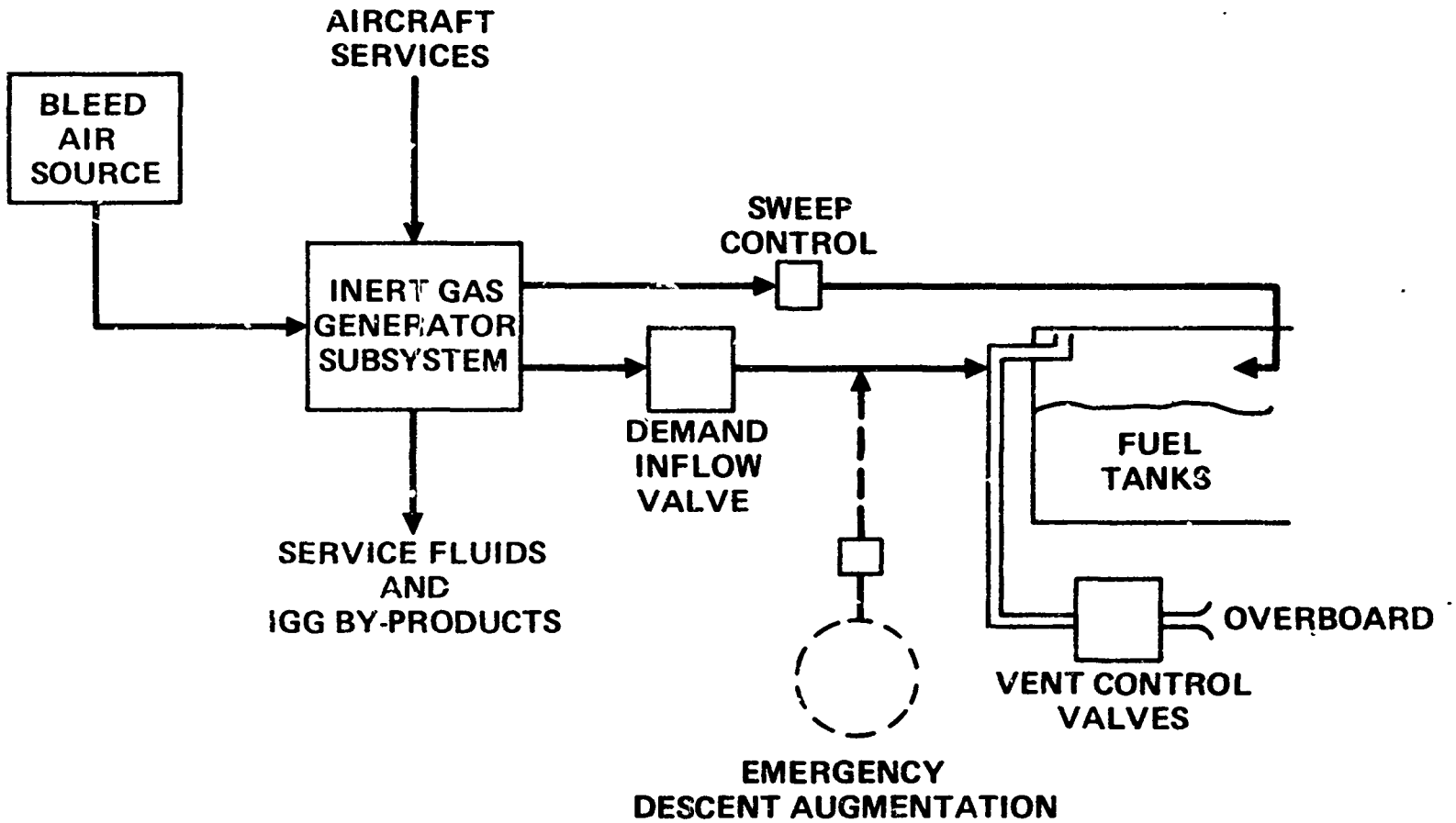

Figure 2-11. Fuel Tank Inerting System Based on Airborne Inert Gas Generation

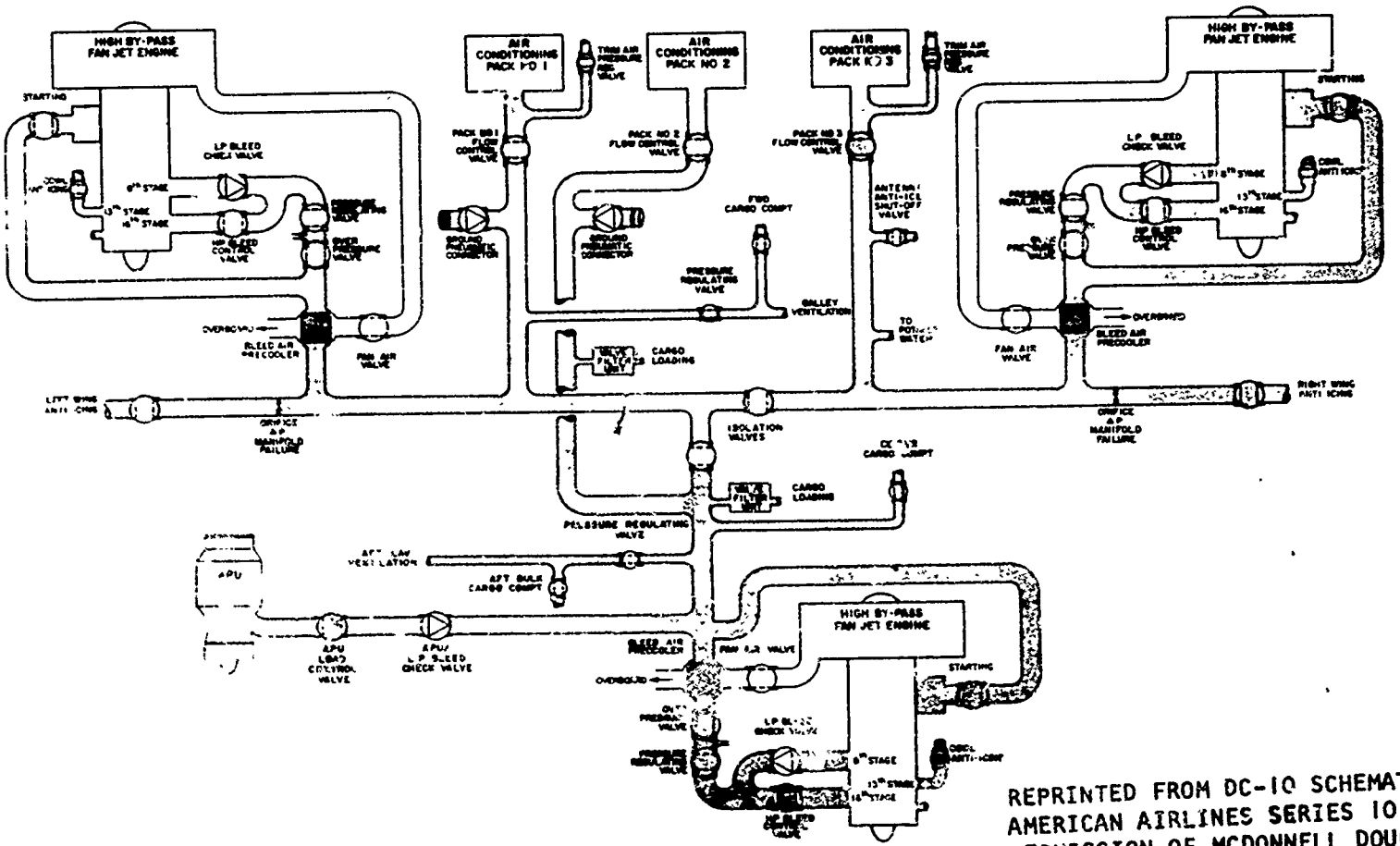

REPRINTED FROM DC-10 SCHEMATICS, AMERICAN AIRLINES SERIES 10 BY PERMISSION OF MCDONNELL DOUGLAS CORPORATION. YEAR OF FIRST PUBLICATION 6-30-1970.

SFA 3241-25

Figure 2-12. DC-10 Pneumatic System

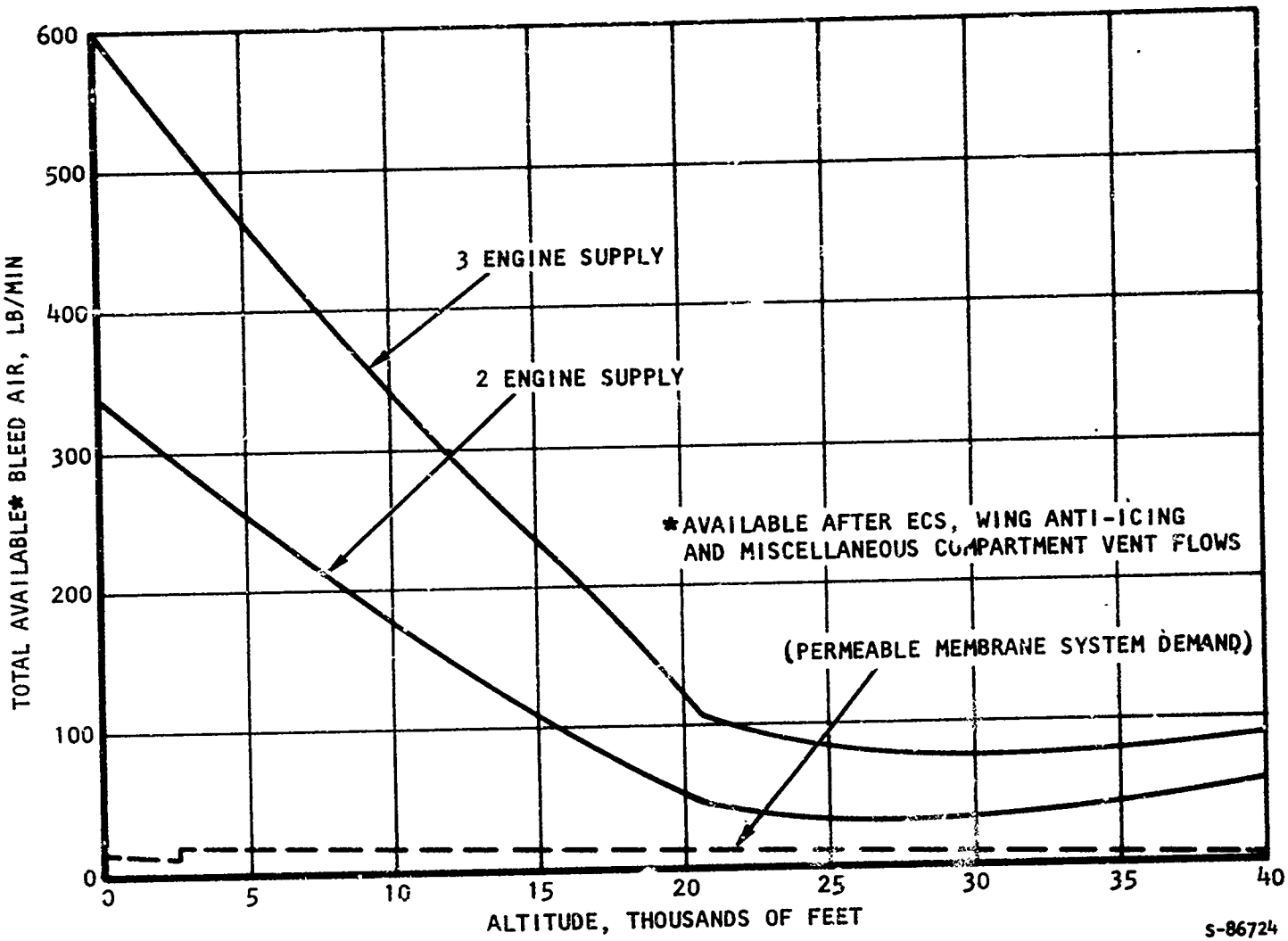

Figure 2-13. Bleed Air Availability (Idle Descent Settings)

is shown for operation in accordance with the design control document[6] for both three- and two-engine operation. Also shown, as a typical IGG requirement, is the bleed air required by the permeable membrane IGG during idle descent at minimum fuel loads (maximum ullage) as discussed previously. As can be seen, the typical permeable membrane fuel tank inerting system does not require all of the available air, even at current minimum engine settings.

Figure 2-13 does not show the data for two-engine out operation in accordance with FAR 121.193(c) due to the fact the required low additional bleed requirements over 1-ECS and 2 wing anti-icing or 2-ECS, no wing anti-icing requirement is readily supplied if the engine is not set at idle.

The physical arrangement of the DC-10 must be considered for IGG subsystem placement utilizing the available aircraft services. Figure 2-14 illustrates the profile view of DC-10. One such potential location for IGG equipment is in the area immediately behind the No. 3 air conditioning ECS pack, just ahead of station 595, on the right side of the nose wheel well. This unpressurized compartment contains bleed air manifolds, ram air, electrical power, and general access to all aircraft services required for IGG operation (with the exception of fuel for a catalytic combustor IGG). Its location, approximately 50 feet in front of the wing station, allows inert gas to be ducted back to the wing area routed parallel to existing bleed air pressure ducts with regulators to be located in the center accessory compartment immediately prior to connection with the existing vent system. In the case of the catalytic combustor, it may be desirable to locate the IGG unit within an existing fire zone, such as the engine nacelle or within the APU area.

Location of the IGG behind the No. 3 ECS provides ready access to ram air from ECS Pack No. 3, to bleed air from the same ECS pack, and via isolation and check valves, potential sources of bleed air from the other two ECS packs located on the opposite side of the nose wheel. Location in the right hand ECS bay, behind ECS Pack No. 3, is accessible either from the existing Pack 3 access door (requires pack removal), or from a potential additional access door similar to the access door for ECS Pack 2 located on the opposite side of

---

[5] DC-10, Series 10, Air Conditioning and Pneumatic System Design Control Document, DCD 50418, May 17, 1971

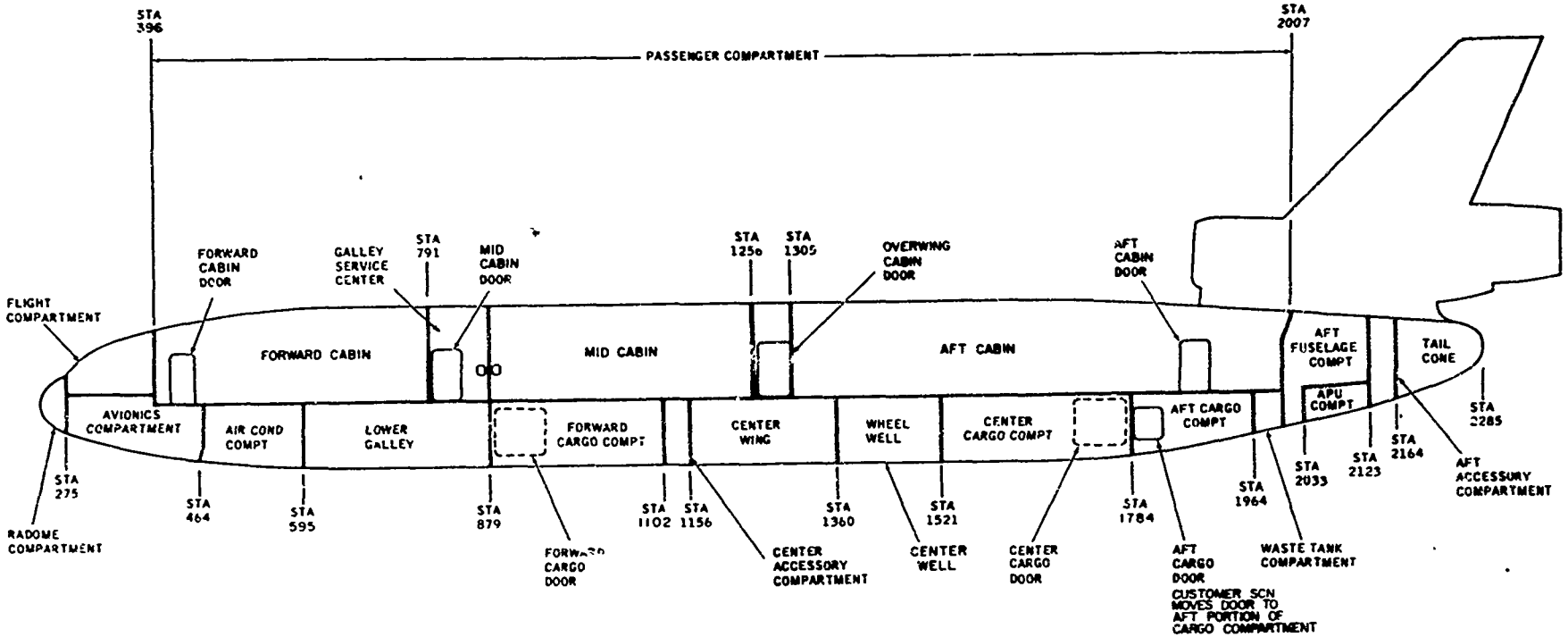

REPRINTED FROM DC-10 SCHEMATICS, AMERICAN AIRLINES SERIES 10 BY PERMISSION OF MCDONNELL DOUGLAS CORPORATION. YEAR OF FIRST PUBLICATION 6-30-1970.

SPA 3241-29

Figure 2-14. DC-10 Profile View

the fuselage. The only piece of equipment currently protruding into this area, as determined by inspection of operational aircraft is a ram air turbine which only requires a portion of the bottom 30 inches of the ECS bay location.

IGG access to existing bleed air and ram air ducts, required for subsystem operation, is shown in Figure 2-15. For an ECS pack independent system, as discussed in this report, prime bleed air tap-off locations would be on the engine side of all ECS isolation and flow control valves with the possibility of multiple IGG bleed sources considered. Ram air can be taken from the existing No. 3 pack ram ducting without impacting its operation. The relatively small quantities of ram air required for IGG operation would tend to result in slightly higher ECS temperatures at the same ram air door settings. This will be compensated for by temperature sensing equipment which will increase the ram door opening.

A secondary source of IGG bleed air is downstream of the ECS heat exchanger. This concept utilizes the existing ECS compressor and heat exchanger making an ECS pack dependent IGG subsystem, with a potential savings in system weight and complexity. Although beyond the scope of this feasibility investigation, any further studies should consider the effects of such an integration in greater detail.

The existing ECS ram ducts are shown in Figure 2-16. The existing linkage, ram inlet, and ram exit door can be seen in this illustration. A potential IGG ram air source is from the aft end of the No. 3 pack ECS ducting immediately prior to its entry into the ram side of the ECS pack heat exchanger. An additional option, to provide more complete independence from ECS pack operations (and potential failures) is to provide a separate ram air inlet scoop and exhaust valve similar to those in existence for ECS pack design.

The existing fuel vent system is schematically shown in Figure 2-17. The system consists of vent lines passing from the outboard end of the No. 1 and No. 3 main tanks across the fuselage and terminating in the vent box of the opposite wing. This design provides two indepe dent vent zones with protection against fuel spillage during aircraft ground and unusual flight operation. The existing vent lines represent an ideal way to distribute inert gases to the individual fuel tanks, however this will require either cross manifolding within the fuselage area to provide inflow from a single demand valve, or alternatively, two demand inflow valves to retain each wing as an independent vent space zone

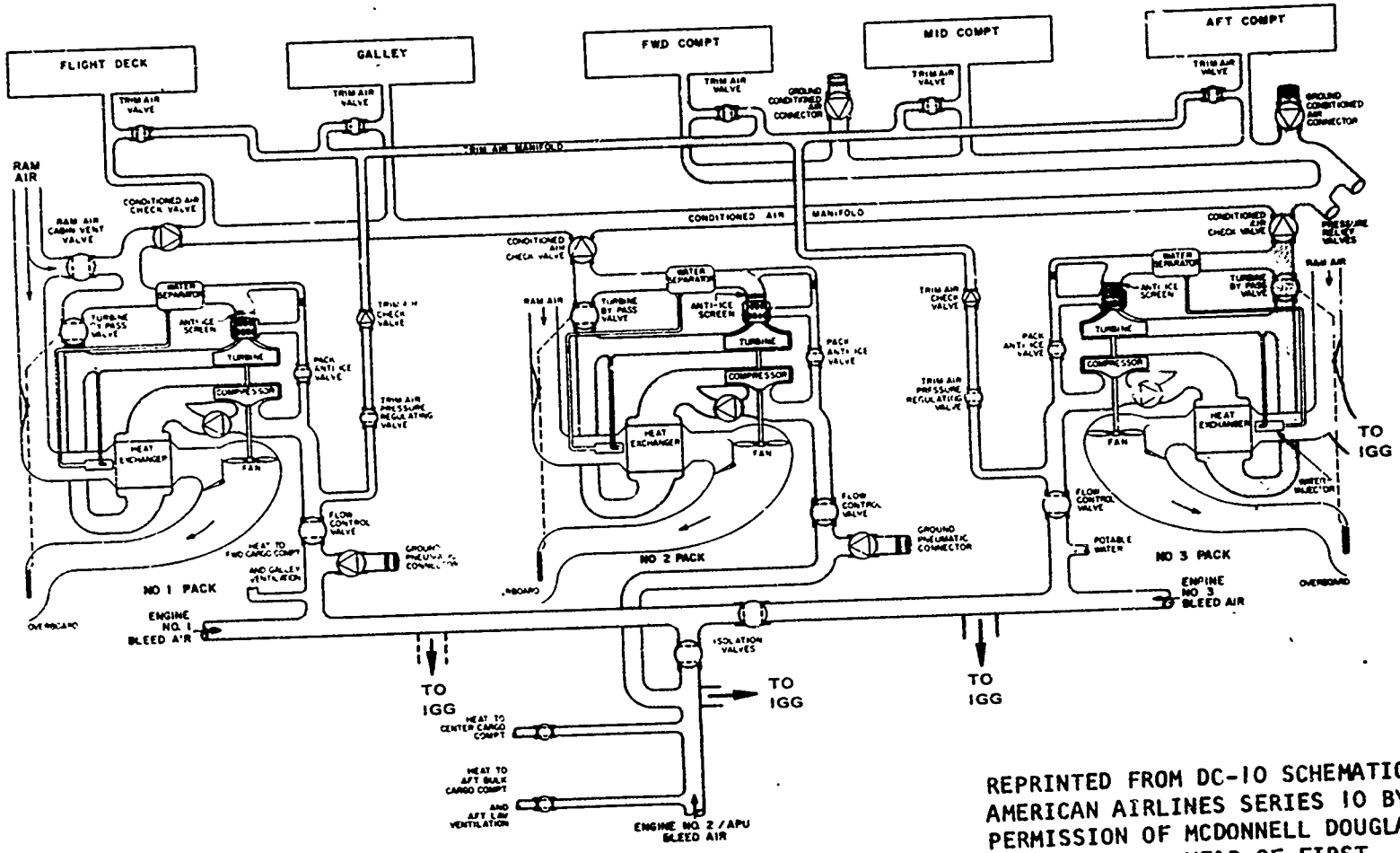

REPRINTED FROM DC-10 SCHEMATICS, AMERICAN AIRLINES SERIES 10 BY PERMISSION OF MCDONNELL DOUGLAS CORPORATION. YEAR OF FIRST PUBLICATION 6-30-1970.

SPA 3241-31

Figure 2-15. DC-10 Air Conditioning System

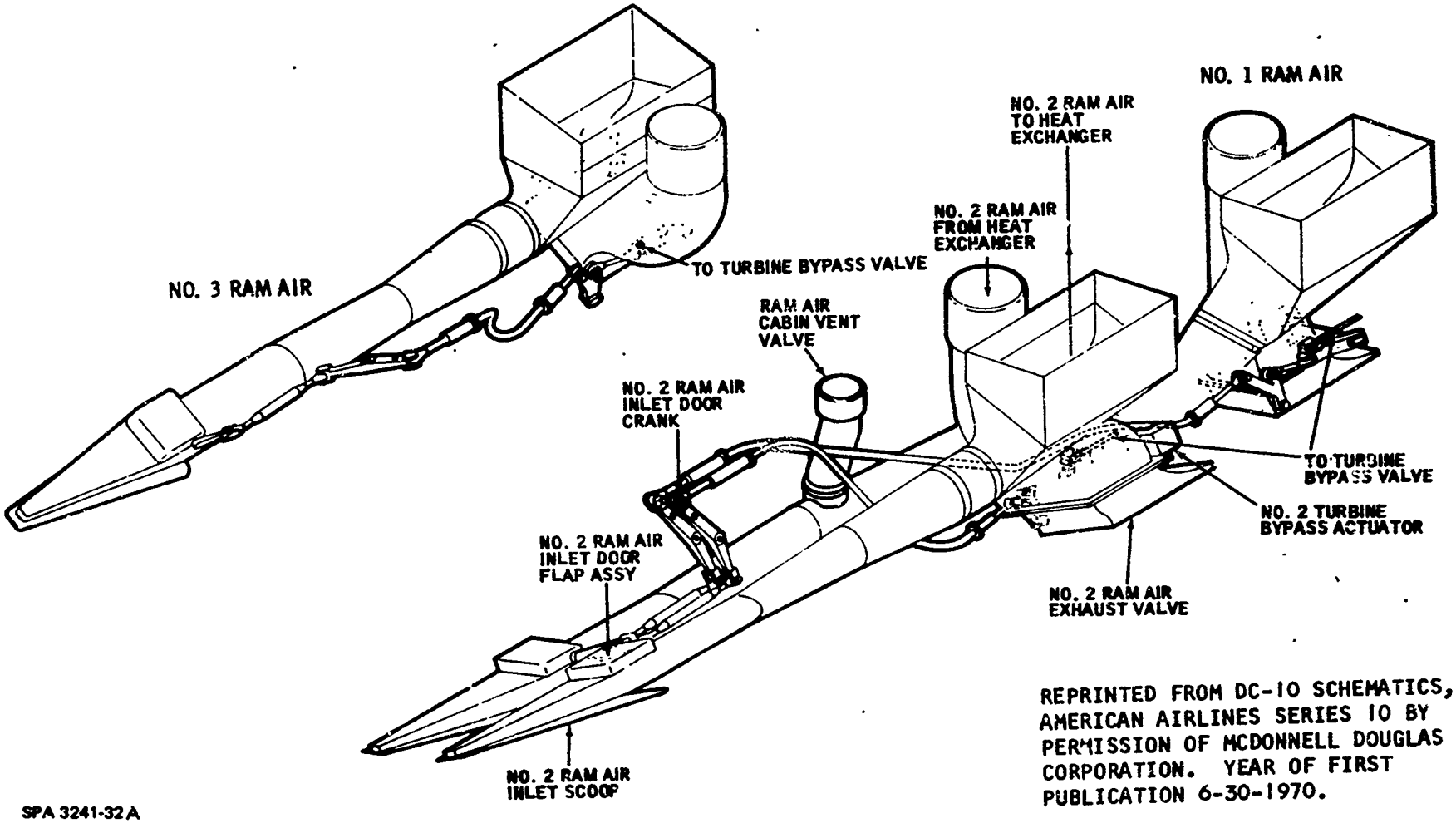

REPRINTED FROM DC-10 SCHEMATICS, AMERICAN AIRLINES SERIES 10 BY PERMISSION OF MCDONNELL DOUGLAS CORPORATION. YEAR OF FIRST PUBLICATION 6-30-1970.

Figure 2-16. ECS Pack Ram Air

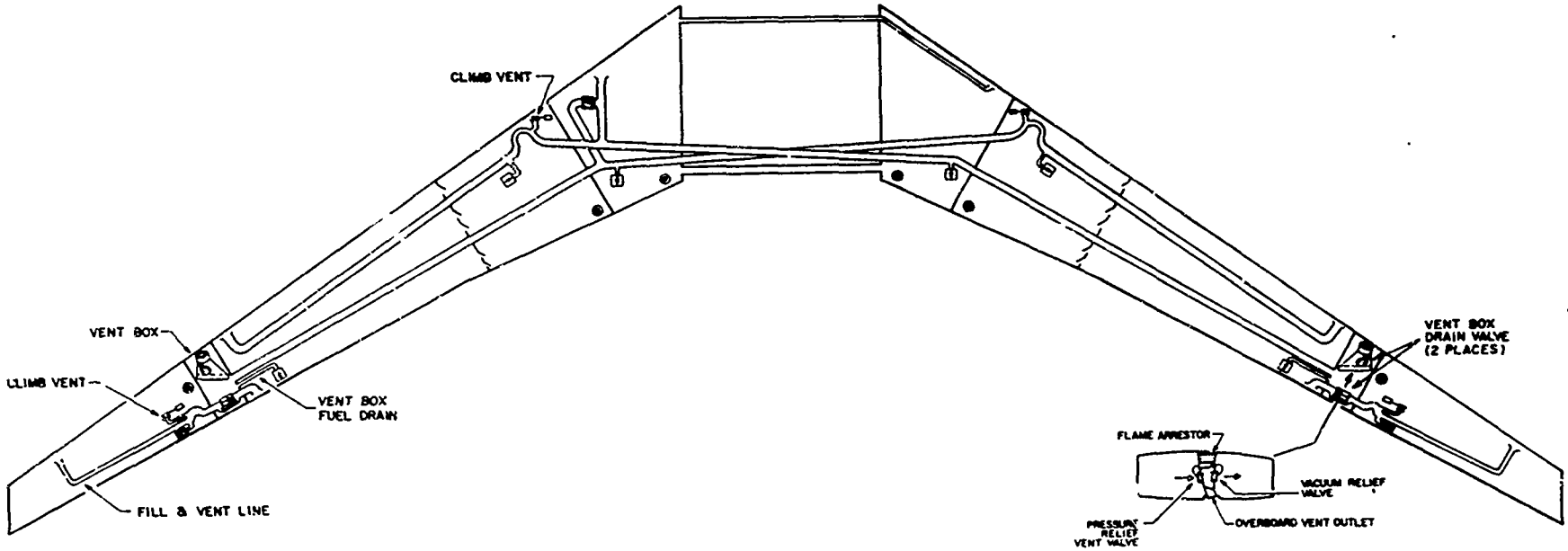

REPRINTED FROM DC-10 SCHEMATICS, AMERICAN AIRLINES SERIES 10 BY PERMISSION OF MCDONNELL DOUGLAS CORPORATION. YEAR OF FIRST PUBLICATION 6-30-1970.

SPA 3241-33

Figure 2-17. DC-10 Fuel Vent System

(No. 2 tanks both left and right hand are part of the left wing vent space and therefore vent to the right wing vent box).

Since IGG systems are sensitive to inflow rate requirements, it follows that changes in this rate will significantly affect the overall weight and size of the IGG subsystem. This rate is strongly a function of the product of fuel tank volume and descent rate (repressurization rate), as can be seen from equation (2-1); resultant rate changes are associated with changes of these terms. The maximum volume of the ullage is determined by the airplane, and the repressurization rate is a function of the flight profile. In order to provide a system having little or no impact upon current airline operations, yet recognize potential weight savings associated with the selection of a design point other than the emergency descent profile, this profile has been singled out as a unique and unusual design point which must be met; however, only during unusual emergency conditions. For this reason, the use of an extinguishing agent such as Halon 1301 for this emergency descent mode only is not inconsistent with the IGG concept of avoiding the use of storable inerting compounds. In order to evaluate the system effects of the use of fluoro-carbon extinguishing agents, it is necessary to evaluate their weight and effectiveness against that achieved by use of an IGG system designed for emergency descent conditions. It has been shown, in tests conducted by DuPont,[7,8] that Halon 1301 offers unusual advantages as a safe and effective fire extinguishing agent against Class A (cellulose materials), Class B (flammable liquids), and Class C (electrical) fires. On a weight of agent basis, Halon 1301 is the most effective gaseous extinguishing agent available. It is up to three times more effective than carbon dioxide and most other halogenated agents; it is approximately equivalent to sodium based dry powder although somewhat less effective than potassium based powder. It has been shown that Halon 1301 concentrations of 6 percent by volume are effective for extinguishing and maintaining inert atmospheres for Class B fires. The use of Halon 1301 will, in addition to providing protection for emergency descent conditions, also be available for

---

7 DuPont, "DuPont 'Freon' FE 1301 Fire Extinguishing Agent," No. B-29B

8 DuPont, "Toxicology of DuPont FE 1301 Fire Extinguishing Agent," No. S35A

system augmentation in the event of a potential failure, wherein the effectiveness of the IGG system is negated due to unusual aircraft damage or other potential problems involving the bleed air or other service required for IGG system. Based on 6 percent by volume requirements (at worst case of full ullage volume and one atmosphere pressure), it is found that 130 cu ft of Halon gas is required for maintaining the inert atmosphere. This will require 70 lb of the extinguishing agent, which when packaged in an ICC-4DA/500 type cylindrical steel container approximately 20 inches long and 15 inches in diameter, weighs approximately 100 lb.

CANDIDATE INERT GAS GENERATION SUBSYSTEMS

The basic goal of all airborne gas generation systems is to take advantage of the media through which the aircraft operates. This environment, the earth's atmosphere, consists largely of nitrogen gas, with a nominal 21 percent oxygen content, available to the aircraft for processing to produce an inert gas. Utilization of the surrounding atmosphere with a reduction of oxygen concentration to approximately 9 percent produces an inertent adequate for fuel tank usage[1,2,3].

A general comparison and screening of conceivable methods for separation or removal of oxygen from the atmosphere resulted in a more detailed evaluation of five feasible techniques to accomplish inert gas generation on-board an aircraft. These concepts considered during the Phase I program, are: (1) air separation by permeable membranes, (2) combustion of aircraft fuel with air, (3) chemical sorption of oxygen from air, (4) physical sorption of oxygen from air, and (5) air rectification. The remainder of this section of the report will briefly present the principle of operation and key application consideration for each of the five IGG concepts identified above. Consideration is given to both the theory of operation and its application to airborne IGG systems.

Following the brief discussions, a comparison summary of the key performance parameters for the DC-10 application is shown. The selection of the permeable membrane system for Phase II study is discussed.

Permeable Membrane Separation Concept and Operation

The concept of separation of oxygen and nitrogen from the air stream utilizing permeable membranes involves a continuous process in which high pressure air is exposed to a large surface of membrane material. The large surface area has been achieved by using a large number of small diameter hollow fiber tubes. The separation process exists due to a preferential membrane permeation to oxygen over nitrogen. A lower pressure on the permeant side of the membrane provides the driving potential for separation to take place. The membrane material itself is chosen for structural and chemical properties as well as for permeability and separation factors. Since the separation of gases is partial pressure driven, additional purge air is provided on the low pressure side of the membranes to avoid an increase in

local oxygen partial pressure. A more detailed discussion of permeable membrane mass transfer is presented in Appendix A to this report.

If sufficient surface area and other conditions are correct, the resultant flow from the membrane fibers is of sufficiently low oxygen concentration to be used as a source of inert gas available, on demand, for introduction into the wing ullage and vent spaces, or for fuel system purging.

In operation, the basic permeable membrane inert gas generation subsystem, shown conceptually in Figure 2-18, uses bleed air from the propulsion engines as a supply gas. The hot bleed supply air passes through the primary heat exchanger where it is cooled. The cooled high pressure bleed air then enters the compressor component of the turbo compressor where the pressure is further increased. Hot bleed air is also supplied from the primary heat exchanger inlet to the turbine component of the turbocompressor to provide shaft power for the compressor. The reheated bleed air from the compressor is then cooled again in the secondary heat exchanger and directed into the membrane canister where reduction of oxygen concentration takes place. The bleed air exits the membrane module at an acceptably low oxygen concentration, available as an inert gas for delivery to the fuel tanks.

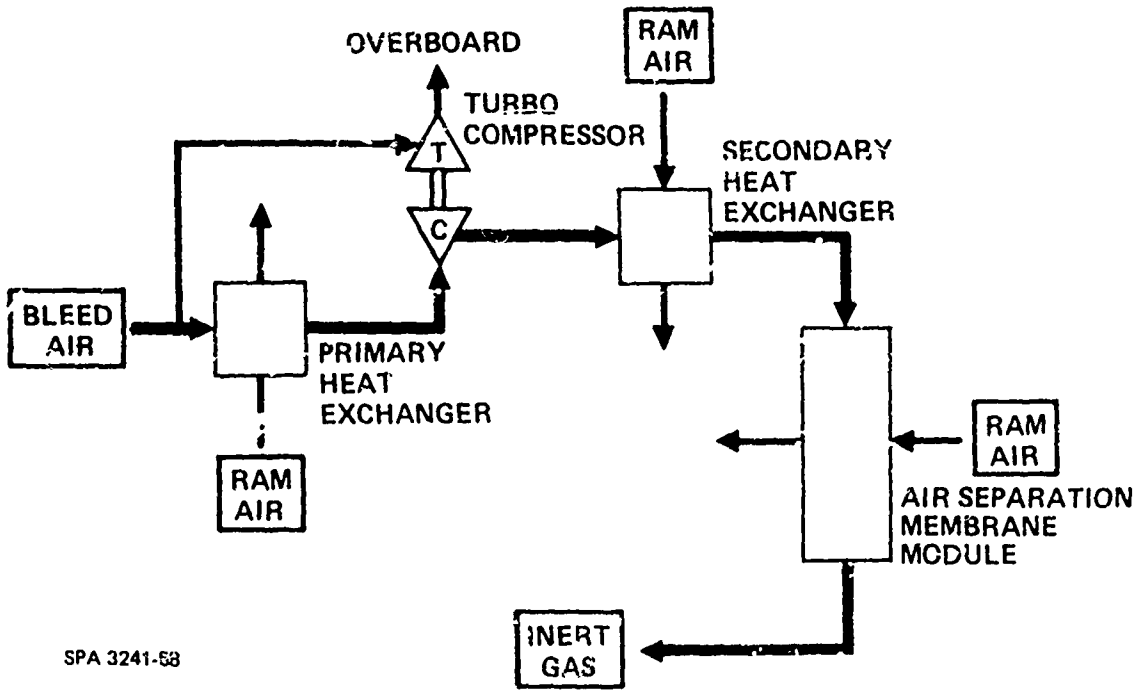

Figure 2-18. Schematic Diagram of a Basic Permeable Membrane IGG

Ram air is utilized as the heat sink for the primary and secondary heat exchangers and is utilized as the purge gas to reduce the oxygen concentration in the permeant side of the membrane canister. Further analysis of the system design and capabilities is presented in Section 3 where the Phase II study of hollow fiber permeable membranes is discussed.

Fuel/Air Combustion

1. Concept and Operation

This concept involves the chemical reaction of aircraft fuel and the oxygen in the air stream. Normal aircraft fuel is mixed with bleed air as it flows into a catalyst packed heat exchanger where controlled chemical reaction takes place. This reaction produces carbon dioxide and water vapor from the burned fuel/oxygen reaction and allows the nitrogen to pass through the catalytic reactor untouched. Cooling the combusted gases and separation of the water produced from reaction results in a suitable inert gas.

The continuous flow process inert gas generator subsystem utilizing catalytic reaction is shown in Figure 2-19. The system consists of the injection and mixing of fuel via fuel nozzles into the hot bleed air supply stream upstream of the catalytic reactor heat exchanger. The mixed gases enter the catalytic reactor where they are subjected to ignition temperatures in the presence of the catalyst where the fuel and oxygen are reduced by chemical reaction to carbon dioxide and water vapor. The hot gases then enter the primary heat exchanger where they are reduced to near ram air temperatures. The flow leaves the primary heat exchanger and enters the cooling turbine which reduces the temperature at the water separator inlet to near freezing conditions. The shaft power produced in the turbine section of the cooling turbine drives the ram air fan which cools the primary heat exchanger and provides temperature control in the combustion zones of the reactor. The cooled inert gas passes through a water separator where the moisture from the chemical reaction is extracted. The cooled, near oxygen free, inert product is then delivered to the fuel tanks, or at high demand, is mixed with untreated bypass bleed air resulting in an overall mixture of acceptably low oxygen concentration.

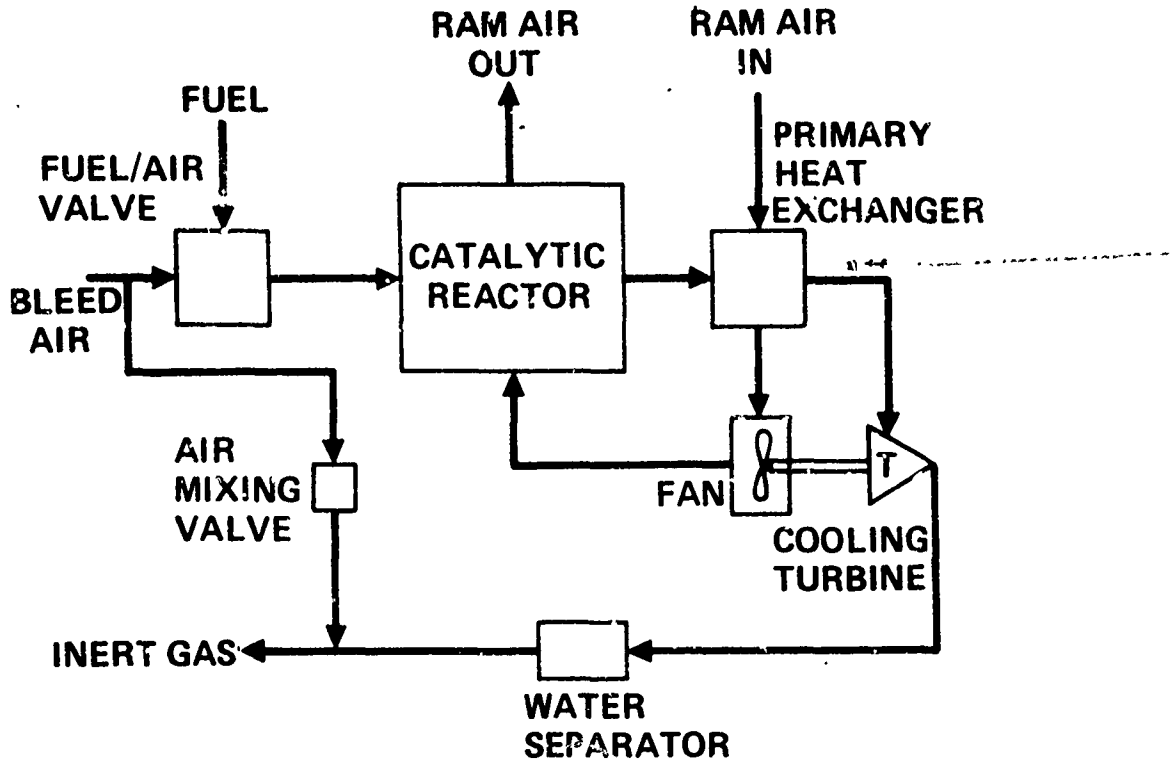

SPA 3241-49

Figure 2-19. Schematic Diagram of a Basic Catalytic Reactor IGG

2. DC-10 System Preliminary Design

The design requirements of the DC-10 IGG indicate two distinct flow requirement periods. The first of these, that associated with ascent and climb is generally characterized by flow rates of 1 lb per minute inert gas requirement maximum; while descent requires flows up to 13.2 lb per minute. In order to establish a steady state output design not requiring a continuous generation of 13 lb per minute, the system has been devised to include two catalytic reactor beds and control schemes in parallel as seen in Figure 2-20. The low flow portion will accommodate maximum inert gas flow rate requirements up to approximately 1 lb per minute. Combined output is designed to provide 13.2 lb per minute. Near stoichiometric mixtures are achieved by the system which has been devised to include the injection of fuel via fuel nozzles into the bleed air stream upstream of the catalytic reactor bed. The gases are mixed and subjected to ignition temperatures in the presence of the catalyst where the fuel is reduced to carbon dioxide and water vapor by chemical reaction with oxygen from the bleed air. The gases then enter the primary heat exchanger where they are reduced to near ram air temperatures. Controls in the ram air circuit prevent the temperature from dropping below freezing in order to prevent freeze up conditions occurring in the primary heat exchanger. Flow leaves the primary heat exchanger and enters the cooling turbine area which reduces the temperature at the water separator to near freezing conditions. This is controlled by the water separator temperature control valve which directs flow either through or bypassing the turbine in correct proportions to control the temperature at the water separator. Flow then passes through the flow control sections and either to the inflow control valve or exits via the excess flow valve.

Ram air enters from the ECS pack duct, (or via another source if an existing fire zone is chosen), receives a small amount of bleed air should its required flow rate result in temperatures at the exit of the primary heat exchanger below freezing, receives water injections from the water separator and primary heat exchanger in order to utilize the latent heat available in the water, passes through the primary heat exchanger cooling the exhaust products and through the reactor for temperature control in the combustion zones.

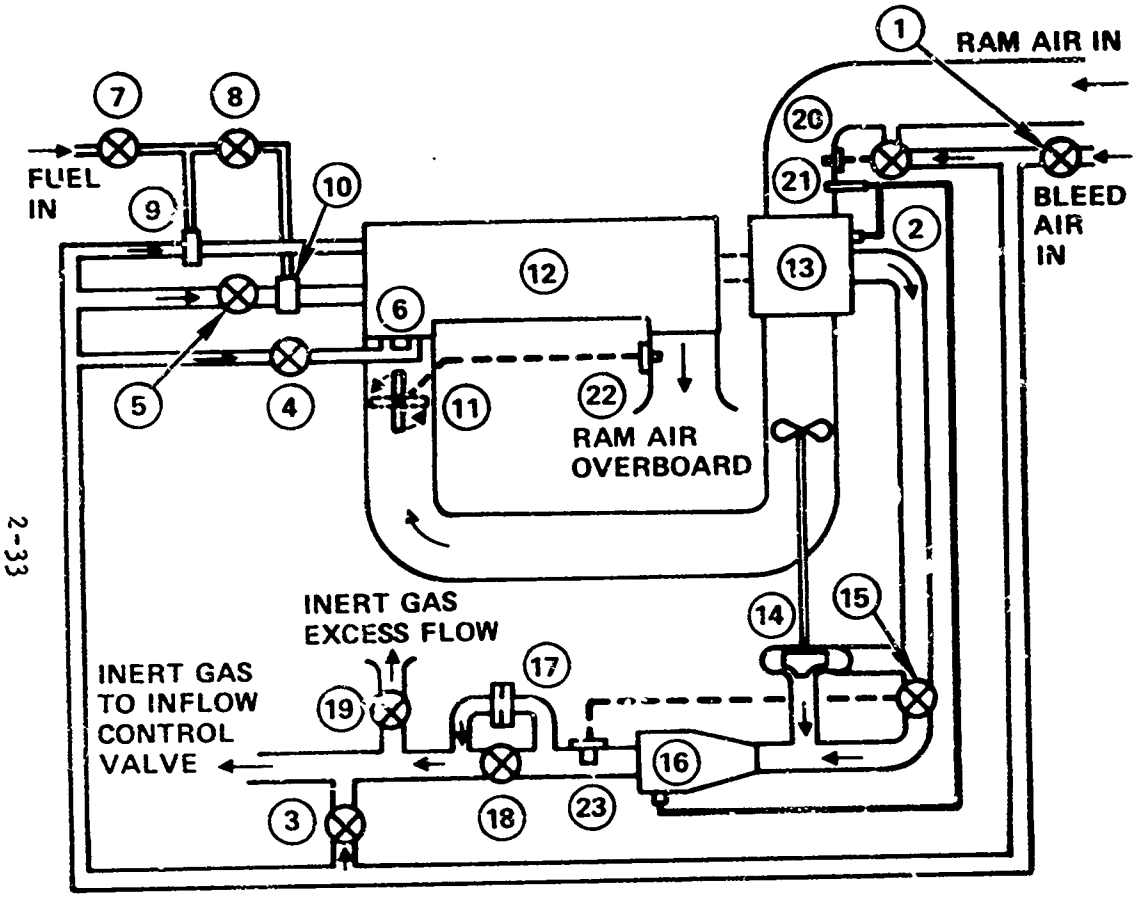

SPA 3241-50

ITEM	DESCRIPTION
1	BLEED AIR PRESSURE REGULATOR AND SHUTOFF VALVE
2	BLEED AIR/RAM AIR MIXING VALVE
3	EXCESS DEMAND FLOW MIXING VALVE
4	STARTUP VALVE
5	HIGH FLOW BLEED AIR VALVE
6	STARTUP BLEED AIR INJECTOR
7	FUEL SHUTOFF VALVE
8	HIGH FLOW FUEL VALVE
9	LOW FLOW FUEL NOZZLE
10	HIGH FLOW FUEL NOZZLE
11	RAM AIR THROTTLE VALVE
12	CATALYTIC REACTOR
13	PRIMARY HEAT EXCHANGER
14	COOLING TURBINE
15	WATER SEPARATOR TEMPERATURE CONTROL VALVE
16	WATER SEPARATOR
17	LOW FLOW RATE CONTROL
18	HIGH FLOW SHUTOFF AND RATE CONTROL
19	EXCESS FLOW RELIEF VALVE
20	RAM AIR INLET TEMPERATURE SENSOR AND CONTROL
21	WATER SPRAY NOZZLE
22	RAM AIR OUTLET TEMPERATURE SENSOR AND CONTROL
23	WATER SEPARATOR TEMPERATURE SENSOR AND CONTROL

Figure 2-20. Catalytic Reactor IGG

The system is designed to work with pressures as low as 15 to 20 psig. This will enable operation compatible with the bleed flow pressures available from the propulsion engines in the DC-10. The controls will accommodate a wide range of inlet temperatures (as will occur in actual DC-10 operation). The catalyst used in testing at the AiResearch laboratories was manufactured by American Cyanamid and designated Aeroband V-HD (Code -A) and is a proprietary catalyst originally designed for automotive applications.

The design point for the catalytic reactor IGG, the 13.2 lb per minute flow requirement which occurs during conditions in the high speed descent, is achieved by producing 9.2 lb per minute of inert gas from the catalytic reactor bed and mixing with approximately 4 lb per minute of bleed bypass air resulting in an overall mixture containing less than 9 percent oxygen by volume. During operation, fuel is injected into the bleed air stream to accomplish a fuel to air ratio near stoichiometric conditions (approximately 6.8 percent). While the fuel/air reaction takes place at approximately 1300°F in the catalytic reactor resulting in bleed and ram air outlet temperatures also near 1300°F the ram air is directed overboard and the bleed air is immediately cooled by the primary heat exchanger reducing the hazard associated with these high temperatures.

The concept of a catalytic reactor IGG has been under study and development since 1968 under the sponsorship of the Air Force Aero Propulsion Laboratory (AFAPL) at Wright-Patterson Air Force Base. At AiResearch under USAF Contract Nos. F33615-70-C-1492 and F33615-71-C-1901, a multi-phase investigation has included the design, fabrication and testing of a laboratory scale model subsystem.

The test setup in the AiResearch laboratories has included all major subsystem components required for the IGG. These have included the fuel injection and mixing chambers, the catalytic reactor bed, of which both a low and high flow range type were provided in parallel flow, the primary heat exchanger, cooling turbine, water separator and all other controls required for subsystem operation.

These tests have resulted in the generation of considerable data which has been used to optimize the system in terms of performance, control, and simplicity of operation.

Physical Sorption Concept and Operation

A typical design for a physical sorption inert gas generation subsystem is shown in Figure 2-21. In this system, bleed air is cooled by a primary heat exchanger after which water is removed in a condensing heat exchanger. A second supply of cooled bleed air from the primary heat exchanger is further cooled by a cooling turbine to provide the heat sink for water condensation from the primary stream. Shaft power from the turbine is used to power a ram air fan for primary heat exchanger cooling. Following water removal, the primary bleed air stream is supplied at a regulated pressure to an adsorbing molecular sieve bed where the resulting gas flow has a reduced oxygen concentration suitable for use as an inert gas, while adsorbed oxygen concentration within the bed increases. At the same time, a second

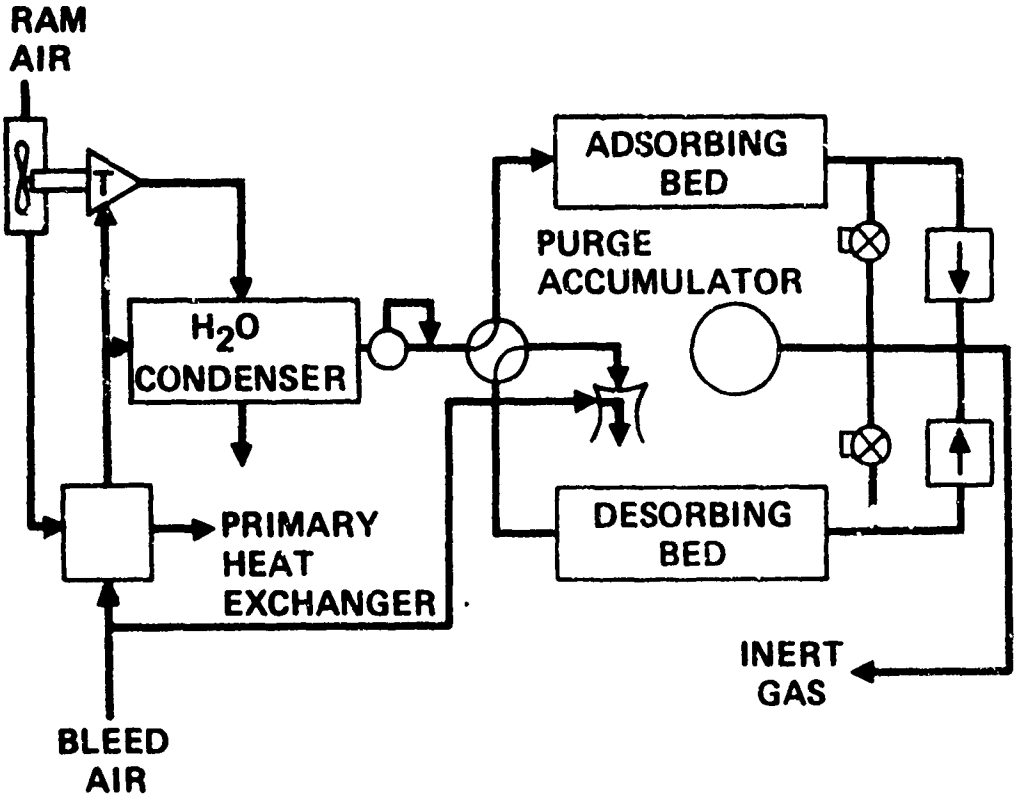

SPA 3241-42

Figure 2-21. Conceptual Operation of Physical Sorption IGG

molecular sieve bed, having been loaded with oxygen during a previous adsorption cycle is desorbed by means of a reduction in bed pressure. Upon completion of the half-cycle, flow in both beds is reversed by means of switching valves, and the cycle of operation begins again.

The principle of physical sorption is based upon the use of synthetically produced crystalline structured compounds known as zeolites or molecular sieves. Molecular sieves retain adsorbates by strong physical forces rather than by chemisorption. Gas molecules enter the internal sieve structure and are held (adsorbed) by physical forces of the Van der Walls type. The concept involved is to adsorb oxygen from the air stream and permit the remaining gas components passing through the material to be sufficiently low in oxygen for use as an inertent.

Co-adsorption curves for molecular sieves can be drawn to indicate gas loading in terms of weight of adsorbed gas to weight of sorbent for both oxygen and nitrogen. These curves show that the loading of both these gases is a function of both temperature and pressure as shown in Figure 2-22. Molecular sieves also have an extremely high equilibrium adsorption capacity for water and polar compounds at very low concentrations and utilization of molecular sieve material requires the prior condensation of moisture from the air stream.

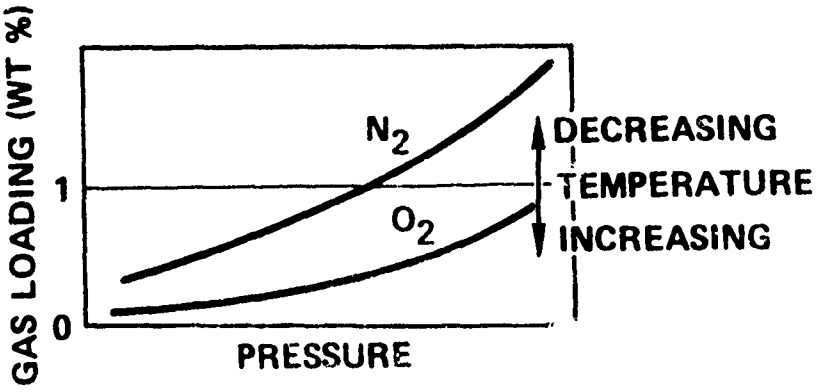

Figure 2-22. Molecular Sieve Co-adsorption Equilibrium Curves

In order for a sorbent bed system to operate at equilibrium, the ratio of oxygen adsorbed at 21 percent of the total pressure when compared to the nitrogen adsorbed at 79 percent of the total pressure must exceed a value of 0.23 (which is the weight percentage of oxygen in the incoming stream). Since none of the molecular sieves evaluated showed this condition, it must be assumed that the operation of molecular sieve as a nitrogen concentration device is based upon rate of adsorption. Figure 2-23 illustrates typical oxygen concentration in molecular sieve material versus time.

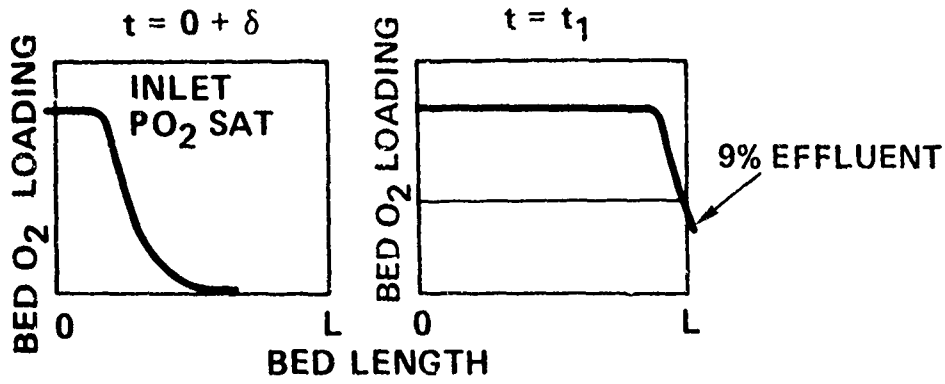

Figure 2-23. Oxygen Loading Within a Molecular Sieve Sorbent Bed as a Function of Time

System operation using molecular sieve requires the use of two sorbent beds, one bed for adsorbing gases while the second bed desorbs by means of reduced bed pressure. Looking at one of the molecular sieve beds, as the bed is loaded ideally and oxygen is being concentrated within the adsorbing bed, the nitrogen pressure wave front passes through the end of the bed first. This results in a low oxygen concentration, however, it begins to increase as the oxygen wave front nears the end of the bed as shown in Figure 2-24. At some time $t = t_1$ the outlet effluent oxygen concentration increases to the limit and the beds must be switched. Resultant sorbent weight as a function of half cycle time for a two-bed system is shown in Figure 2-25.

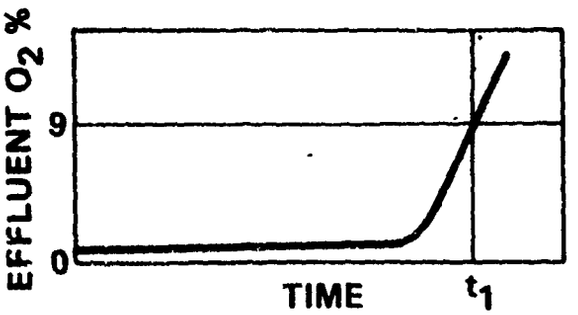

Figure 2-24. Outlet Oxygen Concentration versus Time for Molecular Sieve

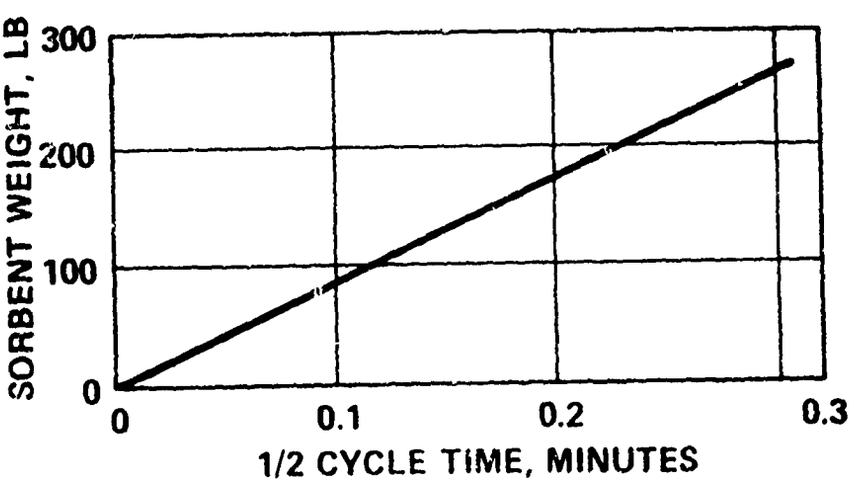

Figure 2-25. Molecular Sieve 4A Required Weight as a Function of Half-Cycle Time

In analyzing practical application of physical sorption IGG systems, several key factors must be considered.

To begin with, considerable development is required before an operational physical sorption IGG can be produced, particularly due to the apparent dependence upon rates which are not characteristic of equilibrium condition. The state of the art of adsorbent materials for the production of inert gas from air has not been developed to a practical standpoint. With available molecular sieve sorbent materials being considered, the system must be designed on dynamic adsorption rates as inert gas production will not occur utilizing equilibrium data. Since this limits bed cycle time, this means that system flexibility is sufficiently reduced to limit the application. The inert gas is in essence a batch process flow where oxygen concentration is time dependent.

Chemical Sorption

1. Concept and Operation

Figure 2-26 shows a simplified schematic of the Chemical Sorption IGG. The process air switching valves and controls have been omitted for clarity and each sorbent bed is shown in a particular mode, either absorbing or desorbing.

Bleed air is used to operate a freon turbocompressor and to provide process air. The process air is cooled in the primary heat exchanger by ram air and then its pressure is increased by a bootstrap turbocompressor. The heat of compression is removed by an intercooler heat exchanger prior to the pressurized air entering the absorbing bed where oxygen is removed. During the absorption process, the heat of reaction is removed from the absorption bed which acts as the evaporator to the freon vapor cycle refrigerator. This heated, pressurized gas then expands through the turbocompressor providing the power for bleed air compression to absorption pressure. The cooled expanded gas is then available for flow to the fuel tank ullage and vent space.

Additional bleed air is required to operate the freon turbocompressor required by the vapor cycle refrigerator. Turbine discharge air from the freon turbocompressor is used for stripping the desorbing sorbent bed and the oxygen rich gas is vented overboard. As with the physical sorption IGG, switching valves are used to alternate the absorption and desorption function of each of the two sorbent beds.

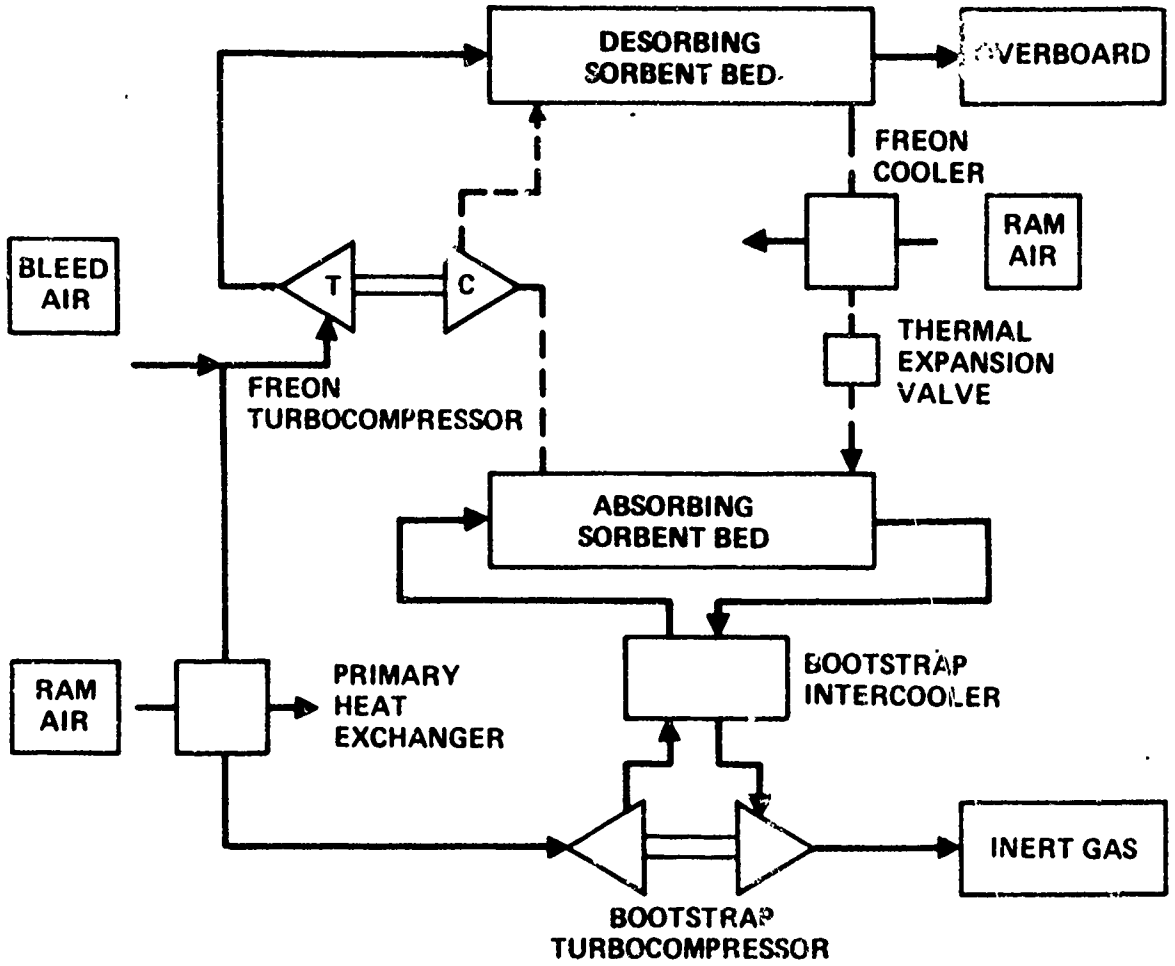

Figure 2-26. Conceptual Operation of Chemical Sorption IGG

The process of inert gas generation by use of chemical sorption techniques is similar to the process of physical sorption. In this concept, oxygen separation is accomplished by the selection of a chemical sorbent material, the chelate Fluomine, which provides several times the absorption capacity of a molecular sieve. Oxygen is chemically absorbed from the air stream allowing the nitrogen to pass through unaffected. Desorption of Fluomine is accomplished by the use of both reduced pressure and increased temperature for maximum effectiveness. The use of a chemical sorbent eliminates co-adsorption of nitrogen gas, further increasing the effectiveness of the system.

The equilibrium curves for the sorbent Fluomine illustrated in Figure 2-27 show that the equilibrium oxygen partial pressure is a function of temperature with a slight hysteresis between absorption and desorption conditions. The rate of absorption or desorption increases as the separation between actual partial pressure and equilibrium conditions occur due to the resultant driving potential towards equilibrium.

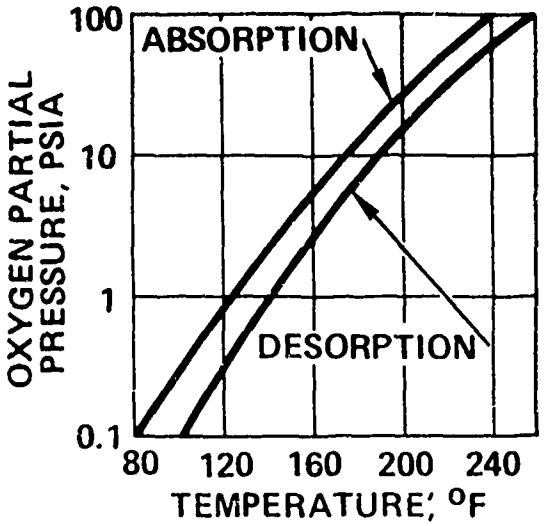

Figure 2-27. Fluomine Equilibrium Curves

Fast Fluomine-oxygen absorption rates, facilitated by efficient sorbent bed design, will result in near oxygen equilibrium between the outlet flow and the fluomine as a function of the sorbent temperatures as shown in Figure 2-27. The fixed oxygen partial pressure in the outlet flow rate, when combined with the total air pressure, determines the outlet concentration as shown in Figure 2-28. As can be seen by this curve, low temperature and higher pressures result in reduced oxygen concentration. This becomes particularly significant due to the temperature fluctuations required by absorption and desorption operations, and the sensible heat required to "swing" these temperatures.

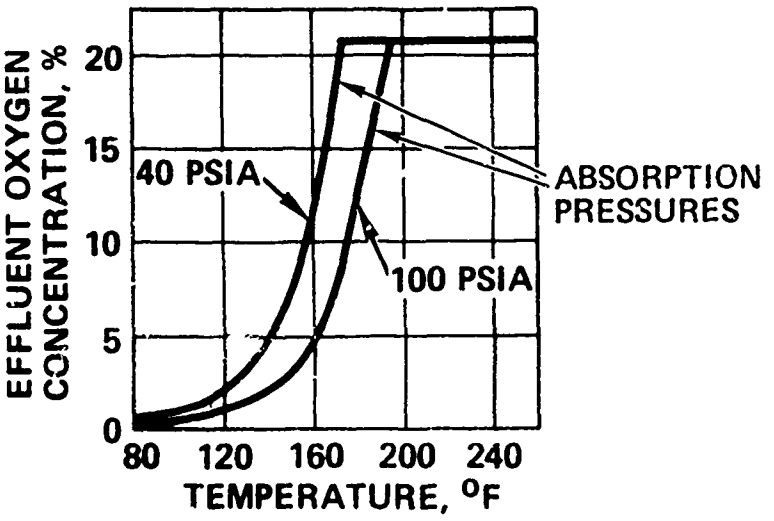

Figure 2-28. Equilibrium Oxygen Concentration for Various Temperatures and Operating Pressures

Utilization of chemical sorption of oxygen involves significant thermodynamic considerations. In chemical sorption, a heat of reaction is usually produced. In the case of Fluomine and oxygen, this heat of reaction is approximately 1075 BTU per lb of oxygen absorbed. Thus, a considerable amount of heat must be removed from the absorbing bed in order to prevent its overheating and loss of oxygen capacity. The desorption of oxygen from Fluomine is an endothermic process also requiring approximately 1075 BTU per lb of oxygen desorbed.

One of the major design considerations is the tradeoff of the system based on thermodynamics consideration. The freon system must provide the heat sink required during absorption, the heat source required during desorption, and the sensible heat transfer required to rapidly change bed temperatures. The resultant systems actually operate throughout a range of temperatures (and therefore oxygen concentrations in the inert gas) in order to "swing" the relatively large masses of sorbent packed beds in achievable time periods.

Since Fluomine loading tends to reach approximately 4 percent oxygen by weight at equilibrium, there is a limit to the cycle time based upon the weight of Fluomine sorbent and the output rate of the bed. Figure 2-29 shows the average temperature within the bed at a typical heat transfer plate. This temperature is increased during a desorb cycle and decreased during an absorb cycle in order to take advantage of the equilibrium partial pressure change as a function of temperature. In a typical temperature cycle, the thermal "swing" is initiated prior to switching flow at half cycle within the beds. This results in absorption at average temperatures around 120°F and desorption temperatures averaging about 180°F. The effect of the thermal swing on effluent oxygen concentration can be seen in Figure 2-30. This indicates that the actual oxygen concentration of the effluent gas is a function of cycle position. The average concentration, while well below the required 9 percent, is not maintained throughout the entire cycle. Oxygen concentration is high during a brief period at the start of the cycle while sorbent temperature is still high, and begins to increase again near the end of a half cycle as the bed begins to achieve equilibrium loading, and the bed temperature is increased in preparation for desorption.

While it remains possible to produce oxygen concentration consistently less than 9 percent, this will require the addition of a third sorbent bed, which will allow for complete cooling following desorption.

2. DC-10 System Preliminary Design

Application of the chemical sorption process for DC-10 design requires a complex system of components and controls as shown in Figure 2-31. For DC-10 operation at the design point, engine bleed flow enters the system to provide power for the freon turbocompressor, sweep for the desorbing bed,

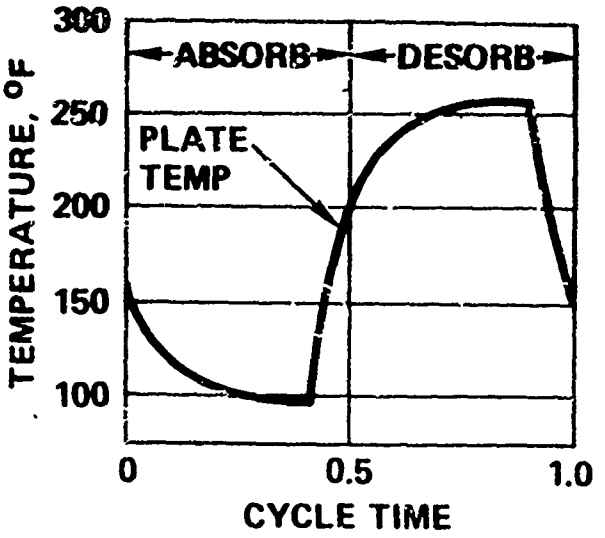

Figure 2-29. Typical Bed Structure Temperature as a Function of Time

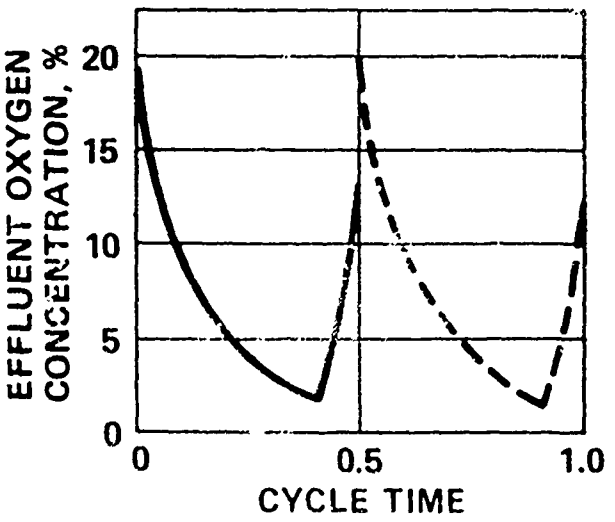

Figure 2-30. Inert Gas Oxygen Concentration as a Function of Time

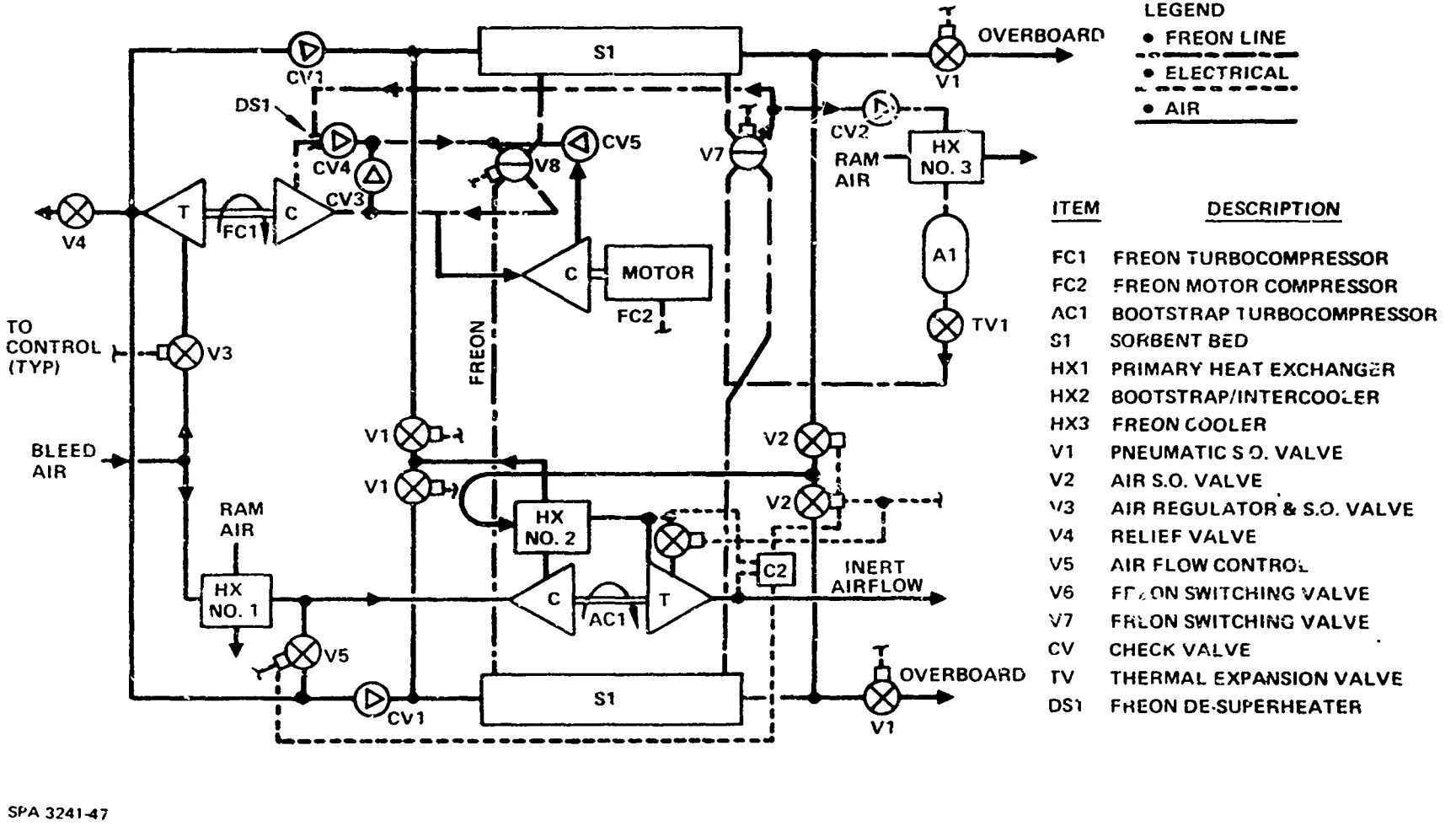

Figure 2-31. DC-10 Chemical Absorption IGG Preliminary System Design

and inert inflow through the absorbing bed to the fuel tanks. The absorbing bed flow proceeds through the No. 1 heat exchanger into the bootstrap turbocompressor, through the No. 2 heat exchanger which acts as a bootstrap intercooler, proceeds into the absorption bed where heat is removed by the freon loop, and oxygen is absorbed from the flow stream. From the absorption bed, flow continues back through the intercooler, through the turbine providing the power for the bootstrap compressor, and to the inflow demand regulator to the fuel tanks. The remaining 90 percent of the flow proceeds through the freon turbocompressor and discharges overboard through valve V4, a small bleed flow being maintained through the desorbing bed in order to lower the oxygen partial pressure. During this process, freon leaves the compressor, passes through a desuperheater which is designed to maintain its condition at the saturated vapor state, passes through the selector valve and into the desorbing bed where heat is transferred to the desorbing Fluomine. From the desorbing bed the freon proceeds through the ram air heat exchanger where heat of compression is removed, is throttled and delivered to the absorbing bed where the heat of reaction is transferred to the freon, vaporizing it prior to return to the freon turbocompressor.

Evaluation of Fluomine sorbents has been undertaken under USAF Contract No. F33615-71-C-1807 with Aero Propulsion Laboratories sponsorship. A final report (AFAPL-TR-72-27) was issued in May 1972. Since this time, evaluation of the Fluomine sorbent under USAF Contract No. F33657-72-C-0729 and Navy Contract No. N62269-72-C-0025, which are contracts for aircraft oxygen generation, has revealed that time dependent equilibrium loading lower than those expected are actually experienced. This new data has been utilized to update the sorbent system design herein reported.

In actual application the Fluomine absorption IGG system requires a fair amount of complexity in terms of controls and components required to achieve cycling. Inert gas production for chemical sorption is a batch process flow where oxygen concentration is time dependent, and exceeds the 9 percent requirement for a portion of each cycle.

Air Rectification

1. Concept and Operation

The basic air rectification (air liquification and distillation) IGG is shown in Figure 2-32. It consists of a precooler to lower the temperature of incoming bleed air followed by a compressor to increase bleed air pressure which is then further cooled in an aftercooler. Condensation of condensable gases such as water and carbon dioxide in the cool high pressure bleed air follows in a condensing heat exchanger following which the air is supplied to both turbine and compressor components of a turbocompressor. Expanded cold air from the turbine then cools the high pressure product from the compressor in a liquifier. The partially liquified gas then enters the separation column where nitrogen and oxygen are separated. A tradeoff exists between added production rate and product storage capacity. For the system size being evaluated, there is a favorable overall weight difference associated with reduced output rates and increased weight of storage containers.

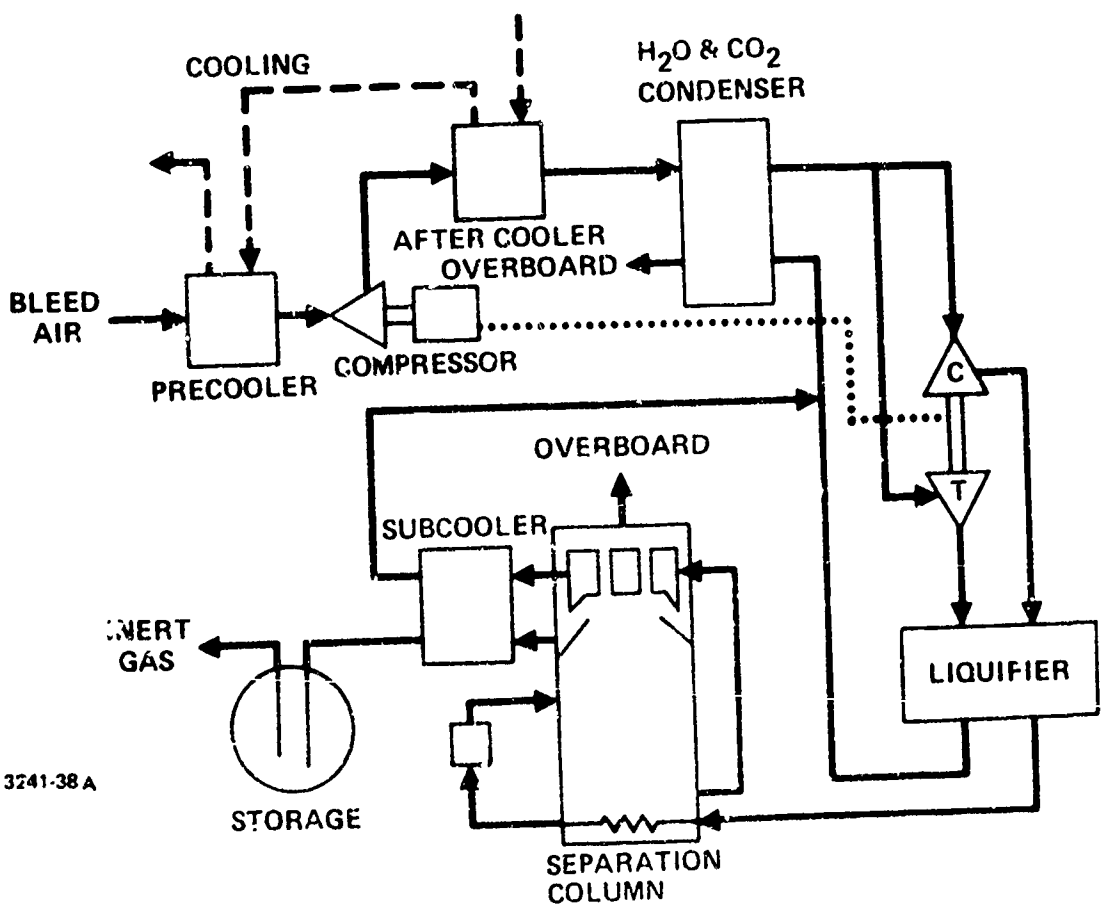

Figure 2-32. Conceptual Operation of an Air Rectification IGG

The technique of air rectification involves the liquification of air followed by separation into its component parts by phase separation principles associated with the physical characteristics of the fluids involved.

An evaluation of the phase diagram shown in Figure 2-33 for a nitrogen-oxygen system at several pressures reveals that single step separation to a level of 9 percent oxygen at pressures of one atmosphere or higher is only marginally possible and is not considered a feasible solution. A separation column is required because single separation, as may be achieved in a liquifier, would require the liquification of an excessively high portion of the incoming vapor stream to achieve reduction in oxygen concentration to 9 percent or below in the remaining vapor. Tradeoffs show the weight, and particularly the air required for the single separation from the packed column separator.

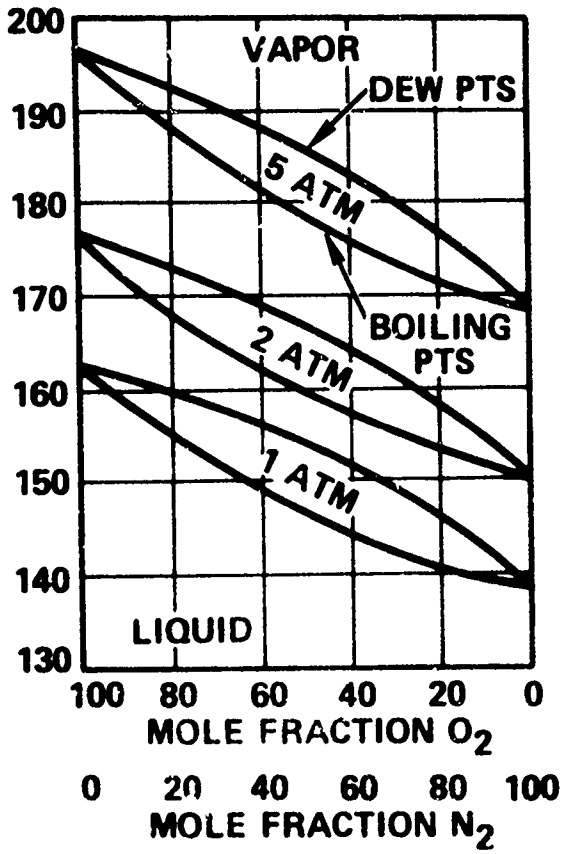

SPA 3241-39

Figure 2-33. Nitrogen-Oxygen Phase Diagram

2. DC-10 System Preliminary Design

The operating schematic as shown in Figure 2-34 of a rectification IGG subsystem is very complex. Conditioned bleed air at approximately 91 psia and 40°F enters the cold box zone through the reversing valve into two reversing heat exchangers; the first of which removes water, the second of which removes carbon dioxide by condensation and exhausting overboard on reverse flow purges. The reversing valve switches every five to seven minutes causing temporary temperature fluxuations which interrupt the output capacity. About 85 percent of the inlet flow passes through the turbo-expander where the pressure is reduced to approximately 20 psia to provide refrigeration to liquify air at about 120 psia, then returns to be exhausted overboard through the reversing heat exchangers. The remaining 15 percent of the incoming air is boosted to 122 psia, passes through the liquifier, and is expanded through a valve into the rectification column at approximately 75 psia. The column separates air into 91 percent nitrogen, collected as a liquid from a reflex condenser at the top of the column, and approximately 28 percent oxygen in the reboiler at the bottom (the heat from the reboiler is taken from the air feed stream at about 113 psia before it is throttled into the column). The oxygen rich bottoms are throttled to about 20 psia into the cold side of the reflux condenser. The nitrogen rich inert gas product is obtained by rectification through a fine mesh screen saddle packed column approximately 24 inches in height containing an equivalent of 6 to 8 theoretical plates. The liquid product (at 75 psia) is then passed through a subcooler (heat is exchanged with the 20 psia oxygen rich bottoms) so that sufficient liquid is retained upon throttling in the storage container at about 20 psia.

While portable units are fully developed and operational in the field today, their startup remains a rather complicated procedure, which must be attended by trained personnel. The fabrication of a unit, which is operational while mobile, requires further development and cannot be considered state-of-the-art.

Typical startup times for an aircraft optimized installation is estimated to be approximately 4 hours. This requires that the system be continually operational or that sufficient time be allowed following down time or

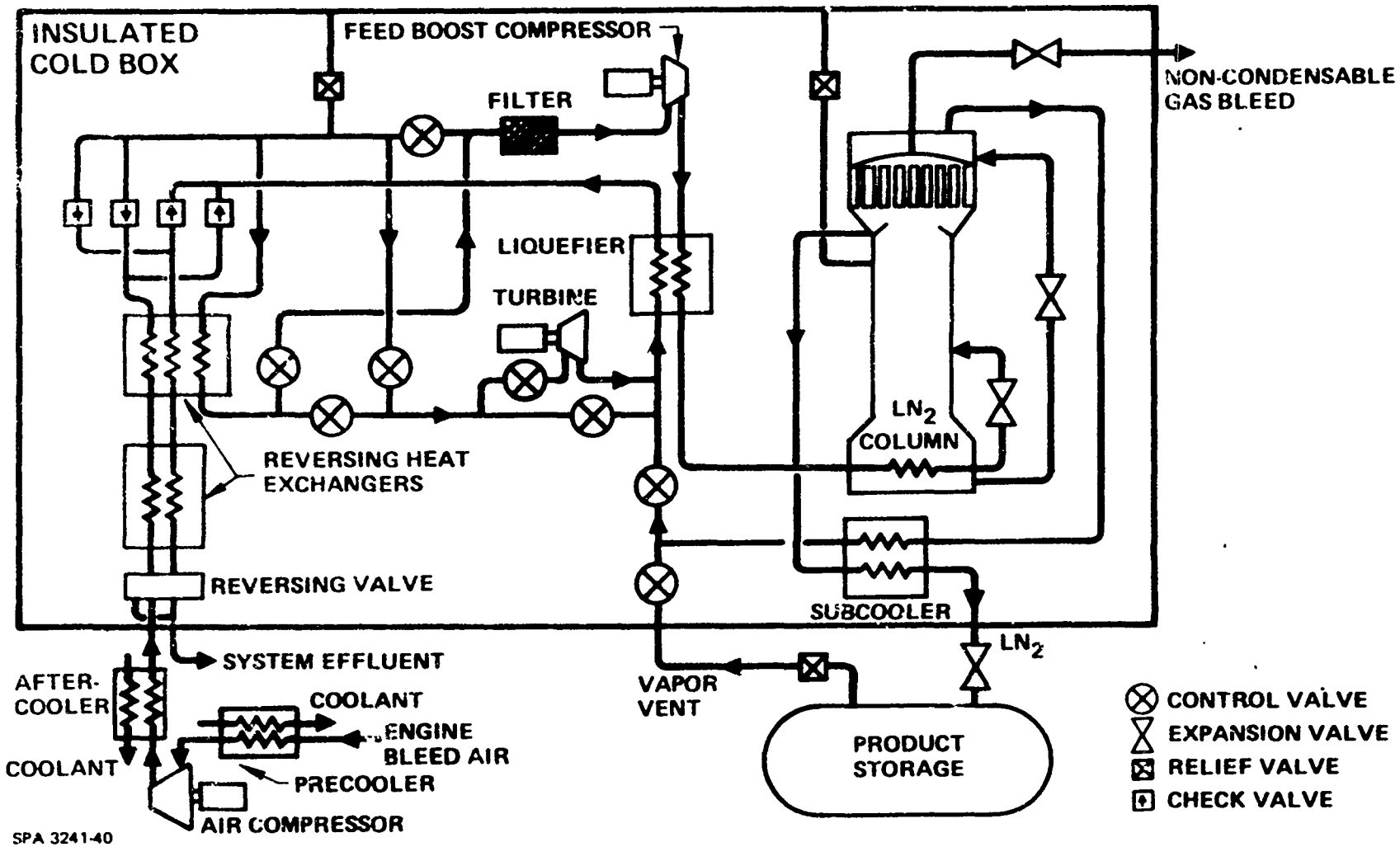

Figure 2-34. DC-10 Rectification IGG System

maintenance, so that the system could be returned to a steady state operating mode prior to use.

In order to make a practical system, an auxiliary means of cooling the incoming bleed air in both the precooler and compressor aftercooler must be considered. A significant problem is the required process air temperature at the inlet to the condensing heat exchangers. The temperature to which the bleed air must be reduced is below the temperature of ram air during many conditions. This requires that an additional refrigeration system (such as freon refrigeration) be considered to refrigerate the incoming bleed air to a temperature below the final air exhaust temperature.

The anticipated development problems and overall system weight and volume make this approach unsuitable for airborne IGG aboard commercial transport aircraft at this time.

Evaluation Summary

The five candidate inert gas generation subsystems discussed above represent a broad scale of technology applications to the separation or removal of oxygen from bleed air to enable its use for fuel tank inerting applications. Although the primary scope of this program has been an evaluation and feasibility demonstration of separation by permeable membranes, the selection of this system from the Phase I candidates requires some additional discussion.

A true comparison of the five Phase I candidate IGG subsystems must consider current development status, potential development risk, probable development cost, initial acquisition cost, operation cost and overall reliability and maintainability considerations as well as performance parameters relating to weight, size and the penalties associated with its use of other aircraft systems such as bleed air, ram air, and so forth. While a full comparison tabulating all of the above is beyond the scope of the current program, all of these factors were considered in the selection of a system for the Phase II program.

Table 2-2 presents a summary of the performance parameters estimated from preliminary designs of DC-10 compatible systems based on the five Phase I candidate subsystems. The table considers five key performance elements for each of the candidate systems; weight, package size, bleed air consumption,

TABLE 2-2. PERFORMANCE CHARACTERISTICS SUMMARY

IGG SUBSYSTEM

IGG Type	Weight, lb	Size, in.	Bleed, lb/min	Ram, lb/min	Power, kw
Permeable membrane	174	24 x 36 x 48	30	120	2.3**
Fuel/air combustion	160*	48 x 51 x 18	15	50	0.1
Physical sorption	460	18 x 24 x 39	75	100	0.1
Chemical sorption	510	51 x 39 x 61	235	250	1.2
Air rectification	2000	72 x 72 x 72	200	500	100

REMAINING SYSTEM COMPONENTS

Component	Weight (typical), lb
Inflow valve	4.
Outflow valve (4)	30.
Emergency descent augmentation	100.

*116 if existing fire zones used
**Ground operation only

ram air consumption, and electrical power requirements. The tabulated values for each of the performance elements are for the highest requirement, which do not necessarily occur simultaneously. For all candidates however, the values given for air use (both bleed and ram) are at the design point. Based only on the tabulated performance parameters, the catalytic combustion IGG is indicated as slightly superior to the permeable membrane IGG, with the two sorption IGG systems a distant second and the air rectification system about equal in weight to an LN_2 system.

Consideration of the development status of the physical sorption system and the required reliance on adsorption rates inconsistent with apparent equilibrium conditions make this system unattractive. The chemical sorption system has an added disadvantage of excessive air penalties, largely as a result of the freon refrigeration system required to transfer the heat of chemical reaction and swing the bed temperature in a reasonable time.

While the preliminary design analysis of the Phase I program indicates that the catalytic reactor IGG system performance slightly exceeds the permeable membrane system in all tabulated performance categories, evaluation of the permeable membranes system penalties in the light of the application, particularly when compared to LN_2 storage as an alternative, show it to be essentially penalty competitive with the catalytic reactor system. In addition, the operational simplicity of the system indicates a potential for high reliability. Further, operation of a system based on the permeable membrane concept will not add a system which represents a potential ignition source (reactor bed temperatures typically exceed 1000^0F) which in turn requires the addition of, or installation into, an airborne fire zone.

Also, permeable membrane separation is not capable of the generation of any products which are not already in the bleed air stream, unlike the catalytic reactor which has some problems associated with the generation of combustion products that may require removal before introduction to the aircraft fuel system in which any contaminants would tend to accumulate and concentrate.

Two viable approaches have been identified as a result of the Phase I analysis. The catalytic reactor approach has been evaluated in some depth and programs for this purpose are currently underway. The permeable membrane

approach, although slightly heavier, offers a potential solution which has many attractive features which could easily negate the slight weight and air penalty advantage of the catalytic reactor.

Perhaps the most significant difference between these approaches is in the current development status. In recognition of the permeable membrane potential and the need for analysis and for the generation of experimental data, the permeable membrane approach was selected for the second phase of the program.

SECTION 3

HOLLOW FIBER PERMEABLE MEMBRANE INERT GAS GENERATION SUBSYSTEM INVESTIGATION

Following the completion of the tradeoff studies and selection of the hollow fiber permeable membrane IGG for further study, the second phase of the program was initiated. This Phase II program included a more detailed analysis of membrane separation and its application to an IGG subsystem for the baseline DC-10 operation. A significant part of the Phase II effort was devoted to the design, fabrication and subsequent testing of hollow fiber permeable membrane air separation test modules which successfully demonstrated the application of the separation theory and the accuracy of the mathematical model.

This section of the final report is divided into three major subsections. First, the mathematical model used for design and performance is described. (The development of the background equations used in the analysis is presented in Appendix A to this report.) Secondly, following the discussion of the analytical techniques, a preliminary design of a hollow fiber permeable membrane IGG for the DC-10 baseline design is described. The IGG subsystem is shown with the major components needed for temperature, pressure and flow controls and the subsystem operation is discussed. The third major subsection is devoted to a discussion of the test program, including the test hardware, and an evaluation of the test data.

ANALYTICAL EVALUATION

To evaluate the application of a permeable membrane IGG subsystem to the generation of inert gas for aircraft fuel system explosion suppression, it is first necessary to understand the basic phenomena of gas permeability. Literature available contains many good discussions of the work of previous experimentors who have carefully developed analytical means of describing the phenomena for a wide variety of membrane/gas systems[9,10,11,12]. A short appendix

[9] R. M. Barrer, Diffusion In and Through Solids, Cambridge Press, London, 1941

[10] C. E. Rogers Chapter "Solubility and Diffusivity" from Physics and Chemistry of the Organic Solid State, Volume II, by David Fox, et. al., 1965, Wylie

[11] R. M. Barrer, "Activated Diffusion in Membranes", page 644 of Faraday Society Transactions, Volume 35, 1939

[12] J. Crank, The Mathematics of Diffusion, Oxford Univ. Press, London 1956

(Appendix A) to this report is included to review or introduce the basic concepts and equations of permeable membrane gas transfer. The material in Appendix A is by no means a complete discussion of permeability, but is sufficient to allow the development of a mathematical model to be used for design and performance analysis. Subsequent use of the mathematical model through test performance verified the modeling results to be of sufficient accuracy for this feasibility evaluation.

Separation Principle

Membrane mass transfer is assumed to be in accordance with the activated diffusion model, that is, the gases transfer through the membrane walls by a process of first dissolving into the polymer surface, then by concentration gradient driven diffusion through the polymer and finally, evolution at the opposite surface. The combination of the processes make up permeable gas transfer. Although gas diffusion is only a part of the transfer mechanism, it usually is rate controlling allowing the surface concentration of dissolved gas to be in near equilibrium concentration with free stream gas partial pressures in accordance with Henry's Law. (A more detailed discussion of this theory is presented in Appendix A).

As derived in Appendix A, the basic relationship to describe mass transfer across a permeable membrane boundary may be described by the following equation.

$$\dot{Q}_i = \frac{TP_i \; A \; \Delta P_i}{th} \qquad (3\text{-}1)$$

where: $\dot{Q}$ = Mass transfer rate through the membrane

A = Surface area of membrane normal to the flow through the material

ΔP = Free stream partial pressure (driving force)

th = Material thickness

TP = Permeability coefficient

subscript i = i^{th} gas

This equation relates mass transfer rate to the partial pressure difference (the driving potential) in a manner similar to Fourier's relationship for heat transfer rate as a function of temperature difference as the driving potential [13]. In the equation above, the proportionality constant is called the permeability coefficient. This coefficient is ideally a function only of the polymeric membrane material and of the gas being transferred at a given temperature.

Hollow Fiber Configuration

Although the property of gas permeation through thin films of solid materials has long been recognized, and data has been collected to show that certain gases permeate through a given material more readily than do other gases, actual practical applications have been limited. With few notable exceptions, gas enrichment by the use of permeable membrane has remained a laboratory curiosity. Perhaps the major drawback limiting the application of membrane separation has been the problems encountered in scaling small laboratory test apparatus to useful separation rates.

The permeability of even the most permeable of materials is seen to be quite low when evaluated in terms of apparatus requirements for even modest separation rates. The low permeabilities require large surface areas of extremely thin membranes. Past practice has required the production of large surface areas of very thin membrane sheets. Total surface area requirement is provided by manifolding the sheets to achieve the required surface area in a compact package geometry. This presents two severe problems: (1) flat sheets of a thin material are incapable of supporting much pressure differential, and (2) a means to manifold alternate passages is required. A number of approaches to increase the structural load bearing capability of the membranes have been tried. In general, the favored approach has been to provide a second material for strength. This usually takes the form of a matrix material either in the form of a porous backing plate, or in the form of a fabric material which has been impregnated with the membrane polymer to form small flat-plate surface between fabric fibers. In either case, care must be taken to provide sufficient separation of alternate plates to allow

[13] H. S. Carslaw and J. C. Jaeger, Conduction of Heat in Solids, Second Edition, Oxford Univ. Press, 1959.

the required flow. While these techniques significantly increase the load bearing capabilities of the membrane surface, they tend to greatly increase the volume required to contain the required active surface area and further complicate the manifolding difficulties.

The second problem, that of manifolding the sheets to interconnect alternate passages, has been a troublesome problem. The difficulty here lies in the fact that not all edges are to be connected but rather adjacent passages must be separately manifolded to form alternate high and low pressure passages, each separated by the thin film membrane.

The development of small hollow fibers has provided a practical breakthrough in the solution of the structural difficulties associated with flat plates. Since hollow fibers form their own pressure vessels, no additional backing material or structural support is required. A high pressure gas stream introduced either into (or around) the hollow fibers can be supported by the proper polymeric material selection and design to limit the resultant hoop stress (or buckling load) to acceptable levels. The selection of a relatively high strength material enables self supporting tube wall thickness to be relatively thin for small tube sizes under hoop stress. In addition, the absence of the requirement for a structural backing material allows the package size to be reasonably small.

The problem of joining alternate flat plates, experienced using thin films, is reduced to manifolding tubes when hollow fiber permeable membranes are considered. This is accomplished by winding the tubes around a core in a manner similar to filament winding processes. Winding results in a continuous fiber which is further processed by [illegible] a bonding agent as a tube-sheet about each end of the unit. By [illegible] the end of the tube-sheet, the loops at the ends of the fibers are [illegible], thereby opening the tubes at the ends to form manifolded [illegible] of tubes similar in resultant structure to a tube and shell heat exchanger.

Mathematical Model

The use of equation [illegible] the [illegible] of mass transfer rates for a given gas through a permeable [illegible] barrier, if the geometry of the membrane, the partial pressure of the gas on either side of the barrier, and the permeability coefficient of the gas/membrane system is known. The

geometry (surface area and material thickness), can usually be measured, calculated, or experimentally determined; thus, the analytical prediction of mass transfer rates depends on the accuracy of the permeability coefficient and the partial pressure of the gas on each side of the membrane barrier.

For the hollow fiber geometry or this study, the surface area normal to net gas transfer is, of course, a function of radius. The surface area used for the mathematical model, and for the calculations from the test data has been based on log-mean surface area, and material thickness, the difference in radial dimension.

Although equation (A-11) yields an accurate prediction of mass transfer, based on total surface area, for a single component gas in a hollow tube, provided the velocity along the tube is low (no fluid flow pressure drop) and the gaseous environment surrounding the tube is uniform, this is not a practical case. The principal difficulty in the application of equation (A-11) to a tubular membrane separation lies in the fact that the partial pressures (even at low flow rates) of the gases vary as a function of location along the tube. The problem then, is to establish the proper mean value of partial pressures on each side of the tube if a single computation is to provide an accurate answer.

For two gas mixtures (air is herein modeled as a mixture of nitrogen and oxygen gases) at low flow rates, the total pressure remains almost constant along the tube length. This pressure is the sum of the partial pressures of both gases. For conditions where the concentration (partial pressure) of the gases change very little from end to end, the use of average values, or log-means, are generally of sufficient accuracy. For use in an IGG subystem, however, the oxygen concentration must be reduced from a nominal 21 percent to a value below 9 percent. No satisfactory means of computation of a mean tube-side partial pressure for a single calculation (for both oxygen and nitrogen gases) over the widely varying conditions encountered has been successful.

Just as the tube-side concentration varies along the length of the tube as a result of gas permeated from the high pressure stream, gas concentration along the length of the shell-side varies from the addition of the gas permeated through the tube walls. In the two-gas oxygen/nitrogen system modeled herein, this results in a reduction of oxygen concentration in the gas flowing inside the tube and an increase in the oxygen concentration around the tubes. Since

the increased oxygen concentration (partial pressure) around the tubes tends to inhibit further oxygen concentration reduction in the tube (oxygen permeation rates are reduced and nitrogen permeation rates increased), it is desirable to prevent this buildup of oxygen concentration. For a system using air, this is easily accomplished by flushing (or purging) the shell-side of the tubes with air to drive the oxygen concentration back toward 21 percent. Ideally, this results in a near constant concentration on the shell side of the tubes if the "wash" air distribution design is properly handled.

Thus, for an IGG system, the problem in computing the mass transfer of oxygen and nitrogen through the tube walls lies in the fact that this rate is a function of position along the tube based on the local value of concentration along the tube. (An analysis shows the gas diffusion rate to be several orders of magnitude greater than the permeability rate thereby allowing the assumption that, at any given distance down the tube, the tube-side gas is homogenous.) The local mass transfer rates for both gases vary as a function of their local tube-side partial pressures (which, in turn, are the cumulative result of mass transfer rates in the preceeding length of tube.) The mathematical formulation of a high pressure side element of mass or volume is further complicated by the fact that both mass and volume of the element change, due to permeation, as it proceeded down the length of the tube.

To allow the evaluation of design requirements, a tradeoff of potential materials, and evaluation of the performance of designs at a number of conditions, a mathematical model was constructed to represent the behavior of the permeable membrane/two-gas system described above. The model investigates the behavior of a single typical tube by approximating its performance in the analysis of a large number of segments. By this means, concentration variations within any one element are small. A typical element is shown in Figure 3-1. If this is the first element of the tube, its inlet conditions (pressure, flow rate, and oxygen concentration) are known. A short distance down the tube (in terms of concentration change) a second node is established.

Based on a linear concentration gradient in the small element, there exists a unique combination of conditions at the second node and permeant gas conditions which will satisfy a set of equations about that element. The major conditions which must be satisfied are the following:

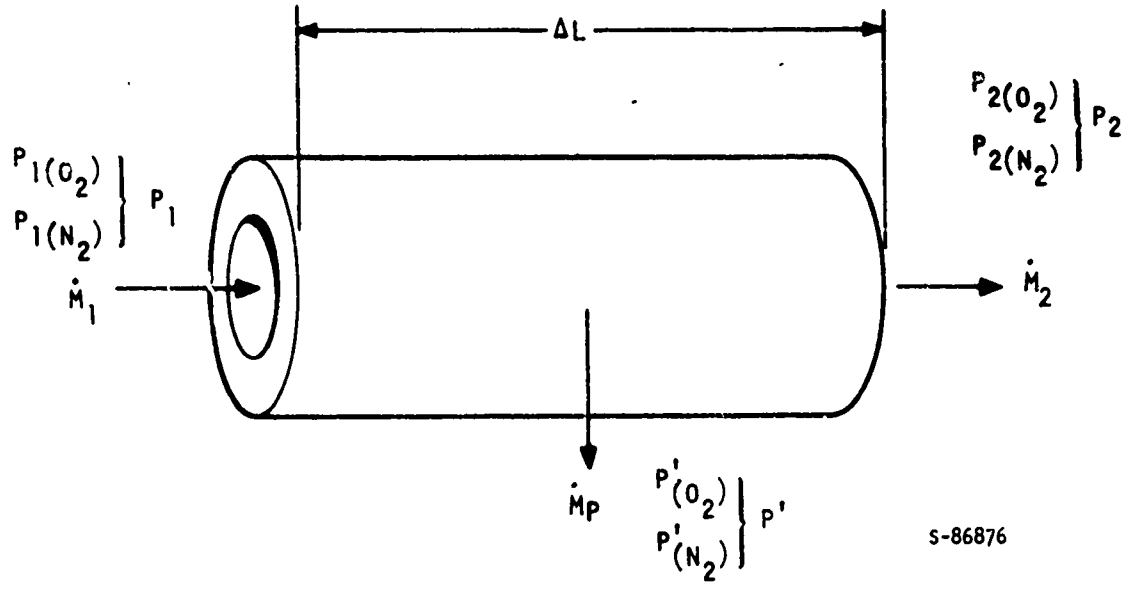

Figure 3-1. Hollow Fiber Permeable Membrane Tube Element

- Conservation of Mass

$$\dot{M}_1 = \dot{M}_P + \dot{M}_2 \tag{3-2}$$

or

$$\dot{M}_1(O_2) = \dot{M}_P(O_2) + \dot{M}_2(O_2) \tag{3-3}$$

and

$$\dot{M}_1(N_2) = \dot{M}_P(N_2) + \dot{M}_2(N_2) \tag{3-4}$$

where:

$\dot{M}$ = Mass flow rate

( ) = Denotes a particular gas

Subscripts 1 = At node 1

2 = At node 2

P = Permeating between nodes 1 and 2

- **Relationship of Partial Pressures**

$$P_1 = P_1(O_2) + P_1(N_2) \qquad (3\text{-}5)$$

and

$$P_2 = P_2(O_2) + P_2(N_2) \qquad (3\text{-}6)$$

where :

P = Tube side static pressure

P() = Partial Pressure on the tube-side

- **Permeable Membrane Mass Transfer**

$$\dot{M}_{P(O_2)} = \frac{TP(O_2)\ A_S \left(\bar{P}_{(O_2)} - P'_{(O_2)}\right)}{th} \qquad (3\text{-}7)$$

and

$$\dot{M}_{P(N_2)} = \frac{TP(N_2)\ A_S \left(\bar{P}_{(N_2)} - P'_{(N_2)}\right)}{th} \qquad (3\text{-}8)$$

where:

$\dot{M}_{P(\ )}$ = Mass permeation rate between nodes 1 and 2

$TP(\ )$ = Permeability coefficient

A_S = Log-mean surface area between nodes 1 and 2

$P(\ )$ = Tube-side mean partial pressure between nodes 1 and 2

$P'(\ )$ = Shell-side (tube environment) partial pressure

th = Tube wall thickness

There exists a unique set of values for $P_2(O_2)$, $P_2(N_2)$, $\dot{M}_P(O_2)$ and $\dot{M}_P(N_2)$ which simultaneously satisfy all seven of the equations above. Once these values are found, all conditions at node 2 are known. This enables the consideration of an additional node and then another and another. Thus, a profile of the tube-side gas flow rate and concentration, and a profile of the permeant gas flow rate and concentration is established as a function of length along the tube.

The simultaneous solution of these equations is best solved by an iteration process of guessing the conditions at node 2, solving for the permeant flow rates of both gases and then calculating the resulting conditions at node 2. The guessed and calculated values are then compared and the guess is corrected until the desired accuracy is achieved Due to the iterative nature of the solution applied to this mathematical model, a

digital computer program, in several versions for special purposes, has been devised.

Current limitations of the existing digital computer programs include a constant total tube-side pressure and a uniform shell-side concentration. Should it become desirable to consider pressure drop due to flow or shell-side concentration as a function of location, these modifications could be made. The current program (currently used in the performance mode with 100 elements) has clearly demonstrated, however, predictions of test results with considerable accuracy.

SYSTEM PRELIMINARY DESIGN

To establish the subsystem weight and size characteristics, and to determine the extent to which interface with other aircraft systems is required, a preliminary design for a fuel tank inerting system based on a hollow fiber permeable membrane IGG subsystem for the DC-10 was established. Although the purpose of the study is primarily concerned with the feasibility of the IGG subsystem, the preliminary design, shown as Figure 3-2, includes the principal ullage pressurization control valves for completeness. The total estimated system weight, including a plumbing allowance, is 320 lb using the published properties of the selected hollow-fiber membrane material subsequently discussed, at the identified optimum (6 micron) wall thickness.

The remainder of this subsection will discuss system operation followed by a brief description of components described in Figure 3-2. The major components used in the system are typical in function and type with aircraft ECS components with the exception of the air separation module (Item No. 14). The design analysis of the air separation module using polymethyl pentene polymer fiber will be discussed in some detail.

Operating Principle

Inert gas generated by the fuel tank inerting system pressurizes and purges the fuel tanks continuously maintaining a non-flammable gas mixture over the fuel. For the operating range of the DC-10 and the type of fuel employed, non-flammability of the nitrogen oxygen-fuel vapor mixture in the tank ullage is ensured if the oxygen concentration is always less than 9 percent by volume. (Air contains a nominal 21 percent oxygen by volume.) The membrane-type inerting system described here is designed to maintain an

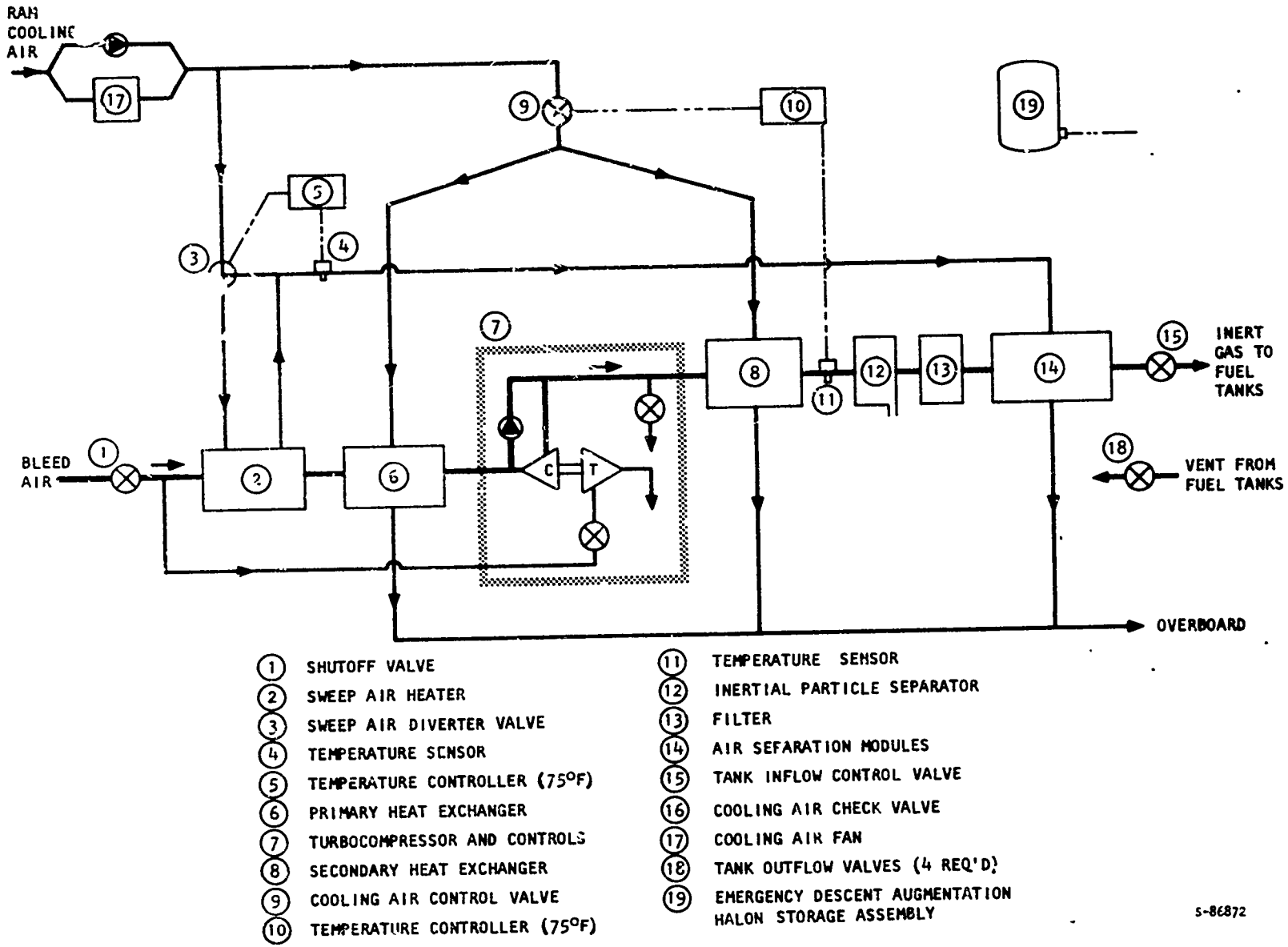

Figure 3-2 Schematic Diagram, Permeable Membrane Fuel Tank Inerting System

inert ullage mixture in two ways: (1) by supplying a nitrogen-rich air mixture containing less than 9 percent oxygen under all normal flight conditions and (2) by providing adequate inert sweep flow in excess of pressurization demands to purge the oxygen-rich mixture that evolves from solution in the fuel during climb and cruise flight when tank pressure is decreasing.

The inerting system generates nitrogen-rich air from normal air by utilizing the selective permeability properties of a selected membrane material, which exhibits several times greater permeability to oxygen than to nitrogen. If a pressurized airflow passes through a tube of this material, the gas mixture permeating through the tube wall is oxygen-rich relative to the incoming airflow and, therefore, the gas mixture in the tube becomes progressively more nitrogen-rich as it passes down the tube. If the tube is long enough, the mixture approaches a limiting concentration which is a function of the pressures as described in Appendix A.

Design Point Selection

Initial tradeoff studies were performed to optimize the preliminary design of the permeable membrane IGG for the DC-10 baseline aircraft. In these studies, inert gas requirements for the fuel tank ullage were calculated for the combined inflow demands during aircraft normal flight profiles. These inert gas requirements included ullage volume pressurization due to fuel consumption and descent repressurization, as well as ullage sweep requirements.

The system performance analysis was calculated using a computer to predict the permeable membrane design performance. Engineering analysis was conducted on a system level to optimize system design based on membrane design.

The first step involves the use of computer techniques for membrane design. The first computer program utilized is the flight design requirements program. Ullage gas inflow demands based on the combined inflow demand equation, previously established in Section 2, are determined by the flight profile information; inert gas requirements are established for the entire mission.

Secondly, these inert gas requirements are combined with the aircraft flight profiles for altitude, bleed air, supply air, and other aircraft services in the membrane design program. Different flight points are evaluated until the design condition is established. This condition is based on the varying parameters of inert gas flow and aircraft services which determines the largest membrane design.

Following establishment of the design point condition, the membrane performance program is used to analyze performance at any given flight condition throughout the mission profile.

The last step in the system performance process is engineering analysis of the system components and their final integration into a system level design.

Results of the analysis has selected the high speed descent at 12,500 foot altitude as the critical design point for this feasibility study based on the DC-10 flight profiles as discussed in section 2. Other conditions at this point are as follows:

- Bleed air pressure — 57 psia
- Bleed air temperature — 425°F
- Ambient pressure — 9.2 psia
- Ambient temperature — 75°F
- Required inert gas inflow (at 60°F) — 13.2 lb/min

A sample digital computer program output sheet is shown as Figure 3-3. The data tabulated in Figure 3-3 shows bleed air pressure at the inlet to the air separator module as 113 psia (following boost by the turbocompressor, and allowing for heat exchanger pressure loss) and local ambient ram air pressure as 9.2 psia. The theoretical minimum oxygen concentration (per the method of Appendix A) is 2.2 percent by volume. The physical characteristics used in the calculation are for 34.5 million fibers of a nominal 50 microns (0.002 in.) inside diameter and 6 microns (0.000235 in.) wall thickness with an active transfer length of 40.3 inches. ICI literature[14] values of permeability coefficients (27.0×10^{-10} and 6.5×10^{-10} $(cm^3/sec\ @\ NTP)\ (cm)/(cm^2)(cm\ Hg)$ for oxygen and nitrogen respectively) are assumed.

The separation profile in Figure 3-3 (in the printout prepared for this report, 25 elements are shown; actual analysis was conducted with 100 elements), shows the distribution of the 21.8 lb/min of bleed air required at the air

separator inlet tabulated as a function of tube length. The profile is divided into three major subsections, that is, "tube length", "inside tube (nitrogen enriched air)", and "permeant (oxygen enriched air)". Tube length is tabulated for both absolute length (inches) and in terms of percent of total length.

The tube-side profile gives bleed air flows in absolute units (lb/min) and in terms of percent of inlet flow. The velocity and oxygen concentration are also tabulated at each of the 26 nodes.

The properties of the bleed air as it permeates in the tube section between each of the nodes is tabulated in the third major column. The rate of gas permeation between each is shown, again, in absolute units (lb/min) and in terms of percent of the bleed air at the air separation module inlet. Finally, the oxygen concentration of the gas permeating between the nodes is tabulated.

The profile shows that at the end of the 25th element, the oxygen concentration has been reduced to 8.9 percent by volume. The summation of oxygen and nitrogen mass permeation rates shows 8.6 lb/min to be permeated (at an integrated oxygen concentration of approximately 40 percent) resulting in the required inert gas flow rate of 13.2 lb/min. Also shown at the bottom of the profile are the log-mean surface area (67,500 ft^2), the frontal area, based on the summation of individual tube outside diameters (165 $in.^2$) and the weight of the polymethyl pentene required to establish the active area (69 lb).

System operation at 40,000 foot cruise has been selected as an example of off-design point operation for the air separation module. Figure 3-4 shows a 1 lb/min inert gas demand flow which, at the 28.1 psia inlet pressure (no boost compressor) requires under 3 lb/min of manifold bleed air. Inert gas oxygen concentration is at 3.9 percent, approaching the 2.6 percent theoretical limit under these conditions. The hollow fiber permeable membrane based IGG is grossly over-sized for this condition, although over 80 percent of the flight is represented by this low output performance.

[14] Imperial Chemical Industries Ltd., Plastics Division, Welwyn Garden City, England, "TP X TM Methylpentene polymers", Technical Bulletin 252.

FINAL REPORT EXAMPLE OF DC-10 AIR SEPARATION DESIGN ANALYSIS
HIGH SPEED DESCENT - 12,500 FT

*** DESIGN CONDITIONS ***

BLEED AIR PRESSURE (PSIA)	INLET MASS FLOW RATE (LBM/MIN)	RAM AIR PRESSURE (PSIA)	THEORETICAL OXYGEN CONCENTRATION LIMIT (PERCENT)
113.000	21.786	9.170	2.199

** MEMBRANE CHARACTERISTICS ** 34,500,000 TUBES

TUBE INSIDE DIAMETER (IN)	TUBE WALL THICKNESS (IN)	PERMEABILITY COEF O2	PERMEABILITY COEF N2
.00200	.00003	27.00-10	6.50-10

*** MEMBRANE SEPARATION PROFILE ***

TUBE LENGTH (IN)	TUBE LENGTH (PERCENT)	INSIDE TUBE (NITROGEN ENRICHED AIR) BLEED AIR MASS FLOW (LBM/MIN)	BLEED AIR MASS FLOW (PERCENT)	VELOCITY (FT/SEC)	O2 CONC (VOL PCNT)	PERMEANT (OXYGEN ENRICHED AIR) BLEED AIR MASS FLOW (LBM/MIN)	BLEED AIR MASS FLOW (PERCENT)	O2 CONC (VOL PCNT)
.0000	.0000	21.7864	100.0000	.8864	21.0000			
						.3990	1.8357	52.0324
1.6120	4.0000	21.3868	98.1643	.8728	20.4440			
						.3948	1.8123	51.1039
3.2240	8.0000	20.9916	96.3520	.8573	19.8911			
						.3898	1.7891	50.1593
4.8360	12.0000	20.6018	94.5629	.8420	19.3419			
						.3848	1.7660	49.2001
6.4480	16.0000	20.2171	92.7968	.8269	18.7966			
						.3798	1.7431	48.2248
8.0600	20.0000	19.8373	91.0537	.8120	18.2557			
						.3748	1.7204	47.2350
9.6720	24.0000	19.4625	89.3333	.7973	17.7195			
						.3699	1.6979	46.2294
11.2840	28.0000	19.0926	87.6354	.7827	17.1886			
						.3651	1.6756	45.2112
12.8960	32.0000	18.7275	85.9597	.7683	16.6632			
						.3603	1.6536	44.1810
14.5080	36.0000	18.3672	84.3061	.7541	16.1437			
						.3555	1.6319	43.1373
16.1200	40.0000	18.0117	82.6742	.7400	15.6303			
						.3508	1.6104	42.0822

17.7320	44.0000	17.6609	81.0639	.7261	15.1240	.3462	1.5892	41.0162
19.3440	48.0000	17.3147	79.4747	.7123	14.6246	.3417	1.5682	39.9401
20.9560	52.0000	16.9730	77.9064	.6988	14.1327	.3372	1.5477	38.8561
22.5680	56.0000	16.6358	76.3588	.6853	13.6486	.3328	1.5274	37.7652
24.1800	60.0000	16.3030	74.8313	.6721	13.1727	.3284	1.5076	36.6682
25.7920	64.0000	15.9746	73.3238	.6590	12.7053	.3242	1.4881	35.5658
27.4040	68.0000	15.6504	71.8357	.6460	12.2467	.3200	1.4689	34.4591
29.0160	72.0000	15.3304	70.3668	.6332	11.7972	.3159	1.4502	33.3491
30.6280	76.0000	15.0144	68.9166	.6205	11.3573	.3119	1.4318	32.2391
32.2400	80.0000	14.7025	67.4848	.6080	10.9271	.3080	1.4139	31.1303
33.8520	84.0000	14.3945	66.0710	.5956	10.5069	.3042	1.3964	30.0239
35.4640	88.0000	14.0902	64.6746	.5834	10.0969	.3005	1.3793	28.9214
37.0760	92.0000	13.7897	63.2952	.5712	9.6975	.2969	1.3627	27.8240
38.6880	96.0000	13.4929	61.9325	.5593	9.3087	.2934	1.3465	26.7332
40.3000	100.0000	13.1995	60.5860	.5474	8.9309			

** PERMEANT FLOWS **

OXYGEN (LBM/MIN)	NITROGEN (LBM/MIN)	TOTAL (LBM/MIN)	O2 CONC (VOL. PCNT)
3.7446	4.8423	8.5869	40.3713

** SURFACE AREA ** (SQ FT)	** FRONYAL AREA ** (SQ IN)	** MATERIAL WEIGHT ** (LBF)
6.754+04	165.307	68.769

Figure 3-3. Sample Computer Output Design Point Performance

FINAL REPORT EXAMPLE OF DC-10 AIR SEPARATION DESIGN ANALYSIS
40,000 FT CRUISE, STANDARD DAY

*** DESIGN CONDITIONS ***

BLEED AIR PRESSURE (PSIA)	INLET MASS FLOW RATE (LBM/MIN)	RAM AIR PRESSURE (PSIA)	THEORETICAL OXYGEN CONCENTRATION LIMIT (PERCENT)
28.100	2.869	2.730	2.622

** MEMBRANE CHARACTERISTICS ** 34,500,000 TUBES

TUBE INSIDE DIAMETER (IN)	TUBE WALL THICKNESS (IN)	PERMEABILITY COEF O2	PERMEABILITY COEF N2
.00200	.00023	27.00-10	6.50-10

*** MEMBRANE SEPARATION PROFILE ***

TUBE LENGTH (IN)	TUBE LENGTH (PERCENT)	INSIDE TUBE (NITROGEN ENRICHED AIR) BLEED AIR MASS FLOW (LBM/MIN)	BLEED AIR MASS FLOW (PERCENT)	VELOCITY (FT/SEC)	O2 CONC (VOL PCNT)	PERMEANT (OXYGEN ENRICHED AIR) BLEED AIR MASS FLOW (LBM/MIN)	BLEED AIR MASS FLOW (PERCENT)	O2 CONC (VOL PCNT)
.0000	.0000	2.8686	100.0000	.4704	21.0000			
						.0972	3.3875	51.6255
1.6120	4.0000	2.7714	96.6125	.4551	19.9712			
						.0948	3.3060	49.8453
3.2240	8.0000	2.6765	93.3065	.4402	18.9562			
						.0925	3.2259	48.0162
4.8360	12.0000	2.5840	90.0807	.4255	17.9571			
						.0903	3.1471	46.1359
6.4480	16.0000	2.4937	86.9336	.4112	16.9767			
						.0881	3.0698	44.2094
8.0600	20.0000	2.4057	83.8638	.3972	16.0175			
						.0859	2.9944	42.2423
9.6720	24.0000	2.3198	80.8694	.3835	15.0818			
						.0838	2.9209	40.2380
11.2840	28.0000	2.2360	77.9484	.3702	14.1722			
						.0817	2.8496	38.2063
12.8960	32.0000	2.1543	75.0988	.3571	13.2909			
						.0798	2.7806	36.1524
14.5080	36.0000	2.0745	72.3182	.3443	12.4400			
						.0779	2.7142	34.0865
16.1200	40.0000	1.9966	69.6040	.3317	11.6217			
						.0760	2.6504	32.0180

17.7320	44.0000	1.9206	66.9337	.3194	10.8375	.0743	2.5893	29.4548
19.3440	48.0000	1.8463	64.3643	.3074	10.0893	.0726	2.5312	27.9105
20.9560	52.0000	1.7737	61.8331	.2956	9.3783	.0710	2.4762	25.8944
22.5680	56.0000	1.7027	59.3569	.2840	8.7055	.0695	2.4241	23.9166
24.1800	60.0000	1.6331	56.9328	.2727	8.0719	.0681	2.3753	21.9913
25.7920	64.0000	1.5650	54.5575	.2615	7.4781	.0668	2.3296	20.1263
27.4040	68.0000	1.4982	52.2280	.2506	6.9242	.0656	2.2871	18.3349
29.0160	72.0000	1.4326	49.9409	.2398	6.4105	.0645	2.2477	16.6240
30.6280	76.0000	1.3681	47.6932	.2291	5.9361	.0634	2.2115	15.0033
32.2400	80.0000	1.3047	45.4817	.2186	5.5010	.0625	2.1784	13.4807
33.8520	84.0000	1.2422	43.3033	.2083	5.1043	.0616	2.1483	12.0619
35.4640	88.0000	1.1806	41.1550	.1980	4.7448	.0608	2.1211	10.7501
37.0760	92.0000	1.1197	39.0338	.1879	4.4214	.0601	2.0967	9.5497
38.6880	96.0000	1.0596	36.9372	.1779	4.1325	.0595	2.0750	8.4614
40.3000	100.0000	1.0000	34.8622	.1680	3.8765			

** PERMEANT FLOWS **

OXYGEN (LBM/MIN)	NITROGEN (LBM/MIN)	TOTAL (LBM/MIN)	O2 CONC (VOL PCNT)
.6241	1.2444	1.8685	30.5098

** SURFACE AREA ** (SQ FT)	** FRONTAL AREA ** (SQ IN)	** MATERIAL WEIGHT ** (LBF)
6.754+04	165.307	68.769

Figure 3-4. Sample Computer Output Off-Design Performance

System Operation

The operation of a hollow fiber permeable membrane IGG based fuel tank inerting system requires interface with several existing aircraft systems. In addition to the membrane air separation device, the fuel tank inerting system requires several additional components for regulating air flows, pressures, temperatures, and cleanliness. Figure 3-2 shows a schematic diagram of the arrangement of these components in the inerting system.

Typical performance of a hollow fiber permeable membrane IGG is shown in Figure 3-5. The altitude profile shown is for a DC-10 long range descent profile. For standard day conditions, with inflow gas temperatures at 60°F and a near zero fuel load at landing, the performance of a subsystem designed to peak at 9 percent oxygen concentration is shown. The curve plots both the average ullage gas mixed concentration and the instantaneous inflow composition. As the aircraft descends, the instantaneous concentration increases from the 3 to 4 percent value experienced during the extended cruise period. Actual instantaneous concentrations begin to peak at about 8 percent at about 22,000 foot altitude. However, at about 9,000 feet, the crossbleed manifold pressure becomes limited by the bleed air system's 48 psig pressure regulator, resulting in a further increase in instantaneous oxygen concentration from the IGG. At 2500 foot elevation, the aircraft descent profile decreases. At that point the peak allowable instantaneous inflow concentration of 9 percent is achieved.

The average ullage composition tends to damp the fluctuations in instantaneous values, however the influences at lower altitude are considerable due to increased density of the inflow gas. Thus, the average composition tends to follow the instantaneous concentration.

1. Inert Gas Flow

For the DC-10 application the inerting system air supply is preconditioned engine bleed air taken from the aircraft crossbleed manifold which also supplies air to the environmental control system and other aircraft systems. Manifold air has been precooled to a maximum 425°F and pressure regulated to limit crossbleed manifold to a nominal 48 psig. This preconditioned bleed

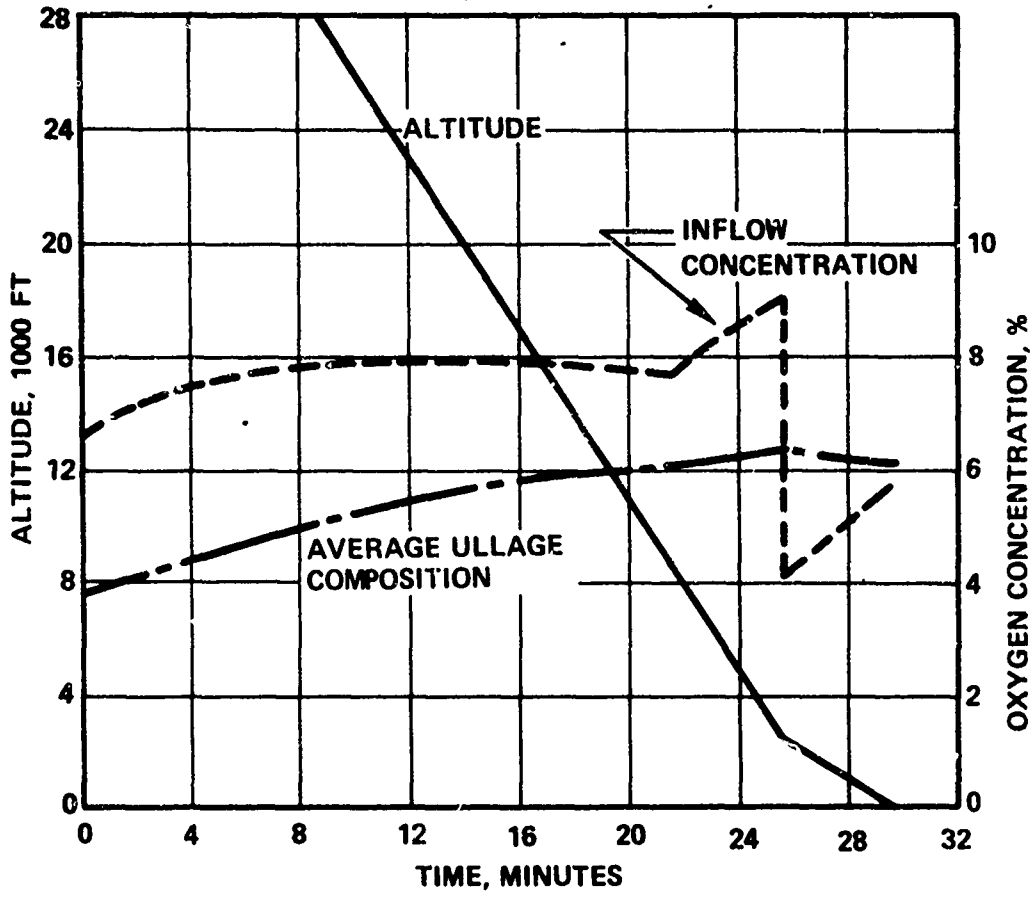

Figure 3-5. Typical Membrane IGG Performance

air enters the inerting system through a shutoff valve (Item 1) and passes through the sweep air heat exchanger (Item 2) and the primary heat exchanger (Item 6) in series where it is cooled by heat transfer to ram air.

The bleed air next flows to the turbocompressor (Item 7) which, during the high flow rate demands of aircraft descent (and during ground operation and climb when high ullage purge flows are desired), boosts the bleed air pressure by a nominal 2:1 compression ratio. Since the membrane separator performance is directly related to pressure difference across the tube walls, this bleed air pressure increase reduces the membrane surface area required during descent when engine bleed pressure is low and inerting flow demand for tank pressurization is high. It is desirable to operate the turbocompressor during climb to produce a low-oxygen-content purge flow to remove oxygen evolving from the fuel as tank pressure reduces with altitude. Turbocompressor operation is not necessary during cruise, the greatest portion of the total flight time, because engine bleed pressure is adequate to meet the low inert gas flow demand.

The turbocompressor assembly, in addition to the radial compressor-turbine rotating assembly, includes all necessary valves and controls. When turbocompressor operation is required, an externally-supplied signal opens the turbine speed control valve admitting bleed air to drive the unit. Turbine exhaust air discharges overboard. The speed control valve modulates the turbine inlet pressure, as required, to maintain the design operating speed. To prevent compressor surging when the demand for inerting flow is low, a surge bleed valve modulates open, discharging bleed flow overboard as required to keep the compressor flow above the surge value. When the compressor is not operating, system bleed flow passes around the compressor through the bypass check valve.

Leaving (or bypassing) the compressor, the bleed air is further cooled by ram air in the secondary heat exchanger (Item 8). Prior to entering the membrane air separation module, the air is cleaned in a two-stage filtration process and removes contaminant particles which could clog the small diameter (nominal 50 micron) membrane tubes. The first filtration stage is an inertial dirt separator (Item 12) designed for high pressure airflows. The static device imparts a tangential swirl to the air stream causing solid particles

to centrifuge outward where they are diverted from the main air stream and exhausted overboard along with approximately two percent of the total airflow. Remaining contaminants, down to the 2-micron size are eliminated by the second-stage particle filter (Item 13).

The bleed air then passes through the membrane air separation module (Item 14) where an oxygen rich gas mixture permeates through the tube walls leaving a nitrogen-rich concentration at the module outlet. To prevent an oxygen concentration buildup outside of the tubes, and the resultant loss of concentration efficiency, the gases permeating through the tube walls are swept away by a proportionally large flow of ram air which enters the center of the cylindrical tube bundle and flows radially outward over the tubes before discharging to ambient.

Inert gas, containing less than nine percent oxygen, is admitted to the fuel tank ullages by the tank inflow control valve (Item 15), as required, to maintain a fixed gauge pressure (about 0.3 psig) relative to ambient. In addition, the valve may be set to maintain a purge flow rate (about 1 to 4 lb/min as required) regardless of pressurization requirements, to remove any oxygen-rich gases which may come out of solution in the fuel.

Fuel tank ullage pressures are also maintained by the redundant pairs of tank outflow valves (Item 18) which begin opening at approximately 0.5 psig venting tank ullage pressure to ambient. When tank pressurization demand exceeds any pre-set purge flow, tank pressure will be controlled by the inflow valve. When purge flow exceeds the flow required for pressurization and during certain types of ascents, tank pressure will be controlled by the outflow valves which are also sized to relieve tank pressure in the event of an inflow valve failure.

2. Temperature Control

To maintain the temperature dependent permeability coefficients in the optimum design range, it is necessary to keep the bleed air passing through the air separator at about 75° to 100°F, a temperature range also suitable for the fuel tank inert gas supply. Since the membrane canister is an excellent heat exchanger, it is necessary to keep the ram air also at 75° to 100°F to prevent it from cooling the bleed air below the desired temperature range. The system incorporates two sets of temperature controls for regulating both the bleed air and the separator ram air temperature.

Before reaching the membrane unit, ram sweep air passes through a diverter valve (Item 3) which divides the sweep flow between the sweep air heat exchanger and a bypass line. Sweep air heated in the heat exchanger recombines with the bypass air and the resulting mixed temperature is measured by the temperature sensor (Item 4) which provides an electrical analog signal of the sensed temperature to the electronic controller (Item 5). The controller compares the sensed temperature with the desired temperature and sends the appropriate electrical signal to the diverter valve. An electropneumatic device on the valve translates the electrical signal to a pneumatic signal which in turn moves the valve to the commanded position. On hot days, when ram air temperature exceeds the control temperature range, the valve will divert the entire sweep airflow to bypass the heat exchanger.

Bleed air temperature is controlled to 75° to 100°F in a similar manner. Signals from a temperature sensor (Item 11) at the separator module bleed inlet are received by the controller (Item 10) which in turn provides command signals to an electropneumatic ram cooling air valve (Item 9). The valve in turn modulates ram cooling airflow through the primary and secondary heat exchangers, as required, to achieve the desired bleed temperature.

3. Ground Cooling Air Supply

During flight, the ram air pressure created by the aircraft's forward motion is sufficient to provide sweep air for the membrane separator and cooling air for the heat exchangers. During ground operation, when no ram pressure exists, an electric-motor-driven fan (Item 17) provides the necessary flows. The fan motor relay can be connected to the aircraft squat switch to turn on and off automatically. During flight, ram air bypasses the inoperative fan through a check valve (Item 16).

4. Emergency Descent Provisions

Certain failures of other systems can cause a rapid cabin depressurization as a result of which the aircraft will be flown rapidly to low altitudes following an emergency descent profile. The rapid descent rates require large inert gas flow rates so that tank repressurization can keep pace with the rapidly increasing atmospheric pressure outside of the tanks. An IGG system designed for the emergency descent profile would be heavier and larger than a system for normal flight operations.

Rather than penalize the aircraft to accommodate a rare occurrence, the proposed system is designed for normal flight profiles only. The resultant total redundancy will enhance overall reliability and is not inconsistent with logistics free operation following an emergency situation where rapid turn-around is not a normal requirement. The emergency descent augmentation selected for this preliminary design is a fluorocarbon fire extinguishing agent (Halon 1301) delivered from an onboard storage tank. When an emergency descent condition is sensed, detonator-actuated burst disks actuate admitting Halon to the fuel tanks. The Halon supply is adequately sized to inert the fuel tanks for the duration of the emergency descent without assistance from the inert gas generating system.

5. Typical Operating Conditions

Although several representative flight conditions could be presented, the heat exchanger design point is presented here as a typical example of system operation. The selected example occurs at a 2500 foot altitude during long range descent on a hot day.

At this point in the descent profile, the demand flow rate to the fuel ullage is 11.2 lb/min (at 60°F). This requires 35.4 lb/min (at 425°F) of bleed air from the bleed air crossmanifold, which is at 60 psia. The compressor requires 15.4 lb/min of the bleed air to boost the pressure of the remaining bleed air to 118 psia, the pressure at the separator module inlet. Ram air, at 14.5 psia and 111°F enters the ram air distribution ducts at 110 lb/min. While 30 lb/min of ram air is used to sweep the air separation module of oxygen rich by-products, 80 lb/min is required for the two (primary and secondary) bleed/ram heat exchangers for reduction of the bleed air temperature to 144°F at the inlet to the air separation module.

Due to the hot day conditions, the sweep air diverter valve bypasses the entire 30 lb/min sweep air around the sweep air heater. The hot day conditions result in hot air at 115°F (though only 4°F hotter than ambient) being input to the ullage. The nominal 8 percent oxygen product is finally throttled by the tank inflow control valve to ullage control pressure.

Component Description

The following brief component description of the particle filters and the air separation module are provided to establish the characteristics of these, the only components not a normal part of an aircraft ECS.

1. Item 12, Inertial Dirt Separator

This unit is a vortex generator that centrifically separates airborne particles while clean air continues its flow through the unit. The separator utilizes a partial reverse flow concept and consists of a static swirl vane section which imparts a centrifugal motion to the entrained inlet air, a collector into which the centrifuged dust is accumulated and discharged, a vortex tube which creates partial reverse air flow and static deswirling vanes at the separator exit. The separated particles are collected in a quiescent manifold chamber and discharged to ambient by scavenging approximately 2.5 percent of the bleed air supply flow.

This same design principle is utilized in the F-15 air cycle refrigeration system in the cabin water separator with approximately 90 percent moisture separation. Testing performed by the Air Force Aerospace Research Laboratory for dust particle separation shows the unit to have separation efficiencies in the range of 70 to 75 percent for fine road dust (0-5μ) and approximately 90 percent for coarse road dust (0-200 μ) composition.

At the system design condition the separator inlet conditions are:

Pressure, psia	115
Temperature, ^{o}F	100
Flow, lb/min	21 (≈40 cfm)

2. Item 13, Filter

This filter provides further filtration of the bleed air inlet to the permeable membrane canister, Item 14, following particle contaminant removal in the inertial dirt separator, Item 12. Conservative estimates of membrane fiber filtration show requirements to be in the two micron range for inlet gas.

In this preliminary design, two types of filter elements are considered. Selection of a final filter design will be based upon the final filtration requirements dictated for the permeable membrane fibers as well as survivability of the filter during flight environment. The first filter considered is of the Balston microfiber type which comprises a medium of glass microfibers bonded with epoxy resin. The bonded fibers are arranged into tubes 2 in. in diameter, 1/8 in. thick and six filter elements are arranged in a circular configuration within an aluminum canister. Filtration utilizing Balston Grade A or Grade B tubes are rated 2 microns "absolute" and 2 microns "nominal" respectively. The second filter under consideration is a single pleated wire mesh type. This filter is rated at 10 microns absolute and 6 microns nominal and its configuration consists of a single wire mesh element housed in an aluminum canister similar to the Balston type.

In the event that 2-micron filtration is required and the epoxy bonded glass fiber matrix is not usable, it is possible to increase the rating of the pleated wire mesh filters by colandering and sinter-bonding, however, this process is expensive and somewhat inconsistent in pore size control. Maintainability costs of both elements are similar on a one time basis since

the Balston filter element cost is estimated to be nearly identical to the unsintered mesh filter cleaning cost, however, any maintainability cost advantage will be determined on relative replacement times.

If final establishment that a 2-micron filtration is required, the mesh filter must be considered for the following reasons. Although the Balston filter rating is better than that of the mesh filter, a bonded glass fiber matrix may not be stable in an aircraft vibration and shock load environment. In addition, the Balston tubes must be discarded and replaced by new elements when particle accumulation raises filter pressure drop, however, the mesh filter element can be cleaned and reused.

3. Item 14, Air Separation Module

This unit is a cylindrical aluminum canister which contains hollow fiber membranes where gas permeation takes place and an inert gas is produced. High pressure bleed air enters the membrane tube inlets, which are 0.002 in. (50μ) inside diameter and 0.000235 in. (6μ) wall thickness, and oxygen from the bleed air permeates through the tube walls. The large number of tubes (34.5 million) and the active tube length (40.3 in.) results in a large active surface area for permeation of approximately 67,500 sq ft. Oxygen permeates through the tube walls at a faster rate than nitrogen resulting in a low oxygen concentration at the tube outlets.

Physically the membrane fibers are spirally wrapped around the perforated ram air inlet tube, and ram air passes down through the center axis of this tube. It then flows radially outward over the membrane fibers, enters a circumferential exit annulus and is vented overboard. The membrane fibers are epoxied together at both bleed air entrance and exit with a plenum at each end for gas distribution.

For an air separation module, packaged as a single unit, the overall length is estimated to be 50 inches, the diameter 24 inches, and the assembled weight to be 90 pounds. Actual practice may, however, form the packaging of the air separation modules into smaller units for reasons of maintenance, commonality of equipment with smaller aircraft systems, and so forth. This would result in a slight weight increase.

Air Separation Module Design

The preliminary design for the DC-10 hollow fiber permeable membrane based IGG is based on design analysis to optimize the subsystem for the application. Many of the subsystem parameters directly affect, and are directly affected by, the air separation module design. To evaluate the subsystem effects of membrane material, fiber geometry, operating pressure, ram air sweep flow, and so forth, the iterative digital computer program was utilized as a design analysis tool. Actual DC-10 design requirements were then considered for a wide range of potential solutions.

One of the first chores for the digital computer mathematical model was the selection of a preliminary design fiber material from numerous potential candidates. The tabulation of a single numerical value as a "merit parameter" for material selection proved unsatisfactory due to the complex relationship of a large number of important considerations. Among these are material density, the permeability properties to oxygen and to nitrogen, and the ratio of those permeability coefficients. Structural properties are also important. A good material must have a high hoop strength, but in addition, should show low fatigue sensitivity and should not be brittle at the operating temperatures. Also important are a high elastic modulus and low thermal expansion coefficient. Finally, the material must be resistant to potential contaminants such as aircraft fluids which could degrade performance. Especially important for the feasibility program was that the material be available and readily manufactured into the desired form.

A large number of available materials were evaluated for the feasibility demonstration. Table 3-1 shows the comparisons of two materials, polymethyl pentene and silicone rubber. While silicone rubber seems a good choice due to its high permeability coefficient to oxygen, the lesser permeable polymethyl exhibits a superior separation factor (ratio of permeability coefficients) and considerably superior structural properties. Without the aid of detailed systems analysis, a superficial examination may have resulted in the selection of the maximization of oxygen permeability as the sole merit parameter. Analysis, however, shows polymethyl pentene to be a superior candidate than silicone rubber.

TABLE 3-1 MEMBRANE PROPERTIES

Property	Membrane Material	
	Polymethyl pentene[14]	Silicone rubber[15]
Permeability coefficient (oxygen)	27.0*	220*
Permeability coefficient (nitrogen)	6.5*	110*
Separation factor	4.15	2.0
Density, lb/ft^3	51.8	65.5
Modulus of elasticity, 10^5 psi (68°F)	1.6 - 2.1	-
Tensile strength at yield, psi (68°F)	3500 - 4000	~3000
Elongation at yield, % (68°F)	~2	~550
Elongation at break, %	13 - 20	-
Thermal expansion, in/in - °C	11.7×10^{-5}	-
Stability to degradation	1 yr at 260°F	200°F continuous
Burning rate, in/min	1.0	-
Resistance to sunlight	Poor	-
Resistance to acids and alkalies	Good	-
Resistance to oils	Good	-

*$\times 10^{-10}(cm^3/sec\ @\ NTP) \times (cm)/(cm^2) \times (cm\ Hg)$

To determine optimum material and tube size, several effects must be simultaneously considered. These are the effects of laminar flow pressure drop due to flow, the stress (or modules) relationship between pressure, tube diameter and required wall thickness, and the state-of-the-art in tube manufacture. Figure 3-6 shows the relationship for pressure loss as a function of gas velocity for tubes of various diameters from 20 to 600 microns. The data plotted is for nitrogen gas at 70°F, but is fairly representative of low oxygen concentration air. Since design analysis indicates that pressure loss at maximum flow should be limited to 5 to 8 psi, a relationship for tube diameter, tube length, and the number of tubes (gas velocity) can be established.

[15] "General Electric Permselective Membranes", Medical Development Operation Chemical and Medical Division, General Electric Co.

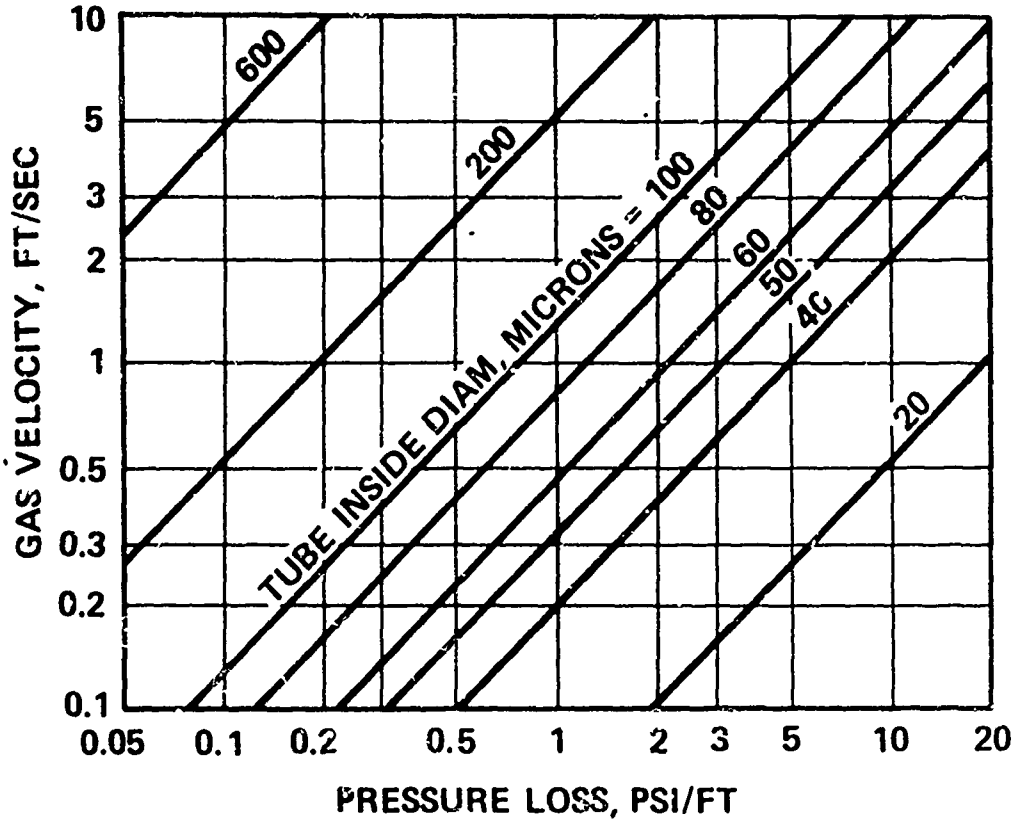

NOTE: 1 INCH = 25,400 MICRONS

SPA 3241-62

Figure 3-6. Pressure Drop in Membrane Tubing

For a margin of safety, it was decided to limit hoop stress to 33 percent of the published values for the candidate materials. For both candidates shown in Table 3-1, this works out to about 1000 psi. However, due to the low modulus of elasticity of silicone rubber, this would result in an elongation of over 100 percent. Obviously an additional structural criteria was required. An arbitrary (albeit high) limit of 10 percent elongation limit was imposed. This resulted in a design working stress of 100 psi for the silicone rubber. Figures 3-7 and 3-8 show the required tube wall thickness for polymenthyl pentene and silicone rubber respectively for various tube diameters and tube pressures. Also shown are estimates of manufacturing minimum tube wall thickness for various diameters of the two materials. As can be seen from Figures 3-7 and 3-8, tube diameters

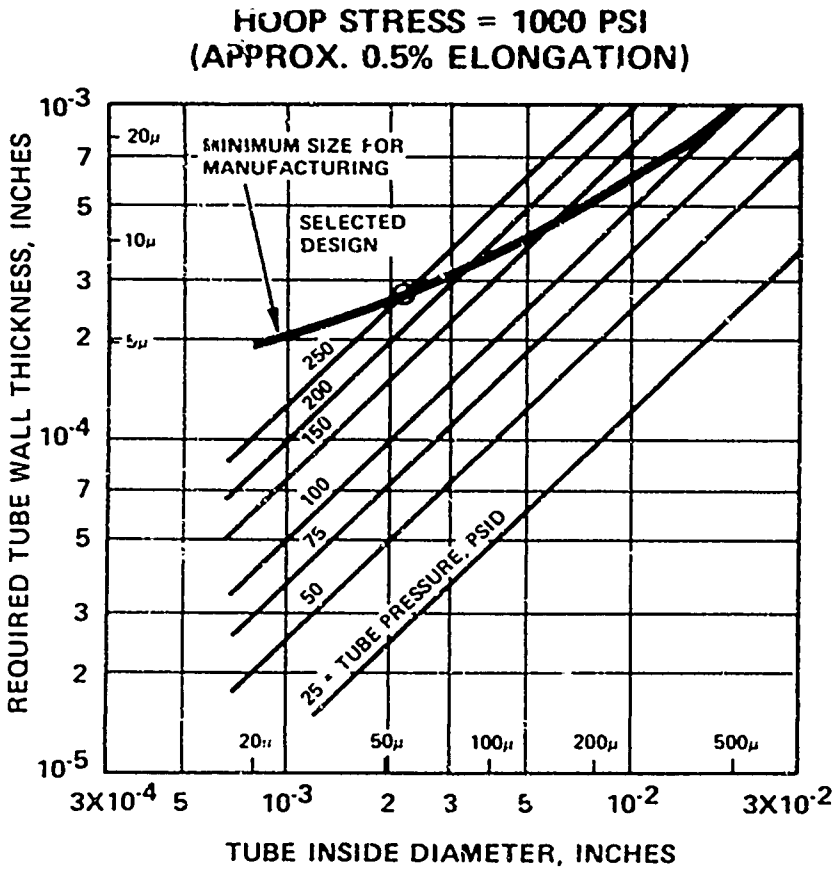

SPA 3241-61

Figure 3-7. Polymethyl Pentene Structural Considerations

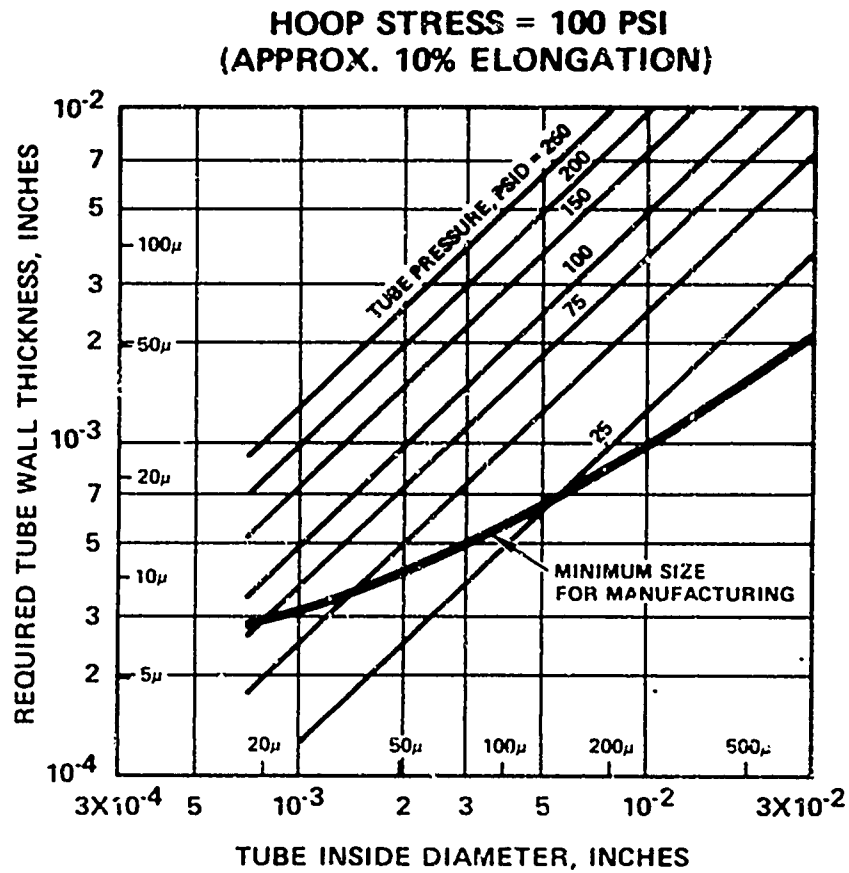

Figure 3-8. Silicone Rubber Structural Considerations

in the 20 to 100 micron range and pressures in the 50 to 200 psid range generally result in polymethyl pentene tubes of wall thickness determined by manufacturing limitations, while silicone rubber tubes are limited by structural requirements.

From the above considerations, a nominal 50 micron tube diameter was selected. Two design points were initially considered from the DC-10 descent requirements shown in section 2. The first condition is for a standard day high speed descent at 12,500 foot altitude resulting in an inert gas inflow requirement of 13.2 lb/min. The second point is for a long-range descent at 2500 foot altitude, which requires 11.2 lb/min. Both conditions were assumed to allow a peak instantaneous inflow concentration of 9 percent oxygen. At these conditions, the crossbleed manifold pressure is assumed to be 57 psia for the first design point (12,500 ft-high speed descent) and 61 psia for the second design point (2500 ft-long range descent). Figure 3-9 shows the required active hollow fiber membrane material weight as a function of turbocompressor boost pressure ratio using ICI published values of permeability coefficient at 75°F [4]. Polymethyl pentene required weight conditions drop until the allowable structural load is achieved, further increases in pressure then begin to increase material weight as the tube wall thickness increases.

Thus the membrane material weight would be optimum for a turbocompressor boost pressure ratio of 4:1 for polymethyl pentene and 1:1 (no boost turbocompressor) for silicone rubber. System preliminary design has resulted in the selection of a 2:1 boost pressure ratio using the polymethyl pentene fibers.

To evaluate the effect of the various design options on the resultant air separation module, several key parameters were parametrically varied about a polymethyl pentene air separator design point with a ram air pressure of 10 psia (10,000 feet) and a bleed air operating pressure of 60 psia producing a 9 percent oxygen product. The figures discussed below show the resultant trend in terms of fiber weight, bleed air inlet flow requirement and minimum oxygen concentration as the design parameters are varied.

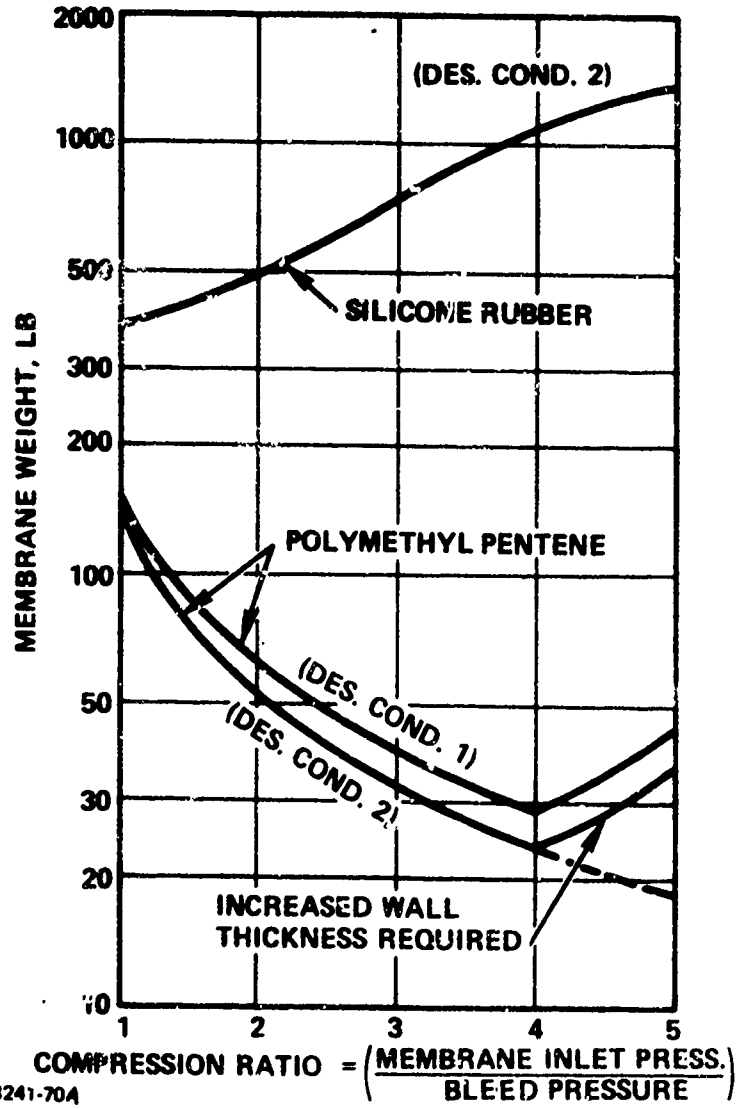

Figure 3-9. Membrane Material Weight for Various Turbocompressor Boost Ratios

Figure 3-10 shows the effect on component design as the bleed air pressure is increased from 60 to 240 psia. Component weight is substantially reduced by increasing the bleed air pressure as long as the allowable structural requirements do not require increases in tube wall thickness. Minimum oxygen concentration also decreases, however the required bleed air flow rate into the module drops only slightly. The effect of ram air pressure also has a substantial effect on the air separator design as can be seen in Figure 3-11. It is as a result of these two somewhat opposed altitude related effects and flow rate peaks at various altitudes that system operation must be simulated to calculate potential design points.

The effect of further reducing the required maximum instantaneous oxygen concentration below 9 percent is seen in Figure 3-12. For the 60 psia hypothetical operating pressure used in this analysis, reduction to 6 percent would more than double the air separation module weight (at higher bleed air pressures, the effect is not nearly as drastic).

Ram air flow rate has been designed to be high relative to permeating gas flow to substantially maintain an ambient oxygen concentration in the ram air (shell-side) of the separation module. If the ram air flows were reduced (or eliminated), the oxygen concentration on the ram air side of the separation module would stabilize at concentration greater than 21 percent thereby increasing the component weight. The reduced minimum concentration and increased bleed air inlet flow required are also shown in Figure 3-13.

The effect of increasing the fiber diameter above the selected nominal 50 micron value is shown in Figure 3-14. If the wall thickness is increased in proportion to the diameter (a constant stress is maintained), the resultant separator weight increased very rapidly. If the wall thickness is maintained at the manufacturing minimum (itself a function of diameter as can be seen in Figure 3-7), the rate at which the weight increases with diameter is substantially reduced. The required tube length however tends to decrease slightly. The minimum tube size considered due to current state-of-the-art practice is 20 microns.

Another significant variation is found in the tube wall thickness. Figure 3-15 shows the results of increased wall thickness for the baseline 50-micron diameter tubes. Thin tube walls are desirable. The weight of the air separator is found to increase as the square of the wall thickness.

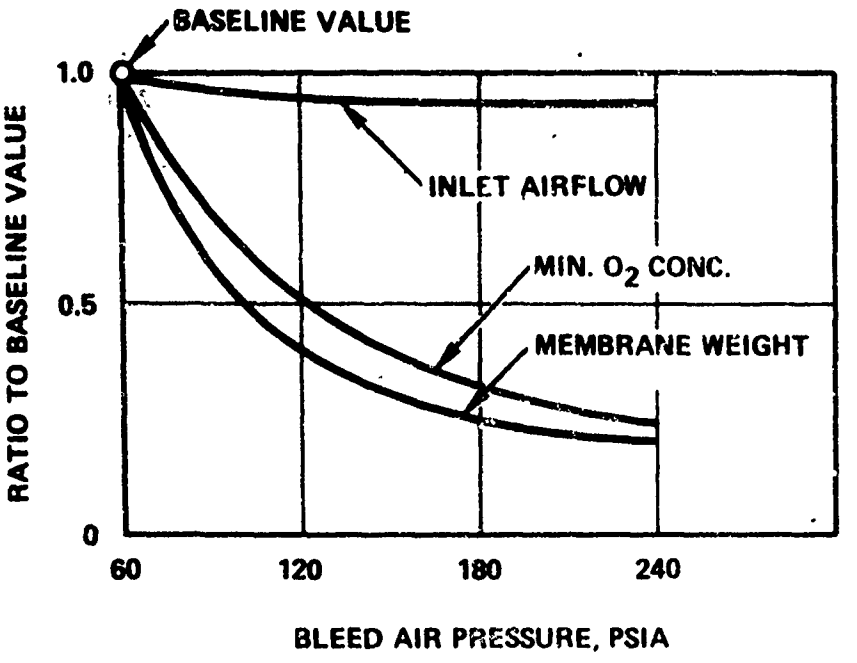

SPA 3241-64

Figure 3-10. Bleed Air Pressure Variation

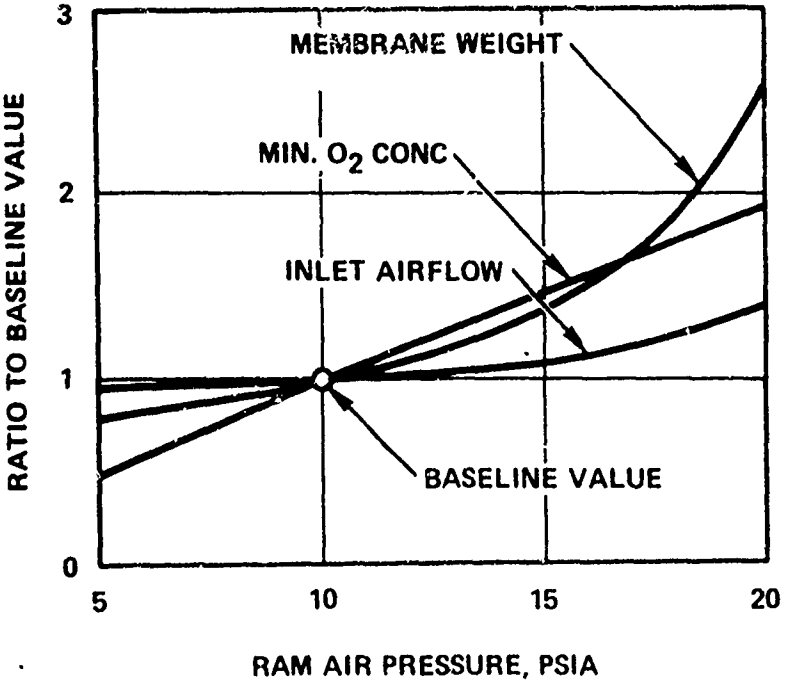

Figure 3-11. Ram Air Pressure Variation

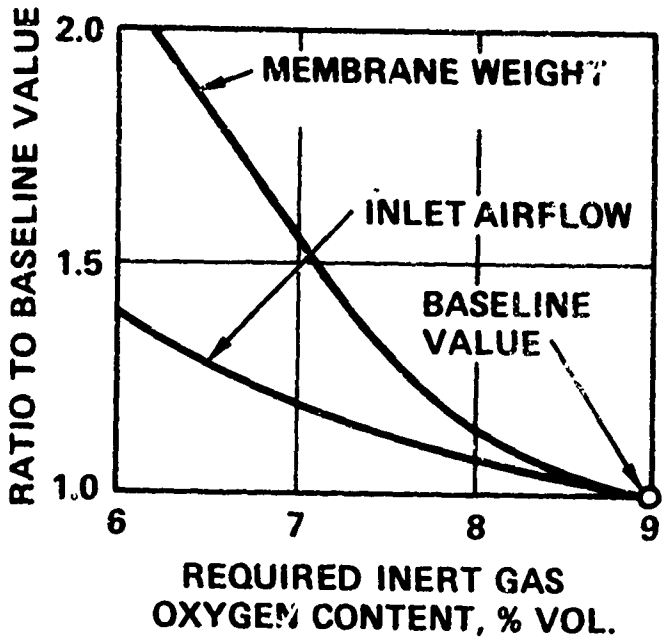

Figure 3-12. Reduction in Inert Gas Oxygen Concentration

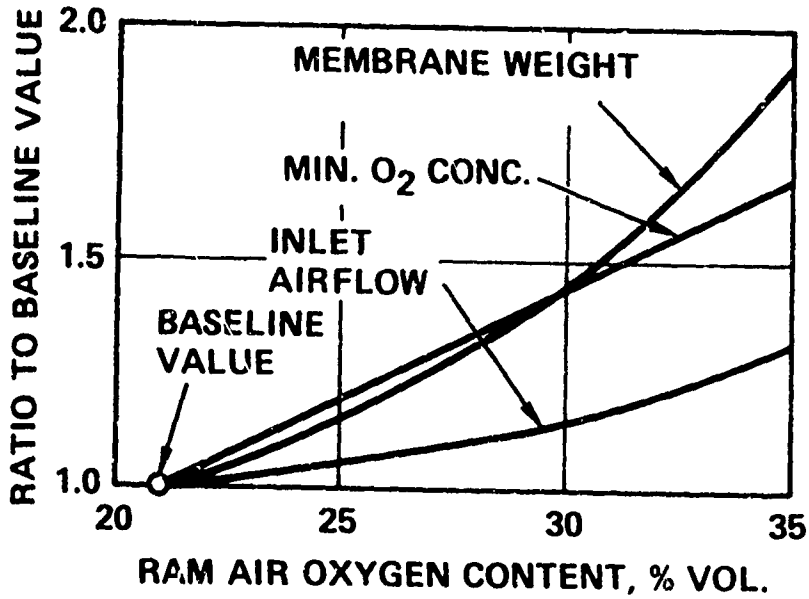

Figure 3-13. The Effect of Reduced Ram Air Flow

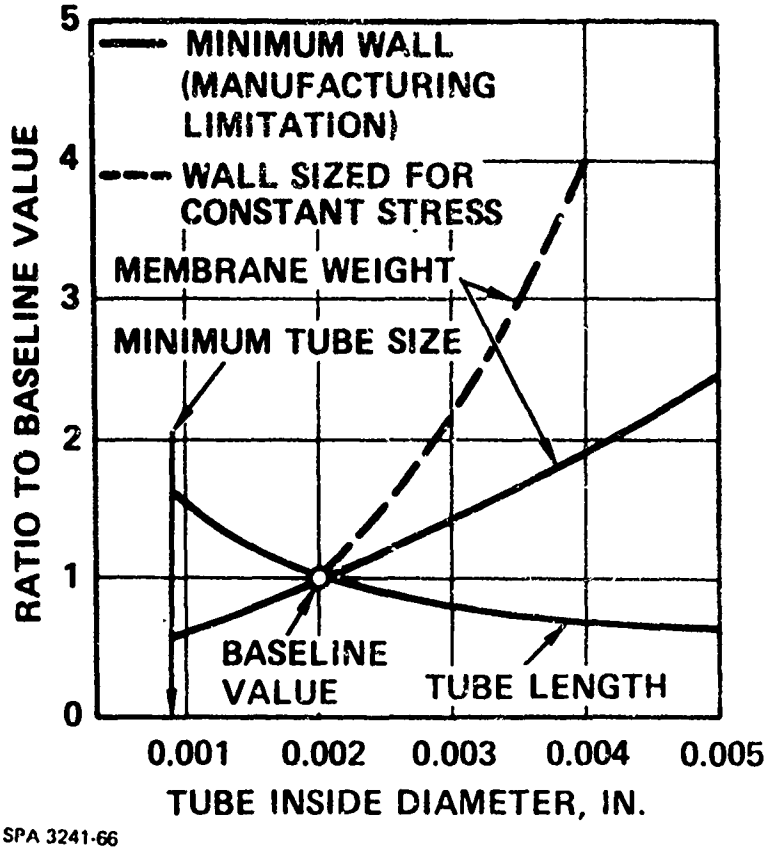

SPA 3241-66

Figure 3-14. The Effect of Tube Diameter

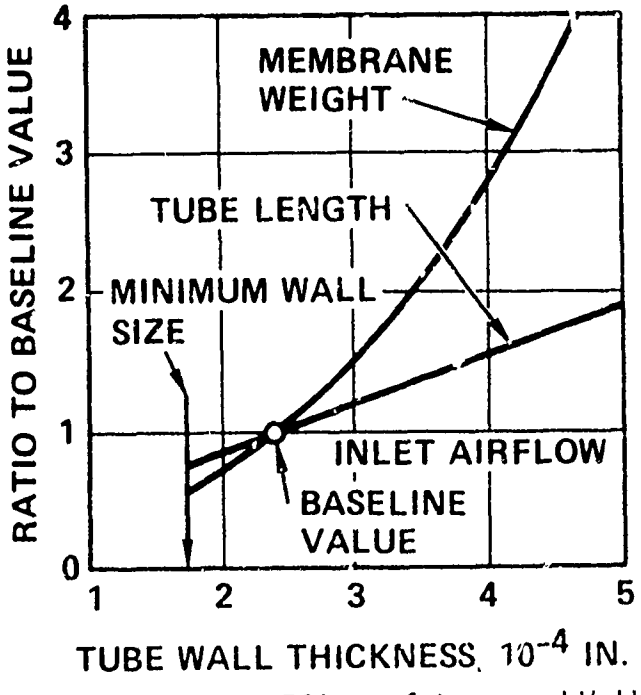

Figure 3-15. The Effect of Increased Wall Thickness

The data shown on Figures 3-14 and 3-15 relate the effects of fiber manufactured on the air separator. As can be seen, close control of both diameter and wall thickness is essential to weight control due to the required increases in module design to accomodate even slightly larger diameter or slightly thicker walls.

Equally important is the material permeability. The data shown in the previous figures has been for assumed permeability coefficients for oxygen and nitrogen respectively of 27.0×10^{-10} and 6.5×10^{-10} $(cm^3/sec\ @\ NTP)(cm)/(cm^2)\ (cm\ Hg)$. The effect of variations on material permeability can also change the design point due to the complex relationship between inert gas flow demand and ram and bleed air pressures. Figures 3-16 and 3-17 show the effect of other values of both oxygen and nitrogen permeability coefficients on separator air inlet flow and fiber weight respectively. The design data shown is for either of two potential design points: high speed descent at 12,500 foot altitude and long range descent at 2500 foot altitude in accordance with the DC-10 profiles shown in Section 2; it is necessary to show both profiles because this high speed descent case is the design point for the values of permeability coefficients used in this analysis, but increased values of permeability coefficients switch the design point to this lower altitude long range descent case. As can be seen from Figures 3-16 and 3-17, reduced nitrogen coefficients and increased oxygen coefficients indicate lighter designs requiring less air. Decreased oxygen coefficients and increased nitrogen coefficients tend to increase the weight and bleed air requirement.

As can be seen from figures 3-16 and 3-17 the effect of permeability coefficients other than the baseline values used not only affects the weight of the air separator, but its bleed air inlet requirement. This in turn affects filter size, turbocompressor size (and turbine flow) and so forth. The effect on this total system weight is shown in Figure 3-18. By selecting adjusted values of permeability coefficient, this adjusted system weight (from preliminary design presented previously in this section) can be determined.

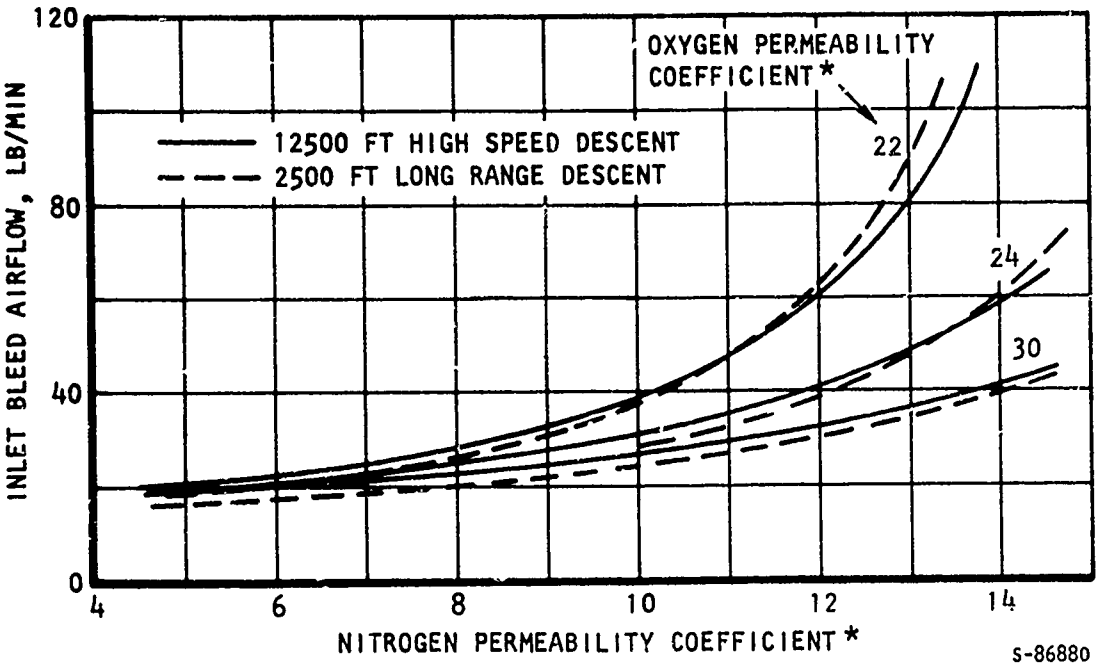

$$* \times 10^{10} \frac{(cm^3/sec\ @\ NTP)(cm)}{(cm^2)(cm\ Hg)}$$

Figure 3-16. The Effect of Permeability Coefficient Variation on Separator Bleed Air Inlet Flow

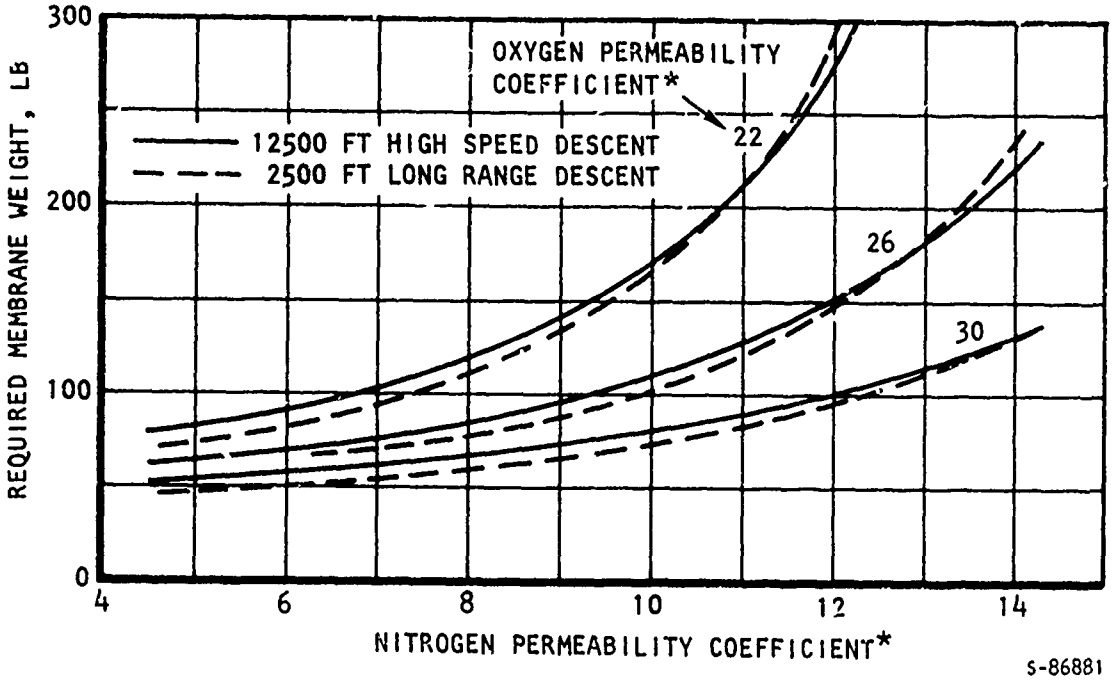

$$* \times 10^{10} \frac{(cm^3/sec\ @\ NTP)(cm)}{(cm^2)(cm\ Hg)}$$

Figure 3-17. The Effect of Permeability Coefficient Variation on Separator Membrane Weight

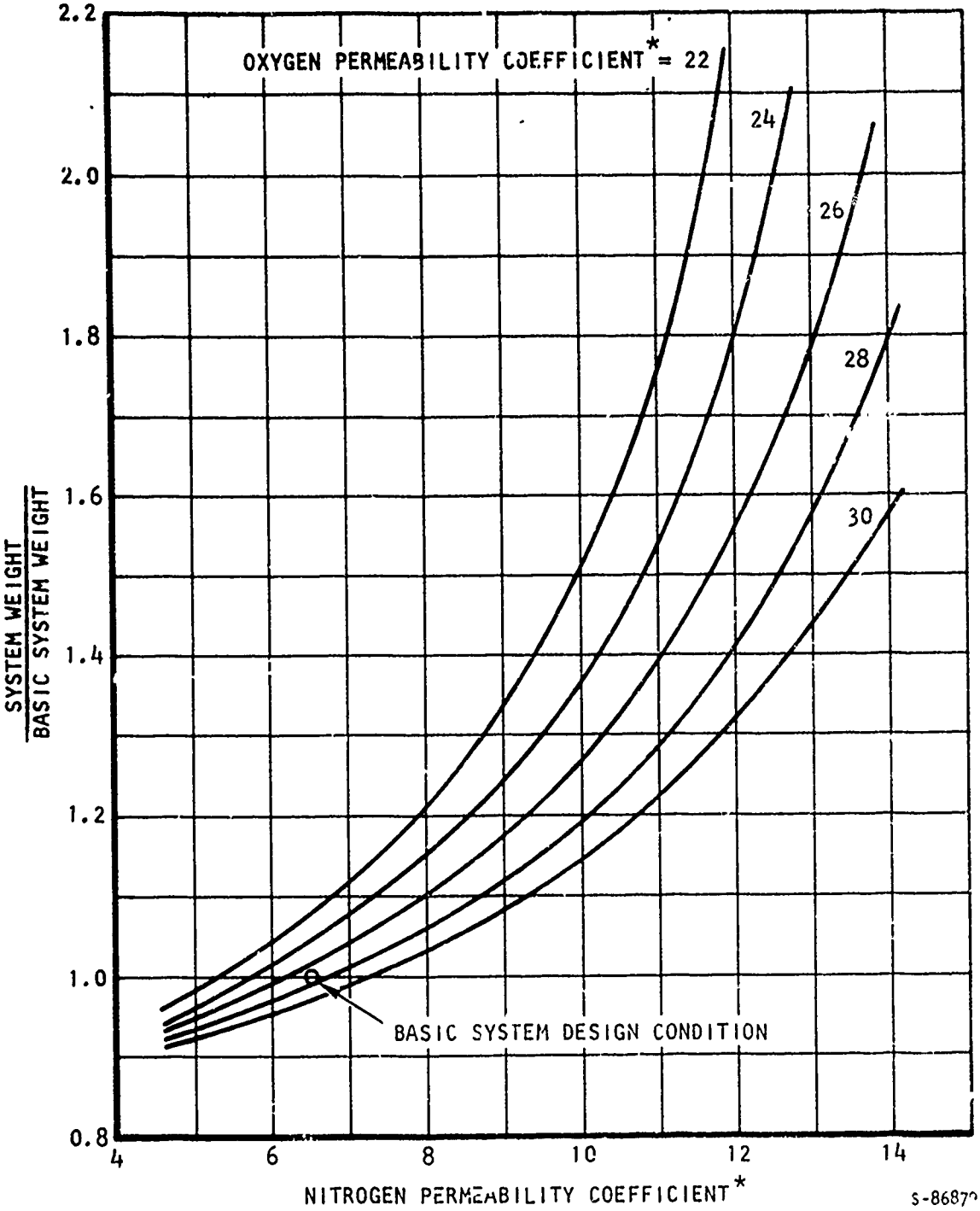

$$* \times 10^{10} \frac{(cm^3/sec\ @\ NTP)(cm)}{(cm^2)(cm\ Hg)}$$

Figure 3-18. The Effect of Permeability Coefficient Variation on System Weight

FEASIBILITY TEST PROGRAM

To further evaluate the feasibility of hollow fiber permeable membranes for the separation of air, an experimental test program was conducted. The feasibility test program had five major goals: (1) the successful spinning of hollow fibers of the material and geometry identified by the preliminary design analysis, (2) the fabrication of test modules of sufficient scale to allow the taking of laboratory data and the accumulation of operating experience, (3) the evaluation of potential chemical degradation of the selected polymeric membrane material due to continued exposure to air, (4) the experimental determination of apparent permeability coefficients for real modules, and (5) the operation as an air separator to demonstrate the feasibility for this purpose and to evaluate the accuracy of predictions based on the iterative digital computer program (a necessary prerequisite to the use of the mathematical model to the design of larger systems).

Although limited by the program schedule and available funding, considerable success was achieved in all five areas, despite the fact that the efforts represented first attempts at the extension of a technology to a new application. The balance of this section is concerned with the fabrication of the test hardware and the results of the test program. The test data and a discussion of the meaning of the data are presented in this section.

Test Hardware

To conduct the test program planned to demonstrate the feasibility of hollow fiber permeable membrane application to inert gas generation subsystems, it was necessary to fabricate unique test hardware. The development of this hardware can be conveniently discussed in three phases: (1) the spinning of a hollow fiber of the selected material to specified dimensions, (2) the assembly of the small spiral wrapped test module used for initial permeability measurements and performance degradation checks; and (3) the fabrication of the large scale parallel fiber module for apparent permeability coefficient testing and air separation tests over a wide temperature range.

1. Polymethyl Pentene Fibers

Following the selection of polymethyl pentene as a candidate membrane material for demonstration of the feasibility of the application of hollow

fiber technology to IGG subsystems, an effort to have tubes of this material manufactured for evaluation was initiated. Dow Chemical, U.S.A., who had assisted AiResearch by supplying data on a number of candidate materials which were analytically evaluated for merit figure, was selected.

The Phase I preliminary design, used in IGG subsystems tradeoff and selection, was based on the use of polymethyl pentene fibers of 50 micron (0.0020 in.) inside diameter and a 6 to 7-micron (0.00025 in.) wall thickness displaying permeability properties per the chemical suppliers data [14]. After a considerable effort, polymethyl pentene fibers with nominal dimensions near the design goals were developed which began to demonstrate structural properties satisfactory for feasibility testing.

Fibers of 50 to 55 micron of a nominal 10 micron wall thickness were continuously spun using modifications to the spinnerettes and tools used for hollow fiber membranes several times the required size for applications to liquid flow. In September 1973, sufficient quantities of fiber of repeatable geometry were manufactured and the decision to fabricate the small-scale spiral wrapped unit for initial testing was made.

2. Small Scale Spiral Wrapped Module

The polymethyl pentene fibers from these initial runs were fed to a textile winder where a fiber wrapped element consisting of 1000 wraps of this small fiber, 16 in tow about a central distribution tube was constructed. The ends of the wrapped element were then bonded by a Dow polyurethane bond into a polycarbonate case used to package laboratory "mini-plant" modules. Finally, the ends of the polyurethane bond and the enclosed loops of the fibers were machined flat to expose the open ends of the polymethyl pentene fibers.

A photograph of the test module, modified at AiResearch to provide external leakage seals consistent with the required test measurements, is shown as Figure 3-19. A schematic diagram of the basic structure and flow passages is shown as Figure 3-20. A photograph showing the resultant spiral wrap for the control of ram air (shell-side) flow channeling is shown as Figure 3-21, and a view of the exposed fiber ends at the ram air inlet end is shown as Figure 3-22. Configuration data is tabulated in Appendix B.

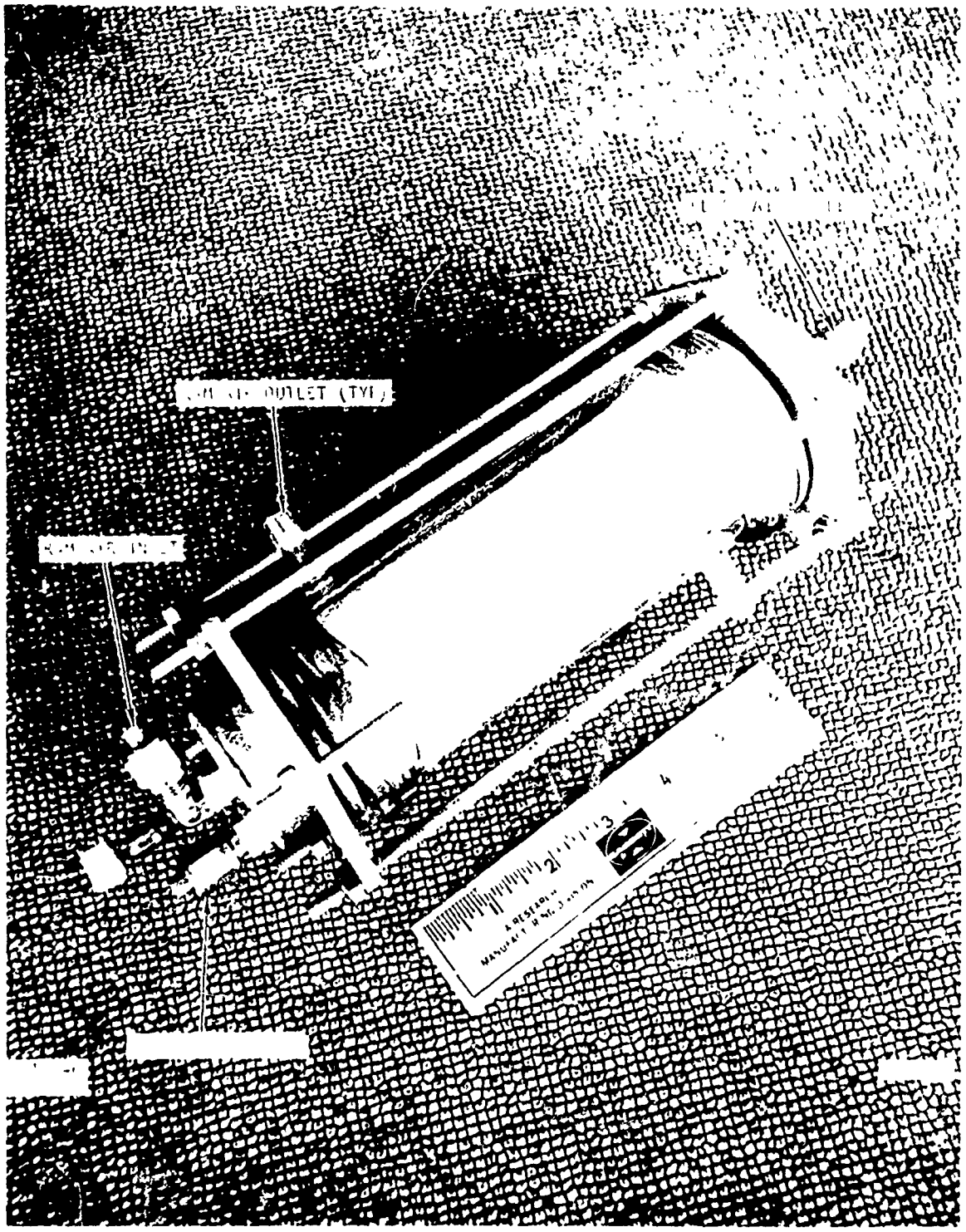

Figure 3-19. Small Spiral Wrapped Test Module Overall Assembled View

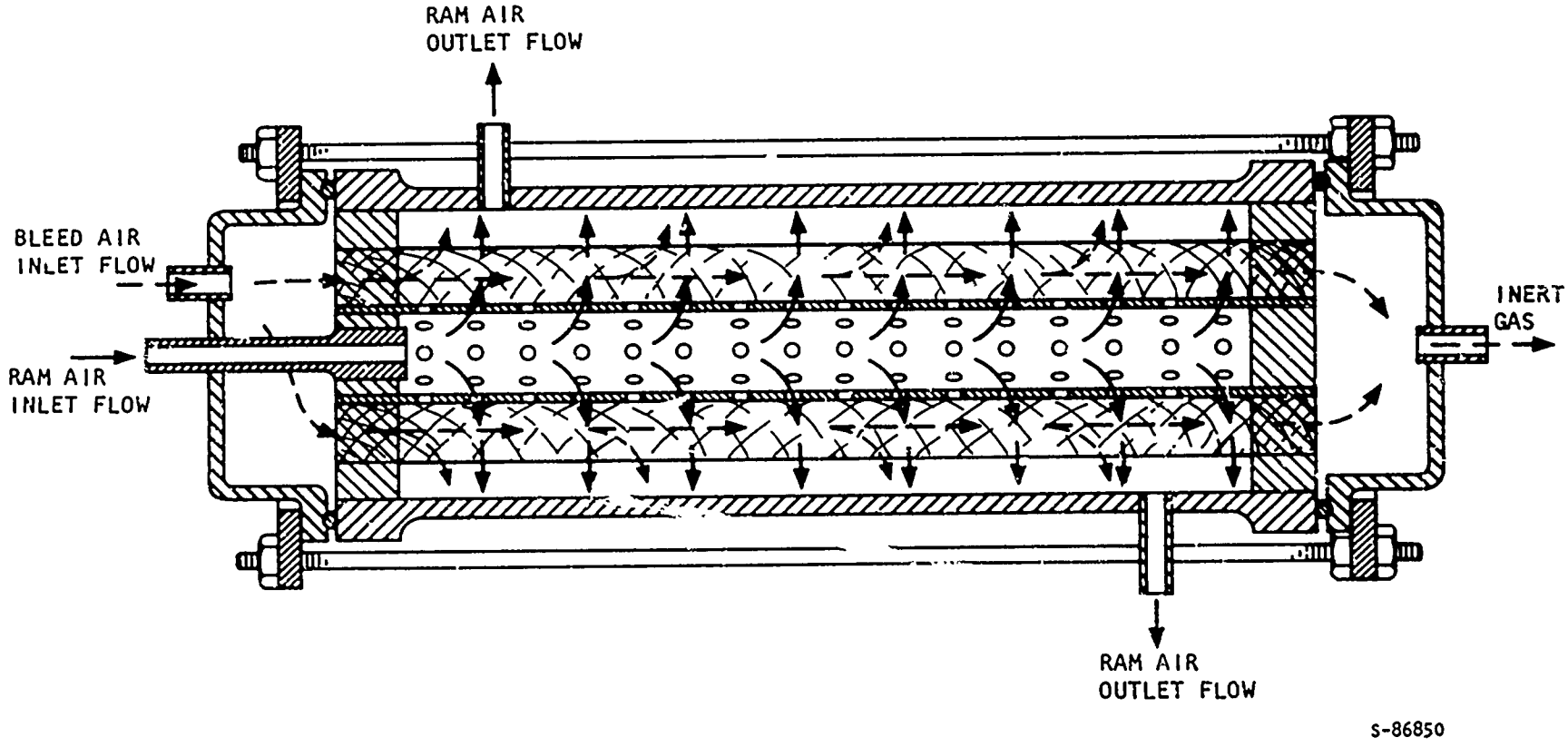

Figure 3-20. Small Spiral Wrap Air Separation Module

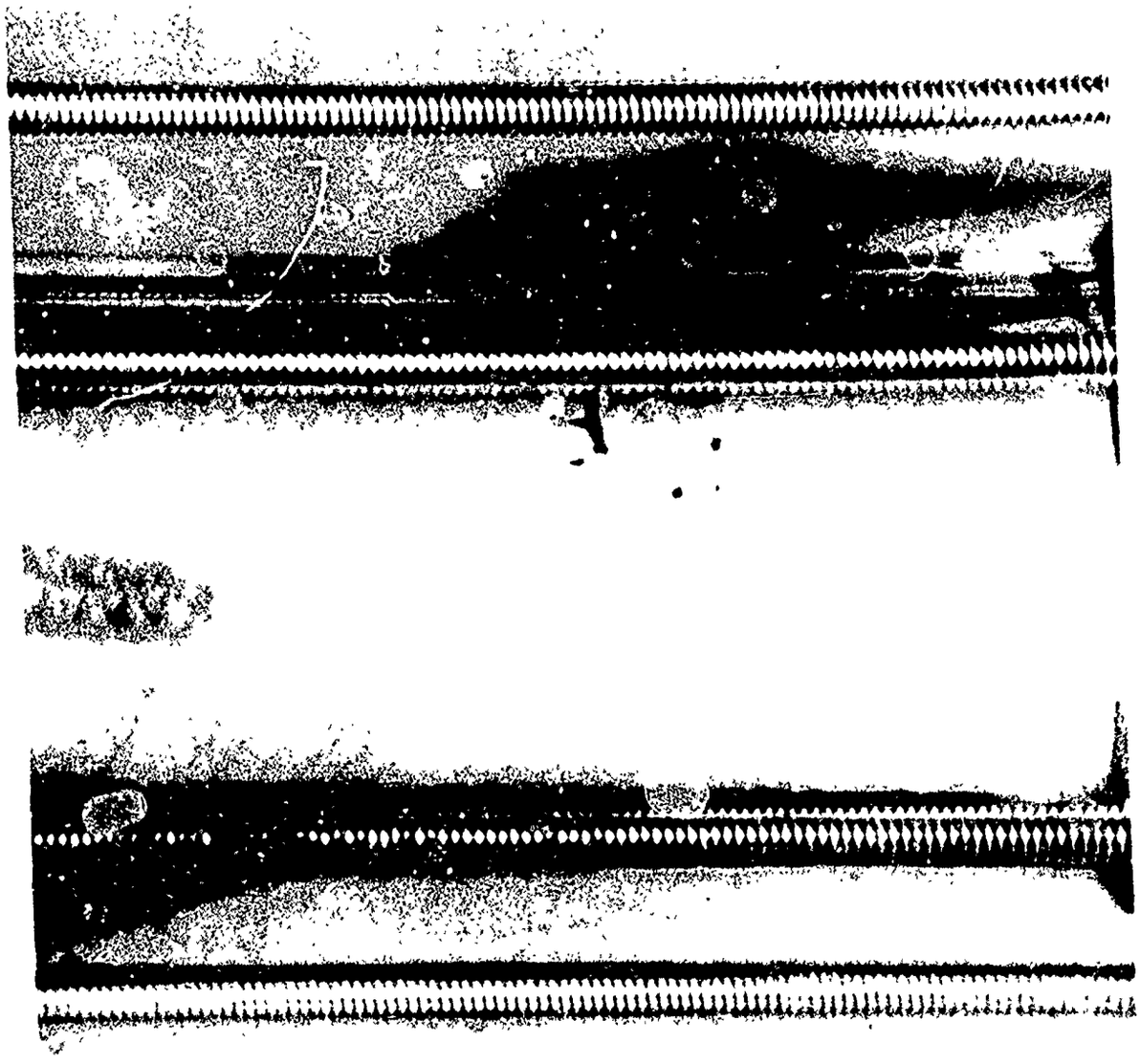

Figure 3-21. Small Spiral Wrapped Test Unit Fiber Wrap Detail

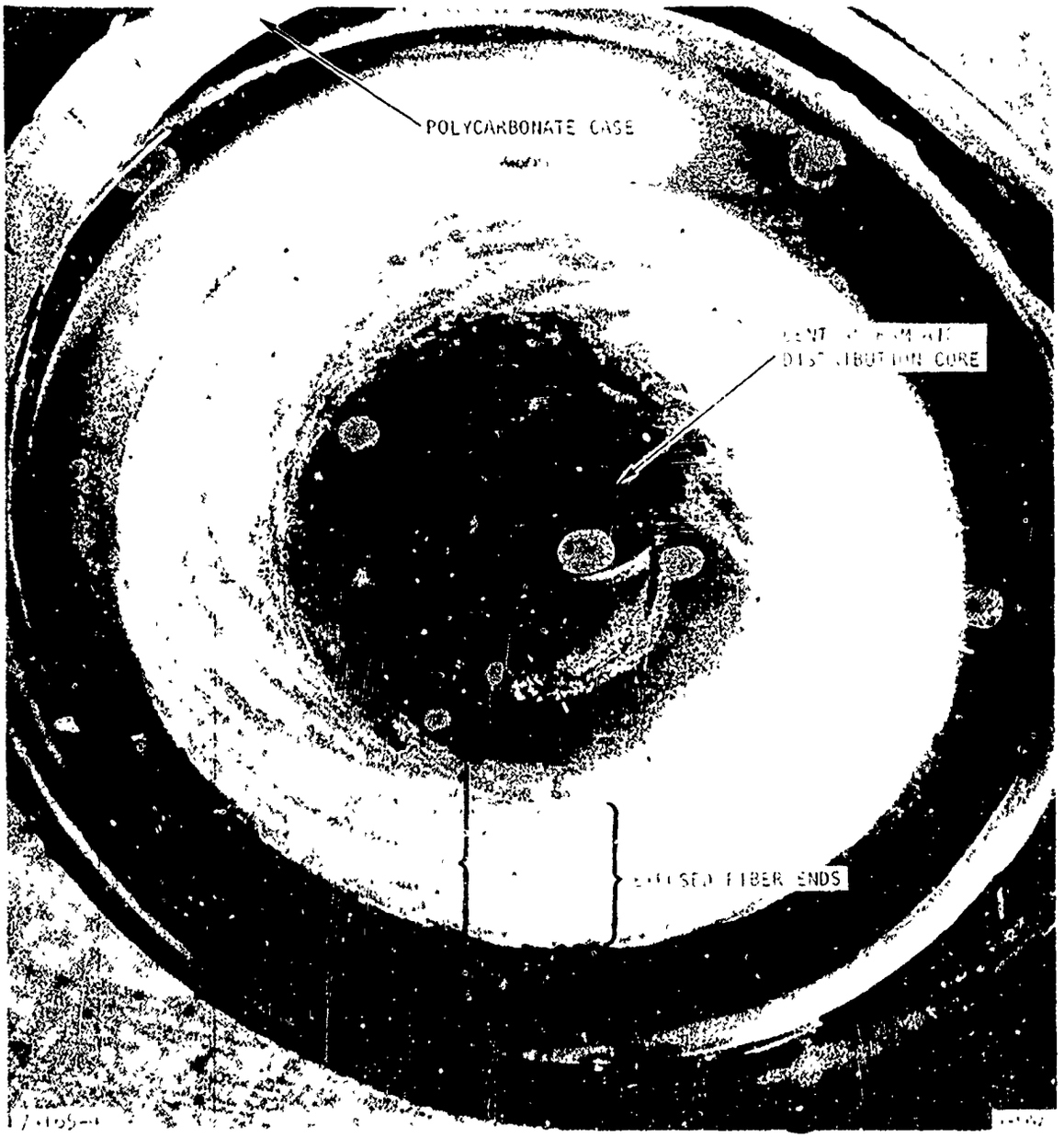

Figure 3-22. Small Spiral Wrapped Test Module End View

Although the test module was successful in providing a test bed for the critical apparent permeability coefficient and successfully operated for 1,000 hours without degradation using laboratory air as a working gas, its use was limited by the applications for which the "mini-plant" design was intended. Most significantly, differential pressure across the tube-sheets was limited to 5 psid. This was to strongly influence the module's testing.

3. Large Scale Parallel Fiber Module

With the encouragement of the initial successes of the small spiral wrapped unit and the continued development of 50 to 55 micron nominal inside diameter polymethyl pentene fibers, a large scale module was assembled which would not be limited by tube sheet differential pressure, and of sufficient size to permit scale laboratory testing (over 2500 ft^2 actual area). This unit was fabricated to allow removal of the hollow fiber assembly from the case, a decision which was to prove invaluable for later disassembly and repair.

Due to limitations requiring the use of existing equipment, the large scale module was constructed by a wrapping procedure resulting in nearly parallel fibers, rather than the spiral wrap used for the small scale module. Limitation to the application of the existing tools to this first assembly of a small fiber resulted in somewhat more damage to fibers than was anticipated (as evidenced by some broken fibers noted during wrapping). Although current technology would permit the construction of a more leak-free unit, again schedule and limited funds were a part in the decision to test this module, felt to be adequate for a feasibility demonstration.

The unit was delivered for testing in December 1973. A schematic drawing of the test module is shown in Figure 3-23. A photograph of the assembled module is shown as Figure 3-24.

Configuration data is tabulated in Appendix B.

Test Program

Experimental feasibility evaluation test programs were initiated for both the small spiral wrapped test module and the large scale parallel fiber test module. The small spiral wrapped test module was used for the first laboratory measurement of polymethyl pentene permeability coefficients under this program. This unit was then subjected to continuous operation with exposure to ambient air in order to evaluate any potential chemical degradation.

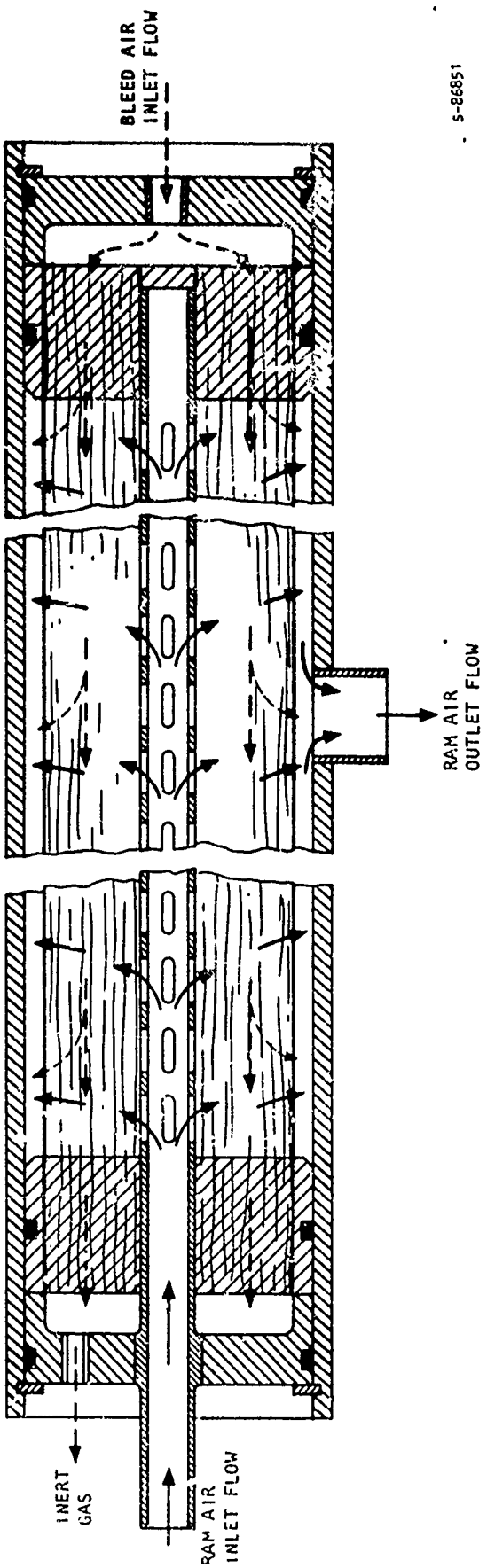

Figure 3-23. Large Scale Parallel Fiber Air Separation Module

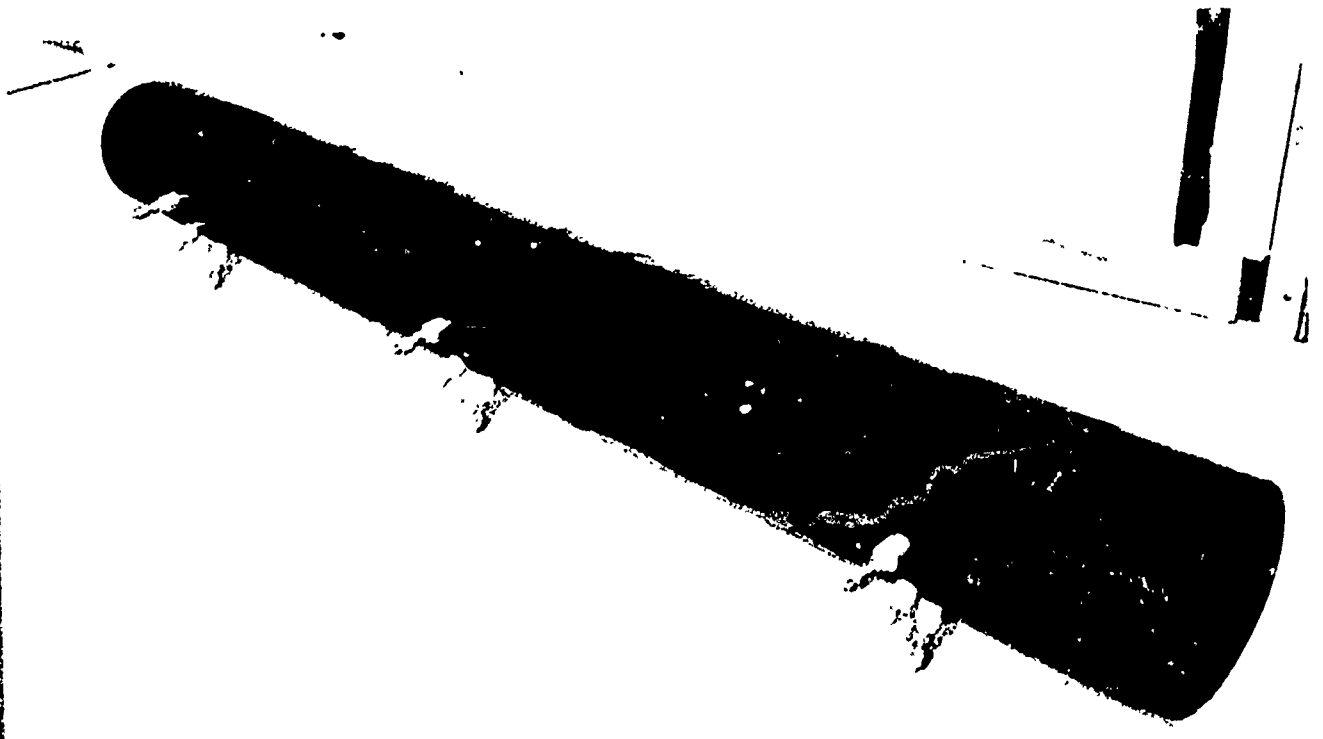

73960-4

Figure 3-24. Large Scale Parallel Fiber Test Module

The large scale parallel fiber test module was subjected to tests for the experimental measurement of permeability coefficients over a wide range of temperatures and pressures This larger unit was also used to demonstrate the air separation capability of polymethyl pentene hollow fiber permeable membrane modules.

In the presentation of the test data that follows, the hollow fiber permeable membrane module is discussed in terms of its installation as a component of an IGG. Thus, the high pressure air on the tube-side of the module is referred to as the bleed air and the low pressure air on the shell-side of the module is referred to as the ram air. The nitrogen enriched bleed air at the outlet of the high pressure tube-side is termed the process gas, which is delivered on demand to the fuel tanks. (The term inert gas has been reserved for process gas with oxygen concentrations below 9%.) The major separation tests were operated over a broad range of process gas demand flows, resulting in process gas oxygen concentrations from the inert gas range through near ambient concentrations to verify analytical predictions for widely varying conditions.

1. Chemical Degradation Life Test

The small spiral wrapped test module was used for the life test program. Due to the 5 psid pressure limitations, operating pressures representative of IGG applications could not be used, therefore, alternate procedures were considered. The procedure selected consisted of introducing laboratory air at a nominal pressure of 5 psig into the bleed air passages (tube-side) and nitrogen gas at pressure slightly above ambient through the ram air passages (shell-side). Bleed air flow rate was controlled by a needle valve on the bleed air outlet. The performance tests consisted of measuring the bleed air outlet concentration as a function of flow rate. An alternative test procedure considered the use of laboratory air in the ram air side at near ambient pressure. While this more closely simulates the actual shell side conditions, the tube side pressure of 5 psig limits the minimum oxygen concentration at the outlet to 17 percent as can be seen from the limit equation developed in Appendix A (Equation A-21). Since it was desirable to measure the performance over a wide range of bleed air outlet concentrations, this procedure was rejected in favor of the use of nitrogen gas on the ram air side.

Life testing was initiated on October 15, 1973 and continued through November 26, 1973. This test period, slightly in excess of 1000 hours, was conducted with the flow rate set to experimentally achieve a nominal 8 percent oxygen concentration in the bleed air outlet flow. At approximately 250 hour intervals, the flow rate was varied over the test range and resultant oxygen concentration was recorded. The test data is shown as Figure 3-25. Experimental test data is summarized in Appendix C.

The experimental data revealed no degradation trend as a result of exposure to laboratory air for the 1000 hour test period. In addition to the test data, Figure 3-25 also shows the results predicted by the finite difference digital computer program. Predictions are shown for permeability coefficients both from ICI literature, and from AiResearch permeability tests conducted prior to the life tests.

The test data clearly shows good correlations with predicted values as well as good stability during the 1,000 hour test period. Following the evaluation of this data, the large scale test module was fabricated.

2. Apparent Permeability Coefficient Measurement

Single gas permeabilities for the large scale laboratory module were determined in the same manner as single gas permeabilities were determined for the small scale module, that is, mass flow measurements were made with essentially constant pressure on each side of the membrane following a purge sweep of sufficient duration of both sides with the test gas. Due to reasonably large permeation rates (as high as 30 lb/hr for oxygen at high differential pressures) there was a measurable pressure drop on the tube side and a smaller but not negligible pressure drop on the shell side. The arithmetic averages of the inlet and outlet pressures were taken as the mean pressures for each side of the membrane. The difference of these mean pressures between the tube and shell side were then used to establish the partial pressure driving force for the permeation in the calculation of apparent permeability coefficient. The inlet tube side pressure, however, has been used as a nominal characteristic pressure for data correlation in the following figures. Experimental evaluation of the permeability coefficients can be expressed by the following equation:

$$TP = \frac{th}{A_s} \left(\frac{\dot{M}}{\Delta P}\right) \qquad (3.9)$$

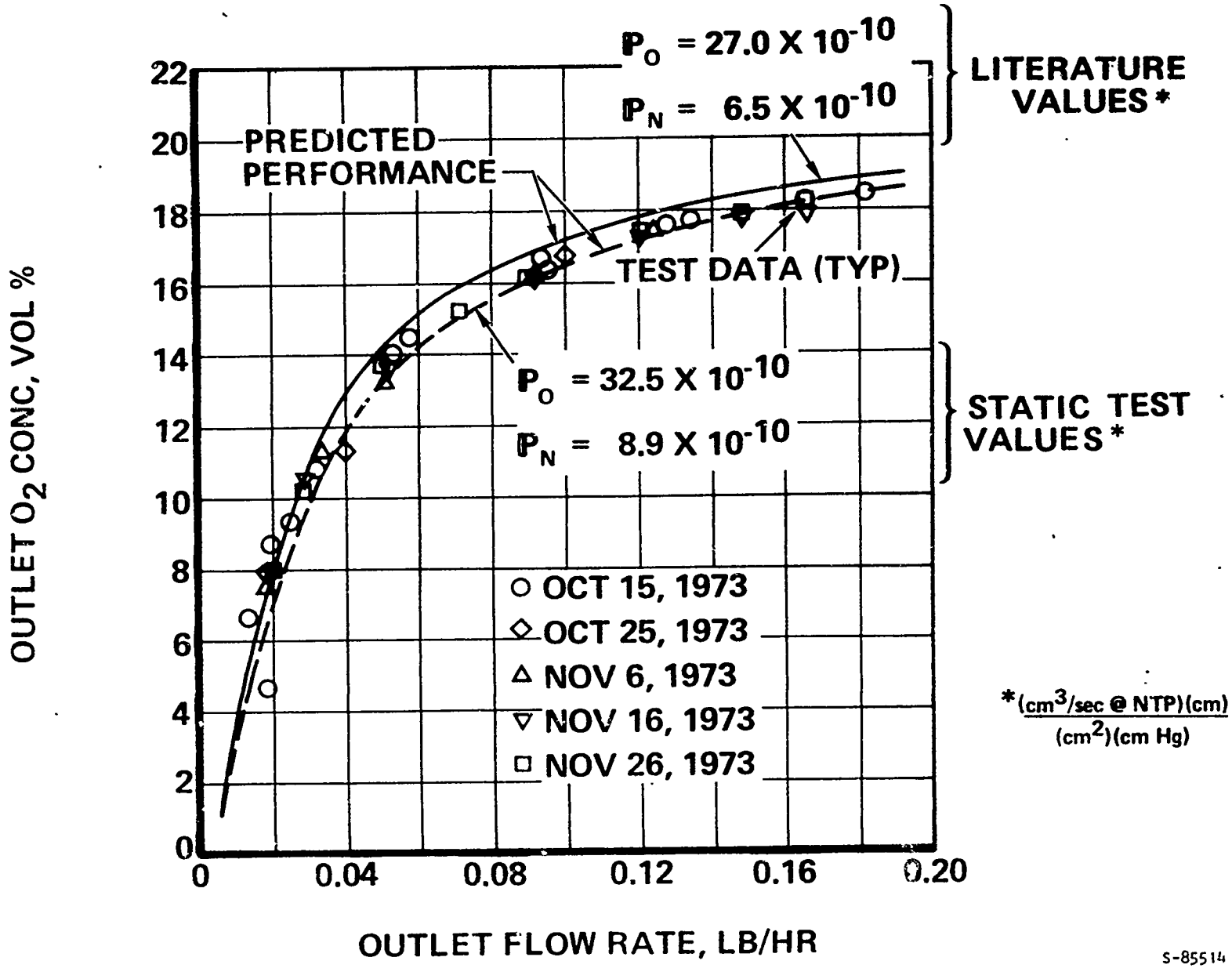

Figure 3-25. IGG Membrane 1000 Hour Performance Test

where $\mathcal{P}$ = the apparent permeability coefficient

A_S = surface area

th = thickness

M = measured mass flow rate

ΔP = mean partial pressure difference driving force

During the course of testing, data were taken and permeability coefficients determined at various temperatures throughout the range of 0^0 to 160^0F and tube side inlet pressures from a nominal 10 to 50 psig. During the evaluation of the initial data, inconsistency in reproducibility was noted, particularly following exposure to sub-ambient temperatures. Subsequent test module disassembly showed this is the result of improperly machined O-ring grooves and some leakage through temporary plugs of voids in the tube sheet at the exit end of the test unit. Both the O-ring sealing problems and the void plugs were repaired and testing continued with subsequent data showing improved reproducibility. Figure 3-26 is a photograph of the disassembled test module showing the general construction. Figure 3-27 shows the O-ring grooves machined into the tube sheet prior to modification. Figures 3-28 and 3-29 show the tube sheet at this exit end of the test module following removal of temporary void plugs and re-drilling and following completion of repairs respectively.

Tube sheet void defects were located by a technique of flooding the tube sheet with water and placing a low nitrogen gas pressure on the ram air (shell-side) of the tube unit. The rate of bubble formation was determined to be an indication of leakage. Small bubbles formed slowly over the entire tube sheet, indicative of gas permeation. In a few select locations, adjacent to the temporary plugs, larger bubbles formed rapidly, indicative of tube sheet void leakage. A photograph of the bubble formation can be seen in Figure 3-30 and 3-31.

Although the tube sheet repairs impacted the test schedule, resulting in the loss of valuable test time, significant experience in the practical repair of a damaged or partially defective module was gained. Since this module is the first of its kind ever assembled, the occurrence of tube-sheet voids is not felt to be representative of production hardware. In addition, the feasibility of module repair was demonstrated.

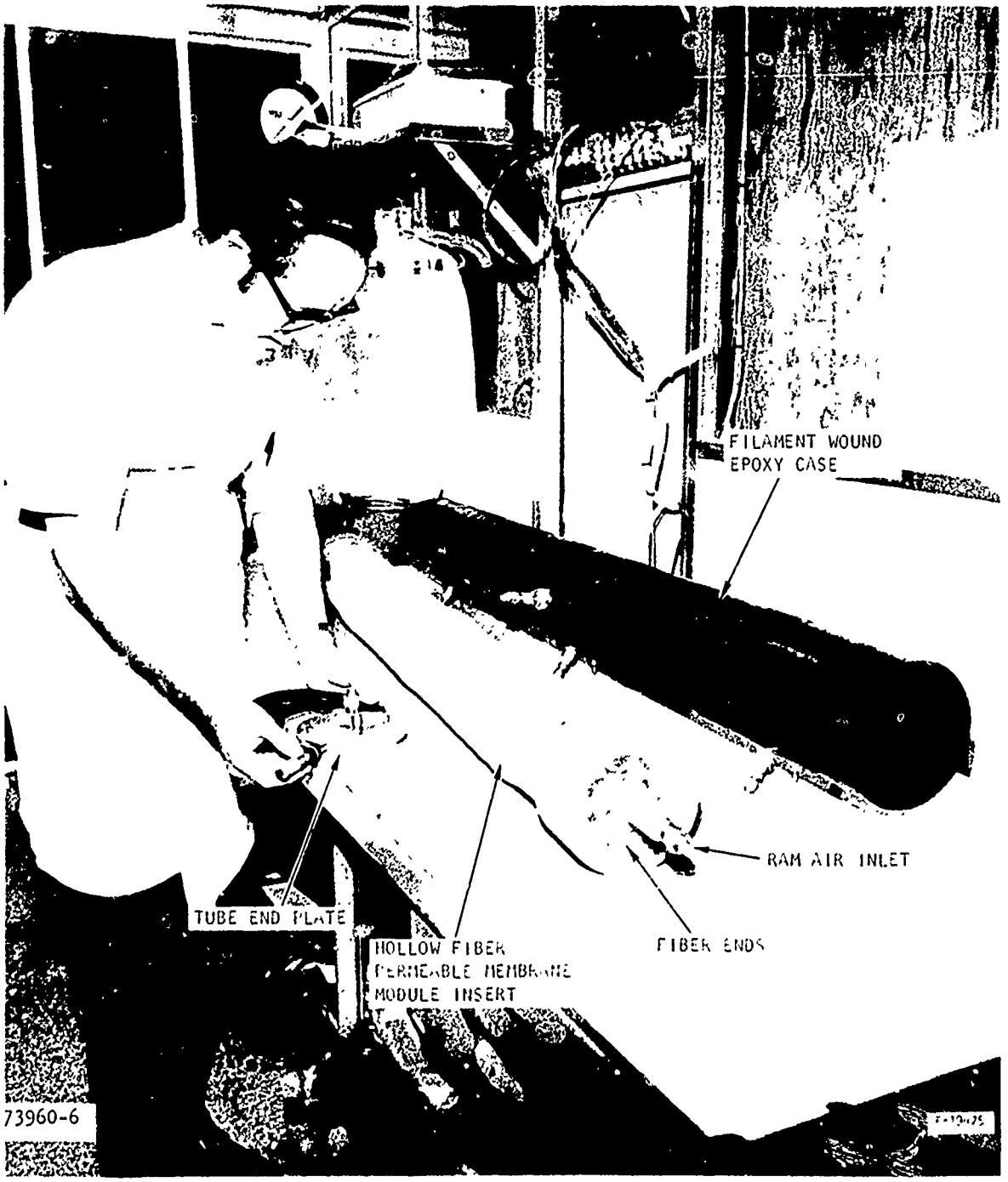

Figure 3-26. Large Scale Parallel Fiber Test Module

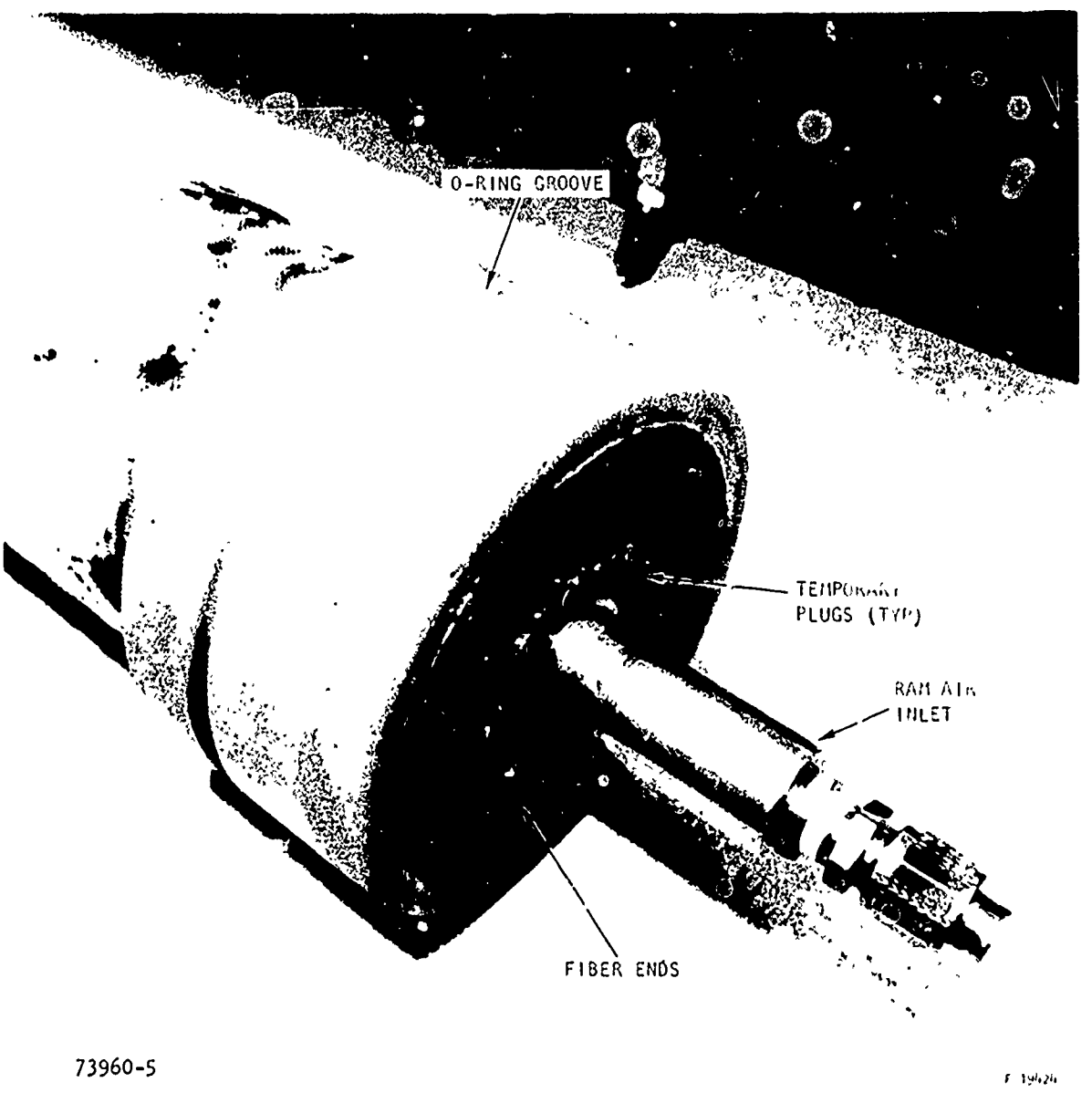

Figure 3-27. Large Scale Test Module Hollow Fiber Permeable Membrane Module Insert

Figure 3-28. Large Scale Test Module During Tube Sheet Void Repair

Figure 3-29. Large Scale Module Following Tube Sheet Void Repair

Figure 3-30.
Initial Leakage Indication

Figure 3-31.
Time Dependent Leakage
and Permeation Indication

Experimentally determined apparent permeability coefficients for nitrogen as a function of time are shown on Figure 3-32. Since data evaluation indicated a slight tendency for permeability coefficient to increase with increasing nominal inlet pressures, this figure represents data taken at nominal 10 psig inlet pressures only. Data is shown for 60°F and 70°F test points. Reduction of the earlier test data indicated the non-reproducibility shown on the left hand side of these figures and led to the unit tear-down and repair. Subsequent to this repair, a definite improvement in data repeatability can be noted. In addition, a significant change in the testing procedure was instituted following these repairs. This established 60°F as a nominal data base point which was repeated, following both the high and low temperature single gas testing and following each air separation test at 40°, 60° and 140°F. The sequence to testing is shown in Table 3-2.

The units of apparent permeability coefficient as shown in the data summary tables of Appendicies D, E and F indicate the apparent transmembrane transfer rate in cubic centimeters per second at normal temperature and pressure. It should be noted that normal temperature and pressure is taken as one atmosphere at 70°F and that volumetric flow rate at a set condition is essentially a unit of mass transfer and not volume.

Because of the unrepeatable nature of the pre-repair test data, (included in summary form, however, in Appendix F) the remainder of the single gas permeation test curves shown in this section exclude this early data and consider only data following the successful repair of the unit. Figures 3-33 and 3-34 show the experimentally measured value of apparent permeability coefficient as a function of temperature for nitrogen and oxygen, respectively, throughout the range of 0° to 160°F. For the baseline 60°F data, test points were taken increasing in 10 psi increments from 10 psig to 50 psig and then decreasing in 10 psi increments again to 10 psig. For other temperatures, that is, 0° to 40°F and 80° to 160°F, a similar sequence of measurements was made. However, the pressures were from 10 to 30 and back to 10 psig. These pressures are nominal inlet pressures to the tube side of the unit. The nominal shell side pressure is slightly in excess of ambient. Actual mean ΔP's were used in computation of the apparent permeability coefficients.

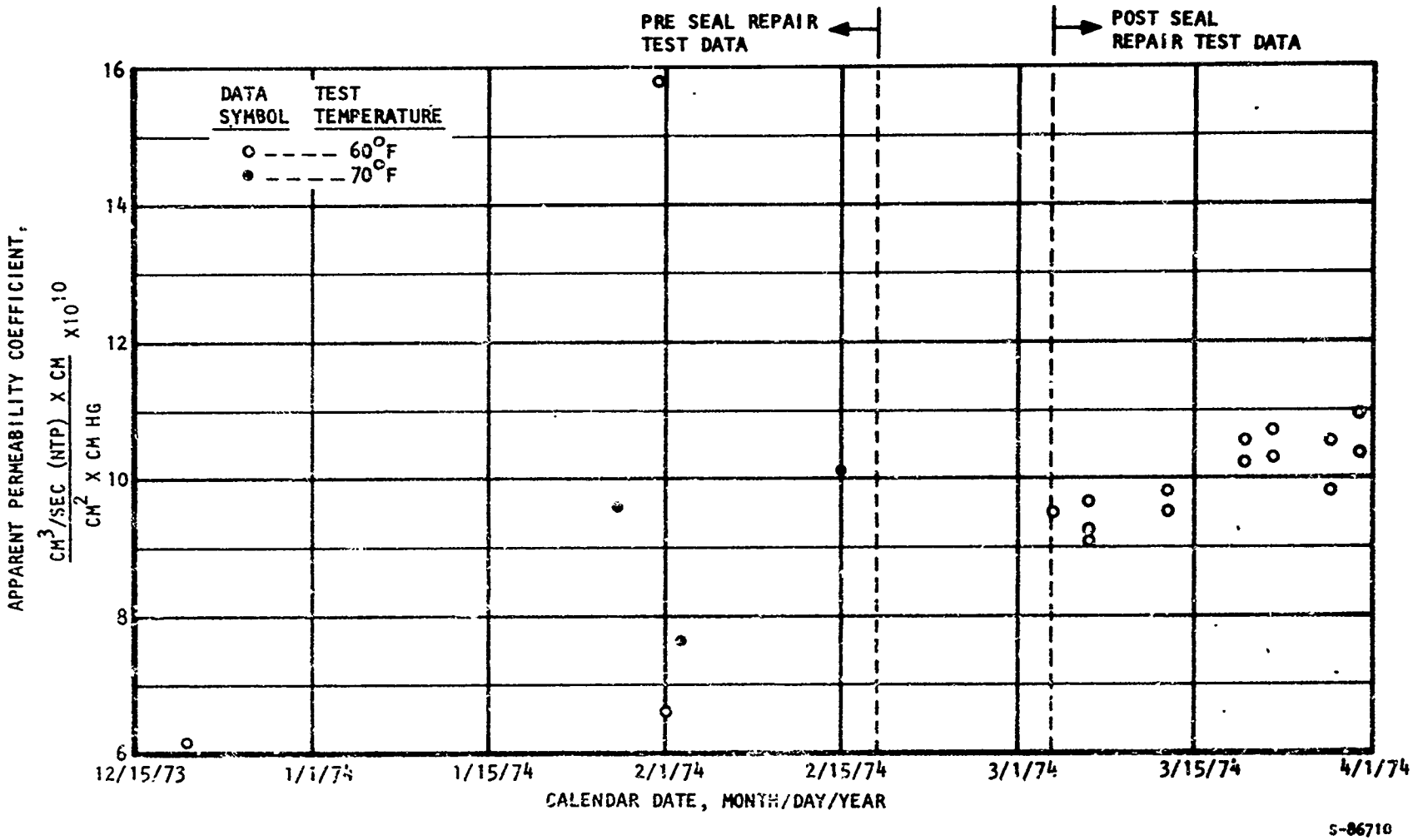

Figure 3-32. Large Scale Polymethyl Pentene Test Module, Experimental Nitrogen Permeability at a Nominal 10 psig Bleed Air Pressure

TABLE 3-2. LARGE SCALE PARALLEL FIBER AIR SEPARATION MODULE TEST SEQUENCE

Bleed Supply Gas	Ram Supply Gas	Test Temperature (°F)	Bleed Air Outlet Flow (lb/hr)	Ram Air Inlet Flow (lb/hr)	Bleed Air Supply Pressure Sequence (psig)
N_2	-	60	-	-	10, 20, 30, 40, 50, 40, 30, 20, 10
O_2	-	60	-	-	10, 20, 30, 40, 50, 40, 30, 20, 10
AIR	AIR	60	0.5	30	30, 50
AIR	AIR	60	1.0	30	30, 50
AIR	AIR	60	2.0	30	30, 50
AIR	AIR	60	4.0	30	30, 50
AIR	AIR	60	6.0	30	30, 50
AIR	AIR	60	8.0	30	30, 50
AIR	AIR	60	10.0	30	30, 50
AIR	AIR	60	2.0	5	30
AIR	AIR	60	2.0	5	30
AIR	AIR	60	2.0	10	30
AIR	AIR	60	2.0	20	30
AIR	AIR	60	6.0	5	50
AIR	AIR	60	6.0	10	50
AIR	AIR	60	6.0	20	50
N_2	-	60	-	-	10, 20, 30, 40, 50, 40, 30, 20, 10
O_2	-	60	-	-	10, 20, 30, 40, 50, 40, 30, 20, 10
N_2	-	80	-	-	10, 20, 30, 20, 10
O_2	-	80	-	-	10, 20, 30, 20, 10
N_2	-	100	-	-	10, 20, 30, 20, 10
O_2	-	100	-	-	10, 20, 30, 20, 10

TABLE 3-2 (Continued)

Bleed Supply Gas	Ram Supply Gas	Test Temperature (°F)	Bleed Air Outlet Flow (lb/hr)	Ram Air Inlet Flow (lb/hr)	Bleed Air Supply Pressure Sequence (psig)
N_2	-	120	-	-	10, 20, 30, 20, 10
O_2	-	120	-	-	10, 20, 30, 20, 10
N_2	-	140	-	-	10, 20, 30, 20, 10
O_2	-	140	-	-	10, 20, 30, 20, 10
N_2	-	160	-	-	10, 20, 30, 20, 10
O_2	-	160	-	-	10, 20, 30, 20, 10
N_2	-	60	-	-	10, 20, 30, 40, 50, 40, 30, 20, 10
O_2	-	60	-	-	10, 20, 30, 40, 50, 40, 30, 20, 10
N_2	-	40	-	-	10, 20, 30, 20, 10
O_2	-	40	-	-	10, 20, 30, 20, 10
N_2	-	20	-	-	10, 20, 30, 20, 10
O_2	-	20	-	-	10, 20, 30, 20, 10
N_2	-	0	-	-	10, 20, 30, 20, 10
O_2	-	0	-	-	10, 20, 30, 20, 10
N_2	-	60	-	-	10, 20, 30, 40, 50, 40, 30, 20, 10
O_2	-	60	-	-	10, 20, 30, 40, 50, 40, 30, 20, 10

TABLE 3-2 (Continued)

Bleed Supply Gas	Ram Supply Gas	Test Temperature (°F)	Bleed Air Outlet Flow (lb/hr)	Ram Air Inlet Flow (lb/hr)	Bleed Air Supply Pressure Sequence (psig)
AIR	AIR	140	0.5	30	30
AIR	AIR	140	1.0	30	30
AIR	AIR	140	2.0	30	30
AIR	AIR	140	4.0	30	30
AIR	AIR	140	6.0	30	30
AIR	AIR	140	8.0	30	30
AIR	AIR	140	10.0	30	30
N_2	-	60	-	-	10, 20, 30, 40, 50, 40, 30, 20, 10
O_2	-	60	-	-	10, 20, 30, 40, 50, 40, 30, 20, 10
AIR	AIR	40	0.5	30	30
AIR	AIR	40	1.0	30	30
AIR	AIR	40	2.0	30	30
AIR	AIR	40	4.0	30	30
AIR	AIR	40	6.0	30	30
AIR	AIR	40	8.0	30	30
AIR	AIR	40	10.0	30	30
N_2	-	60	-	-	10, 20, 30, 40, 50, 40, 30, 20, 10
O_2	-	60	-	-	10, 20, 30, 40, 50, 40, 30, 20, 10

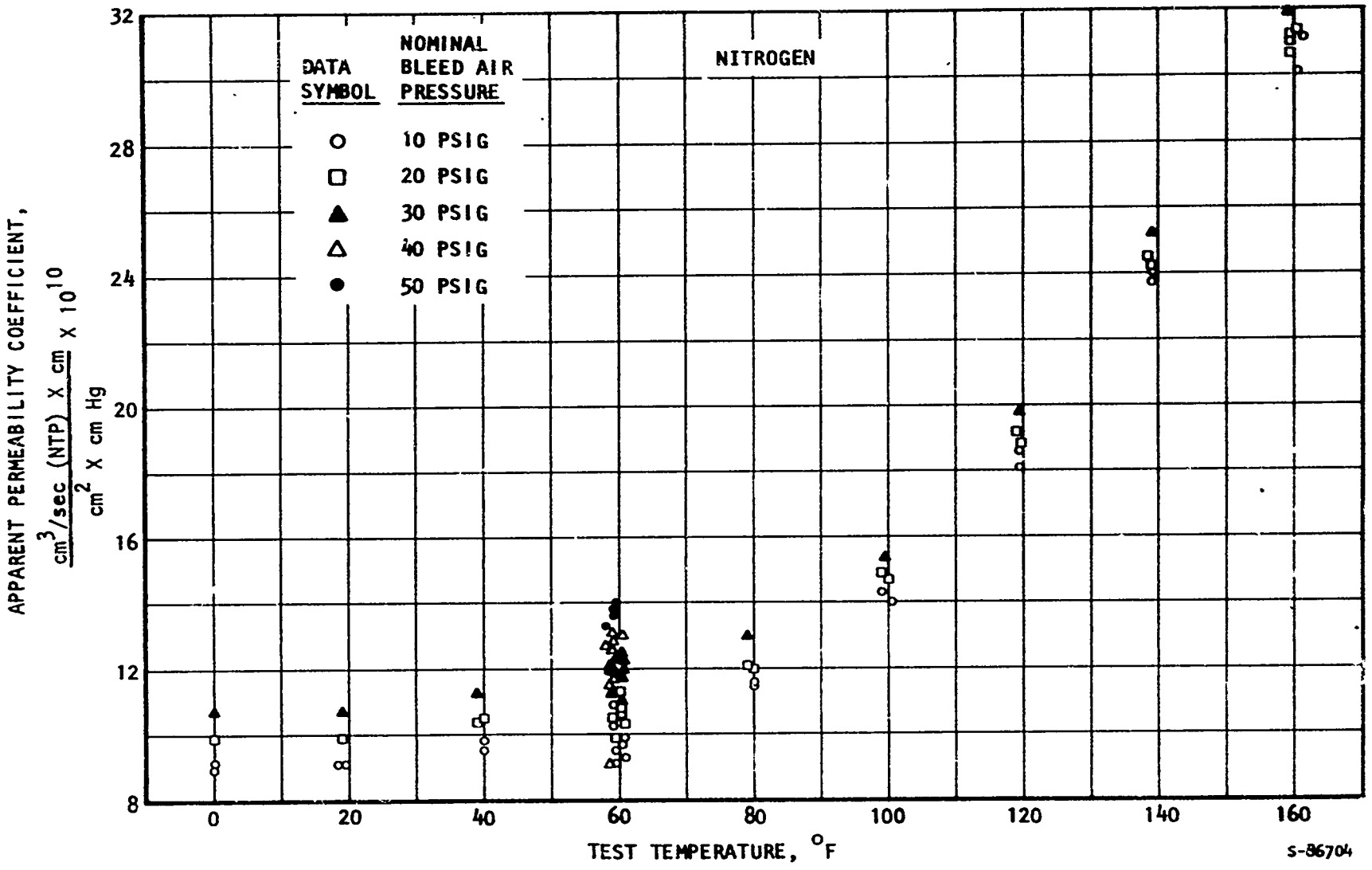

Figure 3-33. Large Scale Polymethyl Pentene Test Module, Experimental Nitrogen Permeability

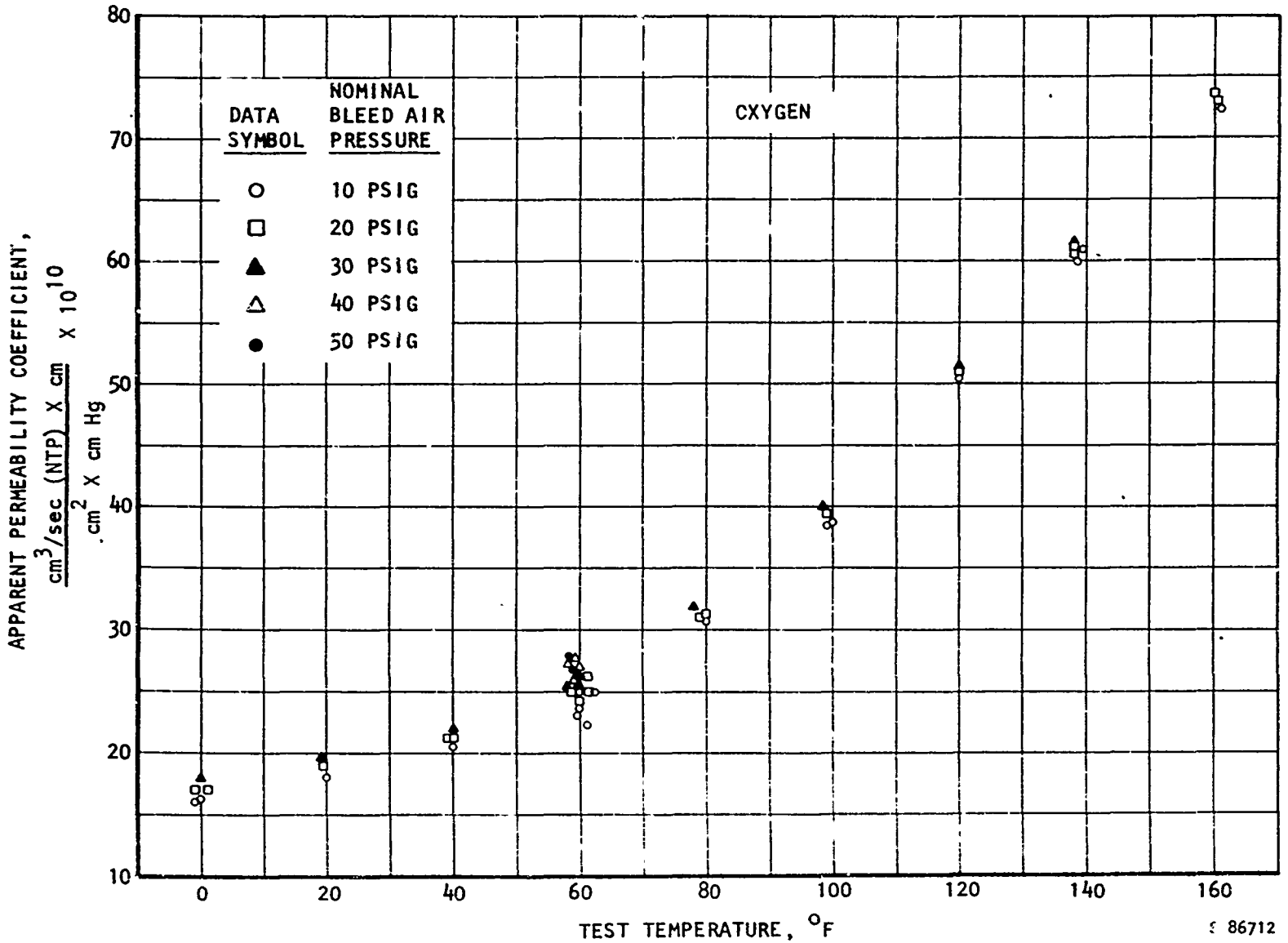

Figure 3-34. Large Scale Polymethyl Pentene Test Module, Experimental Oxygen Permeability

From the data shown on Figures 3-33 and 3-34, it can be seen that the measured values of the apparent permeability coefficient for both nitrogen and oxygen increase with increasing temperatures as may be expected by observation of the equations presented in Appendix A. Two additional effects are tentatively noted. These are an apparent increase in permeability coefficients with increasing pressure at constant temperature, and an apparent hysteresis lag wherein permeability coefficients measured during decreasing pressures are higher than those measured during increasing pressures. A sample plot is shown as Figure 3-35. Although a pattern is difficult to establish due to experimental scatter and the lack of a great number of test data points, the apparent pressure effect, while seemingly an indication that the diffusion coefficient per Fick's first law of diffusion (Equation A-1 of Appendix A), or the solubility coefficient per Henry's law (Equation A-5 of Appendix A) are not in fact constant with pressure. Since these are gross measurements on an engineering unit, they also include a leakage factor which may be somewhat nonlinear with pressure.

The values of apparent permeability coefficients at a nominal 30 psig inlet pressure are plotted as a function of temperature in Figures 3-36 and 3-37 for nitrogen and oxygen, respectively. A smooth curve has been drawn through these points in order to establish permeability coefficients for use in the forward difference digital computer program used to analyze the air separation data reported later in this section.

It is of interest to compare the apparent permeability coefficients from Figures 3-36 and 3-37 with the permeability coefficients of polymethyl pentene found by other investigations. Imperial Chemical Industries [14] report permeabilities of 6.5×10^{-10} and 27×10^{-10} (in consistent units) for nitrogen and oxygen respectively, at 75°F. Yasuda and Rosengren [16] report a permeability range of 6.4 to 13.5×10^{-10} for nitrogen and 26.0 to 45.6×10^{-10} for oxygen at unspecified, but presumably ambient temperature. Neither investigator reports the partial pressure. From Figures 3-36 and 3-37 the apparent permeability coefficient values at 75°F as measured at AiResearch were 12.8 $\times 10^{-10}$ and 30.7×10^{-10} respectively, for nitrogen and oxygen. Although these values are within the range measured by Yasuda and Rosengren, they are both higher than those reported by International Chemical Industries.

[16] H. Yasuda and K. J. Rosengren, J. Appl. Pol. Sci 14, 2839 (1970).

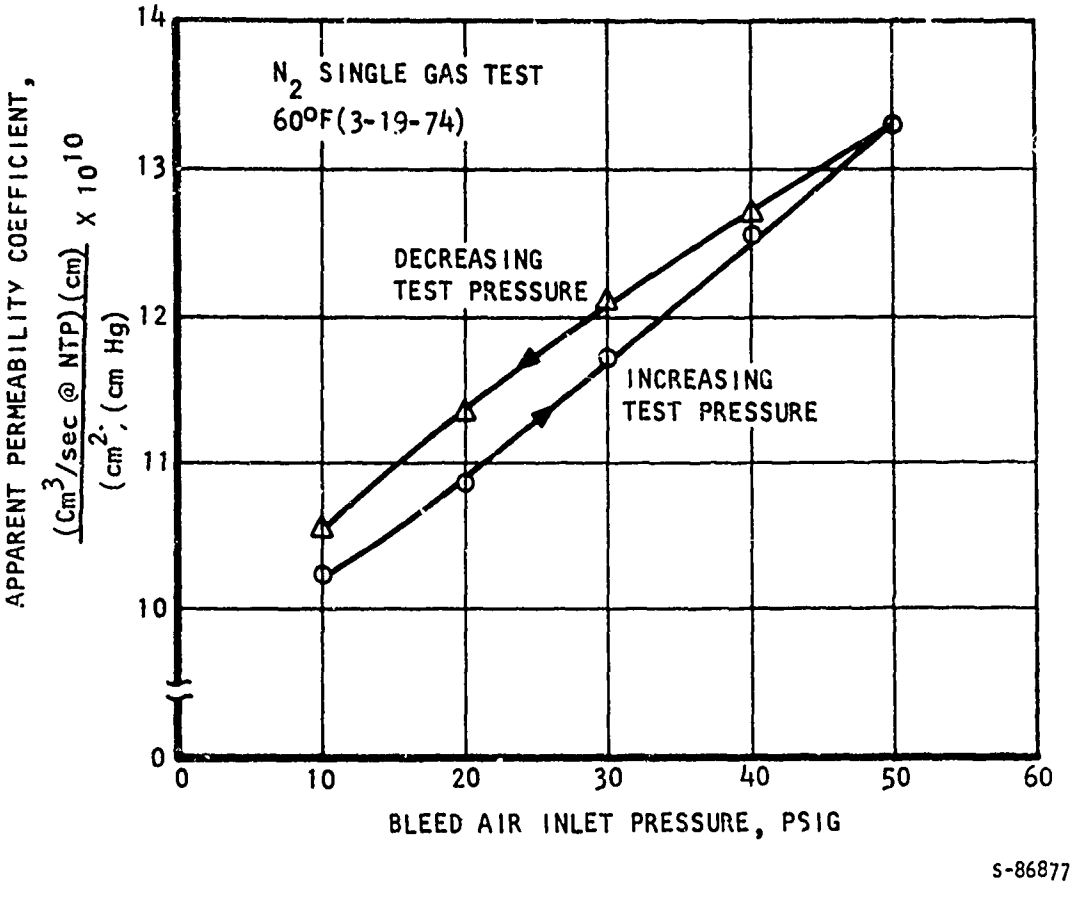

Figure 3-35. Experimental Coefficient as a Function of Test Pressure

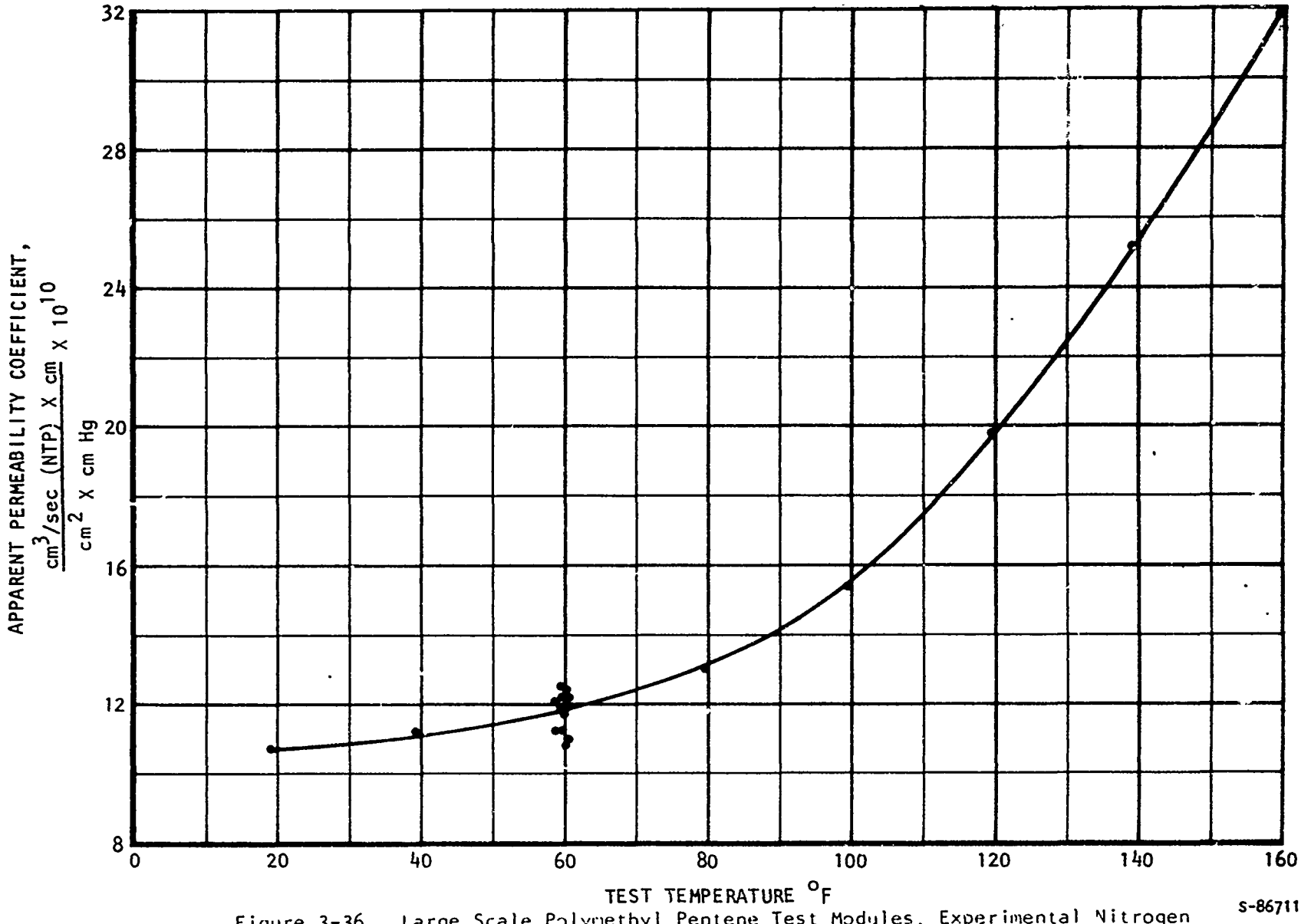

Figure 3-36. Large Scale Polymethyl Pentene Test Modules, Experimental Nitrogen Permeability at 30 psig Nominal Bleed Air Pressure

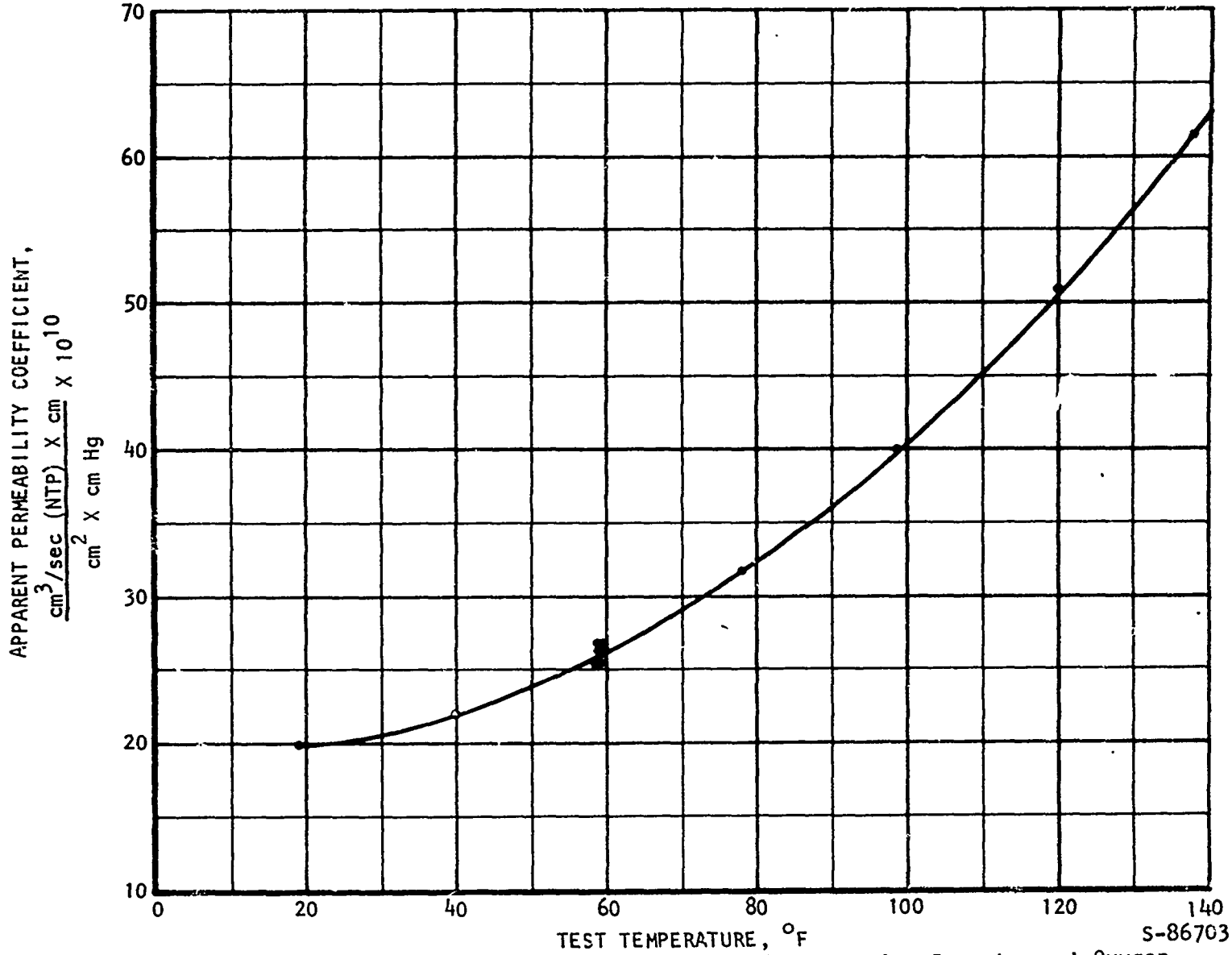

Figure 3-37 Large Scale Polymethyl Pentene Test Module, Experimental Oxygen Permeability at 30 psig Nominal Bleed Air Pressure

When evaluated on a percentage basis, the measured nitrogen permeability coefficient increase seems to be considerably greater than that of the measured oxygen permeability coefficient. It must be remembered that these values include some leakage through fibers, tube sheets, seals, and so forth. The leakage rate of both oxygen and nitrogen through various models can be calculated, it can be shown that the expected leakage rate difference through a given leakage path between oxygen and nitrogen do not differ too widely. Since the apparent permeability coefficient is proportional to the measured mass flow rate at a given pressure difference, it can be expected that whether oxygen or nitrogen is used there is an approximately equal additional component due to leakage, which would of course, tend to reduce the values of the apparent measured permeability coefficients by approximately constant values.

The effect of leakage on permeability separation factor (ratio of oxygen to nitrogen permeability coefficients) can be significant due to its effect on both parameters of the ratio. Uncorrected test results at 75°F show an experimental separator factor of 2.4 (using 30.7×10^{-10} for oxygen and 12.8×10^{-10} for nitrogen). If it is assumed that the large scale module leakage to oxygen was between 0 and 25% of the measured total, the effect of this leakage correction on tube permeability separation factor can be established by applying the assumptions discussed above. Figure 3-38 shows the corrected separator factor as a function of possible oxygen leakage fraction. Thus the separation factor from the previously assumed literature values of permeability coefficients (4.15) could result if approximately 19% of the measured oxygen flow was as a result of leakage. This would reduce corrected permeability coefficients to approximately 24.9×10^{-10} and 6.0×10^{-10} for oxygen and nitrogen respectively. If the ratio of tube wall thickness to membrane surface area used in the calculations were in error by about 15% in addition, the exact values from the ICI literature could be reproduced.

While the above example is merely speculative, since neither the leakage fraction or possible dimensional errors are accurately known, the analysis is demonstrative of the influence of these parameters. The establishment of leakage factors and dimensional uncertainty requirements to reproduce the exact ICI literature values are not impossible. Analysis of the small spiral wrap module's separation factor and that of the large scale parallel fiber module prior to low temperature testing and disassembly for repair show higher separation factors. Since

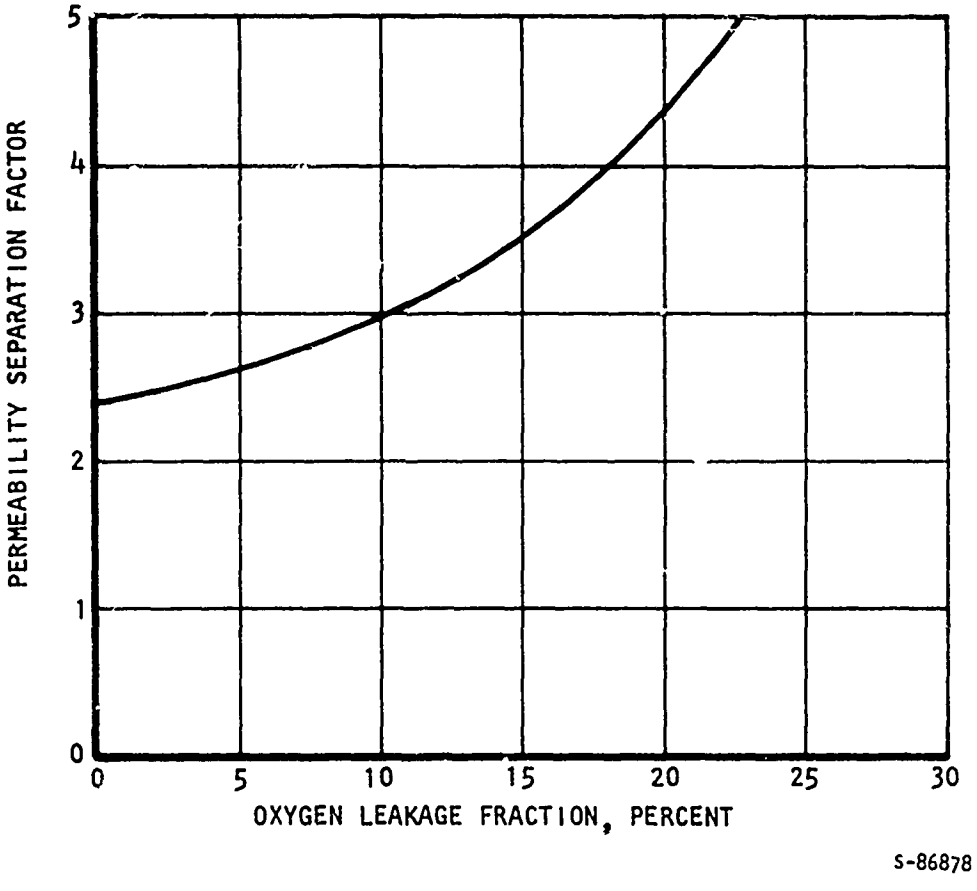

Figure 3-38. The Influence of Internal Leakage on Separation Factor

leakage can never increase the separation factor, the true value can not be less that the highest test value assuming that the two permeability coefficients are stable. A strong case for coefficient stability can be made as a result of the 1000 hour degradation check.

As discussed in Appendix A, it has been suggested that the permeability of certain polymeric materials to gases can be represented by an activation energy equation wherein the permeability at a given temperature is exponentially related to the reciprocal of the absolute temperature. To determine the reliability of this equation, in describing the test data through the test range, the logarithm of the permeability coefficient has been plotted as a function of the reciprocal of the absolute temperature for nitrogen and oxygen in Figure 3-39, for both the 10 psig and 30 psig, tube side nominal inlet pressures. On this semilog plot, if the relationship were valid, the data would fall on a straight line throughout the range of temperatures. As can be seen from Figure 3-39, this is not the case over the entire range, but may be approximately valid over more narrow temperature ranges. Of significance is the fact that the glass transition temperature for the polymethyl pentene fiber is approximately 85°F. At this point, since significant molecular structure transition occurs, some experimenters have reported appropriate changes in the permeability behavior of materials at the glass transition temperature. By considering this data in terms of two ranges, 100° to 160°F, and 60°F to 0°F, it can be seen that fair correlation to the linear relationships are achieved.

3. Air Separation Tests and Performance Prediction

The real significance of measured permeability data can be determined only when these values are used to predict the results, and are compared with experimentally determined air separation data. In order to verify the capability of the finite difference computer program to predict air separation performance, and to evaluate the use of measured apparent permeability coefficients in that program, air separation tests were run at the base line 60°F temperature as well as additional tests at 40° and 140°F. At the base line temperature of 60°F, data were taken for both 30 and 50 psig nominal inlet pressures. At other temperatures of 40° and 140°F, data were taken at only 30 psig inlet pressures. The tube side outlet flow rate was varied from 0.5 to 10 lb per hour while a sweep inlet flow rate was varied from 5 to 30 pounds per hour. Two separate types of tests were conducted. The first maintained

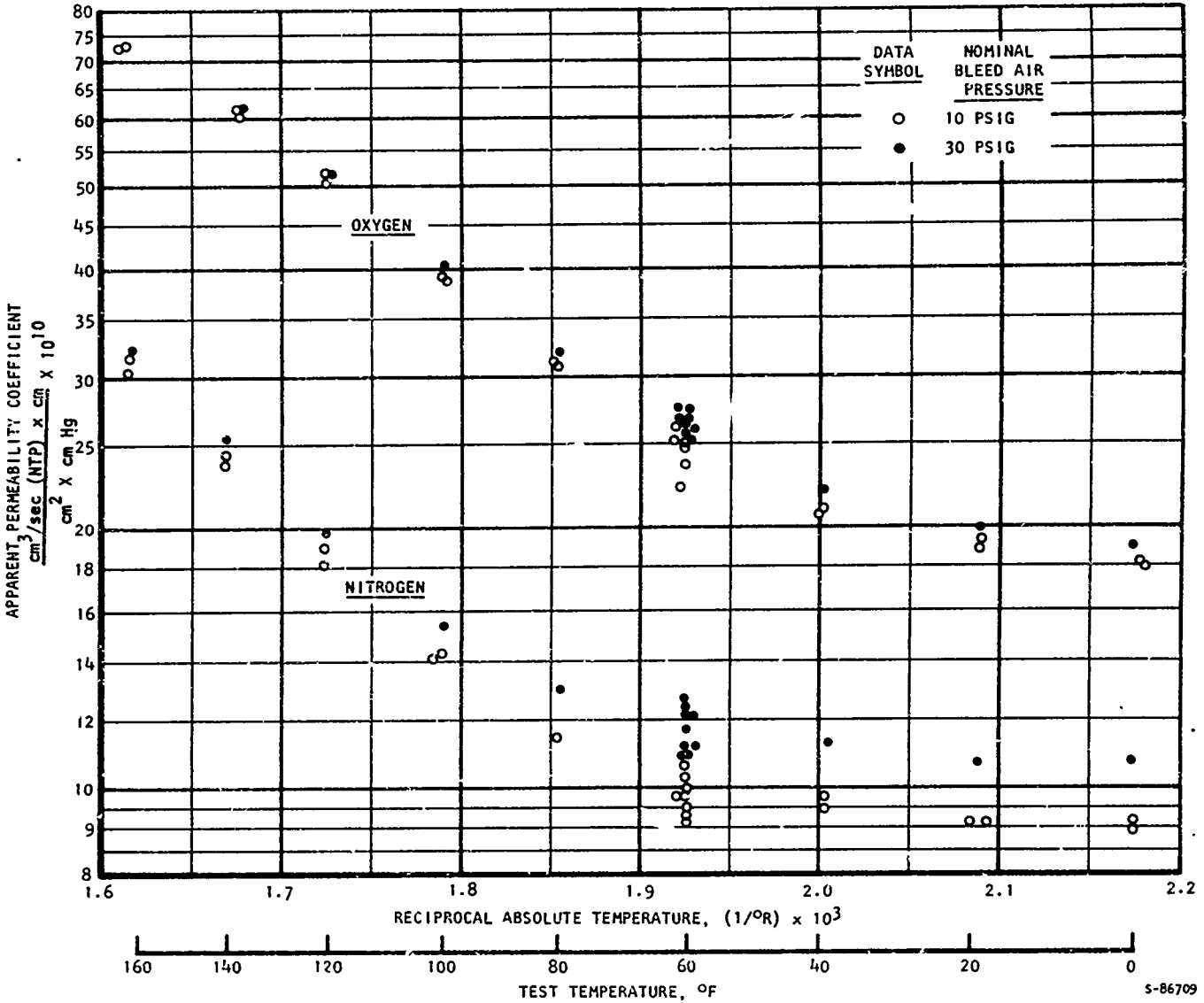

Figure 3-39. Large Scale Polymethyl Pentene Test Module, Experimental Permeability

a constant sweep ram inlet flow with a varied demand outlet tube side flow. The experimentally determined values of process gas outlet oxygen concentration were then plotted against process outlet flow rate. A second type of test held the process outlet flow rate constant and varied the ram side sweep flow to experimentally determine the value of increasing the ram air sweep flow.

Given the necessary parameters, the computer program calculated the tube side outlet oxygen concentration for various tube side flow rates. The necessary input parameters include the unit geometry, oxygen and nitrogen permeability coefficients and tube and shell side total pressures as well as tube side inlet oxygen concentration and an average shell side oxygen concentration. The permeability coefficients used in the program were determined from the previously described single gas permeability data. It was decided to use single gas permeabilities for the same total pressure as the nominal air inlet pressure since there seems to be some indication that the measured apparent permeability coefficients are somewhat pressure dependent functions. Of course, even if permeability is a function of pressure, the single gas tests were unable to differentiate between total pressure and partial pressure dependency. In any case, the permeability coefficients used for the computed curves in Figures 3-40, 3-41, and 3-42, were taken from the smooth curves constructed through the data of Figures 3-36 and 3-37. The actual test temperatures were used at each test data point as were the mean values of pressure on both the tube and shell side of the unit. The data presented on the curves of Figures 3-40, 3-41 and 3-42 however, are grouped into the nominal temperature range for clarity of presentation. The unit temperatures were never more than plus or minus $2^{o}F$ from the nominal range. The data shown on Figure 3-40 clearly indicate the close correlation of experimental values with computer predicted value for both 30 psig and 50 psig cases. It should be noted that since the same computer program was used for the designs discussed earlier in this report, the performance predicted for those designs is felt to be a realistic estimate of that achievable. The sweep inlet flow used in the testing presented in Figure 3-40 was 30 lb/hr. Test data are summarized in Appendix E where an example of the use of the digital computer program for data prediction is shown.

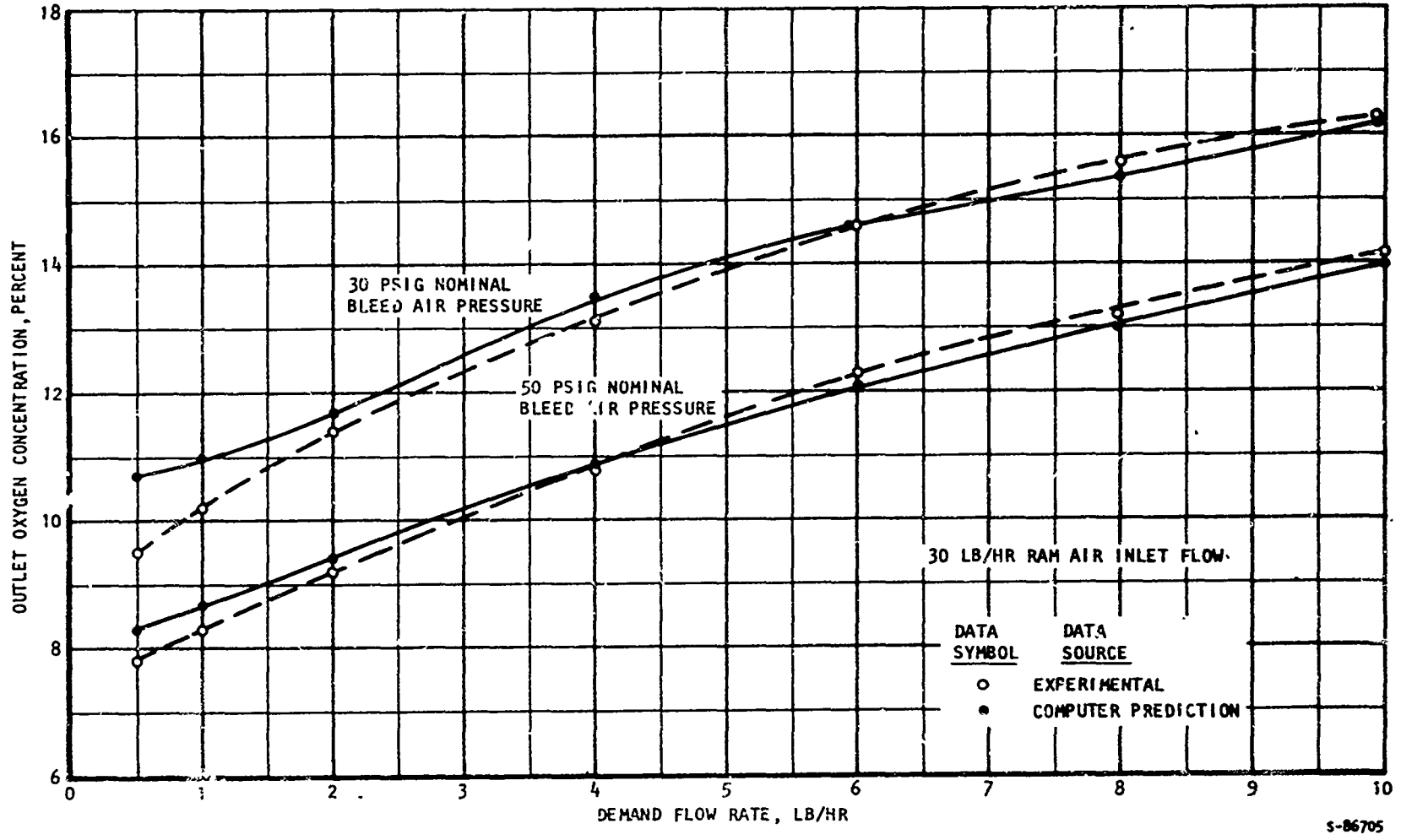

Figure 3-40. Large Scale Polymethyl Pentene Test Module, Air Separation Test at 60°F

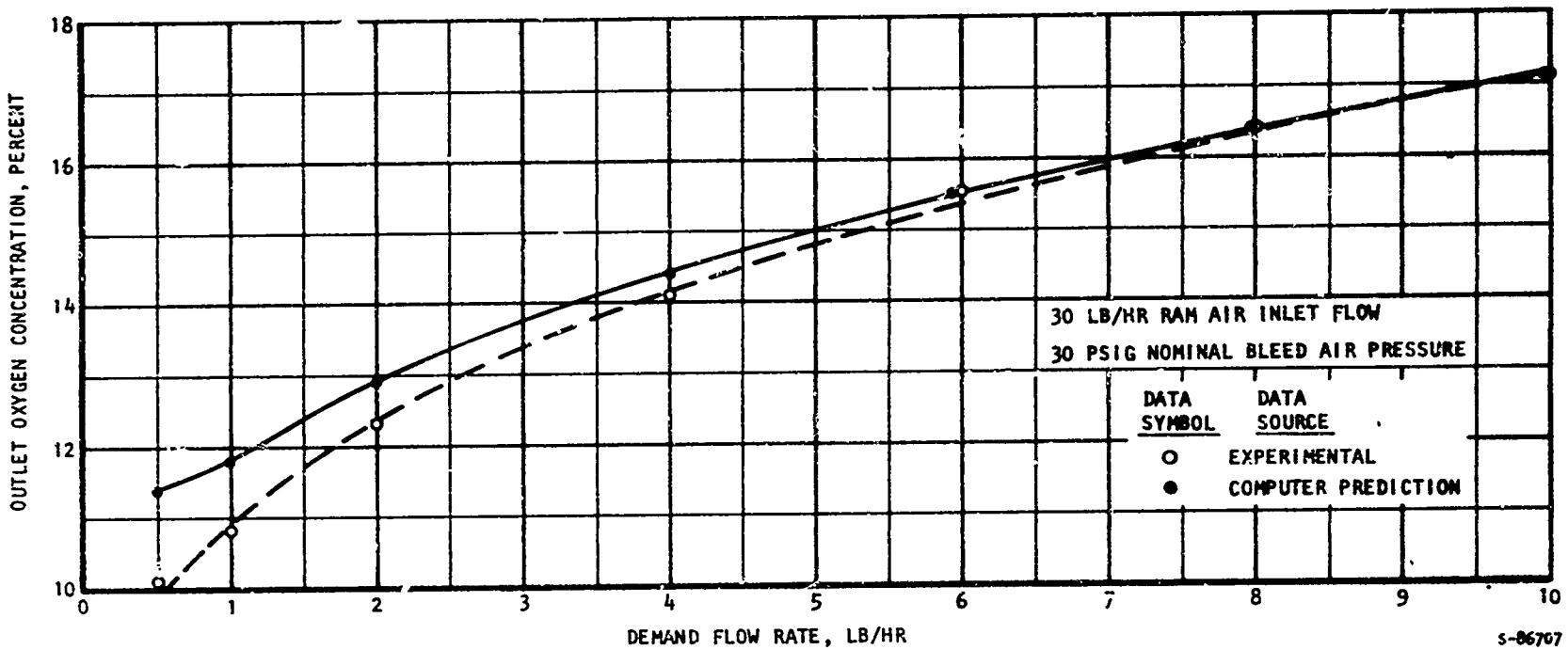

Figure 3-41. Large Scale Polymethyl Pentene Test Module, Air Separation Test at 40°F

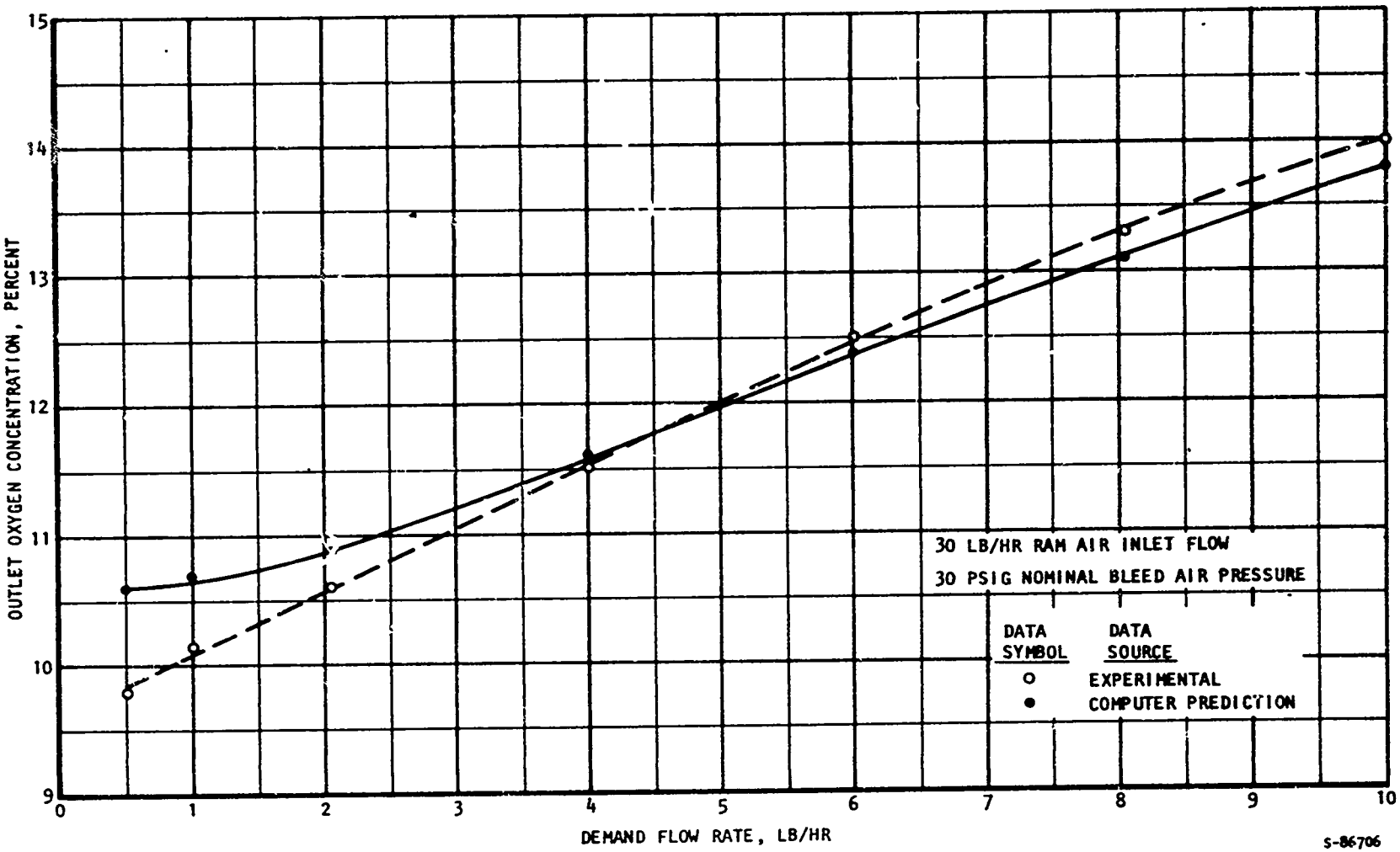

Figure 3-42. Large Scale Polymethyl Pentene Test Module, Air Separation at 140°F

Limitations in the digital computer program require constant total pressures for both tube and shell side as a part of the input. It was found expeditious to use the actual measured pressure drop data to determine mean tube side and shell side total pressures as was done for the single gas calculations. Shell side concentrations were calculated from the measured inlet concentrations and the measured inlet and outlet flow rates. Tube side concentrations were iteratively calculated to determine the tube side oxygen concentration at any given point.

Data for 40°F and 140°F are shown in Figures 3-41 and 3-42 for air separation with 30 lb/hr sweep inflow rate, respectively. This data are for tube side inlet pressures of a nominal 30 psig. Again, computed and experimental data show fairly good correlation.

A comparison of the experimental and computed curves of Figures 3-40, 3-41 and 3-42 indicate the ability of closely predicting the membrane performance of mass transfer units, using the techniques discussed above. In addition, the tests clearly demonstrate the air separation capability of the test units.

Analytical predictions discussed previously in this section indicate the process air outlet concentration to be a function of ram air inlet flow rates to the extent this tends to reduce the resultant oxygen concentration increase on the ram air shell-side of the module. Although the analysis shows the resultant process gas concentration to be a weaker function of ram air flow rate than of process outlet bleed air flow rate, the air separation tests included parametric variations of the ram air inlet flow rate to experimentally determine correlation.

Both experimental and computer prediction data for two conditions are shown in Figure 3-43. Although the data are limited to only three data points for each condition, a general correlation trend is achieved. The 20 lb/hr ram air inlet flow for the 30 psig nominal bleed air pressure case is the sole exception (of the six experimental data points shown). The measured concentration at the high flow rate exceeded those at lower ram air inlet flows. Since this trend would not be predicted by the equations of Appendix A or by the mathematical model, it is assumed that the data point is not typical, or possibly shows some air flow channeling resulting in local oxygen concentration buildup as a result of this very high flow.

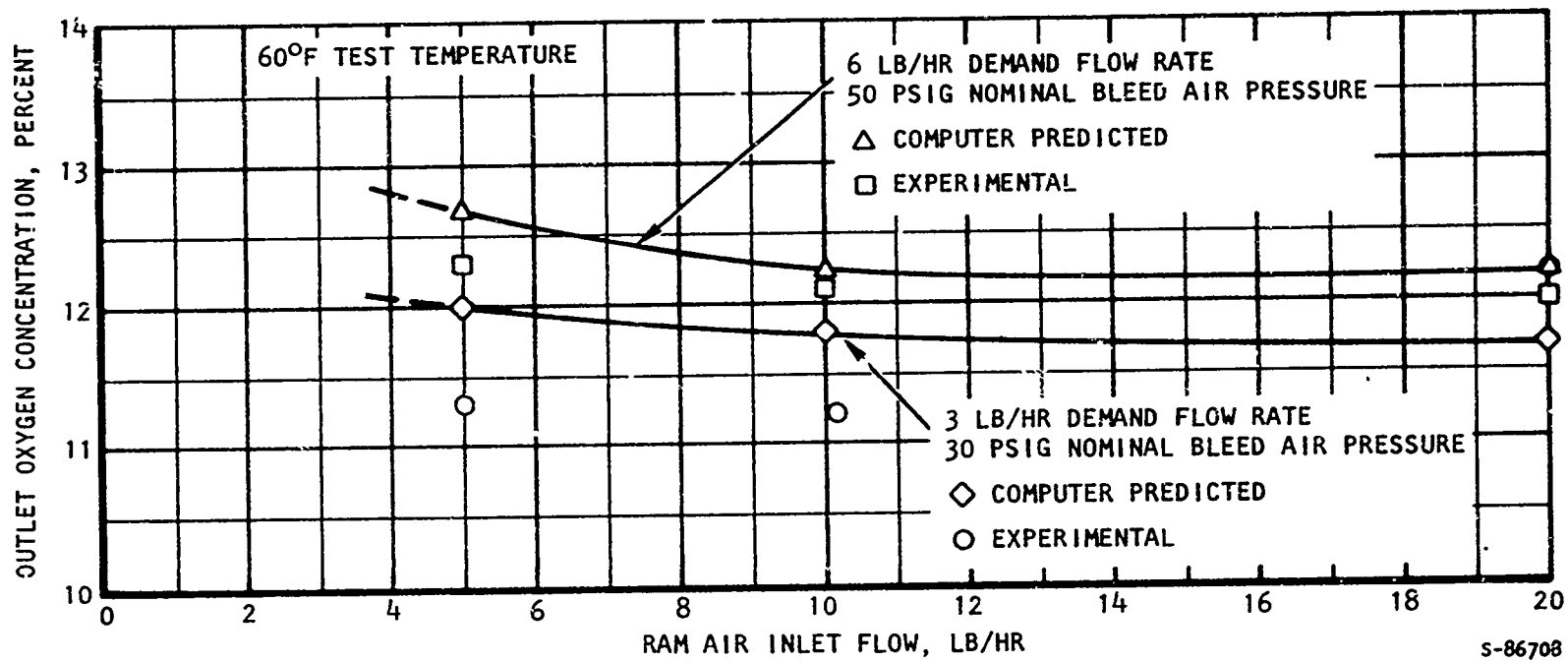

Figure 3-43. Large Scale Polymethyl Pentene Test Module, Air Separation Performance for Varying Ram Air Flow Rates

SECTION 4

OWNERSHIP CONSIDERATIONS

A feasibility analysis of the application of hollow fiber permeable membrane inert gas generator (IGG) to fuel tank inerting must include ownership considerations as well as technical feasibility. Principle ownership considerations of day-to-day operational logistic support and economic viability are discussed in this section.

OPERATING SUPPORT

A principle advantage of IGG based fuel tank inerting, in addition to a considerable projected savings in weight, is found in its freedom from logistical support in day-to-day operation. While maintenance support, typical of airborne pneumatic systems is required, it is the elimination of the resupply of the expendable inert gas to onboard storage vessels that is considered a significant ownership advantage.

The elimination of inert gas resuppl, will allow the adoption of fuel tank inerting without the need for a new class of ground service vehicles to meet and service aircraft during the short turn-around stops which are a normal part of current operations. Also eliminated is the setup of a network of resupply storage equipment at key airports and the expense of an expendable fluid, as well as the risk associated with the operation of an aircraft dispatch required safety system which could be rendered unusable due to resupply problems beyond the control of a commercial carrier.

The flexibility of IGG systems are also a consideration in the feasibility of their potential use. While inert gas storage based fuel tank inerting systems are limited in flight profile flexibility, especially the number of descents prior to resupply, IGG based inerting systems are seen to be independent of flight profile variations subject only to the operation within design descent rates.

COST CONSIDERATIONS

No system is feasible unless it is economically practical. One measure of this feasibility is a comparison of alternatives to determine economic viability. In the case of an airborne system, the cost of ownership over the life of the aircraft must be a factor in the comparison. While the comparative analysis of the hollow fiber permeable membrane IGG of this report with competitive approaches is beyond the scope of this report, an

analysis of the costs associated with this IGG system have been made. The remainder of this section is devoted to a discussion of the rough order of magnitude costs presented and the assumptions upon which they are based. The costs of ownership are discussed under the major cost projection categories: initial costs, maintenance costs, and operating costs.

Initial Costs

Initial cost may, in turn, be considered in terms of hardware procurement costs and the non-recurring costs associated with a particular application.

An estimate of non-recurring costs for the preliminary design of a DC-10 system as discussed in Section 3 has been made. The schematic diagram is repeated as Figure 4-1. Based on 1974 costs, a budgetary $1.5 million has been estimated for the design, development and qualification of a hollow fiber permeable membrane IGG fuel tank inerting system following the completion of the program outlined in Section 5. This figure is exclusive of AGE, ILS or other specific data items as well as airframe installation.

The estimated production hardware cost range has been established at $20,000 to $30,000 per shipset based on the system of figure 4-1 on a 100 unit basis. The air separation module represents the area of the least cost experience. Following the completion of the program recommended in Section 5, large production runs of single modules may reduce air separation module cost below 5¢ per square foot of active surface area. Initial prototype and production material costs however may run as high as an order of magnitude above final production costs for this one component.

The balance of the system components are based on current costs for similar aircraft Environmental Control System (ECS) production components.

Maintenance Costs

Maintenance costs are best considered on a statistical basis over the life of the equipment. To evaluate these costs, the existing, approved, support plan currently in effect for the DC-10 was used as a baseline for the component maintenance and maintenance support used to determine estimated maintenance costs.

Those elements pertinent to the maintenance support cost are summarized in Table 4-1. A number of key cost related assumptions are required to establish operating life. Where background data are available, historical

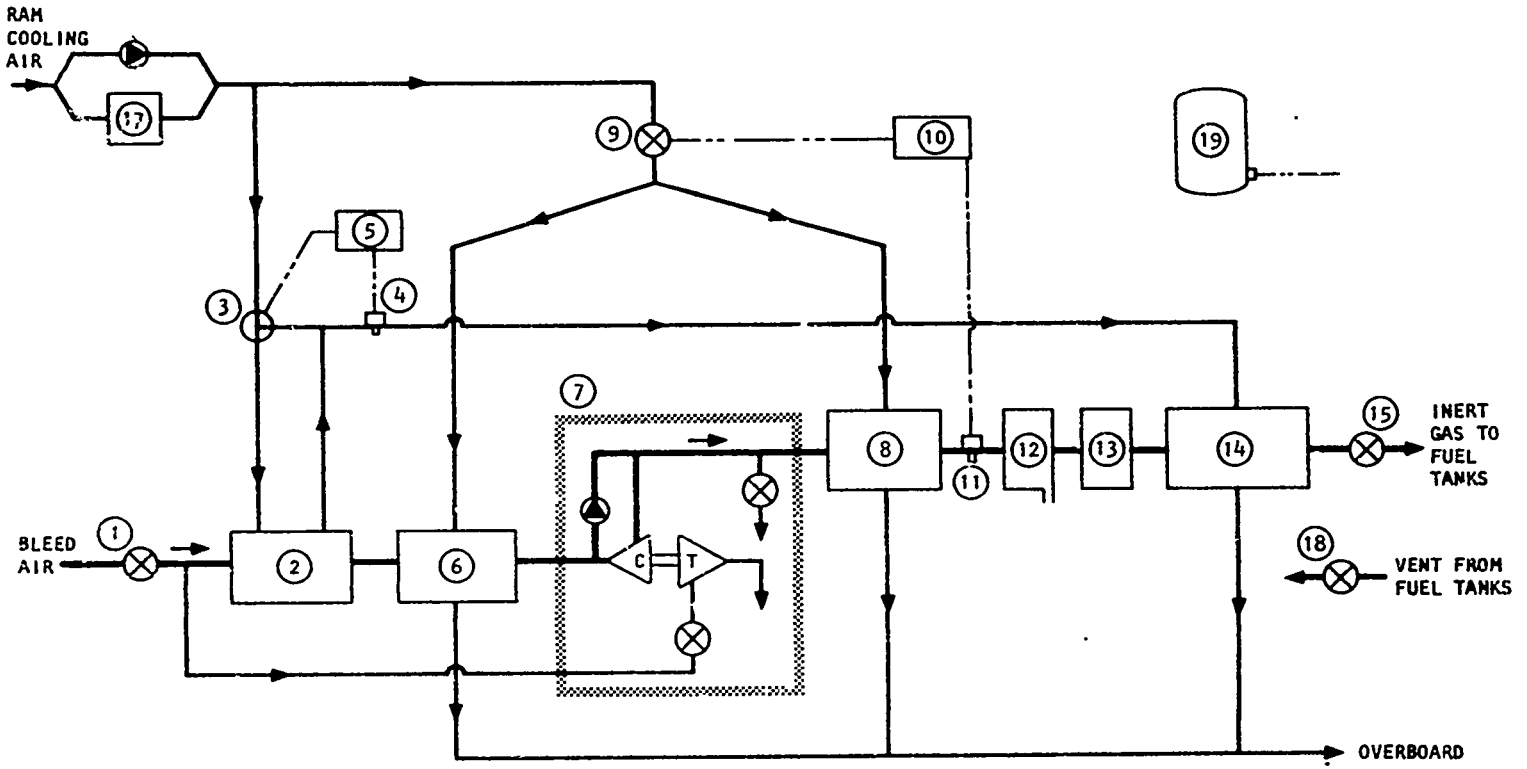

1. SHUTOFF VALVE
2. SWEEP AIR HEATER
3. SWEEP AIR DIVERTER VALVE
4. TEMPERATURE SENSOR
5. TEMPERATURE CONTROLLER (75°F)
6. PRIMARY HEAT EXCHANGER
7. TURBOCOMPRESSOR AND CONTROLS
8. SECONDARY HEAT EXCHANGER
9. COOLING AIR CONTROL VALVE
10. TEMPERATURE CONTROLLER (75°F)
11. TEMPERATURE SENSOR
12. INERTIAL PARTICLE SEPARATOR
13. FILTER
14. AIR SEPARATION MODULES
15. TANK INFLOW CONTROL VALVE
16. COOLING AIR CHECK VALVE
17. COOLING AIR FAN
18. TANK OUTFLOW VALVES (4 REQ'D)
19. EMERGENCY DESCENT AUGMENTATION HALON STORAGE ASSEMBLY

S-86872

Figure 4-1. Schematic Diagram, Permeable Membrane Fuel Tank Inerting System

TABLE 4-1. SUMMARY OF MAINTENANCE COST OF OWNERSHIP ELEMENTS

1.	AGE Costs per Flight Hour	$0.0535555
2.	On-Aircraft Preventive Maintenance Manhour per Flight Hour (MMH/FH)	0.0322500
3.	On-Aircraft Preventive Maintenance Spares Cost per Flight Hour	0.0172500
4.	On-Aircraft Corrective Maintenance Labor Costs (MMH/OH x 2.05 x Rate)	0.0250522
5.	On-Aircraft Corrective Maintenance Material Costs per Flight Hour (Operating Hour Costs x 2.05)	0.1109870
6.	Shop Repair Labor Costs (MMH/OH x 2.05 x Rate)	0.0992877
7.	Shop Repair Materials Costs per Flight Hour (OH x 2.05)	1.4693450
8.	Rotatable Spares Cycle (Price of 1 set of repairables for the life cycle plus 2-1/2% per annum) per Flight Hour to support 1-25 aircraft for 20 years Listed cost to support 25 aircraft	0.0222450
	Maintenance Logistics Costs per Flight Hour, Total	$1.8299724

information has been used per the assumptions outlined in Table 4-2 with the costs based on 1974 dollars. Those cost elements attributable to performance of maintenance are comparable to those presently being demonstrated on other DC-10 pneumatic systems.

The data presented in table 4-1 are the result of a preliminary quantitative maintainability program study to evaluate scheduled on-aircraft preventive maintenance, on-aircraft corrective maintenance, and shop repairs. Each component has been evaluated in terms of task definition, maintenance crew size, maintenance man hours per task, task frequency and finally maintenance man hours per flight hour.

The total cost projection of $1.83 per flight hour shown in Table 4-1 is for the complete inerting system of Figure 4-1. Previous analysis of inert gas storage based fuel tank inerting systems have shown comparable values for LN_2 systems.

Operating Costs

From the same approved DC-10, support plan used for the determination of maintenance costs, a typical flight profile and the average energies used for various flight phases by the IGG fuel tank inerting system have been tabulated in Table 4-3. The standard DC-10 flight profile from the approved support plan while different from the inerting system critical design mission of Section 2, is used for the determination of projected operating costs.

Table 4-4 shows the penalties assumed for the energy usage and system weight. These values were used to compute elements of fuel cost and the cost due to system weight.

Because of the low incremental increase in bleed airflow requirements needed by the IGG based fuel tank inerting system, the existing DC-10 pneumatic system is assumed able to provide the small added requirement. Because of the action of the bleed air control system, as discussed in Section 2, high stage bleed air was used for descent. However, low stage bleed air was used for the balance of the flight profile. The APU was used for all ground operations.

Fuel cost was assumed to be 35¢ per gallon.

Table 4-5 shows the fuel consumed for each of the basic mission elements for each of the energies. The total operating cost is estimated at $3.58/ flight hour based on the 1.6 hour flight profile.

TABLE 4-2. MAINTENANCE COST ASSUMPTIONS

Equipment Design Life (except air separation module) *(years)	20
Aircraft Utilization in Flight Hours (annual)	3600
Typical Operator, Fleet Size (DC-10 aircraft)	25
Ratio Engine Operation to Aircraft Flight Hours	1.3:1
Ratio Aircraft Flight Hours to APU Operating Hours	1:0.75
Ratio Inerting System Operating Hours to Aircraft Flight Hours	2.05:1
Annual Inventory Tax on Non-consumable Spares and AGE	2.5%
Inventory Control and Tax Charges for Repair Materials (Spares cost x 1.15)	15%
AGE Life in Years	20
New (Peculiar) AGE Costs	$64,300.00
Common AGE and Tools	N/A
Labor Rate per Hour	$10.75

*Estimated air separation module life of 2 years was assumed.

TABLE 4-3. ESTIMATED ENERGIES USED DURING A STANDARD DC-10 FLIGHT PROFILE

Flight Condition	Time Increment (Hrs)	Bleed Airflow (lb/min)	Ram Airflow (lb/min)	System Weight (lb)	Installed Weight (lb)
Ground (APU)	0.20	20	4.0 hp for fan	320	416
* Climb	0.30	22	65	320	416
* Cruise	1.0	4	15	320	416
* Descent	0.30	27	50	320	416
Landing rollout and taxi APU	0.20	20	4.0 hp	320	416

*Flight segment = 1.6 hours
Total flight hours/year = 3600 hours

TABLE 4-4. PENALTIES FOR POWER USAGE AND WEIGHT

Power Service or Weight Item	Penalty
Ram air	0.264 $\frac{\text{lb fuel/hr}}{\text{lb air/min}}$
Fan air	0.407 $\frac{\text{lb fuel/hr}}{\text{lb air/min}}$
Midstage bleed air	0.958 $\frac{\text{lb fuel/hr}}{\text{lb air/min}}$
High-stage bleed air	1.531 $\frac{\text{lb fuel/hr}}{\text{lb air/min}}$
Shaft power	0.237 $\frac{\text{lb fuel/hr}}{\text{hp}}$
Fuel (for APU)	1.0 $\frac{\text{lb fuel/hr}}{\text{lb air/min}}$
Equipment weight (except APU)	0.094 $\frac{\text{lb fuel/hr}}{\text{lb equip wt}}$
APU weight	0.130 $\frac{\text{lb fuel/hr}}{\text{lb APU wt}}$
Installed weight (except APU)	1.3 $\frac{\text{lb installed wt}}{\text{lb equip wt}}$
Installed weight (APU)	1.8 $\frac{\text{lb installed wt}}{\text{lb APU wt}}$

TABLE 4-5. FUEL CONSUMPTION PER FLIGHT SEGMENT

Flight Condition	Duration (Hr)	Engine or APU Bleed (lb fuel)	Shaft Power (lb fuel)	Ram Air (lb fuel)	Equipment Weight (lb fuel)
Ground APU	0.20	4.00	0.19	0	0
Climb	0.30	6.50	0	5.15	11.70
Cruise	1.00	3.80	0	4.00	39.00
Descent	0.30	12.40	0	4.00	11.70
Landing and rollout	0.20	6.00	0.19	0	0
	Total	32.7	.38	13.15	62.4

Total fuel per mission = 108.63 lb fuel per flight

= 67.5 lb fuel per flight hour

Fuel cost/flight hour = $\frac{(\$0.35)\ 67.5}{6.6}$ = \$3.58/flight hour

SECTION 5

PROGRAM CONCLUSIONS

From related background reports and as a result of this feasibility study and from laboratory demonstration for the on-board generation of an inert gas suitable for fuel tank inerting of a transport aircraft, a considerable amount of information has been developed. From this information, pertinent conclusions regarding the systems studied for the intended application can be drawn.

The following conclusions are based on the findings of this study and demonstration program as well as a review of related previous programs. The conclusions are summarized and presented with supporting rationale. At the outset, it should be noted that the successful laboratory demonstration of air separation by a hollow fiber permeable membrane module, to produce an inert gas to a predictable performance in concentrations sufficient for explosion suppression, has proven the feasibility of inert gas generation as a viable alternative to LN_2 storage for nitrogen inerting. Detail conclusions follow:

- Various means of explosion prevention systems are being considered for applications to commercial transport aircraft fuel tank ullage and vent systems. One of the systems successfully demonstrated has been the use of nitrogen gas to replace the air environment currently found in the fuel ullage.

  While consideration of fuel tank inerting as a means to reduce the hazard of explosion may be traced to at least the second World War, recent demonstrations using nitrogen gas have been made. These systems have used liquid nitrogen storage to supply the inert gas. Both military and civilian aircraft have been used as flying test beds. More recently, the Air Force has begun the first production contract for a retrofit of the C-5A Galaxy. Liquid nitrogen has been used as a means of reducing the weight and volume penalty associated with these systems.

- Due to the large quantities of inert gas required for fuel replacement and ullage repressurization, a considerable inert gas storage requirement results. The quantity is further increased by the requirement to design for several flight "legs" and by the need for flexibility.

  Economic consideration and past commercial transport experience with LN_2 for other purposes indicate storage and supply at selected airports. Flight variations require the consideration of alternate fields which may result in additional descent repressurization requirements. The overall system weights are largely determined by required LN_2 storage capacity.

- The use of LN_2 storage for fuel tank inerting systems will require modification to existing commercial transport operational procedures and will result in an operating cost associated with the resupply of the inert gas.

  Operational changes will include the need for additional ground service vehicles to resupply LN_2 to meet airport turn-around requirements. Operating costs associated with LN_2 based fuel tank inerting systems will include resupply of the inert gas.

- The complete absence of oxygen is not required to establish a gas suitable for fuel tank inerting purposes.

  Studies conducted by both military and civilian agencies have shown that oxygen concentrations as high as 12% by volume will not support combustion, even under optimum fuel vapor concentrations. For the purposes of this study, a limit of 9% oxygen was established.

- Inert Gas Generation (IGG) systems capable of the generation of a product containing less than 9% oxygen from the air are feasible. Both the use of hollow fiber permeable membranes and the catalytic reaction of oxygen from the air using aircraft fuel has been demonstrated. Preliminary design indicates that an IGG system will weigh a fraction of a liquid nitrogen system designed to DC-10 fuel tank inerting requirements and will require no special logistic considerations.

  Using the DC-10 as a design baseline, several candidate IGG systems were evaluated. The development of the catalytic combustor continues under Air Force sponsorship.

This study is the first to consider the application of hollow fiber permeable membranes. Although preliminary designs show the membrane system to be slightly heavier than the catalytic reactor, the subsystem offers the potential for reliable operation without the addition of new ignition sources or the generation of potentially harmful byproducts which could collect in the fuel tanks.

- A fuel tank inerting system based on hollow fiber permeable membrane generation of inert gas contains many of the components normally a part of an aircraft ECS. Only the hollow fiber module requires adaption of a new technology.

  The balance of the system consists of air-to-air heat exchangers, flow and temperature control valves and sensors, turbocompressors and electronic controls, all of which have established records of reliability and maintainability.

- The feasibility of hollow fiber permeable membrane air separation has been demonstrated analytically and during laboratory testing.

  Laboratory operation using air to simulate both bleed air and ram air flows have demonstrated the capability to produce an inert gas suitable for tank inerting. A mathematical model has been formulated which is capable of closely predicting complex test results. The model has been used to establish a preliminary design for the DC-10.

- Using available materials, fibers closely approaching the specified geometry, and modules demonstrative of air separation were constructed within the limited schedule and funding of the program. The fabrication of fibers of the specified dimension and modules showing full design performance appears possible with additional development.

  The full development cycle for the materials of the feasibility demonstration was approximately six months from design goal identification to delivery of the test hardware. This represents the first attempt to spin the identified material and fabricate modules of the type tested. The learning curve associated with this first attempt indicates continued progress toward meeting all design goals. The material selected for the test program was polymethyl pentene polymer.

- A preliminary design for an inert gas generator (IGG) fuel tank inerting system for a DC-10 has been completed. The system weight is estimated at 320 lb.

  The estimated weight is for a system with a hollow fiber polymethyl pentene air separation module; published material properties and optimum tube geometry were considered.

- Testing has demonstrated the ability of polymethyl pentene to perform without degradation following a continuous exposure to "real" air under simulated operating conditions for over 1000 hours.

  Although necessarily at low test pressures, no permeability degradation was noted by chemical reaction with laboratory air during the test period.

- Repair of test units to seal fiber damage is feasible.

  During the course of the program, the repair of an epoxy tubesheet was required due to voids which occurred during manufacture. A simple mechanical repair was achieved.

APPENDIX A

MEMBRANE GAS TRANSFER

This appendix is included to provide readers unfamiliar with the theory of membrane gas transfer a brief explanation of this mechanism. The treatment herein is not intended to be a comprehensive review of theory but rather is intended to summarize the basic equations to provide an introduction or review of the principles in sufficient detail to permit an understanding of the discussion in the body of the report. While more detailed treatments are available [9,10,11,12], the basic model described herein is sufficient to understand the phenomena of permeable membrane mass transfer to the degree required for this feasibility study. The mass transfer equations for the activated diffusion model are developed for both transient and steady state operation for an isotropic solid with an external penetrant which is in the gaseous state for free stream conditions outside the solid material.

ACTIVATED DIFFUSION MODEL

The activated diffusion model considers the overall mass transfer process, that is, permeation, to consist of a three-step process. Although the net transfer is the statistical result of the behavior of gas molecules in the system, this discussion will consider only the net effects. For a membrane wall with the same gas on either side at identical temperatures yet at different pressures (and therefore, concentrations), the mass transfer occurs in the following manner: First, gas molecules from the high pressure free stream dissolve in the surface of the membrane material, secondly, these molecules then diffuse through the polymer to the opposite surface, then finally, at the low pressure surface, the molecules come out of solution and again enter free stream, this time on the low pressure side of the membrane. In order to clearly understand gas permeation then, this discussion must consider both as desolving and subsequent outgasing at the surfaces, that is, gas solubility, and the diffusion process within the solid. In general, these processes are functions of the chemical and physical nature of both the gases and the polymer and external factors of temperature, pressure and concentration of the gas. The diffusion process in this model considers the actual molecular transfer through the polymer to depend on the formation of "holes" in the polymeric network due to thermal agitation of the polymer chain segments.

The diffusional driving force for transfer can be shown to be equal to the chemical potential gradient across the membrane polymer. For infinitely dilute solutions of the gas penetrant in the polymer, the chemical potential gradient is directly proportional to the concentration gradient. Thus, the mass flux of the gas through a unit surface area normal to the direction of mass flow can be expressed similarly to Fourier's expression for the flux of heat through a surface. The resultant expression is known as Fick's first law of diffusion.

$$J = -D(\partial C/\partial X) \qquad \text{(A-1)}$$

where: J = mass flux
C = gas concentration in polymer
X = space coordinate
D = diffusion coefficient

Fick's first law of diffusion states that the steady state mass flow through a unit area normal to the direction of flow is directly proportional to the gradient of the concentration but in the opposite direction.

For a steady state mass transfer through two unit surface areas normal to the mass flux, separated by a small but finite distance ΔX (Delta X), the flux for an isotropic material with a constant diffusion coefficient may be written as:

$$J = -D(\Delta C/\Delta X) \qquad \text{(A-2)}$$

where: ΔC = the difference between concentrations between the two unit surface areas

The steady state mass flow for any given surface area may then be expressed as:

$$\dot{Q} = -DA(\Delta C/\Delta X) \qquad \text{(A-3)}$$

where: $\dot{Q}$ = mass transfer rate
A = surface area normal to mass transfer

A unidirectional flow over the volume element bounded by two unit areas normal to the directional flow and separated by a small but finite distance has a capacity for mass storage with time. If the diffusion coefficient is assumed to be independent of time and concentration, and the material is isotropic to

diffusion, showing no dependence of the diffusion coefficient to spatial location, a Taylor's expansion of the concentration gradient at each of the unit surface areas may be made. The rate of mass storage may also be expressed in terms of the time rate of change of the average concentration of the volume element. In the limit, as the distance between the unit normal areas is reduced to zero, the following equation results:

$$\frac{\partial C}{\partial t} = D \frac{\partial^2 C}{\partial X^2} \qquad \text{(A-4)}$$

where: t = time

This is known as Fick's second law of diffusion and describes the fundamental transient relationship for a constant diffusion coefficient in an isotropic polymer. Since experimental data taken on this program have shown the transient times to be extremely short, and the quantity of mass actually stored small, no further consideration of transient response will be discussed.

Equilibrium solubility of a gaseous penetrant in a polymer for sufficiently low gaseous concentrations can be related to the partial pressure of the gas by Henry's law.

$$C = SP \qquad \text{(A-5)}$$

where: P = free stream gas partial pressure
S = solubility coefficient

If Henry's law is assumed to hold true throughout the operating range and the solubility coefficient at a given temperature is a function only of the polymer, the gas and their interaction, the gas concentration in membrane surfaces under equilibrium conditions can be established. For the previously discussed model of a permeable membrane separating a gas at two different pressures at the same temperature, the equilibrium concentrations of the gas in each surface of the membrane may now be established as follows:

$$C_1 = SP_1 \qquad \text{(A-6)}$$

$$C_2 = SP_2 \qquad \text{(A-7)}$$

Where condition 1 describes the high pressure gas/polymer interface equilibrium and condition 2 describes the low pressure gas/polymer interface equilibrium.

Since these concentrations, separated by a small finite distance, form the driving force for diffusion, the steady state mass transfer for these concentrations may be written for a finite thickness and surface area normal to the mass flow as follows:

$$\dot{Q} = \frac{-DA(C_1-C_2)}{\Delta X} \qquad \text{(A-8)}$$

Substituting the values of concentrations in terms of the equilibrium solubility coefficients described above, the expression for mass transfer through the polymer may be written in terms of the free stream partial pressures as:

$$\dot{Q} = \frac{-DSA(P_1-P_2)}{\Delta X} \qquad \text{(A-9)}$$

The mass flow rate through the polymer at steady state conditions must equal the free stream mass flow rate from opposite sides of the polymeric membrane. The product of the diffusion and solubility coefficients is defined as the permeability coefficient, thus, the net free stream steady state mass transfer rate may be conveniently expressed as:

$$\dot{Q} = \frac{TPA(P_1-P_2)}{\Delta X} \qquad \text{(A-10)}$$

where: TP = permeability coefficient (-DXS)

Or, when several gases are present the relationship may be expressed as:

$$\dot{Q}_i = \frac{TP_i A(P_1-P_2)_i}{\Delta X} \qquad \text{(A-11)}$$

Where the subscript i denotes the ith gas, that is, the mass transfer rate is proportional to the partial pressure driving force across the membrane wall for the ith gas as proportioned by the ith permeability coefficient.

TEMPERATURE DEPENDENCE

Although the permeability coefficients may in general be a function of temperature, gas concentration, position, and time, the materials selected for this study generally exhibit significant permeability coefficient dependence only on temperature. For many materials, there is some violation of Henry's law, that is, solubility actually varies somewhat with both concentration and total pressure. The major problems with diffusion occur for materials which

exhibit "swelling" with exposure to certain penetrants causing the diffusion coefficient to vary greatly with increasing concentrations. Fortunately, experiments with polymers of the type considered for this study, using atmospheric gases, indicate that the use of permeability coefficients depend only on temperature are of sufficient accuracy for the purpose of this feasibility study.

Temperature dependence of diffusion and solubility coefficients over sufficiently small ranges for the polymeric materials and penetrant gases considered in this study can generally be expressed by Arrhenius relationships.

$$D = D_o e^{-\left(\frac{E_D}{RT}\right)} \qquad \text{(A-12)}$$

$$S = S_o e^{-\left(\frac{\Delta H_s}{RT}\right)} \qquad \text{(A-13)}$$

where: D_o, S_o = frequency factors (constants) for diffusion and solubility respectively

E_D = diffusion activation energy

ΔH_s = heat of solution

R = gas constant

T = absolute temperature

e = base of a Naperian Log System (2.718...)

Since the permeability coefficient is defined as the product of the diffusion and solubility coefficients, the permeability coefficients temperature dependence may also be expressed by an Arrhenius relationship as:

$$P = P_o e^{-\left(\frac{E_p}{RT}\right)} \qquad \text{(A-14)}$$

where: P_o = frequency factor constant for permeability ($D_o \times S_o$)

E_p = pseudo activation energy

Since both solubility and diffusion coefficients, and therefore the permeability coefficients, are functions of temperature, the above expression is useful to estimate permeability coefficients at other temperatures over a limited range, however, solutions for the constants require permeability data be taken at least at two different temperatures. Fortunately, the diffusivity usually

increases and the solubility usually decreases with increasing temperature, thus mitigating some of the temperature dependence of the permeability coefficient.

PERFORMANCE LIMIT

In addition to the equations relating to membrane mass transfer ratio, it is useful to develop an equation to establish the theoretical minimum reduction in oxygen concentration that can be achieved for a given gas mixture/polymer system. In physical terms, the transfer rates across the membrane wall for each gas in the system is dependent upon the local values of partial pressure for the gases on each side of the membrane wall. If a gas is constrained to flow along a membrane wall without access to an infinite source of gas at the original composition (such is the case in a long tube), the local concentration of that gas sample will tend to change with time, as it passes along the membrane wall as a result of the relative rates of permeation of each gas species from the sample through the wall. These rates are in proportion to the permeability coefficient and the local partial pressure driving force. In the case of air under pressure in a hollow fiber, the initial tendency is to transfer oxygen and nitrogen through the membrane, but the proportion of oxygen in the pemeated gas exceeds the proportion of oxygen in the air flow along the tube. As a result of this depletion of oxygen from the original air sample, the driving force for additional oxygen transfer drops as the air proceeds along the tube. If the velocities are low, the pressure drop is also low and the nitrogen driving force will tend to increase.

As the air remaining in the original sample element flows along the tube, the proportion of oxygen in the permeating gas continues to decrease. At the theoretical limit, its oxygen concentration approaches the oxygen concentration of the gas remaining in the sample continuing down the tube. From that point, further tube length will only tend to reduce the flow rate down the tube (due to gas lost in permeation) but will not further decrease the oxygen concentration.

The general form of the mass transfer equation, as shown as equation (A-11) can be written for an oxygen/nitrogen two-gas system as

$$\dot{Q}_0 \qquad \frac{\bar{P}_0 \, A \, \Delta P_0}{\Delta X} \qquad \text{(A-15)}$$

and

$$\dot{Q}_N = \frac{TP_N A \Delta P_N}{\Delta X} \qquad \text{(A-16)}$$

where the subscrips 0 and N denote oxygen and nitrogen, respectively.

At the limiting concentration, as discussed above:

$$\frac{\dot{Q}_O}{\dot{Q}_N} \propto \frac{Conc_O}{Conc_N} \propto \frac{P_O}{P_N} \qquad \text{(A-17)}$$

where P_O and P_N are the tube side oxygen and nitrogen partial pressures, respectively. If the oxygen concentration of the remaining gas sample is denoted by the symbol c , where:

$$c = \frac{P_O}{P_O + P_N} \qquad \text{(A-18)}$$

and the ratio of the permeability coefficients for oxygen and nitrogen defined by the symbol TPr where:

$$TP_r = \frac{TP_O}{TP_N} \qquad \text{(A-19)}$$

an expression for the limiting value of c may be derived. By substituting the definitions of total pressures as the sum of partial pressures, and the tube partial pressures as a sum of the permeant side partial pressure plus the driving force partial pressure for each gas, the following relationship is found to exist as the theoretical minimum oxygen concentration.

$$\frac{P}{P'} = \frac{\left[c' \left(\frac{1-c}{c}\right) TPr - (1-c')\right]}{c\left[\left(\frac{1-c}{c}\right) TPr + 1\right] - 1} \qquad \text{(A-20)}$$

where P = tube side total pressure

P' = shell side total pressure

c' = shell side oxygen concentration

The solution of the above expression for c, the tube side limiting oxygen concentration, results in a quadradic equation. The meaningful root may be expressed as follows:

$$c = \frac{-Y - \sqrt{Y^2 - 4XZ}}{2X} \qquad \text{(A-21)}$$

where: $X = P (\Pi r - 1)$

$Z = c' \Pi r P'$

$Y = (c'-1) P' - X - Z$

A solution may also be determined in terms of the pressure ratio P/P', but the form given above has been found to be most useful in the analysis considered in the feasibility study.

The importance of equation (A-21) can be seen in a simple expression for theoretical inert gas concentration limits expressed in terms of only the gas total pressures (or pressure ratio), the permeability coefficient ratios for oxygen and nitrogen, and the oxygen concentration on the shell side of the concentrator.

As a numerical example, consider tube side air at 65 psia and shell side air at 15 psia. To evaluate the minimum oxygen concentration to which the air may be processed for ideal conditions for a material exhibiting a permeability coefficient to oxygen four times that to nitrogen, the following results:

$X = 65 \times (4-1)$

$= 195.00$

$Z = 0.21 \times 4 \times 15$

$= 12.60$

$Y = (0.21-1.00) \times 15 - 195 - 12.60$

$= -219.45$

$c = 0.061$ (6.1% oxygen by volume)

APPENDIX B

TEST MODULE CHARACTERISTICS

During the second phase of the program, permeable membrane hollow fibers of the required size were prepared and two test modules were constructed. These modules are identified as the small spiral wrapped module and the large scale parallel fiber module. The following configuration data were supplied with these test units.

TABLE B-1

SMALL SPIRAL WRAPPED TEST MODULE CONFIGURATION

MEMBRANE POLYMER: POLYMETHYL PENTENE
NOMINAL FIBER DIAMETER (OUTSIDE/INSIDE): 75μ/53μ
NOMINAL WALL THICKNESS: 11μ
AVERAGE ACTIVE FIBER LENGTH: 14 IN.
AVERAGE TOTAL FIBER LENGTH: 15 IN.
NUMBER OF FIBERS: 16,000
LOG-MEAN SURFACE AREA: 12.2 FT^2
TUBE-SHEET MATERIAL: POLYURETHANE RESIN
CASE MATERIAL: POLYCARBONATE
MODULE TYPE: PERMANENTLY BONDED

TABLE B-2

LARGE SCALE PARALLEL FIBER MODULE CONFIGURATION

MEMBRANE POLYMER: POLYMETHYL PENTENE
NOMINAL FIBER DIAMETER (OUTSIDE/INSIDE): 72μ/54μ
NOMINAL WALL THICKNESS: 9μ
ACTIVE FIBER LENGTH: 50 IN
TOTAL FIBER LENGTH: 56 IN.
NUMBER OF FIBERS: 965,000
LOG-MEAN SURFACE AREA: 2590 FT^2
TUBE SHEET MATERIAL: DOW ADHESIVE DIR 321
CASE MATERIAL: FILAMENT WOUND EPOXY-FIBERGLAS
MODULE TYPE: REMOVABLE MEMBRANE INSERT

Photographs of the modules are included in Section 3 of the body of the report. Data presented in the tables are determined by various test methods. While the accuracy of the fiber geometry and count is not known, use of the value in this appendix produces results within the range of those of earlier polymethyl pentene experimenters. However certain of the conclusions drawn from the Section 3 test data indicate that the large scale polymethyl pentene surface area or thickness may be slightly in error.

APPENDIX C

1000 HOUR DEGRADATION CHECK

TEST DATA

Data taken during the small spiral wrap test module's 1000 hour degradation check are presented in Table C-1.

The data show outlet oxygen concentration as a function of outlet flow rate taken at approximately 250 hour test intervals. Between these performance profile measurement tests, data for continuous operation were continuously recorded on a strip chart. The data sheets show the maximum and minimum values for each of the parameters during the 250 hour steady state operating periods. A more complete discussion of the data is found in Section 3 of this report.

The test gas on the bleed air side (tube-side) of the test module was laboratory air, filtered to remove particulate contamination. Nitrogen gas was used as the test fluid on the ram air side (shell-side) to allow the outlet oxygen concentration to vary between ambient and inert conditions. The use of air as the ram air working fluid would not permit a wide range of oxygen concentration to be achieved in the bleed air outlet flow due to the 5 psid limit imposed by the test module as discussed in Section 3.

The following data columns are for table C-1.

- Test date - the calendar date (month-day-year) on which the data point was recorded (or in the case of the data taken between profile tests, the range of dates is separated by a (1).
- T_B(^{o}F) - the isothermal test temperature measured at the bleed air outlet port.
- P_B (psia) - the bleed air side operating pressure measured at the bleed air inlet port (negligible pressure loss)
- P_R (psia) - the ram air side (nitrogen) pressure
- $\dot{M}_B$ IN (lb/hr) - the bleed air mass flow rate measured at the air separator module's tube side bleed air inlet port
- $\dot{M}_B$ OUT (lb/hr) - the bleed air mass flow rate measured at the air separator module's tube side bleed air outlet port (the processed gas)
- $\dot{M}_R$ IN (lb/hr) - the inlet nitrogen flow rate to the shell side of the module

- O_2B IN (percent) - the oxygen concentration (percent of volume) in the laboratory air used as a test gas
- O_2B OUT (percent) - the oxygen concentration measured in the processed air at the bleed air outlet port

TABLE C-1. 1000 HOUR PERFORMANCE DEGRADATION CHECK TEST DATA SUMMARY

Test Date	T_B (°F)	P_B (psia)	P_R (psia)	$\dot{M}_B$ IN (lb/hr)	$\dot{M}_B$ OUT (lb/hr)	$\dot{M}_R$ IN (lb/hr)	O_2B IN (percent)	O_2B OUT (percent)
10-15-73	72	19.7	14.74	0.02	0.018	0.54	20.7	4.7
	73	19.7	14.74	0.03	0.031	0.54	20.7	10.7
	72	19.7	14.74	0.06	0.057	0.54	20.7	14.4
	72	19.7	14.74	0.10	0.092	0.54	20.7	16.7
	73	19.7	14.74	0.14	0.1335	0.54	20.7	17.7
	73	19.7	14.74	0.18	0.182	0.54	20.7	18.4
	73	19.7	14.74	0.02	0.0184	0.54	20.7	8.7
	73	19.71	14.77	0.02	0.0125	0.54	20.7	6.65
	73	19.71	14.77	0.03	0.0246	0.54	20.7	9.25
	73	19.70	14.77	0.06	0.0531	0.54	20.7	13.95
	73	19.70	14.77	0.100	0.095	0.54	20.7	16.35
	73	19.70	14.77	0.140	0.128	0.54	20.7	17.55
	73	19.70	14.77	0.18	0.166	0.54	20.7	18.2
10-15	73	19.67	19.2	0.025	0.0191	0.58	20.7	8.15
10-25	73	19.4	19.25	0.0246	0.0177	0.57	20.7	7.75
10-25	73	19.7	14.75	0.04	0.0315	0.58	20.7	11.3
	73	19.7	14.75	0.1	0.092	0.058	20.7	16.75

TABLE C-1 (continued)

Test Date	T_B (F)	P_B (psia)	P_R (psia)	$\dot{M}_B$ IN (lb/hr)	$\dot{M}_B$ OUT (lb/hr)	$\dot{M}_R$ IN (lb/hr)	O_2B IN (percent)	O_2B OUT (percent)
10-25	73	19.92	14.90	0.026	0.0199	0.59	20.7	8.
11-6	73	19.7	14.74	0.025	0.0160	0.58	20.7	7.80
11-6-73	73	19.70	14.9	0.04	0.0337	0.58	20.7	11.25
	73	19.70	14.9	0.06	0.0517	0.58	20.7	13.15
	73	19.70	14.9	0.10	0.0903	0.58	20.7	16.20
	73	19.70	14.9	0.16	0.1245	0.58	20.7	17.25
11-6	73	19.72	14.86	0.0254	0.0198	0.58	20.7	7.90
11-16	73	19.70	14.34	0.0254	0.0198	0.58	20.7	7.40
11-16	73	19.	14.84	0.04	0.029	0.58	20.7	10.3
	73	19.	14.84	0.06	0.052	0.58	20.7	13.7
	73	19.	14.84	0.10	0.0897	0.58	20.7	16.1
	73	19.	14.84	0.13	0.1196	0.58	20.7	17.15
	73	19.	14.84	0.16	0.1485	0.58	20.7	17.65
	73	19.	14.84	0.18	0.1662	0.58	20.7	17.85
11-16	73	19.	14.85	0.0254	0.0198	0.058	20.7	8.0
11-26	73	19.60	14.72	0.0254	0.0197	0.054	20.7	7.35

TABLE C-1 (continued)

Test Date	T_B (^oF)	P_B (psia)	P_R (psia)	$\dot{M}_B$ IN (lb/hr)	$\dot{M}_B$ OUT (lb/hr)	$\dot{M}_R$ IN (lb/hr)	O_2B IN (percent)	O_2B OUT (percent)
11-26-73	73	19.7	14.72	0.04	0.028	0.54	20.7	10.1
	73	19.7	14.72	0.06	0.050	0.54	20.7	13.65
	73	19.7	14.72	0.08	0.0715	0.54	20.7	15.30
	73	19.7	14.72	0.10	0.0883	0.54	20.7	16.20
	73	19.7	14.72	0.13	0.1195	0.54	20.7	17.25
	73	19.7	14.72	0.16	0.1486	0.54	20.7	17.85
	73	19.7	14.72	0.18	0.166	0.54	20.7	18.25

APPENDIX D

SINGLE GAS PERMEATION TEST DATA

The single gas permeation test data, discussed in Section 3 of the report are presented in summary form in Table D-I of this appendix. The data presented in this table consist of all single gas permeation data taken subsequent to the repair of the large scale module's O-ring seals as discussed in Section 3.

The data of Table D-1 were taken from the laboratory test data sheets and include the basic measurement data and resultant calculated values required to establish values of apparent permeability coefficient. The apparent permeability coefficient is evaluated by solving equation (A-11) of Appendix A for the permeability coefficient. Since a single gas system is tested, partial pressures are the measured total pressures and equation (A-11) may be rewritten as:

$$TP = \left(\frac{th}{A}\right) \frac{\dot{Q}}{\Delta P} \qquad (D\text{-}1)$$

where TP = experimentally measured permeability coefficient

th = tube wall thickness

A = log mean membrane surface area

$\dot{Q}$ = measured flow rate

ΔP = pressure driving potential

The resultant value of permeability coefficient determined by this test method is denoted as "apparent permeability coefficient" because of the influence of other factors. Most significant are the leakage and geometry uncertainties.

A simplified test schematic is shown as Figure D-1. During testing, both the high pressure tube side (bleed air side) flow rate $\dot{M}_B$, and the low pressure shell side (ram air side) flow rate $\dot{M}_R$, were recorded. The ram air side measured flow rate used in the calculation of apparent permeability coefficient from equation (D-1) includes all internal leakage through fibers damaged in assembly, tube-sheet voids and seal leakages. An additional source of error in the calculation of the apparent permeability coefficient resulted from

TABLE D-1. SINGLE GAS PERMEATION TEST DATA SUMMARY
(POST LEAKAGE REPAIR)

Test Date	Test Time Hr:Min)	Test Gas	T_R OUT (°F)	P_B IN (psig)	$\bar{P}_B$ (psig)	$\bar{P}_R$ (psig)	$\dot{M}_R$ (lb/hr)	$\dot{M}_R/\Delta P$	$\dot{M}_B$ IN (lb/hr)	Flow Balance Error (%)	Apparent Permeability Coefficient $\frac{\left(\frac{cm^3}{sec}\ @\ NTP\right)(cm)}{(cm^2)(cm\ Hg)}$
3-13-74	11:20	N_2	59.9	10.0	9.80	0.06	1.18	0.121	1.125	-4.7	9.51×10^{-10}
	11:55		58.8	20.0	19.68	0.11	2.60	0.133	2.56	-1.5	10.45
	12:15		58.8	29.95	29.55	0.18	4.19	0.143	4.24	1.2	11.24
	12:35		58.8	39.95	39.48	0.26	5.85	0.149	5.96	1.9	11.71
	12:50		59.5	50.0	49.50	0.35	7.69	0.157	7.80	1.4	12.34
	12:55		59.3	40.0	39.54	0.26	5.83	0.148	5.91	1.4	11.63
	13:00		59.5	30.0	29.60	0.19	4.19	0.143	4.24	1.2	11.24
	13:10		59.8	20.0	19.68	0.11	2.64	0.135	2.59	-1.9	10.61
	13:15		60.0	10.0	9.80	0.06	1.22	0.125	1.17	-4.1	9.82
3-13-74	13:50	O_2	60.2	10.05	9.45	0.08	3.32	0.354	3.27	-1.5	24.34
	14:10		59.1	20.1	19.19	0.17	6.89	0.362	6.95	0.9	24.89
	14:20		58.9	30.0	28.89	0.28	10.62	0.371	10.85	2.2	25.51
	14:25		59.0	40.05	38.83	0.43	14.5	0.378	15.0	3.4	26.0
	14:30		59.0	50.0	48.68	0.60	18.7	0.390	19.25	2.9	26.82
	14:35		59.2	40.05	38.83	0.43	14.6	0.372	14.95	2.4	25.58
	14:40		60.0	30.05	28.95	0.29	10.7	0.373	10.9	1.9	25.65
	14:50		61.0	20.10	19.20	0.17	6.95	0.365	6.98	0.4	25.1
	14:55		61.9	10.05	9.40	0.08	3.40	0.365	3.31	-2.6	25.1
3-14-74	9:25	N_2	80.1	10.05	9.80	0.09	1.41	0.145	1.35	-4.3	11.40
	9:30		80.1	20.0	19.59	0.21	2.97	0.153	2.97	0	12.02
	9:40		79.2	30.0	29.50	0.40	4.83	0.166	4.84	0.2	13.05
	9:45		79.2	20.0	19.59	0.22	3.01	0.155	2.99	-0.7	12.18
	9:50		80.0	10.0	9.79	0.09	1.42	0.146	1.36	-4.2	11.47

TABLE D-1 (Continued)

Test Date	Test Time (Hr:Min)	Test Gas	T_R OUT (°F)	P_B IN (psig)	$\bar{P}_B$ (psig)	$\bar{P}_R$ (psig)	$\dot{M}_R$ (lb/hr)	$\dot{M}_R/\Delta P$	$\dot{M}_B$ IN (lb/hr)	Flow Balance Error (%)	Apparent Permeability Coefficient $\left(\frac{cm^3}{sec} @ NTP\right)(cm)$ / $(cm^2)(cm\ Hg)$
3-14-74	10:30	O_2	80.2	10.1	9.30	0.22	4.06	0.447	3.96	-2.5	30.74×10^{-10}
	10:35		79.8	20.0	18.83	0.67	8.21	0.452	8.29	1.0	31.08
	10:45		78.0	29.95	28.55	1.32	12.63	0.464	12.9	2.1	31.91
	10:50		79.6	20.0	18.84	0.65	8.21	0.451	8.30	1.1	31.02
	11:00		79.9	10.1	9.31	0.22	4.06	0.447	3.99	-1.7	30.74
3-14-74	13:05	N_2	100.3	10.0	9.65	0.11	1.70	0.178	1.65	-2.9	13.99
	13:15		99.8	19.95	19.43	0.27	3.58	0.187	3.63	1.4	14.7
	13:25		99.4	30.0	29.35	0.52	5.65	0.196	5.84	3.4	15.4
	13:30		99.1	20.0	19.47	0.28	3.62	0.189	3.64	0.6	14.85
	13:35		99.0	10.0	9.65	0.11	1.74	0.182	1.64	-5.7	14.3
3-14-74	14:15	O_2	99.3	10.0	8.98	0.29	4.87	0.560	4.84	-0.6	38.51
	14:20		98.9	19.9	18.37	0.91	10.0	0.573	10.17	1.7	39.41
	14:25		98.5	30.05	28.20	1.85	15.4	0.584	15.9	3.2	40.16
	14:30		99.1	20.0	18.46	0.92	10.1	0.576	10.2	1.0	39.61
	14:35		99.7	10.0	8.99	0.29	4.90	0.563	4.87	-0.6	38.72
3-15-74	9:30	N_2	119.7	10.0	9.53	0.15	2.16	0.230	2.13	-1.4	18.08
	9:35		119.6	19.95	19.23	0.37	4.53	0.240	4.59	1.3	18.86
	9:40		119.6	29.95	29.07	0.72	7.13	0.252	7.28	2.1	19.8
	9:50		119.2	20.0	19.26	0.38	4.60	0.244	4.64	0.9	19.18
	9:55		119.3	10.0	9.50	0.15	2.23	0.239	2.18	-2.2	18.78
3-15-74	10:40	O_2	120.2	10.05	8.69	0.07	6.33	0.734	6.14	-3.0	50.48
	10:50		120.2	20.0	17.87	0.17	13.05	0.737	13.2	1.1	50.68
	10:55		119.8	30.1	29.50	0.30	20.2	0.743	21.0	4.0	51.1
	11:00		120.0	20.0	19.86	0.17	13.05	0.738	13.2	1.1	50.75
	11:05		120.4	10.0	9.65	0.07	6.38	0.741	6.14	-3.8	50.96

TABLE D-1 (Continued)

Test Date	Test Time (Hr:Min)	Test Gas	T_R OUT (°F)	P_B IN (psig)	$\overline{P}_B$ (psig)	$\overline{P}_R$ (psig)	$\dot{M}_R$ (lb/hr)	$\dot{M}_R/\Delta P$	$\dot{M}_B$ IN (lb/hr)	Flow Balance Error (%)	Apparent Permeability Coefficient $\frac{\left(\frac{cm^3}{sec} @ NTP\right)(cm)}{(cm^2)(cm\ Hg)}$
3-15-74	13:15	N_2	139.2	10.0	9.35	0.20	2.76	0.302	2.77	0.4	23.73×10^{-10}
	13:20		139.1	20.0	19.03	0.53	5.69	0.308	5.82	2.3	24.21
	13:30		139.0	29.95	28.79	1.02	8.90	0.321	9.13	2.6	25.23
	13:35		138.7	20.0	19.02	0.54	5.76	0.312	5.85	1.6	24.52
	13:40		139.0	10.05	9.40	0.20	2.81	0.305	2.80	-0.4	23.97
3-15-74	14:15	O_2	138.5	10.05	8.35	0.09	7.19	0.871	7.30	1.5	59.9
	14:20		138.1	20.0	17.33	0.20	15.1	0.882	15.85	5.0	60.66
	14:25		138.0	30.05	26.74	0.39	23.55	0.894	25.3	7.4	61.48
	14:30		138.0	20.0	17.31	0.22	15.15	0.887	15.82	4.4	61.0
	14:40		139.1	10.0	8.29	0.09	7.29	0.889	7.28	-0.1	61.14
3-18-74	9:55	N_2	160.4	10.0	9.16	0.26	3.41	0.383	3.39	-0.6	30.1
	10:00		159.7	19.95	28.70	0.72	7.08	0.394	7.19	1.6	30.96
	10:10		159.5	19.95	18.65	0.67	7.01	0.390	7.24	3.3	30.65
	10:15		159.2	29.95	28.41	1.33	11.0	0.406	11.4	3.6	31.91
	10:25		159.5	20.0	18.72	0.68	7.14	0.396	7.31	2.4	31.12
	10:30		159.9	20.0	18.72	0.75	7.22	0.402	7.32	1.4	31.59
	10:35		160.7	10.0	9.09	0.27	3.50	0.397	3.50	0	31.2
3-18-74	12:00	O_2	160.9	10.0	7.87	0.11	8.15	1.050	8.60	5.5	72.21
	12:10		160.5	20.0	16.58	0.28	17.3	1.061	18.9	9.2	72.96
	12:15		159.8	30.0	25.70	0.55	27.5	1.093	30.5	10.9	75.17
	12:20		160.0	20.0	16.56	0.29	17.45	1.073	18.95	8.6	73.79
	12:25		160.2	10.05	7.91	0.11	8.26	1.059	8.65	4.7	72.83

TABLE D-1 (Continued)

Test Dat.	Test Time (Hr:Min)	Test Gas	T_R OUT (°F)	P_B IN (psig)	$\bar{P}_B$ (psig)	$\bar{F}_R$ (psig)	$\dot{M}_R$ (lb/hr)	$\dot{M}_R/\Delta P$	$\dot{M}_B$ IN (lb/hr)	Flow Balance Error (%)	Apparent Permeability Coefficient $\left(\frac{cm^3}{sec}\ @\ NTP\right)(cm)$ / $(cm^2)(cm\ Hg)$
3-19-74	8:30	N_2	59.2	10.05	9.84	0.06	1.27	0.130	1.22	-3.9	10.22×10^{-10}
	8:40		59.8	20.0	19.66	0.12	2.70	0.138	2.67	-1.1	10.85
	[illegible]:45		59.9	30.0	29.58	0.19	4.38	0.1[illegible]	4.45	1.6	11.71
	8:50		58.9	39.95	39.45	0.28	6.25	0.160	6.64	6.2	12.60
	9:00		57.8	49.95	49.40	0.41	8.28	0.169	8.53	3.0	13.28
	9:05		57.8	40.0	39.50	0.30	6.30	0.161	6.39	1.4	12.65
	9:10		58.5	30.0	29.56	0.20	4.51	0.154	4.52	0.2	12.1
	9:15		59.9	20.05	19.70	0.12	2.82	0.144	2.77	-1.8	11.32
	9:20		59.9	10.0	9.78	0.06	1.305	0.134	1.41	8.0	10.53
3-19-74	10:05	O_2	60.9	10.05	9.43	0.08	3.50	0.374	3.37	3.7	25.72
	10:10		60.0	20.05	19.11	0.17	7.15	0.378	7.12	-0.4	26.0
	10:20		58.9	30.1	28.96	0.29	11.1	0.383	11.2	0.9	26.34
	10:25		58.2	40.0	38.73	0.47	15.25	0.398	15.6	2.3	27.37
	10:30		57.9	49.95	48.58	0.73	19.55	0.408	20.0	2.3	28.06
	10:35		58.0	40.0	38.74	0.51	15.4	0.403	15.46	0.4	27.71
	10:40		58.4	30.05	28.93	0.30	11.2	0.391	11.2	0	26.89
	10:45		59.0	20.0	19.07	0.17	7.2	0.381	7.10	-1.4	26.2
	10:[illegible]		59.5	10.1	9.49	0.08	3.53	0.375	3.38	-4.2	25.79
3-19-74	13:30	N_2	39.8	10.0	9.81	0.08	1.18	0.121	1.13	-4.2	9.51
	13:35		39.1	20.0	19.71	0.18	2.57	0.132	2.56	-0.4	10.37
	13:40		39.1	30.0	29.63	0.33	4.18	0.143	4.28	2.4	11.24
	13:45		39.9	20.05	19.76	0.18	2.60	0.133	2.56	-1.5	10.45
	13:50		39.9	10.0	9.81	0.08	1.205	0.124	1.15	-4.6	9.75

TABLE D-1 (Continued)

Test Date	Test Time (Hr:Min)	Test Gas	T_R OUT (^{0}F)	P_B IN (psig)	$\bar{P}_B$ (psig)	$\bar{P}_R$ (psig)	$\dot{M}_R$ (lb/hr)	$\dot{M}_R/\Delta P$	$\dot{M}_B$ IN (lb/hr)	Flow Balance Error (%)	Apparent Permeability Coefficient $\frac{\left(\frac{cm^3}{sec} @ NTP\right)(cm)}{(cm^2)(cm\ Hg)}$
3-19-74	14:25	O_2	39.8	10.0	9.50	0.17	2.79	0.299	2.83	1.4	20.56×10^{-10}
	14:30		39.9	20.0	19.26	0.45	5.80	0.308	6.03	4.0	21.18
	14:35		39.7	30.0	29.11	0.88	9.07	0.32[illegible]	9.48	4.5	22.08
	14:45		39.1	20.05	19.[illegible]	0.45	5.81	0.308	6.01	3.4	21.18
	14:50		40.0	10.1	9.51	0.17	2.80	0.300	2.83	1.1	20.03
3-20-74	9:30	N_2	18.6	10.0	9.83	0.07	1.13	0.116	1.07	-5.3	9.12
	9:35		18.9	20.0	19 75	0.17	2.46	0.126	2.45	-0.4	9.90
	9:40		18.9	29.95	29.62	0.31	4.03	0.137	4.10	1.7	10.77
	9:45		19.1	20.0	19.74	0.17	2.49	0.127	2.43	-2.4	9.98
	9:50		19.7	10.0	9.84	0.07	1.13	0.116	1.07	-5.3	9.12
3-20-74	10:25	O_2	19.8	10.0	9.60	0.16	2.48	0.263	2.47	-0.4	18.09
	10:30		19.5	20.0	19.40	0.42	5.21	0.274	5.33	2.3	18.84
	10:35		19.1	30.0	29.26	0.81	8.20	0.288	8.42	2.7	19.81
	10:40		19.7	20.05	19.46	0.42	5.24	0.275	5.31	1.3	18.91
	10:50		19.8	10.0	9.60	0.16	2.50	0.265	2.47	-1.2	18.22
3-20-74	13:25	N_2	0.0	10.05	9.90	0.07	1.12	0.114	1.04	-7.1	8.96
	13:30		0.1	20.0	19.76	0.16	2.46	0.126	2.42	-1.6	9.90
	13:35		0.0	30.0	29.70	0.31	4.03	0.137	4.10	1.7	10.77
	13.40		0.0	20.0	19.76	0.17	2.47	0.126	2.42	-2.0	9.90
	13:45		-0.1	10.0	9.85	0.07	1.13	0.116	1.05	-7.1	9.12

TABLE D-1 (Continued)

Test Date	Test Time (Hr:Min)	Test Gas	T_R OUT (°F)	P_B IN (psig)	P_B (psig)	P_R (psig)	$\dot{M}_R$ (lb/hr)	$\dot{M}_R/\Delta P$	$\dot{M}_B$ IN (lb/hr)	Flow Balance Error (%)	Apparent Permeability Coefficient $\frac{\left(\frac{cm^3}{sec} @ NTP\right)(cm)}{(cm^2)(cm\ Hg)}$
3-20-74	14:15	O_2	-0.1	10.0	9.66	0.15	2.25	0.237	2.22	-1.3	16.3×10^{-10}
	14:25		1.1	20.05	19.55	0.37	4.75	0.248	4.82	1.5	17.05
	14:30		0.1	30.05	29.33	0.70	7.48	0.261	7.77	3.9	17.95
	14:35		-0.8	20.0	19.50	0.37	4.75	0.248	4.80	1.1	17.05
	14:40		-1.1	10.05	9.73	0.15	2.25	0.235	2.22	-1.3	16.16
3-21-74	8:40	N_2	59.5	10.0	9.79	0.06	1.275	0.131	1.21	-5.1	10.3
	8:45		60.2	20.0	19.66	0.12	2.74	0.140	2.74	0	11.0
	8:50		59.2	30.0	29.58	0.20	4.46	0.152	4.52	1.3	11.95
	9:20		59.2	40.0	39.50	0.29	6.38	0.163	6.54	2.5	12.81
	9:25		59.0	50.0	49.45	0.42	8.48	0.173	8.64	1.9	13.6
	9:40		59.6	40.0	39.50	0.30	6.39	0.163	6.44	0.8	12.81
	9:45		59.7	30.0	29.56	0.21	4.58	0.156	4.59	0.2	12.26
	9:50		60.1	20.0	19.65	0.13	2.87	0.147	2.79	-2.8	11.55
	9:55		60.1	10.05	9.83	0.07	1.33	0.136	1.26	-5.3	10.69
3-21-74	10:30	O_2	60.8	10.05	9.45	0.08	3.045	0.325	3.33	9.4	22.35
	10:35		60.1	20.0	19.08	0.17	7.09	0.375	5.91	-16.6	25.79
	10:45		59.7	30.0	28.87	0.29	10.96	0.383	11.14	1.6	26.35
	10:50		59.7	40.0	38.75	0.48	15.05	0.393	15.53	3.2	27.03
	11:05		57.8	50.2	48.84	0.76	19.50	0.406	20.06	2.9	27.92
	11:10		58.5	40.1	38.85	0.53	15.10	0.394	15.47	2.5	27.1
	11:15		58.8	30.0	28.98	0.31	11.05	0.387	11.16	1.0	26.61
	11:20		59.2	20.05	19.13	0.17	7.17	0.378	7.11	-0.8	26.0
	11:25		59.5	(10.0)	9.39	0.08	3.12	0.335	3.37	8.0	23.04

TABLE D-1 (Continued)

Test Date	Test Time (Hr:Min)	Test Gas	T_R OUT (°F)	P_B IN (psig)	$\overline{P}_B$ (psig)	$\overline{P}_R$ (psig)	$\dot{M}_R$ (lb/hr)	$\dot{M}_R/\Delta P$	$\dot{M}_B$ IN (lb/hr)	Flow Balance Error (%)	Apparent Permeability Coefficient $\frac{\left(\frac{cm^3}{sec} @ NTP\right)(cm)}{(cm^2)(cm\ Hg)}$
3-25-74	9:15	N_2	60.8	10.0	9.80	0.06	1.22	0.125	1.17	-4.1	9.82×10^{-10}
	9:20		60.8	20.0	19.69	0.12	2.68	0.137	2.68	0	10.77
	9:25		60.3	29.95	29.53	0.19	4.46	0.152	4.55	2.0	11.95
	9:30		60.2	40.0	39.50	0.28	6.46	0.165	6.60	2.2	12.97
	9:35		59.2	50.0	49.45	0.42	8.56	0.175	8.82	3.0	13.75
	9:40		59.1	40.0	39.50	0.30	6.50	0.166	6.64	2.2	13.05
	9:45		60.1	30.0	29.57	0.21	4.64	0.158	4.70	1.3	12.42
	9:50		59.9	20.05	19.71	0.12	2.85	0.145	2.88	1.1	11.4
	9:55		59.8	10.0	9.80	0.06	1.31	0.134	1.28	-2.3	10.53
3-25-74	10:30	O_2	59.9	10.1	9.50	0.08	3.43	0.364	3.36	-2.0	25.03
	10:35		59.8	20.0	19.09	0.16	7.03	0.371	7.04	0.1	25.51
	10:45		59.2	30.0	28.88	0.29	11.0	0.385	11.22	2.0	26.48
	10:50		59.0	40.05	38.79	0.46	15.15	0.395	15.7	3.6	27.16
	10:55		58.9	50.0	48.63	0.77	19.6	0.410	20.2	3.1	28.2
	11:05		58.8	40.05	38.80	0.52	15.15	0.396	15.6	3.0	27.23
	11:10		58.9	30.0	28.88	0.30	11.1	0.388	11.22	1.1	26.68
	11:15		59.3	20.0	19.08	0.17	7.14	0.378	7.15	0.1	26.0
	11:20		59.5	10.1	9.50	0.08	3.45	0.366	3.35	-2.9	25.17

TABLE D-1 (Continued)

Test Date	Test Time (Hr:Min)	Test Gas	T_R OUT (^oF)	P_B IN (psig)	$\bar{P}_B$ (psig)	$\bar{P}_R$ (psig)	$\dot{M}_R$ (lb/hr)	$\dot{M}_R/\Delta P$	$\dot{M}_B$ IN (lb/hr)	Flow Balance Error (%)	Apparent Permeability Coefficient $\left(\frac{cm^3}{sec} @ NTP\right)(cm)$ / (cm^2) (cm Hg)
3-27-74	9:20	N_2	60.6	10.0	9.80	0.06	1.285	0.132	1.34	4.3	10.37×10^{-10}
	9:30		60.8	20.0	19.66	0.12	2.81	0.144	2.72	-3.2	11.37
	9:35		60.4	30.0	29.51	0.20	4.57	0.156	4.54	-0.7	12.26
	9:40		60.2	40.0	39.50	0.30	6.56	0.167	6.49	-1.1	13.12
	9:45		59.4	49.95	49.40	0.43	8.66	0.177	8.67	0.1	13.91
	9:55		59.2	40.05	39.55	0.30	6.58	0.168	6.49	-1.4	13.2
	10:00		59.2	30.05	29.61	0.21	4.69	0.160	4.60	-1.9	12.57
	10:10		59.3	20.0	19.65	0.12	2.92	0.150	2.76	-5.5	11.79
	10:15		60.0	10.0	9.79	0.06	1.35	0.139	1.25	-7.4	10.92
3-27-74	10:55	O_2	60.8	10.0	9.40	0.08	3.50	0.376	3.23	-7.7	25.86
	11:00		60.1	19.9	18.99	0.17	7.10	0.377	6.88	-3.1	25.93
	11:05		59.9	30.0	28.88	0.29	11.1	0.388	10.97	-1.2	26.68
	11:10		59.8	40.05	38.79	0.47	15.17	0.396	15.2	0.2	27.23
	11:15		59.7	50.0	48.63	0.78	19.5	0.408	19.6	0.5	28.06
	11:20		60.0	40.0	38.75	0.54	15.2	0.398	15.15	-0.3	27.37
	11:30		60.0	30.0	28.87	0.29	11.2	0.392	11.0	-1.8	26.96
	12:30		60.7	19.9	18.98	0.17	7.21	0.383	6.93	-3.9	26 34
	12:45		60.8	10.05	9.45	0.08	3.52	0.376	3.27	-7.1	25.86

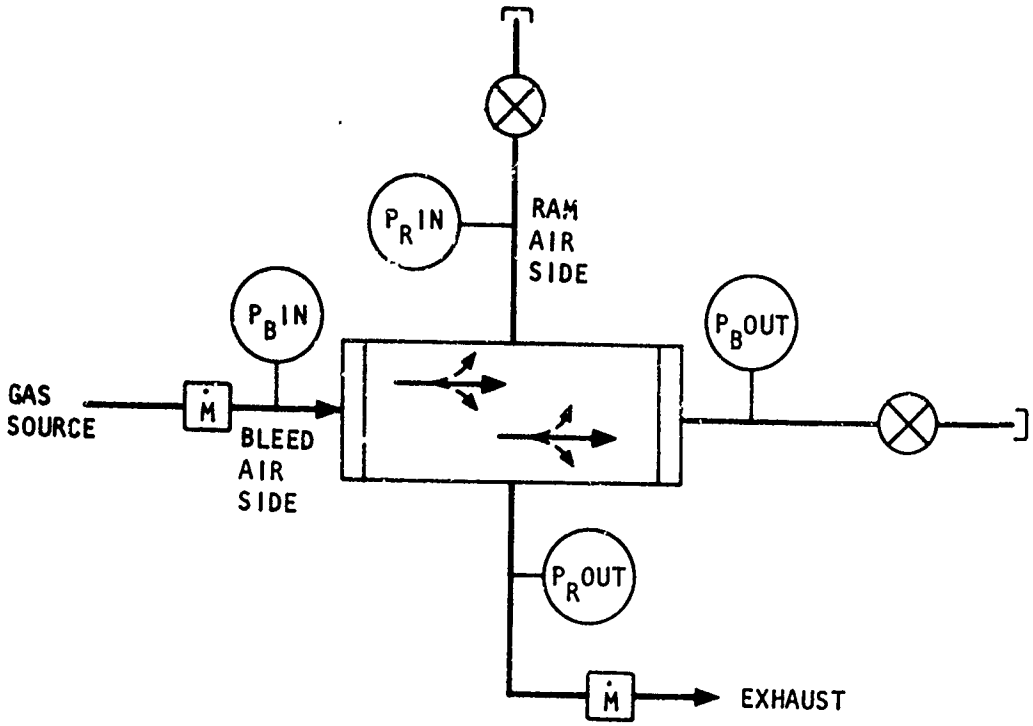

$$\overline{P}_B = \frac{P_B IN + P_B OUT}{2}$$

$$\overline{P}_R = \frac{P_R IN + P_R OUT}{2}$$

S-86726

Figure D-1. Single Gas Permeation Test Data Schematic Diagram

uncertainties in the test unit's geometry. The log mean surface area and nominal wall thickness used in the calculation is based on the mean values of tube inside and outside diameter supplied by the manufacturer (see Appendix B).

The following data columns are on Table C-1:

- Test Date - the calendar date (month-day-year) on which the test point was conducted.
- Test Time (Hr:Min) - The time of day at which the data were recorded. This provides an indication of stabilization time by comparison to the preceeding data point and a correlation to the original laboratory test data sheet.
- Test Gas - Either oxygen (O_2) or nitrogen (N_2)
- T_R OUT (^oF) - Each data point was conducted in a temperature stabilized enclosure with temperature conditioned gas. This is the temperature of the ram outlet gas and within $\pm 2^oF$ of all other temperatures recorded at the time of test.
- P_B IN (psig) - The nominal test pressure. This value is measured at the inlet to the bleed air side.
- $\overline{P}_B$ (psig) - The arithemetic mean pressure on the bleed air side.
- $\overline{P}_R$ (psig) - The arithemetic mean pressure on the ram air side.
- $\dot{M}_R$ (lb/hr) - The apparent permeant rate measured at the ram air outlet.
- $\dot{M}_R / \Delta P$ - The ratio of the apparent permeant rate to the mean driving force.
- $\dot{M}_B$ IN (lb/hr) - The apparent permeant rate measured at the bleed air inlet.
- Flow Balance Error (percent) - The deviation of $\dot{M}_B$ IN from $\dot{M}_R$ OUT.
- Apparent Permeability Coefficient - Calculated value based on test measurements and geometry from Appendix B.

A test equipment list of instrumentation used for the testing of the large scale parallel fiber air separation module is shown as Table D-2. This table is applicable to the test data of Appendicies D, E and F.

TABLE D-2. TEST EQUIPMENT LIST

Instrument Description	Manufacturer and Model No.	Serial No.	Range	Accuracy
Process inlet pressure gage	Martin-Decker	44P352	0-60 psig	±0.2 percent F.S.
Process ΔP pressure gage	Barton	44P404	0-20 psid	±0.5 percent F.S.
Sweep inlet pressure gage	Barton	44S401	0-60 "H_2O	±0.5 percent F.S.
Sweep ΔP pressure gage	Barton	44S401	0-60 "H_2O ΔP	±0.5 percent F.S.
Temperature potentiometer	Leeds and Northrup	43B101	-340 to +230°F	±0.25 percent
Oxygen Analyzer	Beckman F-3	44M001	0-100 percent O_2	±0.3 percent
O_2 analyzer recorder	Leeds and Northrup	43C020	0-100 percent	±0.25 percent
Process inlet flowmeter ΔP gage	Barton	44Q087	0-10" H_2O ΔP	±0.5 percent F.S.
Process inlet flowmeter static gage	Martin-Decker	44P249	0-150 psia	±0.2 percent F.S.
Process outlet flowmeter ΔP gage	Barton	44S137	0-10" H_2O ΔP	±0.5 percent F.S.
Process outlet flowmeter static gage	Wallace and Tiernan	46K566	0-800 mm Hg A	±0.33 percent F.S.

TABLE D-2 (continued)

Instrument Description	Manufacturer and Model No.	Serial No.	Range	Accuracy
Sweep inlet flowmeter ΔP gage	Barton	441446	0-10" H_2O ΔP	±0.5 percent F.S.
Sweep inlet flowmeter static gage	Martin-Decker	44P355	0-150 psia	±0.2 percent F.S.
Sweep outlet flowmeter ΔP gage	Barton	46K265	0-10" H_2O ΔP	±0.5 percent F.S.
Sweep outlet flowmeter static gage	Wallace and Tiernan	46K273-8	0-25 psia	±0.33 percent F.S.
Flowmeter	National Instrument Labs.	2209	0-2.26 lb/hr N_2 @ NTP	
Flowmeter	National Instrument Labs	2379	0-9.2 lb/hr N_2 @ NTP	
Flowmeter	National Instrument Labs	1969	0-9.5 lb/hr N_2 @ NTP TP	
Flowmeter	National Instrument Labs	2373	11.75 lb/hr N_2 @ NTP	
Flowmeter	National Instrument Labs	2309	20.0 lb/hr N_2 @ NTP	
Flowmeter	National Instrument Labs	3118	61.0 lb/hr N_2 @ NTP	

APPENDIX E

AIR SEPARATION TEST DATA

Data taken during the air separation tests are summarized in Table E-1. The data in this appendix are for the time period following the repair of the O-ring seal leakage noted during the early stages of the test program (see Section 3).

Table E-1 data summary sheet include measured data and calculations based on these measurements. In addition, the iterative digital computer program used to optimize material selection and as an aid in system design has been used to predict the performance based on measured pressures and the experimental values of apparent permeability coefficients determined during the single gas permeation tests. The values of apparent permeability coefficient used for the calculation are taken from Figures 3-36 and 3-37 of Section 3. A simplified test schematic is shown as Figure E-1.

During testing, critical pressure, temperature, flow rate and concentration data were recorded. Flow measurements were examined for mass balance closure. Resultant closure balance errors are noted. The output flow range was selected to experimentally determine the resultant output oxygen concentration from near ambient (21 percent) down into the inert range (9 percent).

The following data columns are for Table E-1:

- Test Date - the calendar date (month-day-year) on which the test point was recorded.
- Test Time (Hr:Min) - The time of day at which the data were recorded. This provides a record of stabilization time by comparison to the preceeding data point and a correlation to the original laboratory test data sheet.
- TB OUT (^{o}F) - Each data point was conducted in a temperature stabilized enclosure with temperature conditioned gas. This is the temperature of the bleed outlet flow (the inert gas port) and within $\pm 2^{o}$F of all other temperatures recorded at the time of test.
- P_B IN (psig) - The nominal bleed air test pressure.
- $\overline{P}_B$ (psig) - The arithmetic mean pressure on the bleed air side.
- $\overline{P}_R$ IN (psig) - The arithmetic mean pressure on the ram air side.

TABLE E-1. AIR SEPARATION TEST DATA SUMMARY

(POST LEAKAGE REPAIR)

Test Date	Test Time (Hr:min)	T_B OUT (°F)	P_B IN /psig	$\bar{P}_B$ (psig)	$\bar{P}_R$ IN (psig)	$\dot{M}_B$ IN (lb/hr)	$\dot{M}_B$ OUT (lb/hr)	$\dot{M}_R$ IN (lb/hr)	$\dot{M}_R$ OUT (lb/hr)	O_2 B, R IN (%)	Measured O_2 B OUT (%)	O_2 R OUT (%)	Flow Balance Error (%)	Computed O_2 B OUT (%)
3-11-74	12:30	61.0	29.9	29.35	0.61	5.29	0.506	29.3	34.3	20.9	9.5	21.07	-0.6	10.7
	12:55	61.0	30.0	29.3	0.62	5.82	1.00	30.0	34.4	21.0	10.2	21.32	1.2	11.0
	13:25	60.3	30.1	29.15	0.62	6.96	1.99	30.3	34.7	20.9	11.4	21.44	1.6	11.7
	14:25	59.9	30.1	28.70	0.61	9.00	4.00	30.2	34.5	21.0	13.1	21.91	2.0	13.5
	14:45	60.0	30.0	28.10	0.61	11.00	5.97	29.8	34.4	21.0	14.6	22.11	1.2	14.6
	15:10	59.9	29.95	27.50	0.61	13.0	8.00	29.8	34.1	20.9	15.6	22.13	2.0	15.4
	15:25	59.8	29.8	26.83	0.61	15.2	9.93	29.7	34.1	20.9	16.3	22.22	2.5	16.2
3-12-74	8:35	60.5	50.0	47.70	0.79	19.6	10.00	29.9	38.2	21.0	14.15	22.76	3.3	14.0
	9:05	60.2	50.0	48.08	0.80	17.35	7.98	30.0	38.4	20.8	13.2	22.36	2.5	13.0
	10:20	59.5	49.85	48.28	0.79	15.3	6.00	29.8	38.2	20.9	12.3	22.24	2.3	12.1
	10:55	59.9	50.0	48.78	0.80	13.1	4.00	30.4	38.4	20.9	10.8	21.94	2.8	10.9
	11:15	59.5	50.0	49.10	0.79	11.0	2.00	30.0	38.3	20.9	9.2	21.51	1.8	9.4
	12:25	59.2	50.0	49.25	0.79	9.95	1.005	30.2	38.1	20.9	8.3	21.23	2.7	8.7
	12:35	60.8	49.9	49.25	0.79	8.64	0.506	30.0	38.1	20.9	7.8	21.08	0.1	8.3
	14:05	61.1	30.0	29.05	0.40	6.96	2.00	20.1	25.0	20.9	12.3	21.60	0.2	11.7
	14:35	60.5	30.15	29.20	0.20	7.02	2.00	10.1	15.25	20.9	11.2	22.20	-0.9	11.8
	14:50	60.6	30.0	29.05	0.12	6.96	1.99	4.96	10.0	20.9	11.3	22.86	-0.7	12.0
3-13-74	9:40	60.7	49.9	48.30	0.55	15.4	6.00	20.0	28.8	20.9	12.0	22.74	2.0	12.2
	10:10	60.8	50.0	48.40	0.28	15.4	6.00	10.0	19.1	20.8	12.1	23.53	1.5	12.2
	10:30	60.9	49.75	46.65	0.19	15.3	6.00	4.96	14.25	20.8	12.3	24.44	0.1	12.7
3-22-74	12:10	140.4	29.95	28.40	1.04	11.7	0.497	30.4	39.0	21.0	9.8	21.14	6.3	10.6
	12:35	140.6	30.1	28.40	1.03	12.3	1.01	29.9	38.75	21.1	10.15	21.37	5.9	10.7
	12:50	140.8	30.05	28.03	1.02	13.35	2.04	29.9	38.7	21.0	10.6	21.52	6.1	10.9
3-22-74	13:00	141.1	30.05	27.41	1.02	15.6	4.00	29.9	38.55	20.9	11.5	21.82	7.1	11.6
	13:30	141.5	30.0	26.76	1.01	17.2	6.00	29.9	33.4	21.0	12.5	22.26	6.6	12.4
	14:20	141.3	30.15	26.20	1.01	19.2	8.04	30.0	38.2	21.0	13.3	22.52	7.2	13.1
	14:45	140.7	30.05	25.45	1.00	21.0	10.0	30.1	38.0	21.0	14.0	22.72	7.5	13.8
3-26-74	10:15	39.9	30.0	29.48	0.58	5.32	0.50	30.1	34.35	21.0	10.1	21.16	1.6	11.4
	10:40	39.9	30.0	29.36	0.58	5.89	1.00	30.0	34.4	20.9	10.8	21 19	[illegible]	11.8
	11:00	40.0	30.0	29.13	0.58	7.01	1.99	30.1	34.6	21.0	12.3	21.50	[illegible]	12.9
	12:25	40.8	29.95	28.64	0.58	9.07	3.99	30.0	34.6	21.0	14.1	21.99	[illegible]	14.4
	13:15	41.0	30.0	28.21	0.58	11.02	5.97	30.0	34.5	21.0	15.5	21.95	1.6	15.5
	13:40	40.6	29.95	27.68	0.59	13.1	8.00	30.0	34.6	21.0	16.4	22.06	1.4	16.4
	14:25	39.9	30.0	27.26	0.58	15.2	10.00	29.9	34.35	21.0	17.1	22.12	2.1	17.1

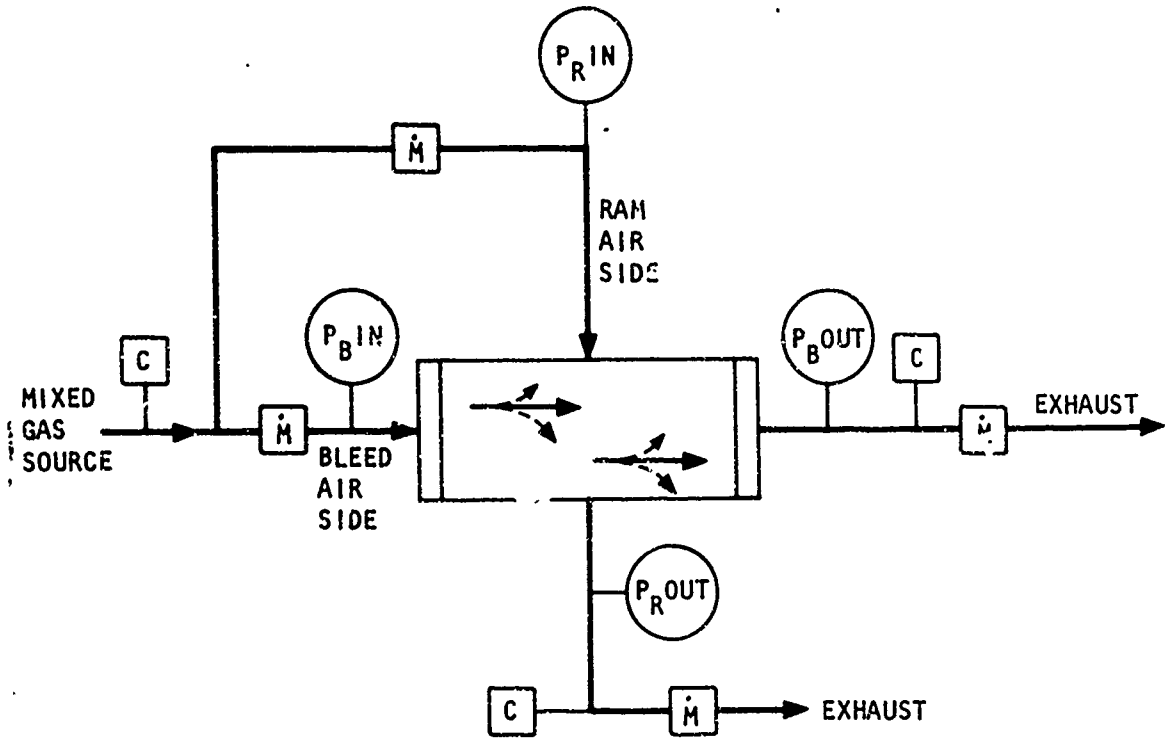

$$\overline{P}_B = \frac{P_B IN + P_B OUT}{2}$$

$$\overline{P}_R = \frac{P_R IN + P_R OUT}{2}$$

S-85725

Figure E-1. Air Separation Test Data Schematic Diagram

- $\dot{M}_B$ IN - The bleed air requirement measured at the inlet to the bleed air side.
- $\dot{M}_B$ OUT - The output flow rate of the unit. This is measured at the bleed air outlet port (the inert-gas port).
- $\dot{M}_R$ IN - The ram air inlet flow used to sweep the low pressure side.
- $\dot{M}_R$ OUT - The exhaust flow at the ram air outlet port. This is a combined flow consisting of the ram air inlet flow and the gas permeated through the membrane from the bleed air side.
- O_2 B, R IN (percent) - The measured oxygen concentration at the bleed and ram inlet ports.
- Measured O_2 B OUT (percent) - The measured oxygen concentration in the output air.
- O_2 R_{OUT} (percent) - The measured oxygen concentration in the ram exhaust air.
- Flow Balance Error (percent) - The density of the measured $\dot{M}_R$ OUT from the measured $\dot{M}_R$ IN + permeant gas ($\dot{M}_B$ IN - $\dot{M}_B$ OUT).
- Computed O_2 B OUT (percent) - The predicted value of O_2 B OUT based on the forward difference digital computer program.

Sample output from the digital computer program used to predict the results of the air separation tests (computed O_2 B OUT - percent) is shown as Figure E-2. The data from March 12, 1974 at 12:25 have been used as an example. The arithmetic mean bleed side and ram side pressures of 49.25 psig and 0.79 psig respectively, are used as input data as are the tube inside diameter and wall thickness and number of tubes from Appendix B. Values of the apparent permeability coefficients for the 59.2°F test temperatures are as determined in Section 3 from the experimental single gas permeability test data summarized in Appendix D.

The theoretical minimum oxygen concentration limit as defined in Appendix A has been calculated as 8.19 percent for the input information.

Next, the membrane separation profile as a function of active tube length is shown. The sample output shows the tube length segmented into 25 finite

(2 inch) elements. (The computed data in Table E-1 are from 100 elements analysis). The "profile" of the bleed air is tabulated over the active length of the fibers. The output notes the conditions of the nitrogen enriched air at each of the 26 nodes, and the conditions of the oxygen evidenced permeant gas between each node.

The tube length at each node is tabulated in both physical dimensions (inches) and in terms of the percent of active length. At each node, the bleed air mass flow rate (in both absolute units and as a percent of bleed air inlet) the velocity, and the oxygen concentration is tabulated. The oxygen enriched air permeating between the nodes is also tabulated. The parameters tabulated are the rate of bleed air permeation between adjacent nodes, the percent of the original inlet bleed air flow rate this represents, and the oxygen concentration of the permeant gas.

Finally, the permeant flow is summarized and the physical characteristics of log-mean surface area, aggregate tube cross sectional area (based on outside diameter) and the weight of the fiber in the active length are noted.

A comparison of the bleed air profile of the computer output sheet with the test data summary sheet shows the two remainder of the fixed input data. The experimentally measured bleed air outlet flow rate of 1.005 lb/min and the air inlet concentration of 20.9 percent oxygen are seen to be the bleed air outlet flow and air inlet concentration of the tabulated profile. The experimentally measured bleed air outlet concentration of 8.3 percent oxygen is closely predicted by the calculated outlet concentration of 8.66 percent. Since, for test conditions, the bleed air's nitrogen content has been enriched to a value near the theoretical limit, a considerable fraction of the bleed air entering the test module leaves as permeant gas. The inlet flow required was measured as 9.95 lb/hr. The computed value is about 5 percent higher.

FINAL REPORT EXAMPLE OF AIR SEPARATION PERFORMANCE PROFILE PREDICTION
DATA FROM 3/12/74 AT 12 25

*** DESIGN CONDITIONS ***

BLEED AIR PRESSURE (PSIG)	INLET MASS FLOW RATE (LBM/HR)	RAM AIR PRESSURE (PSIG)	THEORETICAL OXYGEN CONCENTRATION LIMIT (PERCENT)
49.250	10.468	.790	8.191

** MEMBRANE CHARACTERISTICS ** 965.000 TUBES

TUBE INSIDE DIAMETER (IN)	TUBE WALL THICKNESS (IN)	PERMEABILITY COEF O2	PERMEABILITY COEF N2
.00213	.00035	27.64-10	13.14-10

*** MEMBRANE SEPARATION PROFILE ***

TUBE LENGTH (IN.)	TUBE LENGTH (PERCENT)	INSIDE TUBE (NITROGEN ENRICHED AIR) BLEED AIR MASS FLOW (LBM/HR)	BLEED AIR MASS FLOW (PERCENT)	VELOCITY (FT/SEC)	O2 CONC (VOL PCNT)	PERMEANT (OXYGEN ENRICHED AIR) BLEED AIR MASS FLOW (LBM/HR)	BLEED AIR MASS FLOW (PERCENT)	O2 CONC (VOL PCNT)
.0000	.0000	10.4675	100.0000	.3688	20.9000			
						.0171	3.9852	35.1106
4.0000	4.0000	10.0504	96.0148	.3544	20.3220			
						.0137	3.9520	34.0360
8.0000	8.0000	9.6367	92.0628	.3401	19.7447			
						.0102	3.9190	32.9500
12.0000	12.0000	9.2265	88.1438	.3259	19.1686			
						.0068	3.8861	31.8500
16.0000	16.0000	8.8197	84.2577	.3117	18.5942			
						.0033	3.8531	30.7303
20.0000	20.0000	8.4164	80.4046	.2977	18.0224			
						.3999	3.8205	29.6154
24.0000	24.0000	8.0165	76.5841	.2838	17.4537			
						.3965	3.7880	28.4848
28.0000	28.0000	7.6200	72.7961	.2700	16.8888			
						.3931	3.7558	27.3484
32.0000	32.0000	7.2268	69.0404	.2562	16.3284			
						.3898	3.7238	26.2037
36.0000	36.0000	6.8370	65.3166	.2426	15.7734			
						.3865	3.6921	25.0505
40.0000	40.0000	6.4506	61.6245	.2291	15.2247			
						.3832	3.6609	23.9064

22.0000	44.0000	6.0674	57.9636	.2156	14.6834	.3800	3.6301	22.7579
24.0000	48.0000	5.6874	54.3335	.2023	14.1503	.3766	3.5998	21.6125
26.0000	52.0000	5.3106	50.7537	.1890	13.6267	.3737	3.5701	20.6748
28.0000	56.0000	4.9369	47.1636	.1758	13.1136	.3707	3.5410	19.3848
30.0000	60.0000	4.5662	43.6226	.1627	12.6125	.3677	3.5127	18.2302
32.0000	64.0000	4.1985	40.1100	.1497	12.1247	.3648	3.4851	17.1320
34.0000	68.0000	3.8337	36.6248	.1368	11.6518	.3620	3.4585	16.0576
36.0000	72.0000	3.4717	33.1663	.1240	11.1955	.3593	3.4329	15.0109
38.0000	76.0000	3.1124	29.7335	.1112	10.7576	.3568	3.4084	13.9971
40.0000	80.0000	2.7556	26.3251	.0985	10.2403	.3543	3.3851	13.0250
42.0000	84.0000	2.4013	22.9400	.0859	9.9459	.3520	3.3632	12.1006
44.0000	88.0000	2.0492	19.5768	.0733	9.5770	.3499	3.3429	11.2327
46.0000	92.0000	1.6993	16.2339	.0609	9.2370	.3480	3.3243	10.4334
48.0000	96.0000	1.3513	12.9095	.0484	8.9296	.3462	3.3078	9.7145
50.0000	100.0000	1.0051	9.6017	.0360	8.6596			

** PERMEANT FLOWS **

OXYGEN (LBM/HR)	NITROGEN (LBM/HR)	TOTAL (LBM/HR)	O2 CONC (VOL PCNT)
2.3285	7.1340	9.4625	22.2249

** SURFACE AREA **	** FRONTAL AREA **	** MATERIAL WEIGHT **
(SQ FT)	(SQ IN)	(LBF)
2.593+03	6.090	3.v93

Figure E-2. Sample Test Data Predictions Using Performance Computer Program

APPENDIX F

PRE-REPAIR TEST DATA

Data taken prior to repairing the large scale test module are presented in this appendix. This early data showed poor repeatability of experimentally measured value of apparent permeability coefficient due to an "O-ring" seal leakage problem which tended to vary internal leakages. Because of this difficulty, the early single gas permeation test data, included as Table F-1, have not been considered in the evaluation of apparent permeability coefficient. The air separator test data of Table F-2 are considered in the discussion of Section 3 only to a limited extent.

The pre-repair single gas permeation tests and air separation tests tabular data summaries of this appendix are organized in the same formats as the later data presented in Appendixes D and E respectively.

TABLE F-1. SINGLE GAS PERMEATION TEST DATA SUMMARY (PRE-LEAKAGE REPAIR)

Test Date	Test Time (Hr:Min)	Test Gas	T_R OUT (°F)	P_B IN (psig)	$\bar{P}_B$ (psig)	$\bar{P}_R$ (psig)	$\dot{M}_R$ (lb/hr)	$\dot{M}_R/\Delta P$	$\dot{M}$ IN (lb/hr)	Flow Balance Error (%)	Apparent Permeability Coefficient $\frac{\left(\frac{cm^3}{sec} @ NTP\right)(cm)}{(cm^2)(cm\ Hg)}$
12-20-73	8:30	N_2	57	50.0	49.60	0.23	4.26	0.086	4.50	5.6	6.76×10^{-10}
	8:40		58	39.9	39.53	0.17	3.29	0.084	3.66	11.2	6.60
	8:45		58	30.0	29.68	0.12	2.44	0.083	2.55	4.5	6.52
	8:50		60	20.0	19.73	0.08	1.56	0.079	1.59	1.9	6.21
	9:15		62	9.6	9.43	0.04	0.724	0 077	763	5.4	6.05
12-20-73	12:54	O_2	70	10.0	9.38	0.16	3.18	0.345	3.332	4.7	23.73
	13:00		70	20.2	19.23	0.38	6.74	0.356	7.04	4.5	24.48
	13:15		70	30.2	29.03	0.31	10.8	0.376	10.9	0.9	25.86
	13:20		70	40.15	38.85	0.51	14.35	0.374	14.87	3.6	25.72
	13:25		71	50.0	48.60	0.76	18.3	0.382	18.7	2.2	26.27
1-16-74	8:50	O_2	54	9.8	9.25	0.18	2.67	0.294	2.74	2.6	20.22
	8:55		55	30.1	29.15	0.35	8.36	0.290	8.80	5.3	19.94
	10:40		40.5	9.95	9.00	0.17	3.47	0.393	3.64	4.9	27.03
	11:10		41.5	30.0	29.07	0.34	7.63	0.266	8.19	7.3	18.29
1-21-74	13:20	O_2	81.2	9.9	9.05	0.18	3.97	0.448	4.13	4.0	30.81
	13:45		81.9	28.8	27.35	0.37	12.26	0.454	12.41	1.2	31.22
	14:40		99.2	9.7	8.80	0.19	4.18	0.485	4.21	0.7	33.35
1-23-74	10:10	O_2	99.6	30.25	28.65	0.38	14.1	0.499	14.4	2.1	34.32
	10:25		100.3	10.10	9.15	0.19	4.78	0.533	4.44	-7.1	36.65
	12:20		119.8	30.00	27.80	0.39	18.4	0.671	17.9	-2.7	46.14
	12:35		121.0	9.95	8.68	0.20	5.81	0.685	5.71	-1.7	47.11
	14:05		139.9	30.15	27.30	0.41	22.15	0.824	22.2	0.2	56.67
	14:15		140.5	10.00	8.40	0.20	7.36	0.898	6.55	-5.8	61.76
	15:40		159.2	30.0	26.45	0.42	26.0	0.998	25.95	-0.2	68.63
	15:45		160.0	9.75	7.83	0.21	8.42	1.105	8.00	-5.0	75.99

TABLE F-1 (Continued)

Test Date	Test Time (Hr:Min)	Test Gas	T_R OUT (°F)	P_B IN (psig)	$\overline{P}_B$ (psig)	$\overline{P}_R$ (psig)	$\dot{M}_R$ (lb/hr)	$\dot{M}_R/\Delta P$	$\dot{M}_B$ IN (lb/hr)	Flow Balance Error (%)	Apparent Permeability Coefficient $\frac{\left(\frac{cm^3}{sec} @ NTP\right)(cm)}{(cm^2)(cm\ Hg)}$
1-24-74	9:25	O_2	40.9	30.15	28.70	0.34	10.25	0.362	10.5	2.4	24.89×10^{-10}
	9:30		40.7	9.80	8.75	0.17	3.67	0.428	3.74	1.9	29.43
	12:15		19.1	30.20	29.45	0.33	6.45	0.222	6.75	4.7	15.27
	12:25		20.3	9.80	9.25	0.16	2.455	0.270	2.465	0.4	18.57
	14:15		1.2	10.1	7.20	0.16	9.65	1.371	9.85	2.1	94.28
	14:55		19.1	10.0	7.85	0.16	6.35	0.826	6.48	2.0	56.8
1-25-74	7:40	N_2	44.4	10.0	(9.83)	0.17	3.81	0.394	3.91	2.6	30.96
1-25-74	8:15	O_2	44.0	10.2	8.45	0.17	4.90	0.592	5.08	3.7	40.71
	9:40		68.0	9.85	9.20	0.18	2.96	0.328	3.02	2.0	22.56
	11:05		68.8	30.1	29.00	0.36	9.55	0.333	10.0	4.7	22.9
	11:15		70.0	10.0	9.33	0.18	3.19	0.349	3.20	0.3	24.0
1-25-74	12:30	N_2	69.9	30.1	29.70	0.11	2.83	0.096	2.90	2.5	7.54
	12:40		70.0	9.75	9.45	0.04	1.15	0.122	1.15	0	9.59
	13:15		79.1	29.90	29.50	0.11	2.89	0.098	2.90	0.3	7.70
	13:25		74.1	9.9	9.65	0.04	0.98	0.102	0.925	-5.6	8.02
	14:30		98.2	30.1	29.70	0.12	3.42	0.116	3.52	2.9	9.12
	15:15		99.5	10.1	9.83	0.04	1.24	0.127	1.255	1.2	9.98
1-28-74	10:30	N_2	119.9	30.1	29.43	0.12	5.06	0.173	5.30	4.7	13.60
	10:40		120.3	10.1	9.70	0.04	1.67	0.173	1.69	1.2	13.60
	12:30		139.9	30.4	29.43	0.13	6.90	0.235	7.23	4.8	18.47
	12:35		140.8	10.05	9.50	0.04	2.26	0.239	2.30	1.8	18.78
	15:05		159.7	30.15	28.78	0.13	9.75	0.340	10.13	3.9	26.72
	15:15		160.2	9.95	9.13	0.04	3.14	0.345	3.18	1.3	27.11

TABLE F-1 (Continued)

Test Date	Test Time (Hr:Min)	Test Gas	T_R OUT (°F)	P_B IN (psig)	$\bar{P}_B$ (psig)	$\bar{P}_R$ (psig)	$\dot{M}_R$ (lb/hr)	$\dot{M}_R/\Delta P$	$\dot{M}_B$ IN (lb/hr)	Flow Balance Error (%)	Apparent Permeability Coefficient $\frac{\left(\frac{cm^3}{sec} \text{ @ NTP}\right)(cm)}{(cm^2)(cm\ Hg)}$
1-29-74	8:20	N_2	60.2	29.85	29.08	0.11	4.33	0.149	4.48	3.5	11.71×10^{-10}
	8:30		61.0	9.90	9.28	0.04	1.86	0.201	1.86	0	15.80
	12:05		40.1	29.95	29.65	0.10	2.52	0.085	2.43	-3.6	6.68
	12:10		40.1	9.90	9.73	0.03	0.75	0.077	0.71	-5.3	6.05
	15:00		20.8	30.0	29.73	0.10	2.21	0.075	2.22	0.5	5.89
	15:05		20.0	9.70	9.55	0.07	0.68	0.072	0.63	-7.4	5.66
1-30-74	14:20	N_2	60.0	50.0	49.55	0.22	4.62	0.094	4.72	2.2	7.39
	14:25		59.7	39.65	39.25	0.20	3.58	0.092	3.58	0	7.23
	14:30		59.9	29.70	29.35	0.11	2.62	0.090	2.65	1.1	7.07
	14:40		60.0	20.0	19.70	0.11	1.71	0.087	1.715	0.3	6.84
	14:45		60.8	10.1	9.90	0.04	0.825	0.084	0.792	-4.0	6.60
1-31-74	10:05	N_2	69.9	50.1	50.05	0.22	4.92	0.099	5.31	7.9	7.78
	10:15		70.2	40.1	39.67	0.20	3.96	0.100	4.06	2.5	7.86
	10:25		71.0	30.1	29.71	0.11	2.90	0.098	2.92	0.7	7.70
	10:30		71.6	20.0	19.68	0.08	1.875	0.096	1.89	0.8	7.54
	10:40		72.2	10.05	9.85	0.04	0.93	0.095	0.90	-3.2	7.47
1-31-74	12:35	N_2	69.9	50.0	49.50	0.22	5.16	0.105	5.45	5.6	8.25
	12:40		69.9	39.85	39.40	0.20	4.01	0.137	4.10	2.2	10.77
	12:50		70.0	30.1	29.70	0.11	2.95	0.100	2.98	1.0	7.86
	13:00		70.8	20.1	19.78	0.07	1.92	0.097	1.94	1.0	7.62
	13:10		70.7	10.0	9.78	0.04	0.94	0.097	0.90	-4.3	7.62
1-31-74	15:20	O_2	38.9	30.15	29.25	0.34	7.90	0.169	8.30	5.1	11.62
	15:25		39.4	9.90	9.40	0.17	1.28	0.139	2.45	91.4	9.56

TABLE F-1 (Continued)

Test Date	Test Time (Hr:Min)	Test Gas	T_R OUT (°F)	P_B IN (psig)	$\bar{P}_B$ (psig)	$\bar{P}_R$ (psig)	$\dot{M}_R$ (lb/hr)	$\dot{M}_R/\Delta P$	$\dot{M}_B$ IN (lb/hr)	Flow Balance Error (%)	Apparent Permeability Coefficient $\frac{\left(\frac{cm^3}{sec} @ NTP\right)(cm)}{(cm^2)(cm\ Hg)}$
2-13-74	9:40	N_2	38.2	30.0	29.55	0.32	4.07	0.139	3.92	-3.7	10.92×10^{-10}
	10:50		42.1	10.15	8.48	0.37	4.63	0.574	4.57	-1.3	44.07
	12:35		39.1	30.1	29.65	0.32	4.08	0.139	3.95	-3.2	10.92
	12:45		40.0	10.05	9.83	0.08	1.07	0.110	1.09	1.9	8.64
	12:55		40.2	10.1	9.88	0.19	1.065	0.110	1.07	0.5	8.64
2-13-74	13:30	O_2	38.2	30.0	29.05	0.94	9.08	0.323	9.0	-0.9	22.21
	13:40		39.0	10.05	9.55	0.20	2.82	0.302	2.72	-3.5	20.77
2-14-74	10:20	N_2	20.0	30.0	29.60	0.31	4.00	0.137	3.95	-1.3	10.77
	10:30		20.1	10.1	9.90	0.08	1.11	0.113	1.06	-4.5	8.88
2-14-74	11:00	O_2	21.4	30.05	29.23	0.81	8.27	0.291	8.25	-0.2	20.01
	11:10		20.6	10.0	9.55	0.17	2.46	0.262	2.36	-4.1	18.02
2-14-74	14:15	N_2	24.9	10.0	9.80	0.08	1.09	0.112	1.045	-4.1	8.80
	14:30		26.7	30.0	29.60	0.31	3.98	0.136	3.93	-1.3	10.69
2-15-74	10:25	N_2	70.2	10.05	9.80	0.09	1.25	0.129	1.145	-8.4	10.14
	10:35		69.2	20.0	19.60	0.20	2.75	0.142	2.67	-2.9	11.16
	10:45		68.9	30.0	29.50	0.36	4.43	0.152	4.25	-4.1	11.95
	10:55		69.1	40.05	39.40	0.59	6.33	0.163	6.10	-3.6	12.81
	11:10		69.1	50.05	49.25	0.88	8.25	0.171	8.14	-1.3	13.44
2-25-74	10:45	N_2	75.0	50.05	49.33	1.27	8.94	0.186	8.96	0.2	14.62

TABLE F-1 (Continued)

Test Date	Test Time (Hr:Min)	Test Gas	T_R OUT (°F)	P_B IN (psig)	$\bar{P}_S$ (psig)	$\bar{P}_R$ (psig)	$\dot{M}_R$ (lb/hr)	$\dot{M}_R/\Delta P$	$\dot{M}_B$ IN (lb/hr)	Flow Balance Error (%)	Apparent Permeability Coefficient $\frac{\left(\frac{cm^3}{sec} \bullet NTP\right)(cm)}{(cm^2)(cm\ Hg)}$
2-26-74	10:45	N_2	70.0	50.0	49.30	1.25	8.78	0.183	8.86	0.9	14.38×10^{-10}
	12:15		70.0	40.05	39.43	0.84	6.71	0.174	6.69	-0.3	13.67
	12:55		69.3	30.0	29.40	0.50	4.78	0.165	4.74	-0.8	12.97
2-26-74	14:20	O_2	70.0	10.0	9.25	0.15	3.69	0.405	3.61	-2.2	27.85
	14:30		69.2	20.05	18.90	0.36	7.77	0.419	7.72	-0.6	28.81
	14:40		69.2	30.0	28.63	0.63	12.2	0.436	12.1	-0.8	29.98
	14:45		69.5	40.0	38.45	1.41	16.5	0.445	16.6	+0.6	30.6
	14:55		69.3	49.9	48.25	2.00	21.55	0.466	21.3	-1.2	32.05
2-27	7:55	N_2	51.5	9.95	9.70	0.05	1.22	0.126	1.13	-7.4	9.90
	8:10		51.9	20.0	19.60	0.11	2.70	0.139	2.64	-2.2	10.92
	8:15		51.1	30.0	29.50	0.22	4.40	0.147	4.32	-1.8	11.55
	8:25		51.1	39.95	39.38	0.39	6.21	0.159	6.19	-0.3	12.50
	8:30		51.1	50.05	49.43	0.60	8.21	0.168	8.36	1.8	13.20

TABLE F-1 (Continued)

Test Date	Test Time (Hr:Min)	Test Gas	T_R OUT (°F)	P_B IN (psig)	$\bar{P}_B$ (psig)	$\bar{P}_R$ (psig)	$\dot{M}_R$ (lb/hr)	$\dot{M}_R/\Delta P$	$\dot{M}_B$ IN (lb/hr)	Flow Balance Error (%)	Apparent Permeability Coefficient $\frac{\left(\frac{cm^3}{sec} @ NTP\right)(cm)}{(cm^2)(cm\ Hg)}$
3-6-74	14:50	N_2	59.6	10.0	9.80	0.05	1.18	0.121	1.085	-8.1	9.51×10^{-10}
3-7-74	9:20	N_2	59.6	10.0	9.80	0.05	1.13	0.116	1.035	-8.4	9.12
	10:30		61.1	10.0	9.80	0.06	1.15	0.188	1.037	-9.8	9.27
	10:35		59.7	20.0	19.70	0.11	2.47	0.126	2.41	-2.4	9.90
	10:40		60.1	30.0	29.60	0.23	4.04	0.138	3.94	-2.5	10.85
	10:45		59.1	40.0	39.55	0.43	5.68	0.116	5.65	-0.5	9.12
	10:55		58.3	50.0	49.50	0.67	7.44	0.152	7.46	0.3	11.95
	11:05		58.7	40.0	39.55	0.47	5.69	0.146	5.59	-1.8	11.47
	11:10		60.3	30.0	29.60	0.28	4.10	0.140	3.94	-3.9	11.00
	11:15		60.8	20.07	19.75	0.13	2.58	0.131	2.46	-4.7	10.30
	11:20		60.1	10.05	9.85	0.06	1.20	0.123	1.08	-10.0	9.67
3-7-74	12:30	O_2	59.9	10.05	9.45	0.15	3.20	0.344	3.15	-1.6	23.66
	12:40		60.2	20.0	19.10	0.30	6.65	0.354	6.68	0.5	24.34
	12:55		58.2	30.1	29.0	0.61	10.52	0.371	10.40	-1.1	25.51
	13:10		59.0	40.15	38.95	1.26	14.3	0.379	14.35	0.3	26.06
	13:20		59.1	50.0	48.70	2.04	18.15	0.389	18.40	1.4	26.75
	13:25		58.5	40.0	38.80	1.41	14.25	0.381	14.21	-0.3	26.2
	13:40		58.3	30.0	28.90	0.82	10.50	0.374	10.50	0	25.72
	13:50		59.1	20.0	19.10	0.18	6.91	0.365	6.84	-1.0	25.1
	14:05		59.5	10.0	9.40	0.08	3.39	0.364	3.22	-5.0	25.03

TABLE F-2. AIR SEPARATION TEST DATA SUMMARY

(PRE-LEAKAGE REPAIR)

Test Date	Test Time (Hr:Min)	T_B OUT (°F)	P_B IN (psig)	$\bar{P}_B$ (psig)	$\bar{P}_R$ IN (psig)	$\dot{M}_B$ IN (lb/hr)	$\dot{M}_B$ OUT (lb/hr)	$\dot{M}_R$ IN (lb/hr)	$\dot{M}_R$ OUT (lb/hr)	O_2 B, R IN (%)	Measured O_2 B OUT (%)	O_2 R OUT (%)	Flow Balance Error (%)	Computed O_2 B OUT (%)
2-5-74	12:40	71.2	30.4	29.70	0.49	4.73	1.012	27.10	30.05	21.3	9.7	21.59	2.5	10.7
	13:30	71.9	30.1	28.40	0.50	8.76	5.024	25.48	30.41	21.0	13.3	22.34	4.1	13.4
	14:00	71.3	30.25	27.30	0.50	13.74	9.94	27.34	30.34	21.4	16.3	23.04	2.6	15.9
	14:50	70.5	30.0	25.55	0.51	18.62	14.92	28.30	30.93	21.1	17.4	22.84	3.3	17.1
	15:15	70.0	30.0	24.25	0.51	23.57	20.01	28.10	30.79	20.85	18.0	22.66	2.7	17.9
2-6-74	10:25	71.2	29.9	20.70	0.48	33.63	30.3	27.10	29.48	20.9	19.2	22.60	3.1	19.0
	11:05	71.0	49.9	46.45	0.49	23.88	17.4	4.91	30.21	20.9	15.6	29.15	*	*
	13:30	71.5	49.9	45.80	0.49	27.57	20.38	23.82	30.27	20.8	16.0	23.49	2.4	15.7
	14:10	71.0	50.0	46.85	0.50	22.15	15.15	24.09	30.53	21.2	15.0	24.26	1.8	14.9
	14:50	70.4	50.0	47.75	0.49	16.96	10.09	24.52	30.27	20.8	13.1	23.31	3.6	13.1
2-7-74	10:00	71.2	49.6	43.85	0.49	36.95	30.33	24.02	30.25	20.8	17.2	24.40	1.3	17.2
	10:30	71.0	49.8	48.40	0.50	11.65	5.01	24.29	30.62	20.6	10.3	22.30	1.0	10.4
	11:20	70.5	49.6	48.88	0.49	7.38	1.01	24.12	30.30	21.0	7.1	21.47	0.6	8.0
	13:15	71.7	29.90	28.25	0.12	8.51	4.95	1.19	4.96	21.0	14.1	28.33	-4.4	15.2
	13:35	71.1	30.15	28.48	0.28	8.69	4.98	6.62	10.40	20.9	13.2	26.07	-0.7	14.2
	14:50	71.2	29.9	28.25	0.66	8.62	4.97	16.58	20.07	21.2	13.5	23.12	0.8	13.7
2-8-74	9:10	70.7	49.6	47.35	0.11	16.8	10.0	3.1	10.2	21.0	13.9	28.32	-3.0	14.1
	10:00	71.8	49.75	47.50	0.27	17.0	10.05	13.0	20.0	20.7	13.2	24.54	-0.3	13.1
2-11-74	12:50	140.3	49.8	43.90	0.85	38.5	19.5	18.7	34.2	20.9	13.5	24.79	9.3	12.2
	13:10	140.7	30.3	22.45	0.87	28.5	19.2	29.5	35.6	20.9	16.3	23.20	8.2	16.1
	13:40	140.0	49.9	45.05	0.83	34.0	14.8	18.0	34.2	20.8	12.2	24.28	8.07	12.1
	14:15	140.2	30.0	25.75	0.87	24.75	15.0	28.8	35.6	20.9	15.3	23.10	7.7	15.2
	14:40	140.1	49.95	46.13	0.87	29.4	10.1	18.1	34.9	21.0	10.9	23.78	6.7	10.8
	14:55	140.0	30.0	25.53	0.85	19.9	10.0	27.5	35.2	21.0	13.8	22.95	5.9	13.8
	15:25	139.9	49.95	47.20	0.87	24.4	5.05	17.35	34.2	21.1	9.0	22.80	6.8	9.1
	15:35	139.9	29.9	27.01	0.83	15.3	5.05	26.5	34.6	21.1	11.9	22.38	5.9	12.1
	15:55	140.0	30.0	28.33	0.79	11.5	1.00	25.4	33.9	21.1	9.5	21.43	5.6	10.6
	16:10	140.0	49.75	47.83	0.83	20.2	1.04	16.4	33.4	21.1	7.0	21.52	6.1	7.8

*Relief valve leakage-no entries possible.

TABLE F-2 (Continued)

Test Date	Test Time (Hr:Min)	T_B OUT (°F)	P_B IN (psig)	$\overline{P}_B$ (psig)	$\overline{P}_R$ IN (psig)	$\dot{M}_B$ IN (lb/hr)	$\dot{M}_B$ OUT (lb/hr)	$\dot{M}_R$ IN (lb/hr)	$\dot{M}_R$ OUT (lb/hr)	O_2 B, R IN (%)	Measured O_2 B OUT (%)	O_2 R OUT (%)	Flow Balance Error (%)	Computed O_2 B OUT (%)
2-12-74	9:45	39.8	50.1	49.33	0.46	9.4	1.01	22.5	30.3	21.0	9.3	21.39	1.9	9.2
	10:00	40.0	29.9	29.20	0.39	5.45	1.01	26.8	30.6	21.0	10.8	21.34	2.0	11.9
	10:35	40.1	49.8	48.45	0.47	13.5	4.99	22.6	30.4	21.0	12.9	22.32	2.3	12.7
	10:40	40.1	30.0	28.35	0.46	9.4	5.03	26.7	30.6	21.1	14.9	22.11	1.5	15.2
	11:15	40.1	50.0	47.85	0.47	18.6	9.95	22.95	30.7	21.1	15.2	22.98	2.8	15.1
	11:30	40.6	29.9	27.20	0.48	14.15	9.94	27.5	31.2	21.1	16.9	22.43	1.6	17.2
	12:40	40.3	50.1	47.15	0.46	23.85	15.1	22.4	30.2	21.0	16.4	23.25	3.1	16.4
	12:55	40.5	30.1	26.15	0.46	19.4	15.2	26.85	30.4	20.9	18.0	22.33	2.1	18.1
	13:25	40.3	49.9	46.15	0.46	29.2	20.05	22.35	30.4	21.1	17.4	23.48	3.5	17.4
	13:40	40.1	29.9	24.55	0.46	24.8	20.15	27.1	30.4	21.1	18.8	22.57	4.3	19.0
	14:40	39.8	50.0	44.80	0.46	38.2	30.0	23.0	30.3	20.4	17.6	23.11	2.9	17.8

REFERENCES

1. S.V. Zinn, Jr., Inerted Fuel Tank Oxygen Concentration Requirements, Federal Aviation Administration, Interim Report FAA-RD-71-42, August 1971

2. P.B. Stewart and E.S. Starkeman, Inerting Conditions for Aircraft Fuel Tanks, WADC Technical Report 55-418, University of California, September 1955

3. M.G. Zabetakis, Flammability Characteristics of Combustible Gases and Vapors, Bureau of Mines Bulletin 627, U.S. Department of the Interior.

4. DC-10 Flight Crew Operating Manual, Reference and Performance CAI-52, Vol. 2

5. E.P. Klueg, W.C. McAdoo and W.E. Neese, Performance of a DC-9 Aircraft Liquid Nitrogen Fuel Tank Inerting System, Federal Aviation Administration, Final Report FAA-RD-72-53, August 1972

6. DC-10, Series 10, Air Conditioning and Pneumatic System Design Control Document, DCD 5041B, May 17, 1971

7. DuPont, "DuPont 'Freon' FE 1301 Fire Extinguishing Agent", No. B-29B

8. Dupont, "Toxicology of DuPont FE 1301 Fire Extinguishing Agent," No. S35A

9. R.M. Barrer, Diffusion in and Through Solids, Cambridge Press, London 1941

10. C.E. Rogers Chapter "Solubility and Diffusility" from Physics and Chemistry of the Organic Solid State, Volume II, by David Fox, et. al., 1965, Wylie

11. R.M. Barrer, "Activated Diffusion in Membranes", page 644 of Faraday Society Transactions, Volume 35, 1939

12. J. Crank, The Mathematics of Diffusion, Oxford Univ. Press, London 1956

13. H.S. Carslow and J.C. Jaeger, Conduction of Heat in Solids, Second Edition, Oxford Univ. Press, 1959

14. Imperial Chemical Industires, Ltd., Plastics Division, Welwyn Garden City, England, "TPX ™ methylpentene polymers", Technical Bulletin 252.

15. "General Electric Permselective Membranes", Medical Development Operation Chemical and Medical Division, General Electric Co.

16. H. Yasuda and K.J. Rosengren, J. Appl. Pol. Sci 14, 2839 (1970)

DISCLAIMER NOTICE

THIS DOCUMENT IS BEST QUALITY PRACTICABLE. THE COPY FURNISHED TO DTIC CONTAINED A SIGNIFICANT NUMBER OF PAGES WHICH DO NOT REPRODUCE LEGIBLY.